

tekstilec

4/2024 • vol. 67 • 289–412

ISSN 0351-3386 (tiskano/printed)

ISSN 2350-3696 (elektronsko/online)

UDK 677 + 687 (05)



UNIVERZA
V LJUBLJANI

NTF

Naravoslovnotehniška
fakulteta





<https://journals.uni-lj.si/tekstilec>

Časopisni svet/*Publishing Council*
Barbara Simončič, predsednica/*President*
Katja Burger Kovič, Univerza v Ljubljani
Manja Kurečič, Univerza v Mariboru
Tatjana Kreže, Univerza v Mariboru
Gašper Lesjak, Predilnica Litija, d. o. o.
Nataša Peršuh, Univerza v Ljubljani
Petra Prebil Bašin, Gospodarska zbornica Slovenije

Melita Rebič, Odeja, d. o. o.
Tatjana Rijavec, Univerza v Ljubljani
Simona Strnad, Maribor, SI
Helena Zidarič Kožar, Inplet pletiva, d. o. o.
Vera Žlabravec, Predilnica Litija, d. o. o.

Glavna in odgovorna urednica/
Editor-in-Chief
Tatjana Rijavec

Namestnica glavne in odgovorne
urednice/*Assistant Editor*
Tatjana Kreže

Področni uredniki/*Associate Editors*
Matejka Bizjak, Katja Burger Kovič, Andrej Demšar, Mateja Kos Koklič, Alenka Pavko Čuden, Andreja Rudolf, Barbara Simončič, Dunja Šajn Gorjanc, Sonja Šterman, Brigita Tomšič

Izvršna urednica za podatkovne baze/
Executive Editor for Databases
Irena Sajovic

Mednarodni uredniški odbor/
International Editorial Board

Matej Bračič, Maribor, SI
Inga Dāboliņa, Rīga, LT
Andrea Ehrmann, Bielefeld, DE
Petra Forte Tavčer, Ljubljana, SI
Jelka Geršak, Maribor, SI
Marija Gorjanc, Ljubljana, SI
Lubos Hes, Moka, MU
Aleš Hladnik, Ljubljana, SI
Svjetlana Janjić, Banja Luka, BA
Mateja Kert, Ljubljana, SI
Petra Komarkova, Liberec, CZ
Mateja Kos Koklič, Ljubljana, SI
Mirjana Kostić, Beograd, RS
Manja Kurečič, Maribor, SI
Boris Mahlrig, DE
Subhankar Maity, Kanpur, IN
Małgorzata Matusiak, Łódź, PL
Ida Nuramdhani, ID
Alenka Ojstršek, SI
Željko Penava, Zagreb, HR
Tanja Pušić, Zagreb, HR
Ivana Salopek Čubrić, Zagreb, HR
Snežana Stanković, Beograd, RS
Jovan Stepanović, Leskovac, RS
Antoneta Tomljenović, Zagreb, HR

tekstilec (ISSN: 0351-3386 tiskano, 2350-3696 elektronsko) je znanstvena revija, ki podaja temeljne in aplikativne znanstvene informacije v fizikalni, kemijski in tehnološki znanosti, vezani na tekstilno in oblačilno tehnologijo, oblikovanje in trženje tekstilij in oblačil. V prilogah so v slovenskem jeziku objavljeni strokovni članki in prispevki o novostih v tekstilni tehnologiji iz Slovenije in sveta, prispevki s področja oblikovanja tekstilij in oblačil, informacije o raziskovalnih projektih ipd.

tekstilec (ISSN: 0351-3386 printed, 2350-3696 online) the scientific journal gives fundamental and applied scientific information in the physical, chemical and engineering sciences related to the textile and clothing industry, design and marketing. In the appendices written in Slovene language, are published technical and short articles about the textile-technology novelties from Slovenia and the world, articles on textile and clothing design, information about research projects etc.

Dosegljivo na svetovnem spletu/*Available Online at*
<https://journals.uni-lj.si/tekstilec>



Tekstilec je indeksiran v naslednjih bazah/*Tekstilec is indexed in*
Emerging Sources Citation Index – ESCI (by Clarivate Analytics):

Journal Impact Factor (JIF) for 2023 = 0.7

Journal Citation Indicator (JCI) for 2023 = 0.2

Category Quartile: Q3

Leiden University's Center for Science & Technology Studies:

Source-Normalized Impact per Paper (SNIP) for 2023 = 0.632

SCOPUS/Elsevier for 2023:

Q3, SJR for 2023 = 0.22

Cite Score for 2023 = 1.3

H-Index for 2023 = 15

Ei Compendex

DOAJ

WTI Frankfurt/TEMA® Technology and Management/TOGA® Textile Database

World Textiles/EBSCO Information Services

Textile Technology Complete/EBSCO Information Services

Textile Technology Index/EBSCO Information Services

Chemical Abstracts/ACS

ULRICHWEB – global serials directory

LIBRARY OF THE TECHNICAL UNIVERSITY OF LODZ

dLIB

SICRIS za 2022: 1A3 (Z, A, A1/2); Scopus (d)

tekstilec

Ustanovitelj / *Founded by*

- Zveza inženirjev in tehnikov tekstilcev Slovenije / *Association of Slovene Textile Engineers and Technicians*
- Gospodarska zbornica Slovenije – Združenje za tekstilno, oblačilno in usnjarsko predelovalno industrijo / *Chamber of Commerce and Industry of Slovenia – Textiles, Clothing and Leather Processing Association*

Revijo sofinancirajo / *Journal is Financially Supported*

- Javna agencija za raziskovalno dejavnost Republike Slovenije / *Slovenian Research Agency*
- Univerza v Ljubljani, Naravoslovnotehniška fakulteta / *University of Ljubljana, Faculty of Natural Sciences and Engineering*
- Univerza v Mariboru, Fakulteta za strojništvo / *University of Maribor, Faculty for Mechanical Engineering*

Sponzor / *Sponsor*

Predilnica Litija, d. o. o.

Izdajatelj / *Publisher*

Univerza v Ljubljani, Naravoslovnotehniška fakulteta / *University of Ljubljana, Faculty of Natural Sciences and Engineering*

Revija Tekstilec izhaja pod okriljem Založbe Univerze v Ljubljani / *The journal Tekstilec is published by the University of Ljubljana Press*

Revija Tekstilec izhaja šestkrat letno (štiri znanstveni zvezki in dve strokovni prilogi)

Journal Tekstilec appears six times a year (four scientific issues and two professional supplements)

Revija je pri Ministrstvu za kulturo vpisana v razvid medijev pod številko 583. Letna naročnina za člane Društev inženirjev in tehnikov tekstilcev je vključena v članarino.

Letna naročnina za posameznike 38 € za

- študente 22 €
- za mala podjetja 90 € za velika podjetja 180 €
- za tujino 110 €

Cena posamezne številke 10 €

Na podlagi Zakona o davku na dodano vrednost sodi revija Tekstilec med proizvode, od katerih se obračunava DDV po stopnji 5 %.

Imetnik računa / *Account holder:*
Univerza v Ljubljani,
Naravoslovnotehniška fakulteta,
Askerceva 12, 1000 Ljubljana, SI-Slovenija

Transakcijski račun / *Bank Account:*
SI56 01100-6030708186, Banka Slovenije,
Slovenska 35, 1000 Ljubljana, SI-Slovenija
SWIFT / *SWIFT Code:* BSLJSI2X

Naslov uredništva / *Editorial Office Address:*

Uredništvo Tekstilec, Snežniška 5, SI-1000 Ljubljana

Tel. / *Tel.:* + 386 1 200 32 00, +386 1 200 32 24

Faks / *Fax:* + 386 1 200 32 70

E-pošta / *E-mail:* revija.tekstilec@ntf.uni-lj.si

Spletni naslov / *Internet page:* <https://journals.uni-lj.si/tekstilec>

Lektor za slovenščino / *Slovenian Language Editor* Milojka Mansoor

Lektor za angleščino / *English Language Editor*

Glen Champagne, Barbara Luštek Preskar

Oblikovanje platnice / *Design of the Cover* Tanja Nuša Kočevar

Oblikovanje / *Design* ENOOKI Kraft, Mitja Knapič s.p

Tisk / *Printed by* DEMAT d.o.o.

Copyright © 2024 by Univerza v Ljubljani, Naravoslovnotehniška fakulteta,

Oddelek za tekstilstvo, grafiko in oblikovanje

Revija Tekstilec objavlja članke v skladu z načeli odprtega dostopa pod pogoji licence Creative Commons Attribution 4.0 International License (CC BY 4.0). Uporabnikom je dovoljeno nekomercialno in komercialno reproduciranje, distribuiranje, dajanje v najem, javna priobčitev in predelava avtorskega dela, pod pogojem, da navedejo avtorja izvirnega dela. / *Creative Commons Attribution CC BY 4.0 licence Journal Tekstilec is published under licence Creative Commons CC BY 4.0. This license enables reusers to distribute, remix, adapt, and build upon the material in any medium or format, so long as attribution is given to the creator. The license allows for commercial use.*



SCIENTIFIC ARTICLES/

Znanstveni članki

- 292** *Rochak Rathour, Md. Azharul Islam, Apurba Das, Ramasamy Alagirusamy*
Review of Heat and Moisture Transfer Models of Fire-Protective Clothing
Pregled modelov prenosa toplote in vlage skozi ognjevarna zaščitna oblačila
- 308** *Ida Nuramdhani, Maulana Fahrizal Abdan, Robinson Manalu, Jantera Sekar Tirta, Mohamad Widodo*
Physicochemical Analysis of Dyeing of Cotton Denim with Natural Indigo Dye from *Strobilanthes cusia* Using Green Reducing Agents and Alkalis
*Fizikalno-kemijska analiza barvanja bombažnega denima z naravnim barvilom indigo iz *Strobilanthes cusia* z uporabo zelenih reducentov in alkalij*
- 321** *Md. Zayedul Hasan, Rochak Rathour, Apurba Das, R. Alagirusamy, Nandan Kumar*
Thermophysiological Comfort Behaviour of Cut Protective Workwear Consisting of Filament Twisted Multicomponent Hybrid Yarn
Termofiziološko udobje oblačil za zaščito pred urezom, izdelanih iz oplaščenih prejš s hibridnimi filamentnimi prejami v jedru
- 346** *Mehmet Karahan, Nevin Karahan*
Stiffness Determination of Bi- and Triaxial Flat Braided Carbon/Vinyl Ester Composites Using Micromechanics Method
Določanje togosti kompozitov iz dvo- in triosnih ploskih pletiv iz ogljikovih vlaken in vinilestrske matrice z uporabo metode mikromehanike
- 357** *Vishal Trivedi, Pradeep Joshi*
Exploring the Role of Situational Cues in Apparel Consumers' Impulsive Buying Behaviour
Raziskovanje vloge situacijskih dejavnikov pri impulzivnem nakupovalnem vedenju potrošnikov oblačil
- 370** *Ambreen, Kashif Javed, Asfandyar Khan, Faiza Anwer, Imran Ahmad Khan, Mumtaz Hassan Malik*
Analysis of Identifying and Correcting the Digital Printing Defects in Pakistan's Textile Industry
Analiza prepoznavanja in odpravljanja napak pri digitalnem tisku v pakistanski tekstilni industriji
- 381** *Mehmet Karahan, Muhammad Ali Nasir, Rizwan Ahmed Malik*
Effect of Fibre Type and Fabric Structure on Composite Materials Under Ballistic Shock Impact
Vpliv vrste vlaken in strukture ploskovne tekstilije kompozitnih materialov pri balističnem udaru
- 397** *Viktorija Diak, Andrii Diak*
Features and Limitations of Fused Deposition Modelling (FDM) in Obtaining Textile-like Structures
Značilnosti in omejitve tehnologije modeliranja s spajanjem slojev (FDM) pri pridobivanju tekstilu podobnih struktur

Rochak Rathour,¹ Md. Azharul Islam,^{1,2} Apurba Das,¹ Ramasamy Alagirusamy¹

¹ Department of Textile and Fiber Engineering, Indian Institute of Technology Delhi, Hauz Khas,
110016 New Delhi, India

² Department of Textile Engineering, Mawlana Bhashani Science and Technology University, Santosh,
1902 Tangail, Bangladesh

Review of Heat and Moisture Transfer Models of Fire-Protective Clothing

Pregled modelov prenosa toplote in vlage skozi ognjevarna zaščitna oblačila

Scientific review/Pregledni znanstveni članek

Received/Prispelo 5–2024 • Accepted/Sprejeto 8–2024

Corresponding author/Korespondenčni avtor:

Dr. Rochak Rathour

Tel: +919560821849

E-mail: india.rochak1994@gmail.com

ORCID iD: 0000-0001-7522-2458

Abstract

This paper presents a comprehensive review of previously published research on heat and moisture transfer models applied to fire-protective clothing, which is crucial for ensuring firefighter safety and comfort. By analysing experimental data and numerical simulations from various studies, this review paper tries to explore the intricate interactions between heat, moisture and textile materials. It provides insight into the performance and design optimisation of such clothing, elucidating the dynamic behaviour of heat and moisture transfer within fabric layers. The research results offer valuable guidelines for enhancing protective efficacy while maintaining wearer comfort. This review advances our understanding of fire-protective clothing and lays the groundwork for future innovations in firefighting gear design and material selection.

Keywords: fire-protective clothing, model, heat, moisture, single layer, multilayer

Izvleček

Prispevek prinaša celovit pregled objavljenih raziskav modelov prenosa toplote in vlage, ki se uporabljajo za ognjevarna zaščitna oblačila in so ključna za zagotavljanje varnosti in udobja gasilcev. Z analizo eksperimentalnih podatkov in numeričnih simulacij iz različnih študij skuša avtor raziskati zapletene interakcije med toploto, vlago in tekstilnimi materiali. Prispevek zagotavlja vpogled v učinkovitost in optimizacijo oblikovanja takšnih oblačil, pojasnjuje dinamično obnašanje prenosa toplote in vlage med plastmi tekstilij. Rezultati raziskav ponujajo dragocene smernice za izboljšanje učinkovite zaščite ob ohranjanju udobnosti nošenja. Ta pregled izboljšuje razumevanje ognjevarnih oblačil ter postavlja temelje za prihodnje inovacije v oblikovanju gasilske opreme in pri izbiri materialov.

Ključne besede: ognjevarno zaščitno oblačilo, model, toplota, vlaga, enoslojna, večplastna



Content from this work may be used under the terms of the Creative Commons Attribution CC BY 4.0 licence (<https://creativecommons.org/licenses/by/4.0/>). Authors retain ownership of the copyright for their content, but allow anyone to download, reuse, reprint, modify, distribute and/or copy the content as long as the original authors and source are cited. No permission is required from the authors or the publisher. This journal does not charge APCs or submission charges.

1 Introduction

Structural fires are associated with numerous hazards that pose new challenges with every passing year [1]. Regulatory hazards can lead to minor injuries or fatal accidents resulting in the end of a career or even death [2]. As firefighting technology has improved dramatically in recent decades, firefighters have access to more sophisticated protective equipment. Multidisciplinary research has emphasised the importance of evaluating the performance level of fire-protective clothing to determine its potential to prevent injuries and even save lives. Several factors determine the effectiveness of fire-protective clothing, e.g. the type of fire, design of fire-protective clothing and materials used [3]. The need for fire-protective clothing has been addressed by numerous studies in fire science and technology over the past two decades. An overview of the existing studies and improvements to fire-protective clothing design is presented by Shakeriaski et al. [4]. Periodically documented literature reviews [5–11] provide an overview of current knowledge for future development of products. Fire management is associated with numerous hazards that can endanger the life of workers in extreme conditions of the fire ground. Firefighters wear specialised protective gear depending on the nature of the microclimate [12]. In fire-protective clothing, moisture management presents a challenge since the ensemble must prevent external heat and moisture to penetrate while allowing metabolic heat and sweat to flow in opposite direction through the fabric [13]. Thermal protective clothing (TPC) prevents external heat and moisture from transferring through the fabric to the skin while allowing metabolic heat and perspiration to escape to the environment. It is designed to limit heat stress and minimise hindrances to firefighters' activities. Firefighters deployed to battle fire and rescue victims face life-threatening hazards in an active workplace. The fire-protective clothing should provide basic protection against open flames, heat (radiative, convective etc.) and environmental

hazards. In addition, these fabrics should possess enough mechanical strength to abrasion, cuts, tears and abrasion [14].

This review illuminates the latest advancements in heat and moisture transfer models applied to fire-protective clothing, underscoring their pivotal role in ensuring the safety and comfort of firefighters. By synthesising a breadth of literature spanning experimental studies, numerical simulations and theoretical frameworks, we have identified emergent trends and gaps in knowledge within this interdisciplinary field. Furthermore, we have highlighted recent efforts to incorporate physiological considerations and real-world operational conditions into predictive models, heralding a paradigm shift towards more holistic approaches to fire-protective clothing design and evaluation. Through this comprehensive review, we provide valuable insights that inform future research directions and foster innovation in firefighter safety apparel.

2 Heat and moisture transfer through firefighting clothing

Heat transfer takes place from a medium or high temperature to low temperature until a state of equilibrium between the two media is reached. The process of conduction occurs between textile fabrics in contact with each other or between textile fabrics and human skin when clothing is worn. The temperature gradient between the two mediums and the total heat resistance between them are the two factors that determine the rate of the heat flow. In radiation heat transfer, electromagnetic waves transfer heat from one place to another and do not require material mediums or textile substrates to facilitate the transfer of heat. The role of clothing in heat and moisture management is discussed by Rossi et al. [15]. In order to understand the mechanism of the heat and moisture transfer process through TPC, extensive research has been conducted during the past few decades by the actual measurement

of the desired properties in laboratory simulated conditions in bench top tests and by developing numerical models. The results are well documented in literature [8, 16–18].

2.1 Heat transfer

Firefighters' clothing comprises a fabric structure of at least three layers. Different types of woven and nonwoven materials are used in each layer to meet the functional requirements of a layer in the multi-layered ensemble [19]. The outer layer of fire-protective clothing is the first layer to cope with the incident radiant heat flux from the environment by absorption. The absorbed heat flows via different layers of fire-protective clothing to the basal layer and finally reaches the skin. The heat transmission may occur by conduction through dry fibres and entrapped air bubbles, or by radiation/convection through air gaps between layered structures. Numerous researchers have evaluated the protective properties of fire-protective clothing using mathematical models that considered heat transfer alone and ignored moisture transfer effects completely [20–26]. A multilayer finite element model was developed by Torvi to predict skin temperature and burn time for second- and third-degree burns. There was a small change in second-degree burn predictions when variations in the thermo-physical properties of the skin were considered in multilayer skin models; however, large changes in third-degree burn predictions were observed [27]. Song et al. used a manikin fire-test system, taking into account the air layer between the garment and the manikin exposed to a laboratory-controlled flash fire to study heat-induced changes in fabric thermophysical properties and predict skin burn injury [28]. Finite volume modelling was used to investigate the transient heat transfer effects of protective clothing. Reducing the fabric's rear-side emissivity with fire-resistant coatings improved clothing performance; increasing thermal resistance with this method is more effective than using multiple layers or thickening of fabrics [29]. The conduction and radiation heat transfer

between clothing layers and between the clothing and the skin can be accounted for by an extension of this model. Time-dependent predictions were made for temperature and heat flux distributions in fabric layers, skin and air gaps [30].

A study showed that the predicted temperature on the outer shell of the garment differed the most from experimental values, i.e. by as much as 24 °C [21]. The heat and mechanical protection properties of fire-protective clothing were generally lower after the thermal exposure than in their original state. Heat affected mechanical properties more than heat protective properties. In two cases, the material degradation started before the visual changes, posing potential risk to end users [31]. The degradation of heat resistant fabrics under high radiant heat flux is incorporated in a heat transfer model. The time to second-degree skin burn, mass loss rates, and temperature profiles of the charring material and skin simulant are fairly consistent with the experimental values obtained from radiant protective performance (RPP) tests [32]. Su et al. [33] considered thermal radiation through absorption, transmission, emission and reflection in porous fabrics. Experimental and predicted results were in good agreement with previous Beer's law models. An analysis of radiant heat transfer in a multilayer fabric system, as well as the influence of flame-resistant fabrics' optical properties on heat transfer is presented in this study. With a multilayer fabric system, self-emission enhances both thermal energy transfer to human skin and thermal energy transfer to the atmosphere during cooling [33]. Under three different heat fluxes, full factorial experiments were conducted by varying construction parameters such as pick densities for woven fabrics and punch densities for nonwoven fabrics. These experiments revealed a linear relationship between pick density and punch density, whereas the variation in heat fluxes does not have a linear relationship [34]. Su et al. [35] developed a heat transfer model to predict burn injuries at different contact temperatures and pressures. Contact heat transfer (ASTM F1060-08) is

affected by fabric thickness and thermal conductivity under various applied pressures. In multilayer clothing systems, the thermal protective performance (ASTM F2731) decreases with increasing test temperatures and pressures. Under radiant heat, contact heat transfer can also reduce the importance of the air gap. Using a 3D numerical model, Udayraj et al. [36] investigated heat transfer through fire-protective clothing exposed to flames and radiant heat. The heat transfer through air gaps between the clothing and the human body was analysed using computational fluid dynamics (CFD). Natural convection, conduction and radiation are all accounted for in the model. Various fabric parameters, as well as heat exposure-related parameters, e.g. flame heat transfer coefficient and types of heat exposure, were analysed using a parametric analysis. By simplifying the assumptions used in previous heat transfer models, such as considering constant fabric thermophysical properties and neglecting convection in the air gap, significant deviations can occur in both heat transfer analysis and second-degree burn prediction.

The stored energy in fabric assemblies greatly impacts firefighters' protective clothing when exposed to low intensity radiation heat, which is due to the stored thermal energy contained in the fire-protective clothing weakening the thermal protective performance of those garments. Static air is known to have high thermal resistivity, making it a better heat-insulator. As soon as the moisture barrier in the fabric combination system is removed, T^{RPR} (second-degree burn time) and T^{SET} (minimum value of exposure time) will increase for this fabric system [37]. The relationship between fabric structures, radiant protection and transport properties was explored for providing the most suitable firefighter uniforms. Experiments showed that the thermal protection of single-layer fabrics is affected by their structure, weight and thickness. Transport properties, which are closely related to comfort, are determined by air permeability, thermal resistance and moisture evaporation [38]. Moisture content and perspiration rate within fabric layers affect heat

transfer between multiple air gaps [37, 39]. The measurement of evaporation rates within clothing layers showed that wet clothing layers never reached higher temperatures than dry clothing layers. The temperature increase follows exactly the dry sample curve after all moisture has evaporated [40].

Thermal protective performance against convection (ISO 9151), radiation (ISO 6942) and combined convection/radiation (ISO 17492) heat fluxes was evaluated. As compared to convection heat source, radiation heat source displayed a higher heat transfer index. Heat transfer mechanisms by convection and radiation are fundamentally different, and different heat sources can produce different thermal protective performance values [41]. In human body, mass transfer takes place through fabrics when steam or hot water is present [42]. The transmitted and stored energy in fire-protective clothing after the exposure to low-level thermal radiation was simulated using a finite difference model. The multilayer protective clothing worn by firefighters transmits heat during exposure and discharges heat after exposure, leading to skin burns, particularly third-degree burns [43]. Radiant heat transfer through fabrics is influenced by fabric parameters, structures and properties, and cotton treated with Proban® and thick thermal liner fabrics showed higher radiative protective performance. Multiple linear regression model (Equation 1) is effective at predicting RPP from significant fabric properties [44].

$$\text{Radiative protective performance (RPP)} = 3.02 + 0.02 \times W - 7.9 \times T + 0.29 \times TR + 1.27 \times ER \quad (1)$$

where, W is areal density of fabric (g/m^2), T is thickness (mm), TR is thermal resistance ($^{\circ}\text{Cm}^2\text{W}^{-1}$) and ER is evaporative resistance ($\text{Pam}^2\text{W}^{-1}$).

The cumulative thermal resistance of clothing layers is linearly related to the stored energy in the system. This energy depends not only on the properties of its individual layers, but also on their neighbouring layers. The improvement of thermal insulation for the inner liner in a multilayer fabric system, e.g. by increasing the weight of this layer, in-

creases the stored energy within all fabric layers [45]. A heat transfer level calculation identified fabric properties that significantly affected protective performance at different radiant heat exposure levels. Multiple linear regression models based on these calculations can be applied to predict fabric thermal protective performance effectively [46]. An innovative non-destructive test method for measuring the thermal protective performance was developed with the help of sweating thermal manikin measurements. The fluctuating rate of the core temperature was proposed as a novel objective index for quantifying the thermal protective performance. The thermal protective performance and intrinsic thermal resistance of firefighters' clothing show a positive linear relationship [47]. Radiative protective performance can be improved by increasing the number of fabric layers and air gaps between fabric modular systems; a study was conducted to determine how fabric combinations, air gaps and moisture barrier integrity affected the radiative protective performance of fabric assemblies [37].

2.2 Coupled heat and moisture transfer

Wearing clothing with a high moisture content (near saturation) can provide better thermal protection than wearing clothing without any moisture. However, moisture impacts thermal protection negatively at 100% radiant exposure under 84 kW/m² heat flux. The thermal protection time under low-level heat flux shows anomalies in the presence of moisture. The best thermal protection is offered by bone-dry fibres; however, the protection time rapidly declines as the imbibed moisture rises to a critical value. Beyond this point, there is a gradual rise in protection time with a further increase in moisture [48]. The heat and moisture transfer from the skin to the environment is largely controlled by the microclimate [49]. Firefighters' clothing systems may be affected by moisture, depending on the source, location, timing and sorption level. Moisture from external sources tends to decrease heat transfer through fabric systems when exposed to high-heat flux flames, where-

as moisture from within tends to increase it [50]. Using different barrier material combinations, Fan-glong et al. tested the effect of moisture-permeable and moisture-impermeable barriers on radiant protection, while maintaining a balance between heat and moisture in clothing assemblies. The moisture barrier permeability determines the comfort level of firefighters' protective clothing [51]. In TPC, air gaps and moisture distribution have a large and complicated impact on thermal protection. The amount of moisture added to the fabric influences the air gap effect. When the air gap size was less than 12 mm, moisture accentuated its positive effect, while it had a varying effect when the gap size was larger than 12 mm [52].

In flame and radiant heat transfer and water vapour resistance tests (EN 469), washing improved water vapour transfer, but had a negative impact on heat protection. The material content and material brand have a considerable effect on the required performance levels of heat protection [53]. Direct heat from a heat source and stored thermal energy in the clothing continuously flow during the cooling phase from the clothing to the skin. Thermal protection levels were quantified using a newly developed index and a safety time segment was identified as a measure of thermal insulation for the fabric assembly. Protection levels are controlled not only by the intrinsic properties of the fabrics, but also by exposure and cooling time [54]. Flame retardant fabrics with different moisture contents showed similar variation trends when exposed to a range of radiant heat exposures. When the heat radiation time exceeded 60 seconds, moisture addition during a constant temperature period enhanced thermal protection. The thermal protection of moistened fabrics was generally worsened by heat radiation times longer than 500 seconds [55]. Previous research revealed that skin temperature changes are characterised by four stages, i.e. sharp increase, stable state, gradual rise and decrease. In these four stages, moisture plays different roles based on fabric type, moisture content and exposure time. The increased energy

Table 1: Important findings related to protective performance of single- and multilayer clothing

Reference	Fabric composition	Heat flux/Type and method	Properties studied	Important findings
Day et al. 1987 [57]	Aramid and its blends	8.4 kWm ⁻² Radiant and regression analysis	Non-destructive test method for evaluating RPP of firefighters' garments under moderate heat flux.	1) Vital information on thermal protection during fire ground conditions. 2) Protection time is determined primarily by thickness of garment. 3) Increased thermal inertia of heavier assemblies results in more severe burns.
Yoo et al. 2000 [58]	Cotton and polyester broadcloth and used cotton canvas	Vertical plate sweating skin model	Effect of fibre type, air layer thickness, and garment openness on heat and moisture transport.	Fibre type with desirable comfort effects differs according to sweating time.
Prasad et al. 2002 [59]	Aramid fabric	Radiant heat and Numerical model for moisture transfer	Transient heat and moisture transfer in dry and wet thermal liners under radiant heat flux.	Moisture in the fabric tends to evaporate when heated and some of it condenses inside.
Torvi et al. 2006 [60]	Kevlar, Kevlar/PBI blend Weave type: twill	10 kWm ⁻² and 80 kWm ⁻² Numerical model	A heat transfer model to accurately predict fabric and test sensor temperatures.	1) Developed a heat transfer model to predict inherently flame-resistant fabric temperatures and skin burn injuries during this cooling phase. 2) Effects of various thermal conditions on predicted fabric temperatures and times to produce second- and third-degree skin burns can be predicted.
Barker et al. 2006 [61]	Permeable Kevlar/PBI Impermeable Kevlar/PBI	6.3 kWm ⁻² Radiant and theoretical analysis for heat transfer	Effects of moisture level on predicted second-degree burn injury.	1) Moisture impacts TPP negatively up to a critical value of ~15%. 2) TPP increases beyond this critical point. 3) TPP is a complex function of thermal exposure, added moisture in fire-protective clothing system, and the permeability and insulation of the system.
Song et al. 2008 [23]	Kevlar/PBI, Basofil/aramid, Nomex etc.	Flash fire and Numerical model	A numerical model of coupled heat and moisture transport in protective clothing.	1) Predicted values compared with experimental results. 2) The model can predict the thermal response of a protective fabric and effect of some properties of fabrics and air gap on performance.
Zhu et al. 2009 [62]	FR cotton, Metamax Weave type: twill, sateen	21 kWm ⁻² exposure time – 30 s or 40 s Numerical model	Heat transfer modelling for heat-resistant fabrics and pyrolysis effect under an external heat flux included.	1) A numerical model of heat transfer within heat-resistant fabric layer developed. 2) The model appears to have universal application in scientific and engineering fields involving heat transfer in porous media.
Sawcyn & Torvi 2009 [63]	Aramid and para aramid/PBI blend	80 kWm ⁻² ± 2 kWm ⁻² Improved model based on bench top test results	Heat transfer in air spaces between test specimens and sensors in bench top tests.	1) Fabric cover factor and pore size play crucial role in heat transmission through fabrics. 2) Temperature increases in the test sensor due to convection and radiation heat transfer.
Torvi et al. 2010 [64]		Numerical model based on CFD	Heat transfer inside the air gap of bench top test apparatus. Convective and radiative heat fluxes for air gap. Impact of varying moisture contents in the outer shell on thermal protective performance across various layers of fire-protective clothing.	1) Radiation heat transfer calculations done using FVM. 2) Simulation results of temperature rise agreed well for narrow air gaps.

Song et al. 2011 [65]	Meta aramid and its blends, wool Weave type: plain, twill	6.3–8.3 kWm ⁻² Radiant and traditional TPP/RPP approach (NFPA 1971) with stored energy approach to predict second-degree skin burn	Effect of thickness on predicted skin burn time under different exposure level.	1) A three-layer fire-protective clothing system is essential to protect the wearer from skin burn injury even for low intensity heat flux. 2) Estimated protection times vary between 1 to 5 minutes. 3) Stored energy may cause skin damage after exposure.
Das et al. 2011 [66]		Numerical model	Heat transfer through porous media and thermal resistance.	Strong correlations between the predicted and experimental values of thermal resistance.
Song et al. 2014 [67]		Numerical model	Air permeability, vapour permeation, mass transfer during exposures to hot liquids and steams.	An impermeable fabric or garment provides better performance against hot liquid splashes and pressurised steams.
Onofrei et al. 2015 [18]	Aramid and its blends	5 kWm ⁻² and 10 kWm ⁻² Numerical model based on FEM	Time-temperature profile at the inner face of fire-protective clothing system during exposure to a low radiant heat flux and cooling phase.	1) Prediction range of model extended to predict the first- and second-degree burns. 2) Even for a low-level thermal radiant heat flux, a typical three-layer fire-protective clothing system is required to protect the wearer from skin burn injury.
Fu et al. 2015 [68]		Numerical model	A model of heat and moisture transfer through multilayer fire-protective clothing with air gaps exposed to low level radiation.	A linear correlation between the amount of moisture and the exposed time when moisture is located in the inner layers.
Kakvan et al. 2015 [69]	Kermel (100%) Cotton/nylon (50:50) Blends of 50% cotton/nylon with Kermel	Regression analysis	Thermal comfort: thermal resistance and thermal conductivity, water vapour resistance, air permeability and fabric porosity.	Porosity, air permeability and thermal resistance of fabrics increase with Kermel fibre blend ratio.
Udayraj et al. 2016 [8]	Meta aramid/para aramid (85/15) blended yarns Weave type: Plain, twill, and sateen	40 kWm ⁻² and 84 kWm ⁻² Radiant heat and flame and regression analysis	TPP, Areal density, STR, density, porosity, structural parameters, second-degree burn time.	1) Air permeability was higher for sateen woven fabrics. 2) STR through fabrics depended on porosity, weave, and fabric thickness. 3) New parameter introduced to judge TPP.
Udayraj et al. 2016 [70]	PBI/Kevlar, PBI/Nomex Weave type: plain, 2/1 twill, and sateen	40 kWm ⁻² and 80 kW/m ² Radiant heat and flame exposure, mathematical model	Prediction of TPP and air permeability, validation by experimental data. Spectral transmission of radiation.	As fabric weight increased, TPP also increased, and air permeability decreased for each type of woven structures.
Li et al. 2017 [71]	Cotton Weave type: twill	ALD technology and energy dispersive X-ray spectroscopy	Effect of TiO ₂ nanoparticles deposition on infrared insulation of fabric.	1) Excellent improvement in infrared resistance of TiO ₂ deposited fabrics. 2) Thickness of the fabric increased with the number of ALD cycles.
Zhang et al. 2018 [72]	Nomex IIIA fabric for outer shell and FR viscose blended Kevlar fabric for thermal liner	15.4 kWm ⁻² Radiant heat and regression analysis of stored energy	TPP of outer shell and thermal liner, both in wet condition.	1) Outer shell moisture has a positive and thicker thermal liner has negative effect on fabric TPP. 2) Moisture played a crucial role in heat transfer and TPP in wet conditions for single-layer, two-layer and three-layer systems.
R. Rathour et al. 2022 [11]	Meta aramid Weave type: plain, twill, sateen, honeycomb	80 kWm ⁻² ± 2 kWm ⁻² ANOVA with multiple second-degree polynomial regression analysis	Thermal protective performance rating, thermal resistance and water vapour transmission rate.	1) For same pick density, honeycomb fabrics provided better thermal protective performance and thermal resistance than plain, twill and sateen woven fabrics. 2) Water vapour transmission rate of sateen woven structure is higher.

storage efficiency did not increase energy discharge to the skin simulator, suggesting that moisture in the fabric greatly diminished energy discharge efficiency and that the fabric produced a cooling effect [56]. Important findings related to the protective performance of single- and multilayer fire-protective

clothing are shown in Table 1. Two categories of models that were developed, i.e. one that includes only heat transfer, and the other that incorporates heat and moisture transfer in combination, are summarised in Table 2. In general, models can be descriptive, predictive and numerical.

Table 2: Important models related to protective performance of single- and multilayer clothing

Reference	Model	Notations
Day et al. 1986 [57]	Linear regression analysis, $y = mx + c$	(i) y is parameters (pain time, burn time, pain alarm time), m is slope, x is physical properties (thickness, weight), c is intercept.
Yoo et al. 2000 [58]	$K_d = C/(\alpha_p \times \Delta P_{max} \times t_{max})$ Efficiency of openness (%) = $B/A \times 100$	(ii) K_d is buffering index, C is constant (10,000 mbar ²), (iii) α_p is increase of water vapour pressure, ΔP_{max} is maximum vapour pressure difference, t_{max} is time lapsed to reach maximum vapour pressure, A is area occupied by water-time curve of water and heat impermeable material, B is area occupied by water vapour-time curve of sample.
Prasad et al. 2002 [59]	Radiant heat and numerical model for moisture transfer, $\frac{\partial H}{\partial t} = D \frac{\partial^2 H}{\partial x^2} + S$	(iv) H is moisture content, D is diffusion constant, S is moisture condensation.
Torvi et al. 2006 [60]	$NuL = \frac{h_0 L}{k} = 0.27(GrPr)^{0.25}$	(v) Nu , Gr and Pr are Nusselt, Grashof number, and Prandtl numbers, respectively; h_0 is convective heat transfer coefficient, L is ratio of plate surface area to its perimeter.
Barker et al. 2006 [61]	$\Omega = \int_0^t P \times e^{-\frac{\Delta E}{RT}} dt$	(vi) Ω is Henricque's burn integral, P is human skin system constant, T is basal layer temperature for first- and second-degree burns, t is time, R is ideal gas constant (8.31 Jmol ⁻¹ °C ⁻¹), ΔE is activation energy of human skin (J/mol).
Song et al. 2008 [23]	$\rho c_p \frac{\delta T}{\delta t} + (\Delta h_1 + \Delta h_{vap}) \dot{m}_{sv} = \frac{\partial}{\partial x} (k_{eff} \frac{\delta T}{\delta x}) + \gamma q''_{rad} e^{-\gamma x}$	(vii) ρ is effective density of fabric, c_p is effective specific heat of fabric, T is temperature, t is time, Δh_1 is enthalpy of transition per unit mass, Δh_{vap} is enthalpy of evaporation per unit mass, \dot{m}_{sv} is mass flux of vapour out of fibre, x is linear vertical co-ordinate, k_{eff} is effective thermal conductivity of fabric, γ is extinction coefficient of fabric, q''_{rad} is incident radiation heat flux from flame onto fabric.
Zhu et al. 2009 [32]	$k = k^0 + k(T - T_0)$ $C_p = C_p^0 + C_p^*(T - T_0)$	(viii) k is fabric thermal conductivity, k^0 is thermal conductivity at constant temperature, C_p is specific heat capacity, C_p^0 is thermal capacity at constant temperature.
Sawcyn & Torvi 2009 [63]	$K_{eff} = \left[\frac{\sigma(T_{fab}^2 + T_{sens}^2)(T_{fab} + T_{sens})}{\frac{A_{sens}}{A_{fab}} \left(\frac{1 - \epsilon_{fab}}{\epsilon_{fab}} + \frac{1}{F_{fab-sens}} \right) + \frac{1 - \epsilon_{sens}}{\epsilon_{sens}}} + h_{gap} \right] \delta$	(x) K_{eff} is effective thermal conductivity (W/mK), δ is total width of air gap (m), T_{fab} is temperature of unexposed surface of fabric (K), T_{sens} is temperature of test sensor (K), A_{fab} is surface area of heated portion of fabric (m ²), A_{sens} is surface area of test sensor (m ²), ϵ_{fab} is emissivity of fabric (0.9) or shimstock (0.95), ϵ_{sens} is emissivity of test sensor (0.95), $F_{fab-sens}$ is view factor between heated portion of fabric (square) and circular test sensor.

<p>Torvi et al. 2010 [64]</p>	<p>Continuity: $\frac{\partial \rho}{\partial x} + \frac{\delta(\rho v_j)}{\delta x_j} = 0$ (xi)</p> <p>Momentum: $\frac{\partial \rho_i}{\partial t} + \frac{\delta}{\delta x_j} (\rho v_j v_i - \mu \frac{\delta v_j v_i}{\delta x_j}) = -\frac{\delta P}{\delta x_i} + \rho \beta g_i (T - T_m) + \frac{\delta}{\delta x_j} (\mu \frac{\delta v_j}{\delta x_j})$ (xii)</p> <p>Energy: $\frac{\delta(\rho c_p T)}{\delta x_i} + \frac{\delta}{\delta x_j} (\rho v_j c_p T - k \frac{\delta T}{\delta x_j}) + S_R = 0$ (xiii)</p>	<p>v is velocity factor, P is pressure, T is temperature, ρ is density, μ is viscosity, k is thermal conductivity, c_p is specific heat, β is expansion coefficient, S_R is radiation source per sink.</p>
<p>Song et al. 2011 [65] flame</p>	<p>$(\rho c_p)_s \frac{\partial T}{\partial t} = K_s \frac{\partial^2 T}{\partial x^2} + (\rho c_p)_b \omega_b (T_a - T)$ (xiv)</p>	<p>$(\rho c_p)_s$ is volumetric heat capacity of human tissue, K_s is thermal conductivity of human tissue, $(\rho c_p)_b$ is volumetric heat capacity of blood, ω_b is rate of blood perfusion, T_a is temperature of blood.</p>
<p>Das et al. 2011 [66]</p>	<p>$\frac{\partial T}{\partial t} = \frac{\partial (k \frac{\partial T}{\partial x})}{\partial x}$ (xv)</p>	<p>T is temperature, k is thermal conductivity.</p>
<p>Song et al. 2014 [67]</p>	<p>$\frac{\partial T}{\partial t} = k \frac{\partial^2 T}{\partial x^2} + \beta P$ (xvi)</p>	<p>P is vapour pressure, T is temperature, k is thermal conductivity.</p>
<p>Onofrei et al. 2015 [18]</p>	<p>$\Omega = \int_0^t P e^{-\frac{\Delta E}{\Delta T}} dt$ (xvii)</p> <p>$\rho c_p \frac{\partial T}{\partial t} + \frac{\partial}{\partial x} (-k \frac{\partial T}{\partial x}) = \rho_b c_b \omega_b (T_b - T) + Q_{met}$ (xviii)</p>	<p>Ω is Henrique's burn integral, P is human skin system constant, T is basal layer temperature for first- and second-degree burns, t is time, R is ideal gas constant ($8.31 \text{ Jmol}^{-1}\text{C}^{-1}$), ΔE is activation energy of human skin (J/mol), ρ is density (kg/m^3), c_p is heat capacity (J/kgK), k is thermal conductivity (W/mK), ρ_b is blood density (kg/m^3), c_b is blood specific heat (J/kgK), ω_b is blood profusion rate ($\text{m}^3/\text{s/m}^3$), T_b is arterial blood temperature, T is tissue temperature (K), Q_{met} is metabolic heat source (W/m^3).</p>
<p>Fu et al. 2015 [68]</p>	<p>$\frac{\partial H}{\partial t} = D \frac{\partial^2 H}{\partial x^2} + \gamma T$ (xix)</p>	<p>T is temperature, H is moisture content, D is diffusion constant, γ is reflectivity.</p>
<p>Kakvan et al. 2015 [11, 69]</p>	<p>$Y = \beta_0 + \beta_1 X_1 + \beta_2 X_2 + \dots + \beta_n X_n$ (xx)</p>	<p>Y is independent variable, X is dependent variable and β is constant.</p>
<p>Li et al. 2017 [71]</p>	<p>$W_p = \frac{P_0 - P}{P_0} \times 100\%$ (xxi)</p> <p>$W_T = \frac{T_1 - T}{T_1 - T_0} \times 100\%$ (xxii)</p>	<p>W_p is infrared power insulation rate, P_0 is power reading in absence of any fabric, P is power reading of cotton fabric, W_i is infrared thermal insulation rate, T_i is temperature reading in absence of fabric, T_0 is equal to room temperature, T is temperature reading obtained with cotton fabric.</p>
<p>Zhang et al. 2018 [72]</p>	<p>$\Omega = \int_0^t P e^{-\frac{\Delta E}{\Delta T}} dt$ (xxiii)</p> <p>$q^*(t) = \sqrt{\frac{K_p C_p}{\pi}} \left[\frac{1}{2} \int_0^t \frac{T_s(t) - T_i}{t^{1/2}} \right]$ (xxiv)</p>	<p>Ω is Henrique's burn integral, P is human skin system constant, T is basal layer temperature for first- and second-degree burns, t is time, R is ideal gas constant ($8.31 \text{ Jmol}^{-1}\text{C}^{-1}$), ΔE is activation energy of human skin (J/mol), ρ is density (kg/m^3), k is thermal conductivity ($\text{Wm}^{-1}\text{C}^{-1}$), C_p is specific heat of inorganic material of skin simulant sensor ($\text{Jkg}^{-1}\text{C}^{-1}$); T_i is initial uniform surface temperature ($^{\circ}\text{C}$), $T_s(t)$ is surface temperature ($^{\circ}\text{C}$) at time t (s), $q''(t)$ is heat flux (W/m^2) at time t</p>

3 Discussion

Firefighting is an extreme, arduous and dangerous activity that exposes the person involved to a wide range of exceedingly stressful circumstances requiring exposure to high amounts of heat, fire, toxic materials and gases. Generally, firefighters have to work in conditions where there is less oxygen present. Hence, under these conditions, firefighters can come in contact with high heat exposures multiple times in different time duration. Apart from the danger of extreme heat or toxic chemicals, there are also problems related to heat stress and exertion, biological hazards and long-term problems firefighters experience. Human skin statistics reveal that human skin is very prone to heat flux and high temperature events. A minimum heat intensity of 25.5 kJ/m^2 results in a sense of discomfort, and a maximum heat of 49.23 kJ/m^2 allows the exposed tissues to flame in a second. In terms of temperature, pain sensation at 46°C and 70°C is experienced, then the skin burns to the max. With the evolution of functional textiles, fire-protective clothing became one of the most discussed and researched topics. Operators (firefighters), while working at the site, are exposed to extreme heat environments. This extreme heat causes multiple adverse situations where one feels skin burn, experiencing uncomfortable skin-body temperature. It becomes essential to provide these workers with protective clothing which can help them overcome such conditions and work with full possible efficiency. In the last few years, the fire-protective clothing sector has evolved significantly, with researchers from different regions altering various parameters, fabrics and processes involved in making this type of clothing. During firefighting, a person is exposed to different types of extremely challenging conditions, e.g. high heat flux exposure, hazardous radiation and toxic chemical gases. Experiments showed that the factors affecting the safety of a firefighter are char forma-

tion, shrinkage, melting and dripping of protective clothing etc., while the primary factors which affect the performance and safety offered by a particular clothing assembly are areal density, ignition resistance, thermal inertia, thickness, moisture presence, neatness of reflective surfaces and flammability. It has been observed that a mixture of radiant heat and flame causes less damage to the fabric and provides more protection than exposure to flame or radiant heat alone. Heavily composed woven, knitted or nonwoven fabric clothing shows higher conduction of heat transfer, whereas heat transfer in intense exposure is determined by the air permeability and air volume fraction.

Thermal protective performance (TPP) of fabrics alters with the change in the material of the fabric, fabric structural parameters, e.g. fabric thickness and porosity, air gap width, exposure intensity and heat exposure type, i.e. flame, radiant and combined convective/radiant exposures. Some studies show that protective functionality increases with the increase in layering and thickness of the clothing, while more layering and thickness can without a doubt provide better thermal protection. At the same time, we cannot sideline the importance of comfort in this type of clothing as it plays a vital role in individual's work performance at site. We have looked into the effects of different fabric types and different types of layering arrangement. The fabric thickness also affects the fire protection as if we keep the thickness high then the stored energy in the clothing will also be high and this will damage the skin after coming out of the hazardous place. Moreover, the thickness of the fabric will affect the evaporation of the human skin which is directly related to comfort. To tackle this problem, different layers of different types of fabrics were used in this project. It was found that there was less second-degree burn time (less than 1 minute) in our knit structures. The reason behind this was the porosity or the permeability of the knit structure which is substantially higher compared to woven structures. Similarly, the radiant heat transfer also increases and the sensor senses high heat transmis-

sion compared to woven structures. However, these knit structures also have higher vapour transmission than woven structures, which can be very useful in increasing the comfort level of the fire-protective clothing. The burn time of knit structures is very low compared to woven structures (the data for which we got from the Internet). Typically, the burn time of woven structures made of Nomex and/or Kevlar is between 2–3 minutes, while here, the burn time of knitted structures was less than 1 minute (between 10 to 50 seconds). Therefore, it is not advisable to use a higher percentage of the knitted structure in the fire-protective clothing; nevertheless, we can use them on different parts of the body, e.g. where there is more need for stretch ability, i.e. in the areas of higher movement like on elbows, knees etc.

4 Conclusion

Heat and moisture transfer through the clothing under exposure to different levels of heat flux and flashfire conditions, with special attention to the role of air gaps entrapped within and between different layers of firefighting ensembles on protection times was critically discussed. During decades of research in the area of fire-protective clothing, it has been demonstrated that most burn injuries sustained by firefighters occurred in low level thermal environments. Water penetration test results were not validated by the leakage evaluation tests. Different radiation exposures reduced the tensile strength of three typical fabrics. A different numerical model was developed to quantify the heat and moisture transfer within fire-protective clothing. In conclusion, the synthesis of research on the heat and moisture transfer models in fire-protective clothing underscores the critical importance of advancing our understanding and capabilities in this domain. The reviewed literature collectively demonstrates the complexity of heat and moisture dynamics within protective garments and the necessity of robust modelling frameworks to optimise both safety

and comfort for firefighters. Moreover, integrating multi-scale modelling approaches and accounting for physiological factors and real-world operational conditions will be paramount in enhancing the efficacy of protective clothing designs.

References

1. GUIDOTTI, Tee L., CLOUGH, Veronica M. Occupational health concerns of firefighting. *Annual Review of Public Health*, 1992, **13**(1), 151–171, doi: 10.1146/annurev.pu.13.050192.001055.
2. CHAKRABORTY, Supriyo, KOTHARI V.K. Prediction of radiative protective performance of multilayered clothing. *Indian Journal of Fibre and Textile Research*, 2016, **41**(3), 284–292.
3. SONG, Guowen, LU, Yehu. Flame resistant textiles for structural and proximity fire fighting. In *Handbook of Fire Resistant Textiles*. Edited by F. Selcen Kilinc. Woodhead Publishing, 2013, 520–548, doi: 10.1533/9780857098931.4.520.
4. SHAKERIASKI, Farshad, GHODRAT, Maryam, NELSON, David James. Experimental and numerical studies on efficiency characterization of firefighters' protective clothing: a review. *Journal of the Textile Institute*, 2021, **113**(11), 2549–2568, doi: 10.1080/00405000.2021.1994739.
5. BARR, David, GREGSON, Warren, REILLY, Thomas. The thermal ergonomics of firefighting reviewed. *Applied Ergonomics*, 2010, **41**(1), 161–172, doi: 10.1016/j.apergo.2009.07.001.
6. KAMALHA, Edwin, ZENG, Yongchun, MWASIAGI, Josphat, I., KYATUHEIRE, Salome. The comfort dimension; a review of perception in clothing. *Journal of Sensory Studies*, 2013, **28**(6), 423–444, doi: 10.1111/joss.12070.
7. NAYAK, Rajkishore, HOUSHYAR, Shadi, PADHYE, Rajiv. Recent trends and future scope in the protection and comfort of fire-fighters' personal protective clothing. *Fire Science Reviews*, 2014, **3**(1), 1–19, doi: 10.1186/s40038-014-0004-0.
8. UDAYRAJ, TALUKDAR, Prabal, DAS, Apurba,

- ALAGIRUSAMY, Ramasamy. Heat and mass transfer through thermal protective clothing - a review. *International Journal of Thermal Sciences*, 2016, **106**, 32–56, doi: 10.1016/j.ijthermalsci.2016.03.006.
9. HOSSAIN, M. M., DATTA, E., RAHMAN, S. A review on different factors of woven fabrics' strength prediction. *Science Research*, 2016, **4**(3), 88–97, doi: 10.11648/j.sr.20160403.13.
 10. NAEEM, J., MAZARI, A.A., HAVELKA, A. Review: radiation heat transfer through fire fighter protective clothing. *Fibres and Textiles in Eastern Europe*, 2017, **25**(4), 65–74, doi: 10.5604/01.3001.0010.2665.
 11. RATHOUR, Rochak, DAS, Apurba, ALAGIRUSAMY, Ramasamy. Study on the influence of constructional parameters on performance of outer layer of thermal protective clothing. *Journal of the Textile Institute*, 2023, **114**(9), 1336–1346, doi: 10.1080/00405000.2022.2124650.
 12. RATHOUR, Rochak, RAJPUT, Bhavna, DAS, Apurba, ALAGIRUSAMY, Ramasamy. Performance analysis of shell fabric of fire protective clothing for different process parameters. *The Journal of The Textile Institute*, 2023, **114**(11), 1692–1691, doi: 10.1080/00405000.2022.2145441.
 13. CHAKRABORTY, Supriyo, KOTHARI, V. Effect of moisture and water on thermal protective performance of multilayered fabric assemblies for firefighters. *Indian Journal of Fibre & Textile Research (IJFTR)*, 2017, **42**(1), 94–99.
 14. HOLMES, D.A., HORROCKS, A.R. Technical textiles for survival. In *Handbook of Technical Textiles*. Edited by A. Richard Horrocks and Subhash C. Anand. Elsevier, 2016, **287–323**, 287–323, doi: 10.1016/b978-1-78242-465-9.00010-0.
 15. ROSSI, R. Clothing for protection against heat and flames. In *Protective Clothing*. Edited by Faming Wang and Chuansi Gao. Elsevier, 2014, 70–89, doi: 10.1533/9781782420408.1.70.
 16. SHALEV, Itzhak, BARKER, Roger L. Analysis of heat transfer characteristics of fabrics in an open flame exposure. *Textile Research Journal*, 1983, **53**(8), 475–482, doi: 10.1177/004051758305300806.
 17. MOREL, Aude, BEDEK, Gauthier, SALAÜN, Fabien, DUPONT, Daniel. A review of heat transfer phenomena and the impact of moisture on firefighters' clothing and protection. *Ergonomics*, 2014, **57**(7), 1078–1089, doi: 10.1080/00140139.2014.907447.
 18. ONOFREI, Elena, PETRUSIC, Stojanka, BEDEK, Gauthier, DUPONT, Daniel, SOULAT, Damien, CODAU, Teodor Cezar. Study of heat transfer through multilayer protective clothing at low-level thermal radiation. *Journal of Industrial Textiles*, 2015, **45**(2), 222–238, doi: 10.1177/1528083714529805.
 19. MÄKINEN, H. Firefighters' protective clothing. In *Advances in Fire Retardant Materials*. Edited by A.R. Horrocks and D. Price. Elsevier, 2008, 467–491, doi: 10.1533/9781845694701.3.467.
 20. TORVI, David A., DALE, Douglas J. Heat transfer in thin fibrous materials under high heat flux. *Fire Technology*, 1999, **35**(3), 210–231, doi: 10.1023/A:1015484426361.
 21. MELL, William E., LAWSON J. Randall. A heat transfer model for firefighters' protective clothing. *Fire Technology*, 2000, **36**(1), 39–68, doi: 10.1023/A:1015429820426.
 22. ISMAIL, M. I., A. S.A. AMMAR a M. EL-OKEILY. Heat transfer through textile fabrics: mathematical model. *Mathematical and Computer Modelling*, 1989, **12**(9), 1187, doi: 10.1016/0895-7177(89)90268-9.
 23. SONG, Guowen, DING, Dan, CHITRPHIROMSRI, Patisop. Numerical simulations of heat and moisture transport in thermal protective clothing under flash fire conditions. *International Journal of Occupational Safety and Ergonomics*, 2008, **14**(1), 89–106, doi: 10.1080/10803548.2008.11076752.
 24. PHELPS, Hannah, SIDHU, Harvinder. A mathematical model for heat transfer in fire fighting suits containing phase change materials. *Fire Safety Journal*, 2015, **74**, 43–47, doi: 10.1016/j.

- firesaf.2015.04.007.
25. SU, Yun, HE, Jiazhen, LI, Jun. An improved model to analyze radiative heat transfer in flame-resistant fabrics exposed to low-level radiation. *Textile Research Journal*, 2017, **87**(16), 1953–1967, doi: 10.1177/0040517516660892.
 26. GHAZY, Ahmed. The thermal protective performance of firefighters' clothing: the air gap between the clothing and the body. *Heat Transfer Engineering*, 2017, **38**(10), 975–986, doi: 10.1080/01457632.2016.1212583.
 27. TORVI, D.A., DALE J.D. A finite element model of skin subjected to a flash fire. *Journal of Biomechanical Engineering*, 1994, **116**(3), 250–255, doi: 10.1115/1.2895727.
 28. SONG, Guowen, BARKER, Roger L., HAMOUDA, Hechmi, KUZNETSOV, Andrey V., CHITRPHIROMSRI, Patirop, GRIMES, Robert V. Modeling the thermal protective performance of heat resistant garments in flash fire exposures. *Textile Research Journal*, 2004, **74**(12), 1033–1040, doi: 10.1177/004051750407401201.
 29. GHAZY, Ahmed, BERGSTROM, Donald J. Influence of the air gap between protective clothing and skin on clothing performance during flash fire exposure. *Heat and Mass Transfer/Waerme- und Stoffuebertragung*, 2011, **47**(10), 1275–1288, doi: 10.1007/s00231-011-0791-y.
 30. GHAZY, Ahmed, BERGSTROM, Donald J. Numerical simulation of heat transfer in firefighters' protective clothing with multiple air gaps during flash fire exposure. *Numerical Heat Transfer, Part A: Applications*, 2012, **61**(8), 569–593, doi: 10.1080/10407782.2012.666932.
 31. ROSSI, Renxé M., BOLLI, Walter, STÄMPFLI, Rolf. Performance of firefighters' protective clothing after heat exposure. *International Journal of Occupational Safety and Ergonomics*, 2008, **14**(1), 55–60, doi: 10.1080/10803548.2008.11076747.
 32. ZHU, Fang-Long, ZHANG, Wei-Yuan. Modeling heat transfer for heat-resistant fabrics considering pyrolysis effect under an external heat flux. *Journal of Fire Sciences*, 2009, **27**(1), 81–96, doi: 10.1177/0734904108094960.
 33. SU, Yun, LI, Jun, WANG, Yunyi. Effect of air gap thickness on thermal protection of firefighter's protective clothing against hot steam and thermal radiation. *Fibres and Polymers*, 2017, **18**(3), 582–589, doi: 10.1007/s12221-017-6714-x.
 34. KOTHARI, V. K., CHAKRABORTY, Supriyo. Thermal protective performance of clothing exposed to radiant heat. *Journal of the Textile Institute*, 2015, **106**(12), 1388–1393, doi: 10.1080/00405000.2014.995929.
 35. SU, Yun, HE, Jiazhen, LI, Jun. A model of heat transfer in firefighting protective clothing during compression after radiant heat exposure. *Journal of Industrial Textiles*, 2018, **47**(8), 2128–2152, doi: 10.1177/1528083716644289.
 36. UDAYRAJ, WANG Faming. A three-dimensional conjugate heat transfer model for thermal protective clothing. *International Journal of Thermal Sciences*, 2018, **130**, 28–46, doi: 10.1016/j.ijthermalsci.2018.04.005.
 37. HE, Hualing, YU, Zhicai, ZHANG, Chunbo, LI, Minhua. Thermal protective performance of firefighters' clothing under low-intensity radiation heat exposure. *Autex Research Journal*, 2021, **21**(3), 234–241, doi: 10.2478/aut-2020-0018.
 38. SUN, G., YOO, H.S., ZHANG, X.S., PAN, N. Radiant protective and transport properties of fabrics used by wildland firefighters. *Textile Research Journal*, 2000, **70**(7), 567–573, doi: 10.1177/004051750007000702.
 39. FU, Ming, WENG, Wenguo, YUAN, Hongyong. Effects of multiple air gaps on the thermal performance of firefighter protective clothing under low-level heat exposure. *Textile Research Journal*, 2014, **84**(9), 968–978, doi: 10.1177/0040517513512403.
 40. KEISER, Corinne, ROSSI, Rene M. Temperature analysis for the prediction of steam formation and transfer in multilayer thermal protective clothing at low level thermal radiation. *Textile Research Journal*, 2008, **78**(11), 1025–1035, doi:

- 10.1177/0040517508090484.
41. KIM, Hae-Hyoung, YOO, Seung-Joon, PARK, Pyoung-Kyu, KIM, Young-Soo, HONG, Seung-Tae. Comparison of thermal protective performance test of firefighter's protective clothing against convection and radiation heat sources. *Fire science and engineering*, 2018, **32**(2), 17–23, doi: 10.7731/kifse.2017.31.2.017.
 42. MANDAL, Sumit, SONG, Guowen, ACKERMAN, Mark, PASKALUK, Stephen, GHOLAMREZA, Farzan. Characterization of textile fabrics under various thermal exposures. *Textile Research Journal*, 2013, **83**(10), 1005–1019, doi: 10.1177/0040517512461707.
 43. SU, Yun, HE, Jiazhen, LI, Jun. Modeling the transmitted and stored energy in multilayer protective clothing under low-level radiant exposure. *Applied Thermal Engineering*, 2016, **93**, 1295–1303, doi: 10.1016/j.applthermaleng.2015.10.089.
 44. MANDAL, Sumit, ANNAHEIM, Simon, CAMENZIND, Martin, ROSSI, René M. Radiant heat-protective performance of fabrics used in firefighters' clothing: a scientific study. In *Next Generation Fibers for Smart Products : The Fiber Society 2017 Spring Conference, May 17–19, 2017*. Aachen : Institut für Textiltechnik der RWTH Aachen, 2017, 89.
 45. JIAZHEN, He, YAN, Chen, LICHUAN, Wang, JUN, Li. Quantitative assessment of the thermal stored energy in protective clothing under low-level radiant heat exposure. *Textile Research Journal*, 2018, **88**(24), 2867–2879, doi: 10.1177/0040517517732084.
 46. MANDAL, Sumit, ANNAHEIM, Simon, CAMENZIND, Martin, ROSSI, René M. Characterization and modelling of thermal protective performance of fabrics under different levels of radiant-heat exposures. *Journal of Industrial Textiles*, 2019, **48**(7), 1184–1205, doi: 10.1177/1528083718760801.
 47. LEI, Zhongxiang, QIAN, Xiaoming, ZHANG, Xianglong. Assessment of thermal protective performance of firefighter's clothing by a sweating manikin in low-level radiation. *International Journal of Clothing Science and Technology*, 2019, **31**(1), 145–154, doi: 10.1108/IJCST-04-2018-0061.
 48. LEE, Young Moo, BARKER, Roger L. Effect of moisture on the thermal protective performance of heat-resistant fabrics. *Journal of Fire Sciences*, 1986, **4**(5), 315–331, doi: 10.1177/073490418600400502.
 49. MIN, Kyunghoon, SON, Yangsoo, KIM, Chongyoun, LEE, Yejin, HONG, Kyunghi. Heat and moisture transfer from skin to environment through fabrics: a mathematical model. *International Journal of Heat and Mass Transfer*, 2007, **50**(25–26), 5292–5304, doi: 10.1016/j.ijheatmasstransfer.2007.06.016.
 50. LAWSON, Lelia K., CROWN, Elizabeth M., ACKERMAN, Mark Y., DALE, J. Douglas. Moisture effects in heat transfer through clothing systems for wildland firefighters. *International Journal of Occupational Safety and Ergonomics*, 2004, **10**(3), 227–238, doi: 10.1080/10803548.2004.11076610.
 51. ZHU, Fanglong, ZHANG, Weiyuan, CHEN, Minzhi. Investigation of material combinations for fire-fighter's protective clothing on radiant protective and heat-moisture transfer performance. *Fibres and Textiles in Eastern Europe*, 2007, **15**(1), 72–75.
 52. LU, Yehu, LI, Jun, LI, Xiaohui, SONG Guowen. The effect of air gaps in moist protective clothing on protection from heat and flame. *Journal of Fire Sciences*, 2013, **31**(2), 99–111, doi: 10.1177/0734904112457342.
 53. ATALAY, Ozgur, BAHADIR, Senem Kursun, KALAOGLU, Fatma. An analysis on the moisture and thermal protective performance of firefighter clothing based on different layer combinations and effect of washing on heat protection and vapour transfer performance. *Advances in Materials Science and Engineering*,

- 2015, **2015**, 1–8, doi: 10.1155/2015/540394.
54. HE, Jiazhen, LI, Jun. Quantitatively assessing the effect of exposure time and cooling time of fabric assemblies representative of those used in firefighter clothing on the thermal protection. *Fire and Materials*, 2016, **40**(6), 773–784, doi: 10.1002/fam.2341.
55. CHEN, Meng, ZHU, Fanglong, FENG, Qianqian, LI, Kejing, LIU, Rangtong. Experimental study on moisture transfer through firefighters' protective fabrics in radiant heat exposures. *Thermal Science*, 2017, **21**(4), 1665–1671, doi: 10.2298/TSCI160512051C.
56. SU, Yun, YANG, Jie, LI, Rui, SONG, Guowen, LI, Jun. Experimental study of moisture role and heat transfer in thermal insulation fabric against hot surface contact. *International Journal of Thermal Sciences*, 2020, **156**(1882), 1–7, doi: 10.1016/j.ijthermalsci.2020.106501.
57. DAY, M. Thermal radiative protection of fire fighters' protective clothing. *Fire Technology*, 1987, **23**(1), 49–59, doi: 10.1007/BF01038365.
58. YOO, H.S., HU, Y.S., KIM, E.A. Effects of heat and moisture transport in fabrics and garments determined with a vertical plate sweating skin model. *Textile Research Journal*, 2000, **70**(6), 542–549, doi: 10.1177/004051750007000612.
59. PRASAD, K., TWILLEY, W.H., LAWSON, J.R. *Thermal Performance of Fire Fighters' Protective Clothing: Numerical Study of Transient Heat and Water Vapor Transfer*. Gaithersburg : US Department of Commerce, Technology Administration, National Institute of Standards and Technology, 2002, 1–32.
60. TORVI, David A., THRELFALL Todd G. Heat transfer model of flame resistant fabrics during cooling after exposure to fire. *Fire Technology*, 2006, **42**(1), 27–48, doi: 10.1007/s10694-005-3733-8.
61. BARKER, R.L., GUERTH-SCHACHER, C., GRIMES, R.V., HAMOUDA, H. Effects of moisture on the thermal protective performance of firefighter protective clothing in low-level radiant heat exposures. *Textile Research Journal*, 2006, **76**(1), 27–31, doi: 10.1177/0040517506053947.
62. ZHU, Fang Long, ZHANG, Wei Yuan. Modeling heat transfer for heat-resistant fabrics considering pyrolysis effect under an external heat flux. *Journal of Fire Sciences*, 2009, **27**(1), 81–96, doi: 10.1177/0734904108094960.
63. SAWCYN, Chris M.J., TORVI, David A. Improving heat transfer models of air gaps in bench top tests of thermal protective fabrics. *Textile Research Journal*, 2009, **79**(7), 632–644, doi: 10.1177/0040517508093415.
64. TALUKDAR, Prabal, TORVI, David A., SIMONSON, Carey J., SAWCYN, Chris M.J. Coupled CFD and radiation simulation of air gaps in bench top protective fabric tests. *International Journal of Heat and Mass Transfer*, 2010, **53**(1–3), 526–539, doi: 10.1016/j.ijheat-masstransfer.2009.04.041.
65. SONG, Guowen, CAO, Wei, GHOLAMREZA, Farzan. Analyzing stored thermal energy and thermal protective performance of clothing. *Textile Research Journal*, 2011, **81**(11), 1124–1138, doi: 10.1177/0040517511398943.
66. DAS, Apurba, ALAGIRUSAMY, Ramasamy, KUMAR, Pavan. Study of heat transfer through multilayer clothing assemblies: a theoretical prediction. *Autex Research Journal*, 2011, **11**(2), 54–60, doi: 10.1515/aut-2011-110205.
67. MANDAL, S., SONG, G. An empirical analysis of thermal protective performance of fabrics used in protective clothing. *The Annals of Occupational Hygiene*, 2014, **58**(8), 1065–1077, doi: 10.1093/annhyg/meu052.
68. FU, M., YUAN, M.Q., WENG, W.G. Modeling of heat and moisture transfer within firefighter protective clothing with the moisture absorption of thermal radiation. *International Journal of Thermal Sciences*, 2015, **96**, 201–210, doi: 10.1016/j.ijthermalsci.2015.05.008.
69. KAKVAN, Ali, SHAIKHZADEH NAJAR, Saeed, PSIKUTA Agnes. Study on effect of blend ratio on thermal comfort proper-

- ties of cotton/nylon-blended fabrics with high-performance Kermel fibre. *Journal of the Textile Institute*, 2015, **106**(6), 674–682, doi: 10.1080/00405000.2014.934045.
70. KUTLU, Bengi, CIRELI, Aysun. Thermal analysis and performance properties of thermal protective clothing. *Fibres and Textiles in Eastern Europe*, 2005, **13**(3), 58–62.
71. LI, Linfeng, XU, Weilin, WU, Xi, LIU, Xin, LI, Wenbin. Fabrication and characterization of infrared-insulating cotton fabrics by ALD. *Cellulose*, 2017, **24**(9), 3981–3990, doi: 10.1007/s10570-017-1380-0.
72. ZHANG, Hui, SONG, Guowen, REN, Haitao, CAO, Juan. The effects of moisture on the thermal protective performance of firefighter protective clothing under medium intensity radiant exposure. *Textile Research Journal*, 2018, **88**(8), 847–862, doi: 10.1177/0040517517690620.

Ida Nuramdhani, Maulana Fahrizal Abdan, Robinson Manalu, Jantera Sekar Tirta, Mohamad Widodo
Department of Textile Chemistry, Politeknik STTT Bandung (Polytechnic of Textile Technology), Bandung, Indonesia

Physicochemical Analysis of Dyeing of Cotton Denim with Natural Indigo Dye from *Strobilanthes cusia* Using Green Reducing Agents and Alkalis

*Fizikalno-kemijska analiza barvanja bombažnega denima z naravnim barvilom indigo iz *Strobilanthes cusia* z uporabo zelenih reducentov in alkalij*

Original scientific article/Izvirni znanstveni članek

Received/Prispelo 6–2024 • Accepted/Sprejeto 9–2024

Corresponding author/Korespondenčni avtor:

Assoc. Prof. Dr. Mohamad Widodo

E-mail: mwidodo@stttekstil.ac.id

ORCID iD: 0000-0003-3195-4440

Abstract

Strobilanthes cusia is one of many indigo-producing plants with promising and attractive potentials as an alternative source of natural indigo dye due to its dyeability to cotton fibres with high colour strength, and due to its ease of cultivation. The aim of this research was to utilise natural indigo dye from *Strobilanthes cusia* to dye cotton denim fabric in an environmentally friendly way. The use of D-fructose and D-glucose as well as rice husk ash and lime solutions as reducing agents and alkali sources was explored in this study. The dyeing process was carried out at 30 °C for 30 minutes, followed by the oxidation process in open air for 45 minutes. Colour characteristics and fastness to washing and rubbing were evaluated. The results showed that D-fructose resulted in a higher colour strength than D-glucose, and that lime is better than rice husk ash and even sodium hydroxide in terms of colour strength. The highest colour strength was obtained from the combination of D-fructose and lime solution, with K/S and SUM(K/S) values of 16.02 (at 650 nm) and 8.5 respectively. The colour fastness to washing and rubbing was good for all dyed fabrics, with the staining scale ranging from 3/4 to 4. These results bring a new potential for natural indigo dye from *Strobilanthes cusia* beyond its current and limited use by traditional dyes to a much larger scale of denim dyeing for an eco-friendly fashion industry.

Keywords: natural indigo, *Strobilanthes cusia*, denim dyeing, reducing D-sugars, lime

Izveček

Strobilanthes cusia je ena številnih rastlin, ki proizvajajo indigo. Zaradi preprostega gojenja je obetaven in privlačen potencial alternativnega vira naravnega indiga, ki intenzivno obarva bombaž. Namen raziskave je bil proučiti uporabnost naravnega indiga iz *Strobilanthes cusia* za okolju prijazno barvanje bombažnega denima. Za barvanje so bili uporabljeni reducenta D-fruktoza in D-glukoza ter pepel riževih luščin in apno kot vira alkalij. Barvanje je potekalo 30 minut pri 30 °C, sledil je 45-minutni postopek oksidacije na zraku. Ocenjene so bile barvne lastnosti in obstojnost pri pranju in drgnjenju. Uporaba D-fruktoze je vplivala na večjo intenziteto barve kot D-glukoze, apno pa je bilo glede



Content from this work may be used under the terms of the Creative Commons Attribution CC BY 4.0 licence (<https://creativecommons.org/licenses/by/4.0/>). Authors retain ownership of the copyright for their content, but allow anyone to download, reuse, reprint, modify, distribute and/or copy the content as long as the original authors and source are cited. No permission is required from the authors or the publisher. This journal does not charge APCs or submission charges.

intenzivnosti barve boljše od pepela riževih lupin in celo boljše od natrijevega hidroksida. Najvišja intenziteta barve je bila dosežena pri kombiniranju D-fruktoze in raztopine apna, in sicer so bile vrednosti K/S in SUM(K/S) 16,02 (pri 650 nm) oziroma 8,5. Barvna obstojnost pri pranju in drgnjenju je bila dobra za vse obarvane tkanine, ocene po barvni lestvici so bile med 3/4 in 4. Rezultati so pokazali, da ima naravni indigo, ekstrahiran iz *Strobilanthes cusia*, velik potencial za barvanje denima za okolju prijazno modno industrijo, ki presega njegovo trenutno in omejeno uporabo pri tradicionalnih barvarjih.

Ključne besede: naravni indigo, *Strobilanthes cusia*, barvanje denima, reducirajoči D-sladkorji, limeta

1 Introduction

Environmental awareness and health consciousness have renewed demand for natural dyes on the global market, including natural indigo dye. The annual global production of indigo in 2010 is estimated at around 80,000 tonnes, with 95% of that production being used to produce denim [1]. Currently, natural indigo pigment represents less than one percent of the indigo dye produced and used worldwide [2]. There are almost 800 species of Indigofera plants [3, 4], but only a handful of these have a high content of indican, with the most widely exploited of all being

Indigofera tinctoria. Other major indigo-producing plants include *Isatis tinctoria*, *Polygonum tinctoria*, *Persicaria tinctoria* and *Strobilanthes flaccidifolius* (or *Strobilanthes cusia*) [3]. Figure 1 shows the different appearances of *Strobilanthes cusia* and *I. tinctoria*. Recently, there is an increasing interest in natural indigo dye from *Strobilanthes cusia* [5–12]. In Indonesia, natural indigo is very popular and demand is high, especially for artisanal products such as batik and tie-dye, in particular for products where *Strobilanthes cusia* is used [13, 14].



a)



b)

Figure 1: a) *Strobilanthes cusia* and b) *I. tinctoria* plant showing the differences in the shape and size of the leaves and flowers

Historically, Indonesia has been an important player in the international trade of indigo, which centred in particular around the species of Indigofera [3]. It is only recently that *Strobilanthes cusia* was introduced to Indonesian indigo farmers and the natural indigo dyer community particularly on the

island of Java. A new indigo plantation was launched in the highland area of Tretep, Temanggung District, Central Java, at an altitude of around 1,000–1,200 m (average temperature 23–25 °C) on the backside of Mount Prau (2,565 m) (Figure 2b). It has now expanded to a total of approximately 65 ha of land,

which is distributed over 15 villages. The plant has been successfully cultivated in a polyculture system, side by side and under preexisting local main crops

such as coffee and guava, providing a more sustainable practice of cultivation with an opportunity for the farmers to double their income.

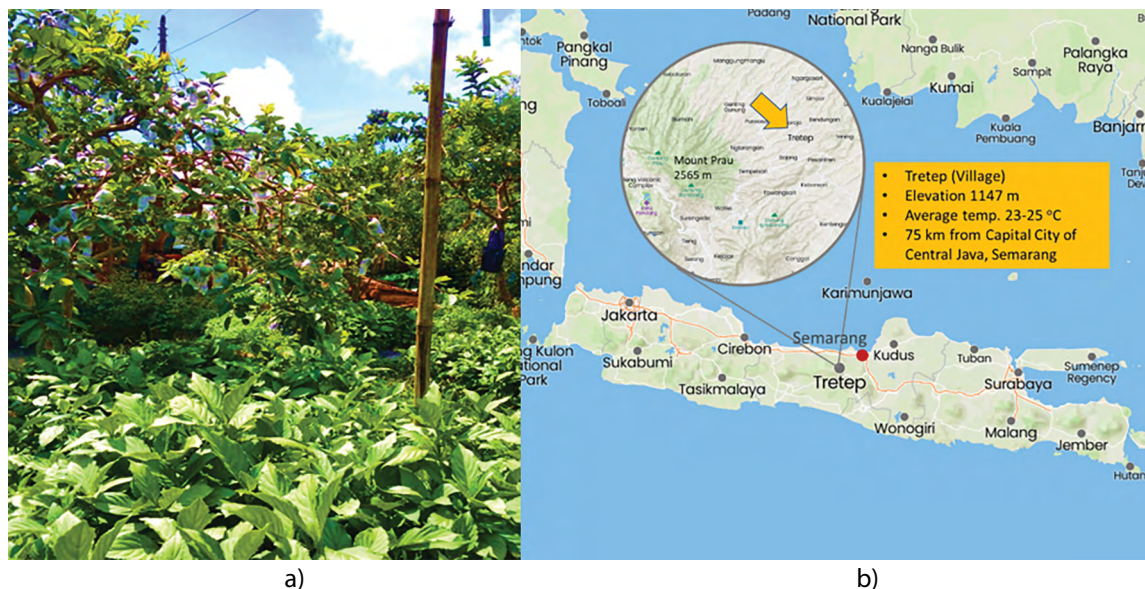


Figure 2: (a) *Strobilanthes cusia* in the field (side-by-side and under guava trees, seen in the background) and (b) the location of the plantation area in Tretep, Temanggung District, Central Java, Indonesia (<https://mapcarta.com/15592174>)

Figure 3 shows the reduction of indigo dye by a reducing agent under alkaline conditions. Dyers in the traditional community use mixed fruits in their system of traditional indigo dyeing. Fruits are a good source of sugar and contain primarily D-fructose, a monosaccharide. In light of this observation, Shin et al. [15] and Hossain et al. [16] investigated the use of different fruits and their wastes as natural reducing agents for the reduction of indigo dye. Both studies confirmed that fruits are a good source of an effective natural reducing agent, as shown by their reduction potential and the results of dyeing. Furthermore, both studies also highlighted the role of D-fructose as one of the main reducing sugars found in fruits. It was later shown by Saikhao et al. [17] in a study with synthetic indigo dye that D-fructose has indeed the highest reducing power among other monosaccharides (D-glucose, D-fructose and D-galactose) and disaccharides (lactose and maltose).

In this research, D-fructose and D-glucose were investigated as green reducing agents in the dyeing

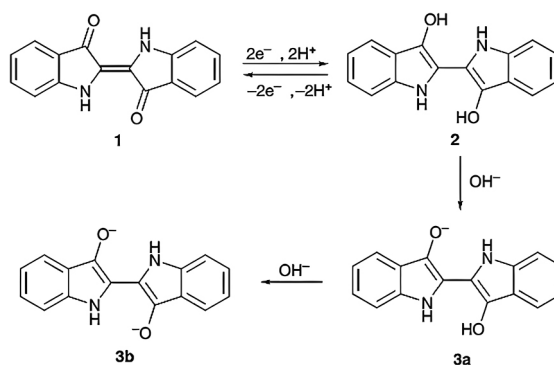


Figure 3: Reduction of indigo dye under alkaline conditions: insoluble indigo (1), indigo acid leuco (2), partly soluble monophenolate alkaline leuco indigo formed at a lower alkaline pH (3a), completely soluble biphenolate alkaline leuco indigo at a higher alkaline pH (3b) [18]

of denim using natural indigo extracted from *Strobilanthes cusia*. There has been no report on such studies in literature, particularly concerning the use of natural indigo dye from *Strobilanthes cusia* for denim dyeing. Additionally, in attempt to explore

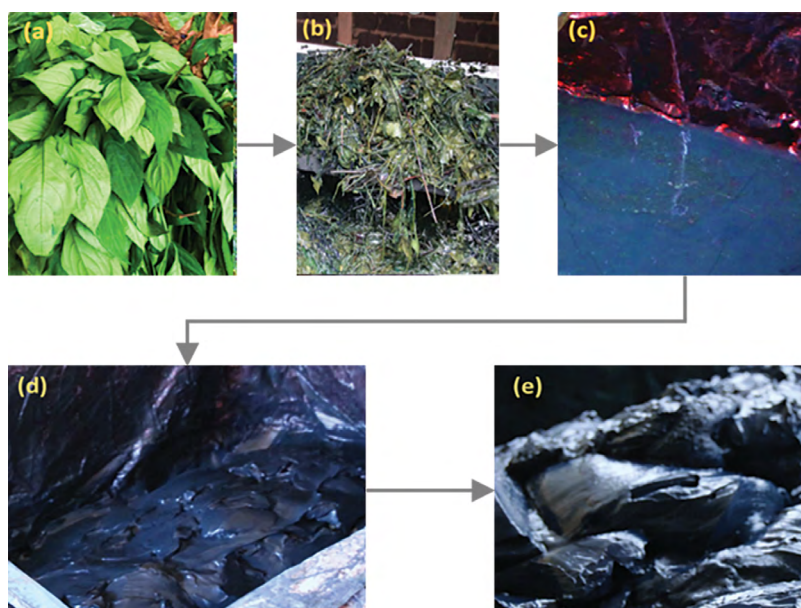


Figure 4: *Strobilanthes cusia*: a) fresh and b) extracted leaves and branches, c) remaining extract after addition of lime, d) precipitate of the oxidized leuco indigo, and e) resulting indigo paste (personal documentation: photos were taken from the field during the production of indigo paste)

the possibility of a more environmentally friendly and sustainable process of dyeing, the use of lime and rice husk ash as an alternative source of alkali was also investigated in this study.

2 Materials and methods

2.1 Materials

Fresh leaves and branches of *Strobilanthes cusia* were provided by the indigo cultivation centre in Temanggung, Central Java, Indonesia (CV Sidhobiru). Industrial grade lime (calcium hydroxide, $\text{Ca}(\text{OH})_2$) from a particular source was purchased from the local market. D-glucose and D-fructose, both of food grade, were purchased from the local market and used without any further purification or pretreatment. NaOH (flake) was purchased from PT Bratachem (Bandung, Indonesia). Denim cotton (100%) fabric, with a 2/1 twill weaving construction and RFD (ready for dyeing) quality, was obtained from PT Indah Mas Tekstil (Bandung, Indonesia). Rice husks were obtained from the local paddy field close to the indigo cultivation centre in Temanggung.

2.2 Methods

2.2.1 Preparation of natural indigo paste from *Strobilanthes cusia*

To produce 1 kg of natural indigo paste, about 10 kg of fresh leaves and branches of *Strobilanthes cusia* (Figure 4a) were prepared. Washed leaves and branches of *Strobilanthes cusia* were soaked in 20 L water (ratio of 1:2 for fresh leaves and branches and water) for 48 hours for the purpose of anaerobic fermentation. During immersion, the soaking water slowly turned from clear to greenish-yellow over the next two days, which indicated the hydrolysis of indican to indoxyl and eventually to soluble leuco indigo. After removing the plant matter (Figure 4b) from the soaking water, a certain dose of strong alkali (slaked lime $\text{Ca}(\text{OH})_2$, pH 10-11) was added to the vat (Figure 4c). Normally, 1% of lime would be required for 1 kg of plant material. Thus, in this experiment, 10 g of lime was added for every 1 kg of plant material. The addition of lime, in addition to helping the hydrolysis of indican and accelerating the formation of indoxyl, is also intended to help the precipitation of the resulting indigo dye particles. Churning the vat then oxidized the leuco

indigo, leading to the formation of a blue complex with the lime that precipitated to the bottom of the vat over the course of another day (Figure 4d). Decanting the liquid from the vat and straining the precipitate resulted in a blue paste of indigo dye (Figure 4e). The amount of indigo paste obtained from this procedure was 1 kg.

2.2.2 Dyeing process for denim using natural indigo paste from *Strobilanthes cusia*

The resulting natural indigo paste obtained as described in section 2.2.1 was collected and used for the dyeing of denim cotton. The dyeing experiments were carried out in the Laboratory of Dyeing Technology at the Department of Textile Chemistry, Politeknik STTT Bandung, Indonesia.

During the preliminary study, several reducing sugars were explored, i.e. palm sugar, D-glucose, and D-fructose as alternative reducing agents, as well as sodium dithionite for comparison. Different sources of alkali were also explored, such as solutions of natural lime and husk ash, as well as sodium hydroxide for comparison. The preliminary study was carried out to standardize the recipe, which was optimized from the recipe commonly used by SME's in the field. The amount of substances used was optimized during the preliminary study. Based on those results, the dyeing recipe and variations thereof for this research were determined as shown in Table 1 (note that palm sugar was removed from the recipe due to unsatisfactory results).

Table 1: Recipes of indigo dyeing using different reducing sugars and alkali

Substance	Concentration in the dyeing bath (g/L)					
	R-1	R-2	R-3	R-4	R-5	R-6
Dye paste of <i>Strobilanthes cusia</i>	50	50	50	50	50	50
Fructose	12.5	12.5	12.5	0	0	0
Glucose	0	0	0	12.5	12.5	12.5
Lime (pH 12)	40	0	0	40	0	0
Husk ash (pH 12)	0	40	0	0	40	0
NaOH flake (pH 12)	0	0	2.5	0	0	2.5

All dyeing processes were carried out at room temperature for 30 minutes, followed by a 45-minute ox-

idation process by airing in the ambient atmosphere, using the dyeing scheme presented in Figure 5.

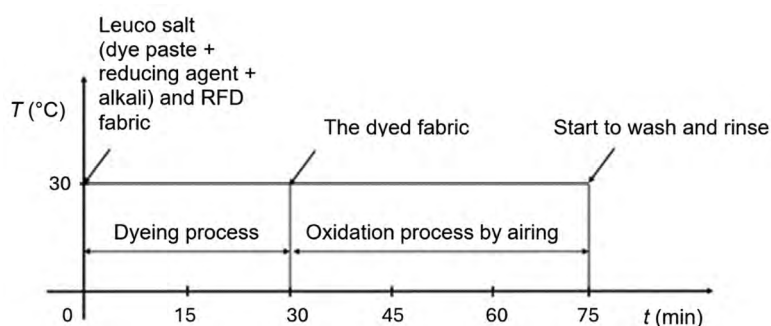


Figure 5: Dyeing scheme of denim cotton with *Strobilanthes cusia* indigo dye

To prepare the dyeing bath, alkaline solution was first prepared by mixing either lime, husk ash or NaOH flake to obtain a pH of 12. The indigo dye paste of *Strobilanthes cusia* and the reducing sugar

were added to the alkaline solution that had been prepared according to the recipe. The mixture was constantly stirred until leuco was formed through the reduction of the indigo pigment. When the

colour of the solution changed from indigo blue to yellowish green, the fabric was immersed and kept in the newly-formed leuco indigo solution for 30 minutes for dyeing to take place. At the end of the dyeing process, the fabric was removed from the solution and then aired for 45 minutes by hanging. Oxidation took place when the fabric was in contact with the oxygen in the air, and changed its colour from yellowish green to the characteristic indigo blue. All resulting dyed fabrics were then washed and rinsed in water at room temperature before being dried. To ensure reproducibility, all dyeing processes were repeated twice for each recipe.

2.3 Evaluation of dyed fabrics

2.3.1 Colour evaluation

The colour strength of each dyed fabric was measured using a Minolta CM-3600d visible light spectrophotometer, under a light source of D65 in a 10° observer position. Black and white calibrations were taken before each measurement. Every sample was measured in three different areas to cover any possible variations across the sample. The results of the measurement were expressed as a K/S value, which is calculated using the Kubelka-Munk equation (eq. 1) and corresponds to the amount of dyes being fixed on the substrate.

$$K/S = \frac{(1 - R)^2}{2R} \quad (1)$$

The colour strength of the dyeing over the whole visible spectrum (SUM) was determined according to the method described by Blackburn and Harvey [19]. The K/S values obtained from eq. 1 were summed and the resultant single value was then normalized by dividing it by the number of intervals/data summed (eq. 2)

$$SUM K/S = \frac{\sum_{i=1}^n (K/S)_i}{n} \quad (2)$$

2.3.2 Measurements of pH and redox potentials

To check the pH of the alkali solution and the redox potential of each reducing agent used in this research,

measurements were taken using a pH-meter (Beeco BT 600, Germany), with a platinum electrode used to measure the oxidation-reduction potential, and Ag/AgCl as a reference electrode. The redox potential measurements were taken from each leuco salt produced before and after dyeing process.

2.3.3 Colour fastness to washing and rubbing

The tests of colour fastness to washing and rubbing were carried out according to the standard method prescribed by ISO 105 C06 and ISO 105 A02 respectively.

3 Results and discussion

Being classified as vat dyes, whatever the source, the process of dyeing with natural and synthetic indigo is in principles similar. Insoluble indigo dye must be converted to its soluble form of dye leuco by the addition of a reducing agent under alkaline conditions. The conversion can be observed by the change from a suspension of dark blue to a clear solution of yellowish-green colour. The cotton fabric or yarn is then submerged in the solution of reduced indigo dye to let the molecules diffuse into the fibre, which is subsequently followed by air oxidation when the substrate is taken out of the solution and the dyes convert back to insoluble form and are locked in the fibre. The usual practice of indigo dyeing in traditional communities, either for batik making or yarn dyeing, is carried out by repeatedly immersing and removing the substrate from the dyeing bath, depending on the desired depth of shade. The procedure is similar with warp dyeing for denim to produce ring dyeing required for a worn denim look. The natural indigo dye being investigated in this research, however, was from *Strobilanthes cusia*, which has not been explored extensively in literature. Interesting results were obtained from its use in the dyeing of cotton denim fabric, with the aim of exploring its use in garment dyeing for the fashion industry.

Table 2 shows the redox potentials of leuco indigo dyebath before and after dyeing. As expected, based on the observation from the works of other researchers in the field [17, 19] as well as the chemistry of the reducing sugars, the redox potentials of leuco from fructose are higher than those from the glucose, regardless of the type of alkali source used in the reduction reaction. Despite the absence of an aldehyde group in the molecule, D-fructose readily undergoes keto-enol tautomerism at a high pH, forming a mixture of D-glucose and D-mannose, and also decomposes when treated with alkali to several other products with reducing capability [17, 19]. The reactions are shown in Figure 6. These products of tautomerism and decomposition gives D-fructose a supposedly higher reducing power than D-glucose that only possesses one form of product. That explains the higher colour strength that was obtained from D-fructose at all alkali variations (Table 3, and Figure 6 and 7), which also aligns well with data reported in literature. Saikhao et al. [17], for example, reported a redox potential of -716.3 mV and -702.5, and an absorbance result of 0.94 and 0.55 for D-fructose and D-glucose respectively. Blackburn and Harvey [19], in their investigation on the application of various reducing sugars in the sulphur dyeing, made the same observation and observed the trend that D-fructose has a slightly higher

redox potential, leading to a higher colour yield than D-glucose.

Another important observation from the data in Table 2 is that the redox potential of leuco dyebaths from those prepared with lime and husk ash remained virtually unchanged after being used to dye the fabric. This indicates the stability of the dyebaths against oxidation by air, which normally takes place during the dyeing process, leading to the decreased reducing capability of the dyebath and hence a reduced level of colour. The dyebaths that used sodium hydroxide, however, showed a significant decrease in redox potential, which may indicate that oxidation had taken place in the dyebaths. This suggests that a dyebath with a high alkali, such as sodium hydroxide, is prone to oxidation. This observation, however, may explain the low level of colour strength obtained from the sodium hydroxide, despite having the highest redox potential, as will be discussed further later in this paper. Additionally, it is also noteworthy that the redox potentials from lime and husk ash dyebaths are not significantly different from each other. The smaller values of redox potentials of the dyebaths in our research is most probably due to the impurities in the materials being used, which were obtained from the same local market accessed by traditional dyers.

Table 2: Redox potentials of each leuco dye before and after dyeing

Leuco dyebath	Redox potentials (mV) (at 22.9 °C for 2 min)					
	R-1 (F+L)	R-2 (F+A)	R-3 (F+NaOH)	R-4 (G+L)	R-5 (G+A)	R-6 (G+NaOH)
Before dyeing	-271.5	-272.9	-309.1	-267.6	-268.6	-306.6
After dyeing	-268.1	-272.7	-303.4	-267.6	-260.2	-301.8

The results of dyeing with different reducing sugars and alkali sources are presented in Table 3, together with their corresponding redox potentials. Additionally, the quantitative measures of the colour are provided in Figures 8 and 9, which are expressed both as *K/S* and *SUM(K/S)* values.

The data is correlates well with and supports the

visual observation made in Table 3. It was hypothesized that dyebaths with higher redox potential should result in a better reduction of indigo dye particles, and hence better dyeing and higher colour strength. The results are, however, quite the contrary. The lime dyebaths, having lower redox potentials (-271.5 mV and -267.6 mV for D-fructose and D-glucose respec-

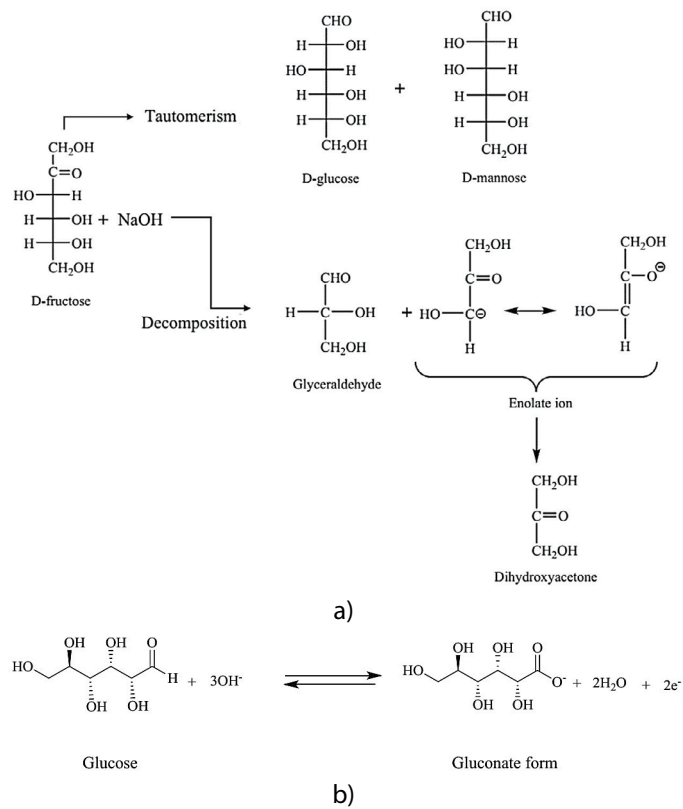


Figure 6: Reactions of D-fructose and D-glucose in alkaline conditions [17]

tively), unexpectedly produced the darkest colours with *K/S* values of 16.02 and 11.87 for D-fructose and D-glucose respectively and *SUM(K/S)* of 8.5 and 6.08 accordingly. On the other hand, denim cotton fabrics

dyed in the sodium hydroxide dyebaths, having the highest redox potentials (-309.1 mV and -306.6 mV), are lighter in colour and have the lowest colour strength (*K/S* values of 9.74 and 3.70).

Table 3: Photo images of dyed samples from all variations of dyeing recipes in Table 1

Reducing sugar	Alkali		
	Lime	Husk ash	NaOH flakes
Fructose	R-1	R-2	R-3
	-271.5 mV	-272.9 mV	-309.1 mV
Glucose	R-4	R-5	R-6
	-267.6 mV	-268.6 mV	-306.6 mV

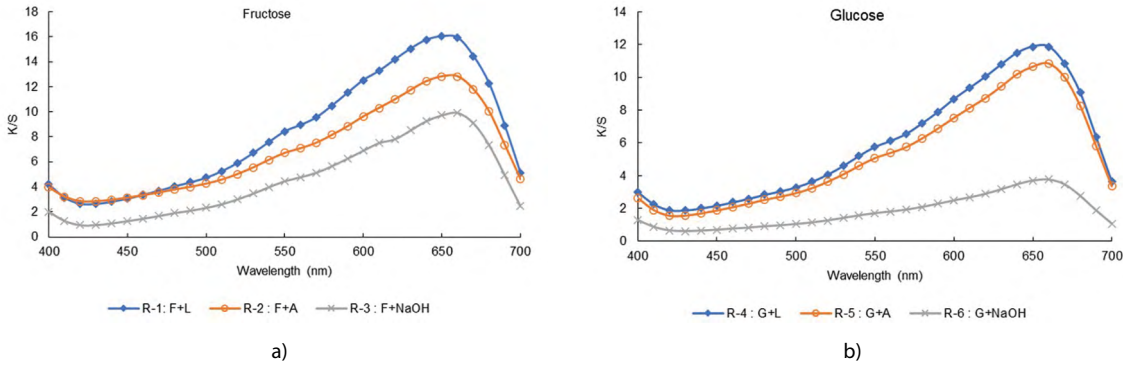


Figure 7: Colour spectra of the dyed fabrics obtained from all variations of recipe in Table 1

From this observation, it is evident that redox potential, which is a direct indicator of the reducing capability of a substance, is not the only factor that affects the dyeing process and the resulting colour. The strength of the alkali and the resulting pH of the dyebath played an important part in the colour yield of indigo dyeing. Important works by J.N. Ethers and colleagues at the University of Georgia, USA [20–22], as have been cited by many [17–19, 23], revealed the effect of pH on the dyeing behaviour of indigo, and described the existence of different forms of leuco indigo under different pH values.

indigo leads to the formation of monophenolate which increases with the further addition of alkali and reaches its peak at pH 10–11, as shown in Figure 9. At this point, all acid leuco indigo has converted to monophenolate or mono-ionic leuco indigo. The ionization of monophenolate to di-ionic biphenolate starts to occur when the pH of the dyebath is approximately 11. As the pH increases, more and more of the reduced mono-ionic indigo ionized further to produce a more soluble di-ionic form, reaching 50% conversion at an approximate pH value of 12.7. The proportions of the three forms of leuco indigo depicted in Figure 9 were calculated using equations 3–5 by taking the pK_1 and pK_2 values of 7.97 and 12.68 respectively [18, 21]:

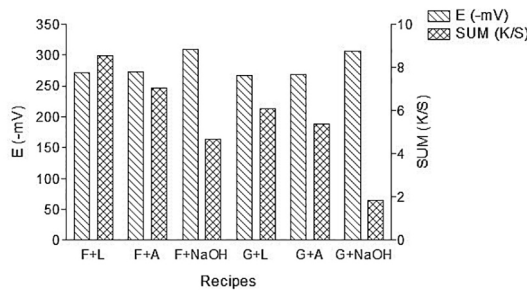


Figure 8: Redox potential of dyebath before dyeing and the resulting colour strength (K/S) of the corresponding dyed fabric

As shown in Figure 3, the leuco indigo in the dyebath is present in the form of acid leuco indigo [2], monophenolate (mono-ionic) leuco indigo (3a), and biphenolate (di-ionic) leuco indigo (3b), depending on the pH of the dyebath that impacts the degree of ionisation. The addition of alkali to the acid leuco

$$\text{acid leuco} = \frac{1}{1 + 10^{(pH - pK_1)} + 10^{(2pH - pK_1 - pK_2)}} \quad (3)$$

$$\text{monophenolate} = \frac{1}{1 + 10^{(pK_1 - pH)} + 10^{(pH - pK_2)}} \quad (4)$$

$$\text{biphenolate} = \frac{1}{1 + 10^{(pK_1 + pK_2 - 2pH)} + 10^{(pK_2 - pH)}} \quad (5)$$

On the other hand, studies by Ethers and et al. [21, 22] have shown that the isothermal sorption of indigo and the resulting colour strength (K/S) were both highest at a pH value of around 11, which coincides with the pH value at which the proportion of leuco indigo species is predominated by monophenolate ions. The sorption and K/S values were significantly lower at higher pH values of around 13. It can be

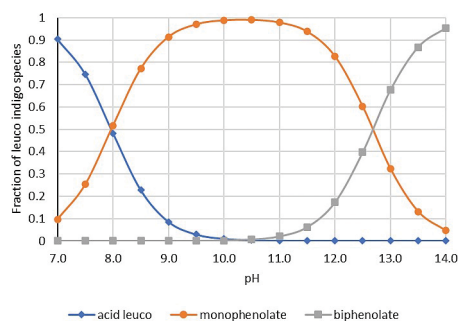


Figure 9: Fraction of leuco indigo species in the dye-bath as a function of pH

concluded that the substantivity of indigo is highest when it is in the form of monophenolate ions, despite the fact that it is less soluble than the di-ionic leuco indigo. In this regard, however, it must be remembered that the hydroxy groups of cellulose ionize at pH 11 create negative sites along cellulose molecular chains. The degree of ionization increases exponentially with an increase in the pH value. At pH values higher than 11, both the fibre and the dye are highly negatively charged. Repulsion thus occurs and prevents the adsorption of dyes on the fibre surface, resulting in low dye-fibre substantivity.

It was presumably suggested that the difference in colour strength was due to pH differences among the three dyebaths. However, by adjusting the concentration of alkali used, all the leuco indigo dyebaths in this study had a pH value of around 12, which is a normal practice in industry and for traditional dyers. Thus, according to equations 3–5 and Figure 7, they must have the same fractions of monophenolate (83%) and biphenolate ions (17%), and hence same level of colour strength. Since pH alone cannot explain the difference of colour strength, we must investigate the species that make up the alkali and their corresponding strengths.

Calcium hydroxide and sodium hydroxide are both strong alkalis. Given pure substances, they can easily reach pH 12 by a concentration as low as 0.4 g/L or 0.005 M for calcium hydroxide and 0.01 M for sodium hydroxide. The calcium hydroxide used in this experiment, however, was purchased from the local market and was not of industrial grade.

Due to the high content of impurities, it required a concentration of up to 40 g/L to reach pH 12. The alkali from husk ash, which most probably contained sodium carbonate, on the other hand, is a weaker alkali than both calcium and sodium hydroxide. Being a weaker alkali means that it dissociates less in water at equilibrium. A solution of 5 g/L pure sodium carbonate would normally have a pH value of around 11. According to this observation, dyeing from dyebaths with lime and sodium hydroxide should have had higher colour strength than those from husk ash. However, this is only true for lime. Sodium hydroxide dyeing, on the contrary, is significantly lighter than husk ash dyeing. It has been suggested that the charge on each of the alkali ions explains this observation. Calcium hydroxide has a charge of +2 on its calcium ion (Ca^{2+}), whereas sodium hydroxide and sodium carbonate each has a charge of only +1 (Na^+). It has been proposed that the larger charge on calcium ions created a larger attraction force to the anionic leuco indigo molecules in the dyebath, which leads to higher dye adsorption on the fibre surface and hence more dye molecules penetrating into the fibre. Additionally, in the bulk solution, each of the calcium ions can hold two leuco indigo anions creating a complex of larger size, resulting in a higher affinity for cellulose. In this regard, it is interesting to note how the leuco indigo associates with calcium ions in the form of monophenolates and biphenolates. For biphenolate ions, the association may lead to an even larger complex due to the di-ionic character of the leuco indigo, resulting in a significant reduction of dye penetration into the fibre.

Another possible explanation for the lighter colour of dyeing from the sodium hydroxide dyebaths is due to the stability of the leuco indigo against oxidation during the course of dyeing, as indicated by the lower redox potential of the used dyebaths (–303.4 and –301.8 mV as opposed to –309.1 and –306.6 mV before dyeing). This is only the case with the use of sodium hydroxide, which is a strong alkali, and not with lime and husk ash.

Table 4 presents the colour fastness of the dyed fabrics to washing and rubbing. The results show that all samples had good fastness to washing and rubbing, with the value of staining scales ranging from 3/4 to 4. As understood, cellulose and indigo dyes interact with each other physically through Van der Waals forces. The insoluble indigo pigments are trapped in the polymer structure of cellulose

without making any chemical bonding. With a high concentration of dye diffusion, ring dyeing is formed, so that the colour fastness to wet rubbing is lower than the colour fastness to dry rubbing. In the denim fashion industry, these disadvantages of low fastness to rubbing and washing are used to obtain a vintage effect through an intentional stripping-like process by the mechanical washing treatment.

Table 4: Colour fastness to washing and rubbing

Type of fastness		Staining scale value					
		R-1	R-2	R-3	R-4	R-5	R-6
Colour fastness to washing (ISO 105 C06)	Staining on cotton	3/4	3/4	4	3/4	3/4	3/4
	Staining on polyester	4	4	4	4	4	4
Colour fastness to rubbing (ISO 105 A02)	Staining on cotton after wet rubbing	3/4	3/4	4	3/4	3/4	4
	Staining on cotton after dry rubbing	4	4	4	4	4	4

4 Conclusion

A systematic study of the dyeing of denim using natural indigo paste from *Strobilanthes cusia* was carried out. It was demonstrated that *Strobilanthes cusia* produced a strong and deep indigo blue. The natural reducing sugars D-fructose and D-glucose were shown in this research to effectively reduce the insoluble indigo dye of *Strobilanthes cusia* to soluble leuco indigo, with D-fructose giving a higher colour strength or K/S values than D-glucose. The trend is similar to that shown in studies by others using different types of indigo dye. Lime or calcium hydroxide gave the highest colour strength with K/S and SUM(K/S) values of 16.02 and 8.5 respectively. The colour strength of indigo dyeing was found to depend on the reducing power of sugars, pH, alkali strength and the charge of ions in the alkali. The fastness to washing and rubbing of all dyeing recipes were good and not affected by the use of different reducing sugars and alkali sources.

Acknowledgment

The authors wish to thank the Agency of Industrial Human Resources Development, Ministry of Industry of Republic of Indonesia for the research grant (SPIRIT 2020) to conduct this research, and Mr. Fatah Syaifur from CV. Sidhobiru for the provision of raw materials of *S. cusia* and assistance in the preparation of indigo dye paste.

References

- FRANSSSEN, Maurice C.R., KIRCHER, Manfred, WOHLGEMUTH, Roland. Industrial biotechnology in the chemical and pharmaceutical industries. In *Industrial Biotechnology: Sustainable Growth and Economic Success*. Edited by Wim Soetaert and Erick J. Vandamme. Weinheim : Wiley, 2010, 323–351, doi: 10.1002/9783527630233.ch9.

2. WENNER, N., FORKIN, M. Indigo: sources, processes and possibilities for bioregional blue [online]. FIBERSHED [accessed 23 May 2021]. Available on World Wide Web: <<https://fibershed.org/wp-content/uploads/2017/08/indigo-sources-processes-possibilities-june2017.pdf>>.
3. BALFOUR-PAUL, J. Indigo in South and South-East Asia. *Textile History*, 1999, **30**(1), 98–112, doi: 10.1179/004049699793710688.
4. MUZAYYINAH, M. Jejak evolusi dan spesiasi marga indigofera. *Bioedukasi: Jurnal Pendidikan Biologi*, 2012, **5**(2), 1–12, <https://jurnal.uns.ac.id/bioedukasi/article/view/3922>.
5. HARTL, A., POLLEICHTNER, A., NOVAK, J. “Purplish Blue” or “Greenish Grey”? Indigo qualities and extraction yields from six species. *Plants*, 2024, **13**(7), 1–32, doi: 10.3390/plants13070918.
6. DEVI, R.L., DEVI, S.T., SANATOMBI, K. Hairy root culture of *Strobilanthes cusia* for the production and enhancement of indigo biosynthesis. *Plant Cell, Tissue and Organ Culture*, 2024, **157**(3), 1–14, doi: 10.1007/s11240-024-02791-9.
7. HU, Kun, JIANG, Yipeng, XIAO, Ying, WANG, Zikang, YU, Hao, CHEN, Zhihao, YAO, Cheng, CHENG, Zetong, ZHANG, Tian-Ao, HU, Jiajun, GAO, Min-Tian. *ACS Sustainable Chemistry & Engineering*, 2023, **11**(1), 426–435, doi: 10.1021/acssuschemeng.2c06375.
8. ZHANG, L., YANG, H., WANG, Y., ZHUANG, H., CHEN, W., LIN, Z., XU, J., WANG, Y. Blue footprint: distribution and use of indigo-yielding plant species. *Strobilanthes cusia* (Nees) Kuntze. *Global Ecology and Conservation*, 2021, **30**, 1–10, doi: 10.1016/j.gecco.2021.e01795.
9. XU, W., ZHANG, L., CUNNINGHAM, A.B., LI, S., ZHUANG, H., WANG, Y., LIU, A. Blue genome: chromosome-scale genome reveals the evolutionary and molecular basis of indigo biosynthesis in *Strobilanthes cusia*. *Plant Journal*, 2020, **104**(4), 864–879, doi: 10.1111/tpj.14992.
10. SUSAWAENGSP, C., CHOENGPANYA, K., SORNSAKDANUPHAP, J., TABTIMMAI, L., CHAIHARN, M., BHUYAR, P. Phytochemical and pharmacological properties of a traditional herb, *Strobilanthes Cusia* (Nees) Kuntze. *Molecular Biotechnology*, 2023, **66**, 1–12, doi:10.1007/s12033-023-00897-7.
11. LI, S., CUNNINGHAM, A.B., FAN, R., WANG, Y. Identity blues: the ethnobotany of the indigo dyeing by Landian Yao (Iu Mien) in Yunnan, Southwest China. *Journal of Ethnobiology and Ethnomedicine*, 2019, **15**, 1–14, doi: 10.1186/s13002-019-0289-0.
12. ZHANG, L., WANG, L., CUNNINGHAM, A.B., SHI, Y., WANG, Y. Island blues: indigenous knowledge of indigo-yielding plant species used by Hainan Miao and Li dyers on Hainan Island, China. *Journal of Ethnobiology and Ethnomedicine*, 2019, **15**, 1–9, doi: 10.1186/s13002-019-0314-3.
13. KURNIAWAN, C. Ekstraksi indigo dari daun strobilanthes cusia dan kajian pembentukan kompleks dengan ion Ni²⁺. *Jurnal Kimia dan Kemasan*, 2020, **42**(2), 93–99, doi: 10.24817/jkk.v42i2.5977.
14. ARTA, T.K., ATIKA, V., HAERUDIN, A., ISNAINI, I., MASISWO, M. Kualitas pewarnaan batik menggunakan bubuk indigofera tinctoria dan strobilanthes cusia. *Dinamika Kerajinan dan Batik*, 2019, **36**(2), 163–172, doi: 10.22322/dkb.V36i2.5421.
15. SHIN, Y., CHOI, M., YOO, D.I. Utilization of fruit by-products for organic reducing agent in indigo dyeing. *Fibres and Polymers*, 2013, **14**, 2027–2031, doi: 10.1007/s12221-013-2027-x.
16. HOSSAIN, M.D., KHAN, M.M.R., UDDIN, M.Z. Fastness properties and colour analysis of natural indigo dye and compatibility study of different natural reducing agents. *Journal of Polymers and the Environment*, 2017, **25**, 1219–1230, doi: 10.1007/s10924-016-0900-6.
17. SAIKHAO, L., SETTHAYANOND, J., KARP-KIRD, T., BECHTOLD, T., SUWANRUJI, P. Green reducing agents for indigo dyeing on cotton fabrics. *Journal of Cleaner Production*, 2018, **197**, 106–113, doi: 10.1016/j.jclepro.2018.06.199.

18. BLACKBURN, R.S., BECHTOLD, T., JOHN, P. The development of indigo reduction methods and pre-reduced indigo products. *Colouration Technology*, 2009, **125**(4), 193–207, doi: 10.1111/j.1478-4408.2009.00197.x.
19. BLACKBURN, R.S., HARVEY, A. Green chemistry methods in sulfur dyeing: application of various reducing D-sugars and analysis of the importance of optimum redox potential. *Environmental Science & Technology*, 2004, **38**(14), 4034–4039, doi: 10.1021/es0498484.
20. ETTERS, J.N. Recent progress in indigo dyeing of cotton denim yarn. *Indian Journal of Fibre & Textile Research (IJFTR)*, 1996, **21**(1), 30–34, <http://nopr.niscpr.res.in/handle/123456789/19246>.
21. ETTERS, J.N. Indigo dyeing of cotton denim yarn: correlating theory with practice. *Journal of the Society of Dyers and Colourists*, 1993, **109**(7–8), 251–255, doi: 10.1111/j.1478-4408.1993.tb01569.x.
22. ETTERS, J.N., HOU, M. Equilibrium sorption isotherms of indigo on cotton denim yarn: effect of pH. *Textile Research Journal*, 1991, **61**(12), 773–776, doi: 10.1177/004051759106101211.
23. VUOREMA, A. *Reduction and Analysis Methods of Indigo*. Turku : University of Turku, 2008, <https://core.ac.uk/reader/52209950>.

Md. Zayedul Hasan^{1,2}, Rochak Rathour¹, Apurba Das¹, R. Alagirusamy¹, Nandan Kumar³

¹ Department of Textile and Fiber Engineering, Indian Institute of Technology Delhi, Hauz Khas, New Delhi-110016, India

² Department of Textile Engineering, Mawlana Bhashani Science and Technology University, Santosh, Tangail-1902, Bangladesh

³ HHigh-Performance Textiles Pvt. Ltd., Panipat, Haryana-132103, India

Thermophysiological Comfort Behaviour of Cut Protective Workwear Consisting of Filament Twisted Multicomponent Hybrid Yarn

Termofiziološko udobje oblačil za zaščito pred urezom, izdelanih iz oplaščenih prej s hibridnimi filamentnimi prejami v jedru

Original scientific article/Izvirni znanstveni članek

Received/Prispelo 7–2024 • Accepted/Sprejeto 9–2024

Corresponding author/Korespondenčni avtor:

Dr. Rochak Rathour

Tel: +919560821849

E-mail: india.rochak1994@gmail.com

ORCID iD: 0000-0001-7522-2458

Abstract

Current cut protective gear is subject to several difficulties, such as the use of heavy fabric, complicated donning processes, lack of comfort and limited movement. When selecting the most comfortable cut protective fabric, it is important to consider the end users' specific needs. The aim of this study was to enhance the comprehension and optimisation of protective apparel for superior occupational safety and protection by exploring the intricate link between material composition, yarn structure and comfort parameters. Various combinations of filament twisted core sheath yarn consisting of stainless-steel/glass with high-performance polyethylene and polyester wraps were used to fabricate thermo-physiological comfortable cut protective workwear fabric. Twelve cut protective fabrics with the same areal density (200 g/m²) were prepared with 6-end satin weave using filament twisted core sheath yarn of five distinct linear densities (98.4 tex, 73.8 tex, 59.1 tex, 49.2 tex and 39.4 tex). These fabric samples were used to evaluate thermophysiological characteristics, including air permeability, dry and evaporative heat resistance, thermal conductivity, moisture permeability, wettability and moisture wicking according to the established standard. The cut protection of each sample was also measured according to EN 13997. The cut protection and thermo-physiological comfort attributes of cut-resistant clothing are greatly influenced by the proportion of core material (stainless-steel/glass) and yarn structural parameters (linear density and twist direction), which was observed by analysing the results. An increased core material percentage (stainless-steel/glass) contributes to increased fabric thickness and reduced bulk density, which influences the thermophysiological comfort attributes of the developed cut protective workwear fabric. Fabric made from a



Content from this work may be used under the terms of the Creative Commons Attribution CC BY 4.0 licence (<https://creativecommons.org/licenses/by/4.0/>). Authors retain ownership of the copyright for their content, but allow anyone to download, reuse, reprint, modify, distribute and/or copy the content as long as the original authors and source are cited. No permission is required from the authors or the publisher. This journal does not charge APCs or submission charges.

higher proportion of core material (stainless-steel/glass) with a lower bulk density exhibited an acceptable cut protection level and performed better in terms of thermo-physiological comfort attributes.

Keywords: Protective workwear, cut-resistant, filament twisted core sheath yarn, bulk density, thermal and moisture transmission

Izvleček

Sodobna oprema za zaščito pred urezom je izdelana iz težkih tkanin, zaradi katerih so načini oblačenja zapleteni, oblačila neudobna, gibanje v njih je močno omejeno. Pri izbiri najudobnejše tkanine za zaščito pred urezom je pomembno upoštevati specifične potrebe porabnika. Pričujoča raziskava zapletenih povezav med surovinsko sestavo materiala, strukturo preje in parametri udobja je bila izvedena z namenom izboljšati razumevanje in optimizacijo zaščitnih oblačil za čim večjo varnost in zaščito pri delu. Za izdelavo termofiziološko udobne tkanine za zaščito pred urezom so bile uporabljene oplaščene preje z jedrom iz hibridnih prej (filamentov nerjavnega jekla in stekla) in dvojnimi plaščem iz visokozmogljivih polietilenskih in poliestrskih filamentnih prej. Iz petih različnih oplaščenih prej, ki so se med seboj razlikovale po dolžinski masi jedra (98,4 tex, 73,8 tex, 59,1 tex, 49,2 tex in 39,4 tex), je bilo v vezavi saten 6 izdelanih dvanajst tkanin za zaščito pred urezom z enako površinsko maso (200 g/m²). Na vzorcih tkanin so bile izvedene meritve termofizioloških lastnosti, vključno z zračno prepustnostjo, toplotnim uporom in uporom prehodu vodne pare, toplotno prevodnostjo, indeksom prepustnosti vodne pare, omočljivostjo in odvajanjem vlage v skladu z uveljavljenimi standardi. Zaščita pred urezom je bila za vzorce določena skladno s standardom EN 13997. Analiza je pokazala, da na zaščito pred urezom in termofiziološko udobje zaščitnih tkanin močno vplivajo odstotni delež jedra iz nerjavnega jekla in stekla ter strukturni parametri preje (linearna gostota in smer vitja). Večji delež jedra pripomore k večji debelini tkanine in nižji volumski gostoti, kar vpliva na termofiziološke lastnosti tkanine za zaščito pred urezom. Tkanine z višjim odstotnim deležem jedra in nižjo volumsko gostoto imajo sprejemljivo raven zaščite pred urezom ob boljši toplotni udobnosti kot tkanine z nižjim odstotnim deležem jedra.

Ključne besede: zaščitna oblačila, varovalna oblačila, odpornost proti urezu, dvojno ovita preja, volumska gostota, prenos toplote in vlage

1 Introduction

Human nature dictates that a person will react when given visual information about an object, such as clothing, other everyday things or objects in their surrounding area. Clothing is one of our most basic needs; it emphasizes safety and modesty. Over time, the need for safety was superseded by the desire for beauty. The protective clothing market is now driven by a trend towards protection as the primary functionality. The primary objective of protective clothing is to protect workers from hazards that are mechanical, chemical and physical. However, the requirement to follow safety and protection standards may limit the effectiveness of protective fabrics [1, 2]. Cut risks are present everywhere. For every 10,000

employees, there are 8.1 instances of cuts and laceration injuries [3]. There are still several problems with contemporary cut-resistant workwear clothing, such as bulky fabric, challenging donning techniques, uncomfortable fit and unnatural movement. Most cut protective workwear designs incorporate increased size and areal density, resulting in a 20% increase in energy consumed during activities [4, 5]. Wearing cut protective clothing in excessively humid circumstances can cause significant physical strain, leading to intellectual incapacity, pain, exhaustion, reduced operational effectiveness and harm to the body [6]. The way heat is transferred throughout the body and its surroundings controls the temperature of the human body [7, 8]. Once this process is unable to counteract heat accumulation, core temperature

may rise to dangerous levels, leading to heat stress, a serious threat to one's health and ability to operate in many industrial contexts [9]. The temperature environment, the amount and length of physical activity required for activities and clothing are important risk factors associated with heat stress sickness [10]. Understanding these components and their underlying concepts is necessary for assessing heat stress. At present, the importance of the wearer's health is growing when using cut protective workwear [11–16]. Even though India has many glass and sheet metal manufacturing companies, the notion of protective workwear is still in its early stage. The remedy to this issue lies in instructing personnel about safe material handling. Employees are supplied with cut protective workwear for safety protection during physical activity, but they are not interested in utilizing it frequently due to the inconvenience of wearing them in hot and humid surroundings [17]. The needs particular to the user form the basis and culmination of the process of creating cut protective workwear. The user's operating environment and the activities that are carried out by them establish these needs, whether for comfort or performance [18–19].

Cut protective clothing prioritizes functionality, thermal comfort and human movement, yet aesthetic elements are necessary for all garment systems. In cut protective clothing, the human body-environment system, the relationship between clothing and the human body, creates a micro-environment that affects human comfort. This interaction serves as an inhibitor to prevent the human body from being exposed to potentially hazardous situations. The main purpose of cut protection gear is to shield the wearer from potential cuts and slashes. Psychological comfort is provided, especially in terms of sensory and thermal comfort, which facilitates human mobility while a user is engaged in certain tasks. During the use of cut protective workwear in hot and humid working conditions, the ambient air temperature is much higher than the human body temperature. In this condition, the temperature differential between the skin and the surrounding air becomes negative.

As a result, the body produces heat, even when its metabolic heat loss is greatly reduced [20]. This is offset by the human body's capacity to perspire. Furthermore, the human body possesses a significant ability to release heat through evaporation, thus aiding in the regulation of its thermal balance [21, 22]. If thermal balance is not achieved, it will lead to heat stress and the microenvironment near the skin will become saturated with high humidity, causing liquid from perspiration to condense on the skin. This might result in elevated heat load and discomfort, thereby limiting the working hours of employees. Ensuring proper body temperature is crucial in high-stress sectors such as the metal and automobile industries. Inadequate thermal comfort can lead to overheating, profuse perspiration and dehydration, which can undermine the protective capabilities of the garment and increase the likelihood of injuries. This highlights the importance of developing materials that are resistant to cuts while continuing to provide thermal comfort. This may lead to better adherence to safety standards, a decrease in heat-related health problems and the overall improvement in the well-being of workers.

Thermophysiological is a critical aspect of cut-resistant fabrics and garments, directly impacting their effectiveness and suitability for various applications. By integrating features that enhance breathability, moisture management and thermal regulation, manufacturers can ensure that cut-resistant garments not only provide necessary protection but also support the health, safety and performance of workers in demanding industries such as manufacturing, construction, law enforcement and the military. In the field of occupational safety, the design and effectiveness of protective clothing are essential for ensuring the thermophysiological comfort of workers in different circumstances. The level of comfort provided is especially crucial in industries that demand cut protection, since the balance between safety and the comfort of the end user is of the utmost importance. Ensuring thermal balance is a crucial factor in the design of garments, particularly in the context of

protective clothing [23, 24]. Appropriate selections of fabric raw materials and weaving structures may enhance airflow and moisture evaporation, and provide safety protection [25]. An important breakthrough in this field is the use of filament twisted core sheath multicomponent hybrid yarns. These sophisticated yarns not only improve the mechanical durability and protective qualities of workwear but also have a significant impact on thermophysiological comfort. This research investigated the behaviour of cut protective workwear that incorporates filament twisted core-sheath hybrid yarns, focusing on their effects on thermophysiological comfort. The aim of this study is to expand the understanding and optimization of protective clothing for improved occupational safety and protection by investigating the complex relationship between material composition, yarn structure and comfort measures.

2 Materials and methods

2.1 Materials

2.1.1 Preparation of filament twisted core sheath yarn

To explore the impact of core material and yarn twist direction on thermo-physiological comfort features, a

total of 12 distinct filament twisted core sheath hybrid yarns were manufactured for study using a HKV141 hollow spindle wrapping machine, maintained at a consistent twist level (400 twists/m). Stainless-steel (SS), glass (GF), polyester (PES) and high-performance polyethylene (HPPE) filament threads were chosen as raw materials. The specifications of the filament yarn and structural properties of produced yarns are given in Tables 1 and 2. Produced filament twisted core sheath yarns contained a core yarn (SS/GF) in the middle and two surrounding yarns (inner yarn: PES, outer yarn: HPPE) in the structure as shown in Figure 1.

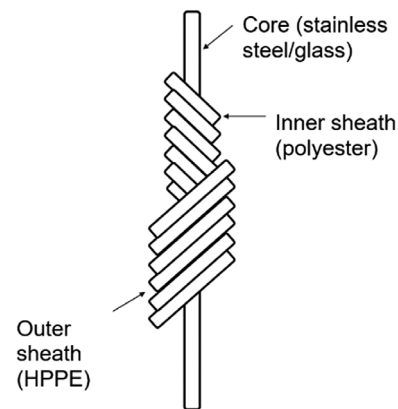


Figure 1: Filament twisted core sheath yarn

Table 1: Specifications of high-performance filament yarn

Filament thread	Linear density (dtex)	Diameter of individual fibre (μm)	Number of filaments
Stainless-steel (SS) ^{a)}	55.56–166.67	30–50	1
Glass (GF) ^{a)}	111.11–333.33	5.5–9.5	200–400
High-performance polyethylene (HPPE) ^{a)}	222.22–444.44	20–30	90–180
Polyester (PES) ^{a)}	111.11	20	36

^{a)} High-performance textiles limited, Panipat, Haryana, India

Table 2: Specifications of prepared filament twisted core sheath yarn

Yarn sample code	Diameter or fineness of core material	Fineness of inner sheath material (den/dtex)	Fineness of outer sheath material (den/dtex)	Composition (%) of core/inner sheath/outer sheath	Yarn linear density (Ne/tex)	Twist multiplier, direction	Breaking stress (cN/tex)	Breaking elongation (%)
Y1	SS 30 μm	PES 100/111.11	HPPE 200/222.22	15.25/28.25/56.50	15/39.4	2.62 S and Z	129.27	6.28
Y2	SS 40 μm	PES 100/111.11	HPPE 300/333.33	24.70/18.80/56.50	10/59.1	3.21 S and Z	66.23	5.94

Y3	SS 50 μ m	PES 100/111.11	HPPE 400/444.44	28.44/15.06/56.50	8/73.8	3.59 S and Z	107.02	7.51
Y4	SS 30 μ m	PES 100/111.11	HPPE 200/222.22	15.25/28.25/56.50	15/39.4	2.62 S and S	133.95	5.72
Y5	SS 40 μ m	PES 100/111.11	HPPE 300/333.33	24.70/18.80/56.50	10/59.1	3.21 S and S	53.18	6.89
Y6	SS 50 μ m	PES 100/111.11	HPPE 400/444.44	28.44/15.06/56.50	8/73.8	3.59 S and S	79.21	7.37
Y7	GF 100 den	PES 100/111.11	HPPE 200/222.22	22.58/22.58/54.84	12/49.2	2.93 S and Z	94.13	7.62
Y8	GF 200 den	PES 100/111.11	HPPE 300/333.33	30.12/15.04/54.84	873.8	3.59 S and Z	44.24	8.12
Y9	GF 300 den	PES 100/111.11	HPPE 400/444.44	33.85/11.31/54.84	6/98.4	4.15 S and Z	66.40	9.80
Y10	GF 100 den	PES 100/111.11	HPPE 200/222.22	22.58/22.58/54.84	12/49.2	2.93 S and S	91.57	9.45
Y11	GF 200 den	PES 100/111.11	HPPE 300/333.33	30.12/15.04/54.84	8/73.8	3.59 S and S	43.71	9.08
Y12	GF 300 den	PES 100/111.11	HPPE 400/444.44	33.85/11.31/54.84	6/98.4	4.15 S and S	61.90	8.89

2.1.2 Preparation of woven fabrics from filament twisted core sheath yarn

In this research work, twelve fabric samples were woven using five distinct yarn counts (98.4 tex, 73.8 tex, 59.1 tex, 49.2 tex and 39.4 tex (15 Ne, 12 Ne, 10 Ne, 8 Ne and 6 Ne)) of filament twisted core sheath yarn as both the weft and warp yarn. The particulars of these various fabric specimens with are given in Table 3. Fabric specimens were woven using a 6-end satin design with various thread densities. As shown in Figure 2, the 6-end satin design was chosen because it has a tight structure with fewer interlaces

than other weaves such as plain or twill weave. This tightness enhances the fabric's ability to resist cuts by reducing the spaces where a blade can penetrate.

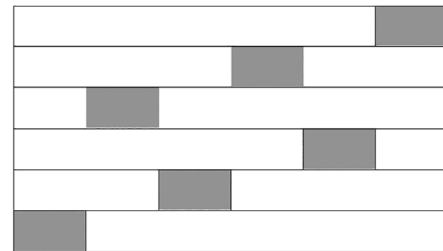


Figure 2: 6-end satin weave design

Table 3: Specifications of manufactured woven 6-end satin fabrics

Sample code	Yarn material	Linear density (Ne/tex)		Thread density (cm ⁻¹ /inch ⁻¹)	
		Warp yarn	Weft yarn	Ends	Picks
SSS30	UHMWPE/PES/SS	15/39.4	15/39.4	23.62/60	23.62/60
SSS40	UHMWPE/PES/SS	10/59.1	10/59.1	15.74/40	15.74/40
SSS50	UHMWPE/PES/SS	8/73.8	8/73.8	11.81/30	13.78/35
SZS30	UHMWPE/PES/SS	15/39.4	15/39.4	23.62/60	23.62/60
SZS40	UHMWPE/PES/SS	10/59.1	10/59.1	15.74/40	15.74/40
SZS50	UHMWPE/PES/SS	8/73.8	8/73.8	11.81/30	13.78/35
SSG10	UHMWPE/PES/GF	12/49.2	12/49.2	19.685/50	19.685/50
SSG20	UHMWPE/PES/GF	8/73.8	8/73.8	11.81/30	13.78/35
SSG30	UHMWPE/PES/GF	6/98.4	6/98.4	9.45/24	9.45/24
SZG10	UHMWPE/PES/GF	8/73.8	8/73.8	19.685/50	19.685/50
SZG20	UHMWPE/PES/GF	12/49.2	12/49.2	11.81/30	13.78/35
SZG30	UHMWPE/PES/GF	6/98.4	6/98.4	9.45/24	9.45/24

2.2 Methods

2.2.1 Physical properties

The ASTM standards were followed to assess the physical properties of each fabric sample [26, 27]. According to ASTM D 3775-12, counting glass was used to measure the thread density in both directions of each specimen. The mean value of ten readings was recorded to obtain the precise value of thread density. Each sample's areal density was measured according to the ASTM D 3776-09 standard. Each specimen's thickness was assessed using a digital thickness gauge at a pressure of 20 N/cm², and then according to the ASTM D 1777-96 standard. The ratio of the areal density and thickness of fabric was used to assess the fabric density (kg/m³). The porosity of each sample was calculated using equation 1.

$$\text{Porosity} = 1 - \frac{\text{Fabric density}}{\text{Fibre density}} \quad (1)$$

2.2.2 Cut protective performance

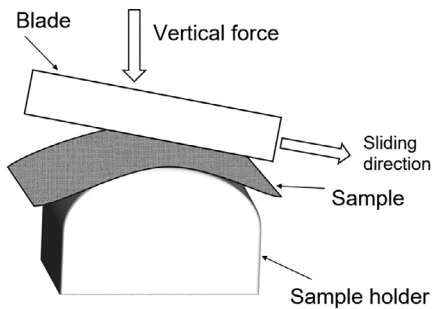


Figure 3: Schematic diagram of the functioning of the TDM100 cut test machine

A TDM-100 cut-resistant tester was used to assess the cut protection capabilities of covered yarn fabrics in accordance with the ISO 13997-1999 standard [28]. The fabrics were sliced in the warp direction to create standard samples. The fabrics were subjected to fifteen cuts under different weights, resulting in a distribution of cut distances of between 5~15 mm, 15~30 mm and 30~50 mm. Every experiment's different cut load and matching distances were noted. The ideal fitting curve for the load and normalized cut distance was created using it as a basis. Subsequently, the load necessary for

a cutting distance of 20 mm may be ascertained based on this curve. Figure 3 displays the schematic diagram of the cut test instrument.

Table 4 presents the grading for levels of cut resistance performance according to the EN 388:2016 standard. The amount of cut resistance of the material increases in direct proportion to its index value [34]. Several factors, such as weaving construction, fabric thickness, areal density, thread density, coating and source material, influence the cut resistance properties of a fabric [35].

Grading	A	B	C	D	E	F
Cut resistance (N)	≥ 2	≥ 5	≥ 10	≥ 15	≥ 22	≥ 32

Table 4: Grading of cut resistance according to the ISO13997 method in EN388:2016

2.2.3 Comfort properties

a) Air permeability

The air permeability of each fabric sample was assessed using a TEXTEST FX3300 air permeability tester (Figure 4), following the guidelines of the ASTM D737-96 standard. Air permeation was calculated by determining the air circulation rate over a 38.26 cm² circumference, while both surfaces had a predefined pressure of air variation. The size of each specimen was 20 cm², while maintaining the air pressure at 100 Pa. The mean of five readings of samples was taken and recorded.

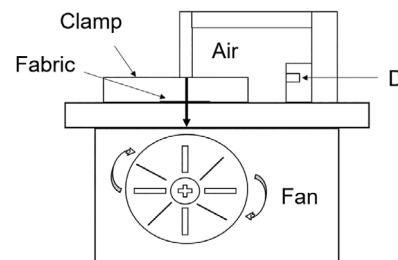


Figure 4: Schematic diagram of the functioning of the air permeability tester

b) Dry and evaporative heat resistance

The fabric's dry heat resistance (R_{cl}) and evaporative heat resistance (R_{et}) were evaluated according to

ASTM1868 F, Part-C under steady-state conditions using an Atlas sweating guarded hot plate (Figure 5) (SGHP, Model M259B). Each fabric was measured using three 52 cm × 52 cm specimens, and the R_{ct} and R_{et} values were calculated using the means of nine readings (assuming the test parameters were within the tolerance limit).

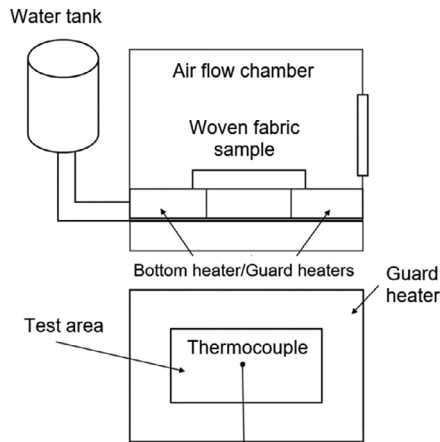


Figure 5: Schematic diagram of the functioning of the sweating guarded hot plate

c) Thermal conductivity

The sample's thermal conductivity (λ) was measured using a dry-contact KES-F7 Thermolabo tester. The test specimen (20 cm × 20 cm) was kept on the warmth plate at a consistent air temperature (10 °C above ambient temperature) with a constant air stream. The amount of heat lost was measured to determine the fabric's thermal conductivity using equation 2.

$$\lambda = q \frac{L}{\Delta T} \quad (2)$$

where, q represents the heat flow rate (W/m^2), L represents the thickness of the specimen (m), ΔT represents temperature (K) and λ represents the coefficient of thermal conductivity ($Wm^{-1}K^{-1}$).

d) Moisture permeability index

The moisture permeability index (i_{mt}) measures how clothing allows for evaporative cooling. The permeability index is a quantitative measure that relates the

dry and evaporative heat resistance of clothing. It is determined by calculating the R_{ct} and R_{et} values using equation 3.

$$i_{mt} = K \frac{R_{ct}}{R_{et}} \quad (3)$$

where K represents a constant with a value of 60.6515 Pa/°C [29].

e) Contact angle

The contact angle was measured using a contact angle meter (OCA30) manufactured by Data Physics in Germany, as shown in Figure 6. The contact angle was calculated using the goniometric method. The process involved extracting distilled water from a Hamilton syringe in a controlled manner, releasing it in precise, changeable volumes using software-controlled droplets. The instrument itself is responsible for moving the base plate and applying pressure to the piston. After the drop has reached a stable state on the surface, accurate measurements are taken for a duration of 30 seconds. The device was located in a laboratory maintained at a temperature of 23 °C ± 1 °C and a relative humidity of 50% ± 4% [30].

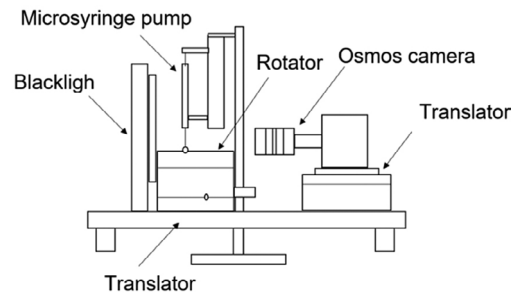


Figure 6: Schematic diagram of the functioning of the contact angle measurement meter

f) Moisture wicking

The impact of core material and yarn twist direction on the vertical capillary action of textiles was evaluated by measuring the height of liquid absorption against the force of gravity along the lengthwise and widthwise directions of the fabric. The test was performed using a vertical wicking tester following the DIN 53924 technique [31]. Figure 7 illustrates the

schematic diagram of the moisture wicking instrument. A 200 mm × 25 mm strip of fabric was hung vertically, with its lower end submerged in a reservoir of distilled water. Reactive dye (1% Prussian blue) was added to the water to track its movement, and a scale was used to measure the height at which the water in the fabric reached regularly.

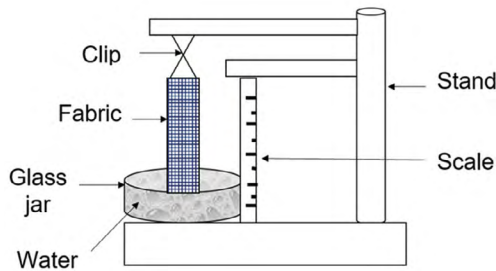


Figure 7: Schematic diagram of the functioning of the moisture wicking tester

2.2.4 ANOVA test

Completely randomized one-factor analysis of variance (ANOVA) test was performed to determine the effect of the percentage of core material and yarn structural parameters on the thermophysiological comfort properties of cut protective fabric. Statistical evaluations were performed using a statistical software package (XLMiner Analysis Toolpak). A p-value indicates the probability of getting an effect no less than that observed in the sample data. If $p < 0.05$, the result is considered statistically significant. F-value is the result of the ANOVA test to determine if the variances of the means of two populations are different when there are multiple variables.

3 Results and discussion

3.1 Physical properties

The microscopic images of the prepared cut protective fabric are presented in Table 5. To study the impact of yarn count on the physical characteristics of the cut protective fabric, we analysed the variations in fabric thickness and fabric bulk density. These findings are presented in Table 6. The thread

density of each sample was measured in warp and weft directions, as shown in Table 3. Table 6 shows that the cut protective fabrics SSS 50, SZS 50, SSG 50 and SZG 50 showed the highest fabric thickness. These cut protective fabrics were made with a coarser yarn count. When coarser yarn is used in fabric, yarn diameter and thickness increase. An increase in fabric thickness results in a decrease in bulk density.

Cut protective fabrics SSS 50 and SZS 50 exhibited the highest porosity. Fabric specimens SSS 50 and SZS 50 possessed a lower bulk density. Fabric with low bulk density indicates more void space or pores in the fabric structure, since there is less mass in each volume. Because there are larger gaps between all the fibres or threads in fabrics with low bulk density, more things such as air can exist there. This results in fabrics with increased porosity. Porosity declined as the bulk density of each sample tended to rise. This showed, as other researchers have already demonstrated, that a larger bulk density reduces porosity [32, 33]. Porosity impacts several attributes of clothing, such as its capacity to facilitate air permeation, absorb moisture and offer thermal insulation. Fabrics with higher porosity often have better breathability and moisture absorption characteristics, making them beneficial in certain situations such as protective clothing.

Table 5: Microscopic images of cut protective fabrics made from filament twisted core sheath yarn, taken by a microscope camera Axiocam 208c at magnification 1 x

SSS30	SSS40	SSS50	SZS30	SZS40	SZS50
SSG10	SSG20	SSG30	SZG10	SZG20	SZG30

Table 6: Physical properties (arithmetic mean \pm error) of cut protective fabrics made from filament twisted core sheath yarn

Sample code	Areal density (g/m ²)	Thickness (mm)	Bulk density (kg/m ³)	Porosity
SSS30	200	0.58 \pm 0.05	344.83 \pm 1.26	0.838 \pm 0.016
SSS40	200	0.74 \pm 0.07	270.27 \pm 2.07	0.902 \pm 0.024
SSS50	200	0.77 \pm 0.04	259.74 \pm 1.82	0.913 \pm 0.021
SZS30	200	0.58 \pm 0.05	344.83 \pm 1.26	0.838 \pm 0.016
SZS40	200	0.74 \pm 0.07	270.27 \pm 2.07	0.902 \pm 0.024
SZS50	200	0.77 \pm 0.04	259.74 \pm 1.82	0.913 \pm 0.021
SSG10	200	0.62 \pm 0.03	322.58 \pm 1.04	0.744 \pm 0.011
SSG20	200	0.82 \pm 0.06	243.90 \pm 3.52	0.812 \pm 0.025
SSG30	200	0.85 \pm 0.04	235.29 \pm 1.72	0.821 \pm 0.013
SZG10	200	0.62 \pm 0.03	322.58 \pm 1.04	0.744 \pm 0.011
SZG20	200	0.82 \pm 0.06	243.90 \pm 3.52	0.812 \pm 0.025
SZG30	200	0.85 \pm 0.04	235.29 \pm 1.72	0.821 \pm 0.011

3.2 Cut resistance

Each fabric sample achieved cut protection level D according to EN 388:2016. Cut protection level D indicates that a garment can endure a downward force of up to 15 N. This level of cut protection is optimal for environments with an elevated risk of cuts from dangers, including construction sites, industries and warehouses.

Effect of stainless-steel content

As evident from Figure 8, cut resistance performance improves with an increase in stainless-steel content as core material in filament twisted core sheath yarn made fabrics. After a certain level, however, it decreases. This may be due to the bulk density of the clothing. Fabrics with a higher proportion of stainless-steel may have a more relaxed weave structure with less bulk density to accommodate the rigidity of the stainless-steel. A less dense structure can result in wider spaces between fibres, which may facilitate the penetration of a cutting edge into the fabric, as opposed to a closely woven fabric with a lower proportion of stainless-steel. Among the different fabrics made from filament twisted core-sheath yarn, the ranking of cut-resistant performance of the fabrics was: SSS30, SZS30 > SSS40, SZS40 > SSS50 and SZS50. The cut protection level of the fabric samples SSS30

and SZS30 was 20% higher than the SSS50 and SZS50 samples. This may be also explained in terms of yarn count. Fabrics made with coarser yarn demonstrate less bulk density, which directly impacts cut resistance performance. To observe the effect of the core material (stainless-steel content) and yarn structural parameters on cut resistance, a one-way ANOVA test was also performed. According to the p-value (Table 7), the stainless-steel content had significant effect on cut resistance properties.

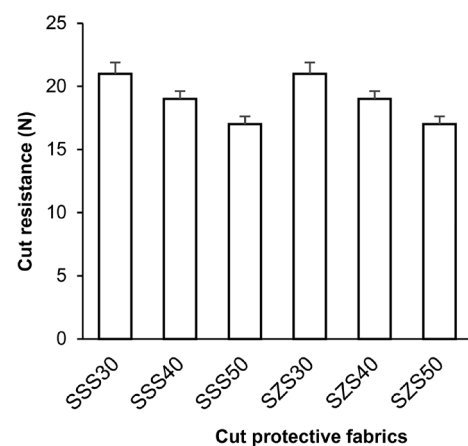


Figure 8: Influence of core material (stainless-steel content) and yarn structural parameter on cut resistance

Table 7: ANOVA test for the impact of core material (stainless-steel content) and yarn structural parameter on cut resistance

Source of variation	SS	df	MS	F	p-value	F _{critical}
Between groups	20	5	4	6	0.000977	2.620654
Within groups	16	24	0.666667			

Effect of glass content

Figure 9 shows that the cut resistance performance of clothing produced from filament twisted core sheath yarn improves as the percentage of glass increases as the core material increases. However, there is a point when the cut resistance performance begins to decrease. This might be attributed to the clothing's bulk density. Fabrics with a higher percentage of glass may have a looser weave structure and lower bulk density to accommodate the stiffness of the glass fibres. A lower-density fabric allows for more spacing between fibres, making it easier for a cutting edge to penetrate the fabric. This is in contrast to a tightly woven fabric with a smaller amount of glass. The cut-resistant performance of the materials, ranked from highest to lowest, is as follows: SSG10, SZG10 > SSG20, SZG20 > SSG30 and SZG30. This may also be elucidated to yarn count. Fabrics produced with thicker yarn have lower bulk density, resulting in a direct influence on the cut resistance performance.

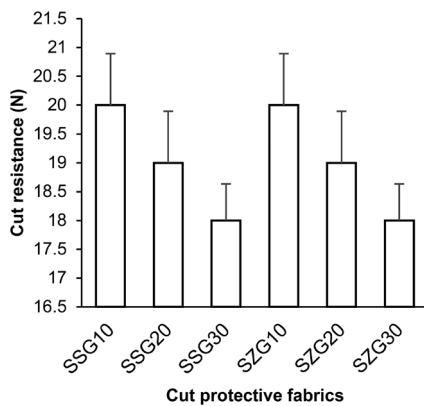


Figure 9: Influence of core material (glass content) and yarn structural parameter on cut resistance

A one-way ANOVA test was also performed to see how the yarn structural characteristics and the percentage of glass used in the core material affected cut resistance. Table 8 shows that the p-value is significant.

Table 8: ANOVA test for the impact of core material (glass content) and yarn structural parameter on cut resistance

Source of variation	SS	MS	F	p-value	F _{critical}
Between groups	80	16	19.2	1.09 × 10 ⁻⁷	2.620654
Within groups	20	0.833333333			

3.3 Air permeability

A fabric's air permeability refers to its capacity to allow air to pass through it, and it is commonly used to evaluate its air transmission characteristics. Air quantity and flow impact numerous garment characteristics, such as thermal insulation, resistance to wind and rain, and other factors that determine the selection of materials for different end uses. Air permeability is influenced by several elements, such as the type of yarn used, constructional variables of the fabric and bulk characteristics, which include thickness, mass per unit area and porosity. The openness of the fabric structure is primarily determined by the interstices between the yarns [36-38]. Porosity is often regarded as the primary component that influences air permeability. Fabric openness is a measure of the total amount of vacant space inside a certain region. The air permeability of a fabric is determined by the number and size of pores in its structure [39].

Effect of stainless-steel content

As evident from Figure 10, air permeability improves with an increase in stainless-steel content as core material in filament twisted core sheath yarn made fabrics. It can also be observed from Figure 10 that fabric specimens SSS50 and SZS50 exhibit air

permeation. Both fabric specimens were prepared with coarser yarn, which has a lower bulk density, resulting in a direct influence on the porousness of the clothing. It is evident from Table 4 that a lower bulk density results in the higher porosity of clothing, which in turn indicates greater air permeability. In order to observe the effect of the core material (stainless-steel content) and yarn structural parameters on air permeability, a one-way ANOVA test was also performed. According to Table 9, the p-value is significant.

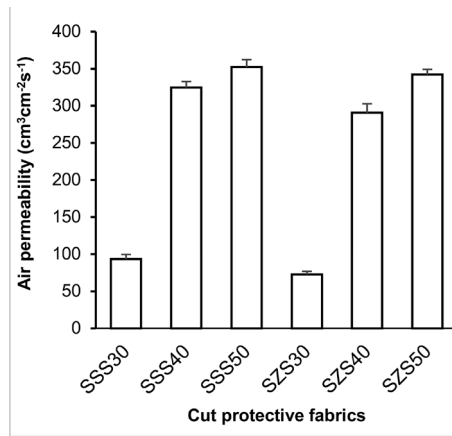


Figure 10: Influence of core material (stainless-steel content) and yarn structural parameter on air permeability

Effect of glass content

Figure 11 shows that the air permeability of clothing

produced from filament twisted core sheath yarn improves as the percentage of glass used as the core material increases. Figure 11 shows that fabric samples SSG30 and SZG30 demonstrate air permeability. Both fabric specimens were manufactured with coarser yarn, which has a lower bulk density. This directly affects the porosity of clothing. According to Table 4, the lower bulk density of clothing results in higher porosity, which in turn indicates greater air permeability. To investigate the impact of the core material composition (glass percentage) and yarn structural factors on air permeability, a one-way ANOVA test was conducted. Based on the data presented in Table 10, the p-value is statistically significant.

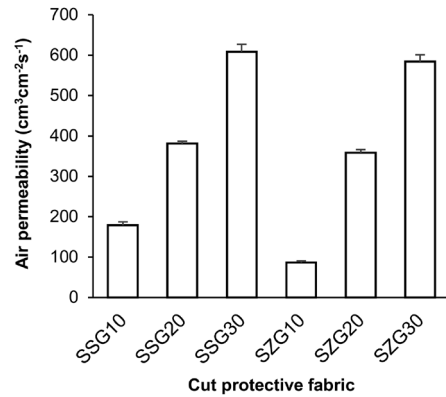


Figure 11: Influence of core material (glass content) and yarn structural parameter on air permeability

Table 9: ANOVA test for the impact of core material (stainless-steel content) and yarn structural parameter on air permeability

Source of variation	SS	df	MS	F	p-value	F _{critical}
Between groups	409996.594	5	81999.3188	934.3444965	0	2.620654
Within groups	2106.272	24	87.76133333			

Table 10: ANOVA test for the impact of core material (glass content) and yarn structural parameter on air permeability

Source of variation	SS	df	MS	F	p-value	F _{critical}
Between groups	1098628.242	5	219725.65	1305.81157	0	2.620654
Within groups	4038.42	24	168.2675			

3.4 Dry heat resistance

To maintain a state of thermo-physiological contentment, human beings must maintain thermal balance. This implies that the thermal acquisition and drop should be closely synchronized. If thermal equilibrium is not achieved, it can lead to either an elevation or reduction in body temperature, which might be life-threatening. The primary factor influencing the heat balance of a fabric is its dry heat resistance, which pertains to the speed at which heat passes through the fabric. The dry heat resistance of a fabric is influenced by several factors, such as the kind of fibre, the structure of the fabric and its thickness. High dry heat resistance prevents the flow of metabolic body heat to the surrounding environment. Thus, the use of cut protective fabric might result in heat stress, since the protective gear has increased resistance to dry heat. The dry heat resistance of fabrics is closely correlated with their thickness and bulk density [40].

Effect of stainless-steel content

It is evident from Figure 12 that increasing the core material content (stainless-steel) reduces the dry heat resistance of cut protective fabric. A higher proportion of core material contributes to a decrease in fabric bulk density, which is also mentioned in Table 4. Fabric specimens SSS30 and SZS30 exhibit the maximum dry heat resistance. This phenomenon may be explained in terms of bulk density. Both fabric specimens possess a higher bulk density. Fabrics that possess a higher bulk density typically have a

more compact structure and less air permeability. The higher density of the fabric reduces the number of air pockets, which in turn improves its insulating properties by minimizing heat transfer. On the other hand, it was also observed that S-S twisted yarn made fabrics have a higher thermal resistance than the S-Z twisted yarn made fabrics. The direction of twist has an impact on the yarn's structure and tightness. While S-Z twist can produce more open and elastic yarns, S-S twist tends to produce more compact and denser yarns. This structural variation affects a fabric's resistance to dry heat. A one-way ANOVA test was also performed to investigate how the core material (stainless-steel content) and yarn structural factors affected dry heat resistance. Table 11 indicates a significant p-value.

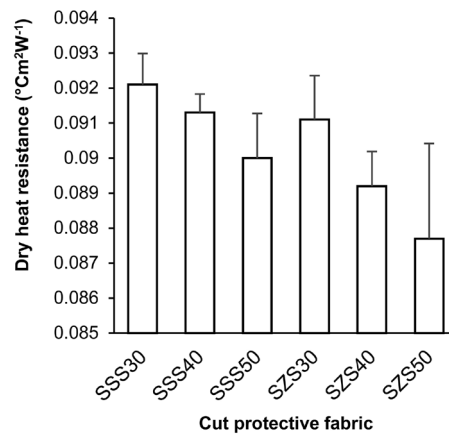


Figure 12: Influence of core material content (stainless-steel) and yarn structural parameters on dry heat resistance

Table 11: ANOVA test for the impact of core material (stainless-steel content) and yarn structural parameters on dry heat resistance

Source of variation	SS	df	MS	F	p-value	F _{critical}
Between groups	0.000116	5	2.32×10^{-5}	9.72364	1.85×10^{-6}	2.408514
Within groups	0.000115	48	2.39×10^{-6}			

Effect of glass content

Figure 13 shows that an increase in the percentage of core material (glass) leads to a decrease in the fabric's resistance to dry heat. A higher amount of

core material leads to a reduction in the bulk density of the fabric, as seen in Table 4. The fabric samples SSG10 and SZG10 demonstrate the highest level of resistance to dry heat. This phenomenon can be

elucidated concerning bulk density. Both fabric samples have a greater bulk density. Fabrics with a higher bulk density often have a denser structure and lower air permeability. The increased density of the cloth decreases the quantity of air pockets, hence enhancing its insulating characteristics by minimizing heat transmission. Conversely, clothing manufactured from S-S twisted yarn has superior thermal resistance compared to fabrics created from S-Z twisted yarn. The orientation of the spiral has a significant effect on the composition and tautness of the yarn. While the S-Z twist can result in yarns that have a looser and more stretchy structure, the S-S twist tends to create yarns that are more tightly packed and denser. This diversity in structure impacts the fabric's ability to heat transfer. A one-way ANOVA test was also performed to examine the

impact of yarn structural characteristics and core material percentage on dry heat resistance. Table 12 shows that the p-value is statistically significant.

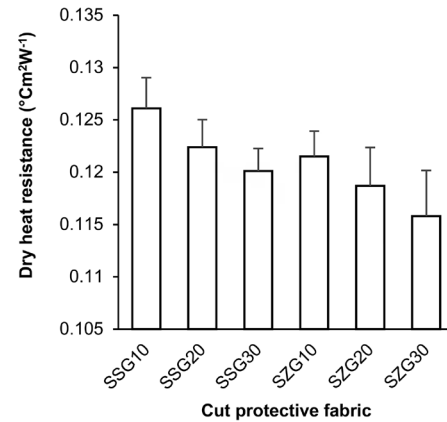


Figure 13: Influence of core material content (glass) and yarn structural parameters on dry heat resistance

Table 12: ANOVA test for the impact of core material (glass content) and yarn structural parameters on dry heat resistance

Source of variation	SS	df	MS	F	p-value	F _{critical}
Between groups	0.000306	5	6.11×10^{-5}	5.019531	0.002748	2.620654
Within groups	0.000292	24	1.22×10^{-5}			

3.5 Evaporative heat resistance

A material's water vapour resistance tells us how resistant it is to letting water vapour pass through, relative to air properties. This feature has a major effect on how people perceive warmth and coldness. Humans produce moisture by sweating to keep the skin dry and stop the garment from sticking to their

skin, which lowers stress levels [41]. The comfort attributes of textiles are affected by their water vapour resistance, with a preference for fabrics that have low water vapour resistance and promote sweating. The resistance to water vapour is affected by variables such as the fabric thickness and bulk density [42].

Table 13: Water vapour resistance of the different cut protective fabric [20]

R _{et} range (m ² Pa/W)	Performance	Specimen
0–6	Very good or extremely breathable. Comfortable at higher activity rate. Good or very breathable	–
6–13	Good or very breathable. Comfortable at moderate activity rate	SSS30, SSS40, SSS50, SZS30, SZS40, SZS50, SSG10, SSG20, SSG30, SZG10, SZG20, SZG30
13–20	Satisfactory or breathable. Uncomfortable at high activity rate	–
30+	Unsatisfactory or not breathable. Uncomfortable and short tolerance time	–

Effect of stainless-steel content

Figure 14 shows that cut protective fabric’s evaporative heat resistance decreases when the core material content (stainless-steel) is increased. Table 4 shows that a higher core material percentage lowers fabric bulk density. SSS30 and SZS30 fabrics tolerate evaporative heat well. This can be explained by bulk density. Bulk density is greater in both fabrics. Denser fabrics are more compact and less air permeable. The fabric’s increased density decreases air pockets, thereby reducing heat transmission and improving insulation. Moreover, S-S twisted yarn fabrics have stronger heat resistance than S-Z fabrics. Twist direction affects yarn structure and tightness. An S-Z twist produces open, elastic yarns, whereas an S-S twist produces denser, compact yarns. Structural diversity impacts fabric evaporative heat resistance. Table 13 presents the water vapour resistance rating and the level of comfort attained by the wearer, as determined by the Hohenstein Institute’s comfort rating system [20]. Table 13 indicates that all fabrics were assigned ratings within the range of 6–13.

This findings suggest that these fabrics exhibit a satisfactory level of comfort when utilized as cut protective workwear. A one-way ANOVA test was also performed to investigate how core material (stainless-steel content) and yarn structural characteristics affect evaporative heat resistance. Table 14 indicates a significant p-value.

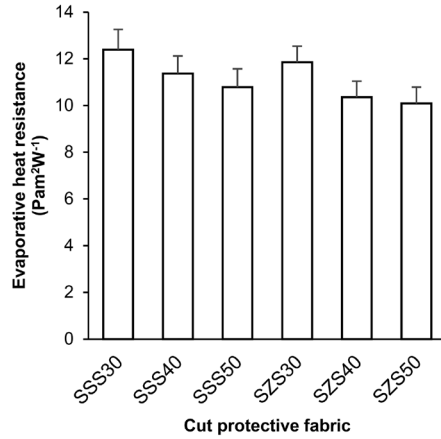


Figure 14: Influence of core material content (stainless-steel) and yarn structural parameters on evaporative heat resistance

Table 14: ANOVA test for the impact of core material (stainless-steel content) and yarn structural parameters on evaporative heat resistance

Source of variation	SS	df	MS	F	p-value	F _{critical}
Between groups	19.79098	5	3.958197	5.619742	0.001445	2.620654
Within groups	16.90411	24	0.704338			

Effect of glass content

Figure 15 and Table 13 show that the R_{et} values of the cut protective fabric SSG10 and SZG10 showed a similar trend that was comparable to the R_{ct} . It is possible to explain the higher R_{et} values of the cut protective fabric by pointing to their increased bulk density. Comparing the R_{ct} and R_{et} values to the fabric’s air permeability, the latter revealed a reversal trend. Clothing manufactured from S-S twisted yarn has superior thermal resistance compared to fabrics created from S-Z twisted yarn, as seen in Figure 15. Fabrics produced from yarns with an S-S twist have a higher density and a more tightly packed structure.

The configuration of this structure can impact a fabric’s ability to absorb and release moisture. S-S twist yarns have lesser moisture absorption than S-Z twist yarns, which may result in a slower rate of moisture drainage from the fabric. Table 13 shows the water vapour resistance rating and the level of comfort attained by the wearer, as determined by the Hohenstein Institute’s comfort rating system [20]. Table 13 shows that all fabrics were assigned ratings within the range of 6–13. The findings suggest that these fabrics exhibit a satisfactory level of comfort when utilized as cut protective workwear. A one-way

ANOVA test was used to investigate the influence of the core material (glass content) and yarn structural factors on evaporative heat resistance. According to Table 15, the p-value is significant.

Table 15: ANOVA test for the impact of core material (glass content) and yarn structural parameters on evaporative heat resistance

Source of variation	SS	df	MS	F	p-value	F _{critical}
Between groups	2.492258	5	0.498452	5.594945	0.001483	2.620654
Within groups	2.1381512	24	0.08909			

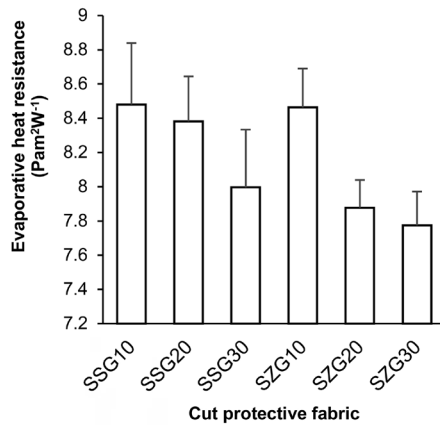


Figure 15: Influence of core material content (glass) and yarn structural parameters on evaporative heat resistance

3.6 Thermal conductivity

Thermal conductivity plays a crucial role in thermo-physiological comfort, which refers to how individuals subjectively perceive their comfort levels in their thermal environment. There is a relationship between the thermal conductivity of materials and the body's capacity to control its temperature. Apparel with effective thermal conductivity management can help regulate body temperature, reducing the risk of overheating or chilling, and enhancing comfort in different weather conditions. Thermal conductivity determines the speed at which heat is transferred through substances. The thickness and density of the fabric affect the thermal conductivity of clothes.

Effect of stainless-steel content

It is evident from Figure 16 that the test findings indicated that thermal conductivity diminishes as the percentage of core material increases. The increasing proportion of core material leads to an improvement in fabric thickness and a reduction in bulk density. Fabric specimens SSS50 and SZS50 possess higher thickness and lower bulk density, resulting in better performance in terms of thermal conductivity, which can also be seen in Figure 16. Fabrics with greater thickness typically exhibit reduced thermal conductivity due to their enhanced ability to insulate against heat transfer. Fabrics with a higher thickness possess a larger quantity of air that becomes entrapped within them, thereby functioning as a thermal insulator. The presence of trapped air within the fabric hinders the transfer of heat, leading to a decrease in thermal conductivity [43]. It was also observed that fabric made with S-S twisted yarn exhibits higher thermal conductivity than S-Z twisted yarn fabrics. S-S twist yarns generally exhibit a higher density and a more compact structure than S-Z twist yarns. The higher density of S-S twist yarns might limit the airflow within the fabric, thus impacting its thermal conductivity. Fabrics with higher bulk density exhibit reduced thermal conductivity due to the presence of fewer air spaces, which limits the flow of heat. A one-way ANOVA test was also performed to examine the impact of the yarn structural characteristics and the core material (stainless-steel content) on thermal conductivity. Table 16 indicates that the p-value is significant.

Table 16: ANOVA test for the impact of core material (stainless-steel content) and yarn structural parameters on thermal conductivity

Source of variation	SS	df	MS	F	p-value	F _{critical}
Between groups	3.06×10^{-5}	5	6.13×10^{-6}	90.82325	8.66×10^{-15}	2.620654
Within groups	1.62×10^{-6}	24	6.75×10^{-8}			

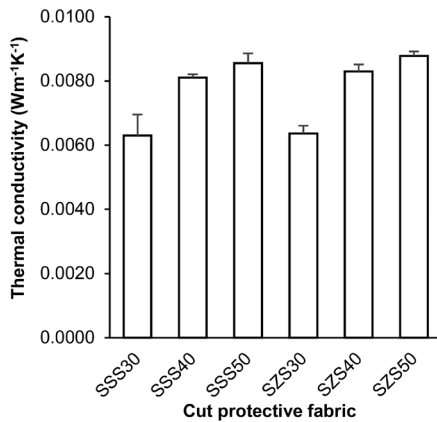


Figure 16: Influence of core material content (stainless-steel) and yarn structural parameters on thermal conductivity

Effect of glass content

According to Figure 17, the test results showed that thermal conductivity decreases as the proportion of core material increases. An increasing amount of core material results in enhanced fabric thickness and decreased bulk density. Fabric specimens SSG30 and SZG30 exhibit greater thickness and lower bulk density, leading to superior thermal conductivity performance, as seen in Figure 17. Thicker fabrics often have lower thermal conductivity because they are better at insulating against heat transfer. Fabrics with greater thickness contain a higher amount of trapped air, which acts as a thermal insulator. The existence of entrapped air within a fabric obstructs

the flow of heat, resulting in a reduction in thermal conductivity [44]. It was observed that fabric manufactured with S-S twisted yarn has a greater heat conductivity than textiles made with S-Z twisted yarn. S-S twist yarns often have a greater density and a more condensed structure than S-Z twist yarns. The increased density of S-S twist yarns may restrict the movement of air within the fabric, thus affecting its heat conductivity. Fabrics with greater bulk density demonstrate less thermal conductivity as a result of having fewer air gaps, which restricts the transfer of heat. A one-way ANOVA test was also done to determine how the core material (glass content) and yarn structural factors affected the ability to transfer heat. Table 17 shows that the p-value is significant.

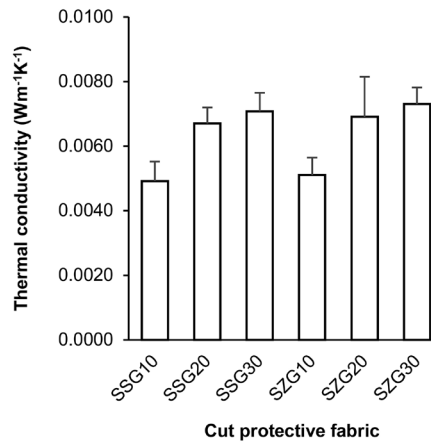


Figure 17: Influence of core material content (glass) and yarn structural parameters on thermal conductivity

Table 17: ANOVA test for the impact of core material (glass content) and yarn structural parameters on thermal conductivity

Source of variation	SS	df	MS	F	p-value	F _{critical}
Between groups	2.78×10^{-5}	5	5.55×10^{-6}	8.80317	7.49×10^{-5}	2.620654
Within groups	1.51×10^{-5}	24	6.31×10^{-7}			

3.7 Moisture permeability index

The water vapour permeability index evaluates a fabric's capacity to facilitate the passage of water vapour (perspiration) through it. Fabrics having a greater water vapour permeability index facilitate the evaporation of moisture, thus improving moisture management. Ensuring dryness next to the skin is essential for avoiding discomfort, such as clamminess or stickiness.

Effect of stainless-steel content

The moisture permeability index was computed for each fabric, in addition to the R_{ct} and R_{et} values. This index spans from 0 to 1. Figure 18 presents the impact of core material content (stainless-steel) and yarn structural parameter on the moisture permeability index, where SSS30 and SZS30 exhibit the lowest moisture vapour permeability index value. This may be attributed to the bulk density and yarn structural parameters. Fabrics that possess a greater bulk density often have a more compact structure, with a reduced number and size of pores or spaces between the fibres. The increased density of this structure might impede the passage of moisture vapour through the fabric, thus decreasing its permeability. Consequently, textiles that have a greater density are likely to have lower moisture vapour permeability index values, which suggests that they have a reduced ability to transmit moisture vapour. It is also evident from Figure 18 that S-Z twisted

yarn made fabrics performs better than S-S twisted yarn produced clothing in terms of moisture vapour permeability. Yarns that have an S-Z twist tend to produce a fabric structure that is more relaxed and has larger gaps between the threads. This configuration enables enhanced air circulation and promotes the transmission of moisture vapour throughout the cloth. Fabrics containing yarns with an S-Z twist generally exhibit increased water vapour permeability, as indicated by their higher moisture vapour permeability values. A one-way ANOVA test was also performed to determine how the yarn structural factors and core material (stainless-steel percentage) affected moisture permeability. Table 18 shows that the p-value is statistically significant.

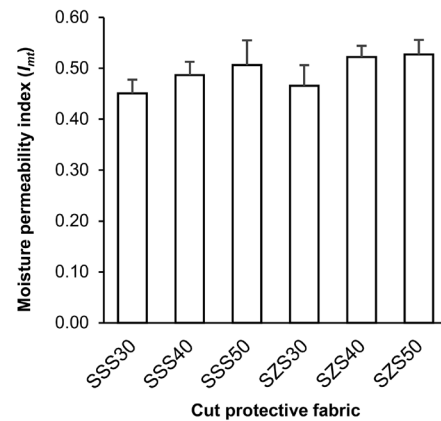


Figure 18: Influence of core material content (stainless-steel) and yarn structural parameters on moisture permeability index

Table 18: ANOVA test for the impact of core material (stainless-steel content) and yarn structural parameters on the moisture permeability index

Source of variation	SS	df	MS	F	p-value	F _{critical}
Between groups	0.024017	5	0.004803	3.422803	0.017833	2.620654
Within groups	0.03368	24	0.001403			

Effect of glass content

The water vapour permeability index was obtained for each fabric, together with the R_{ct} and R_{et} values. This index ranges from 0 to 1. Figure 19 illustrates the relationship between the percentage of core material (glass) and the structural characteristic of the

yarn on the moisture permeability index. It shows that SSG10 and SZG10 have the lowest water vapour permeability index value. This can be ascribed to the bulk density and structural characteristics of the yarn. Fabrics with a higher bulk density often have a denser structure, characterized by fewer

and smaller pores or gaps between the fibres. The increased density of this structure might hinder the flow of moisture vapour through the cloth, thus reducing its permeability. Therefore, fabrics with higher density tend to have lower moisture vapour permeability index values, indicating a decreased capacity to transport moisture vapour. Figure 19 shows that fabrics prepared from S-Z twisted yarn have a superior moisture vapour permeability than apparel produced from S-S twisted yarn. Yarns with an S-Z twist tend to create a fabric with a more relaxed structure and wider spaces between the threads. This arrangement facilitates improved air circulation and the diffusion of moisture vapour throughout the fabric. Fabrics that include yarns with an S-Z twist typically show higher levels of water vapour permeability, as seen by their elevated water vapour permeability ratings. A one-way ANOVA test was also performed to investigate how core material

(glass content) and yarn structural factors affected moisture permeability. Table 19 states a significant p-value.

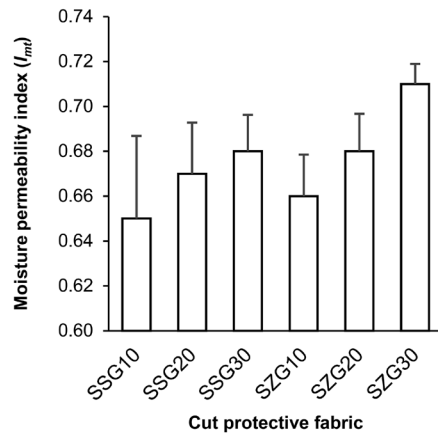


Figure 19: Influence of core material (glass content) and yarn structural parameters on moisture permeability index

Table 19: ANOVA test for the impact of core material (glass content) and yarn structural parameters on the moisture permeability index

Source of variation	SS	df	MS	F	p-value	F _{critical}
Between groups	0.01011	5	0.00202	3.407865	0.018169	2.620654
Within groups	0.01424	24	0.00059			

3.8 Contact angle (wettability)

The degree to which a liquid may spread across a surface is known as wettability, and it has a significant effect on how comfortable clothing is in terms of body temperature. Wettability affects the formation and maintenance of the microclimate that exists between the skin and clothing. Materials with a lower wettability may offer better ventilation and moisture vapour movement, maintaining a cosy microclimate around the skin. Conversely, fabrics with a high wettability may retain moisture and heat, which might be uncomfortable and even result in symptoms such as heat rash, chafing or worse [44].

Effect of stainless-steel content

According to Figure 20, the test results showed that the contact angle decreases as the proportion

of core material increases, which means improved wettability. An increasing amount of core material results in enhanced fabric thickness and decreased bulk density. Fabric specimens SSS30 and SZS30 exhibit a lower contact angle, as seen in Figure 20. These fabric specimens have a higher bulk density. Surfaces of fabrics with higher bulk densities are often denser and smoother. When exposed to liquids, this smoother surface may provide a reduced contact angle, suggesting increased wettability. Liquids have an easier time spreading across the fabric's surface, which speeds up absorption and may increase moisture retention. Conversely, S-S twisted yarn made fabric demonstrates a lower contact angle than S-Z twisted yarn produced fabric. Yarns that have an S-S twist typically lead to a more compact and closely

woven fabric structure. The increased density of this structure results in a more even fabric surface with less imperfections. When liquids are applied, smoother surfaces often exhibit lower contact angles, which indicates greater wettability. S-S twist yarns enhance the ability of liquids to disperse across fabric surfaces, resulting in quicker absorption and perhaps increased moisture retention. A one-way ANOVA test was used to determine the influence of the core material (stainless-steel content) and yarn structural characteristics on wettability. According to Table 20, the p-value is statistically significant.

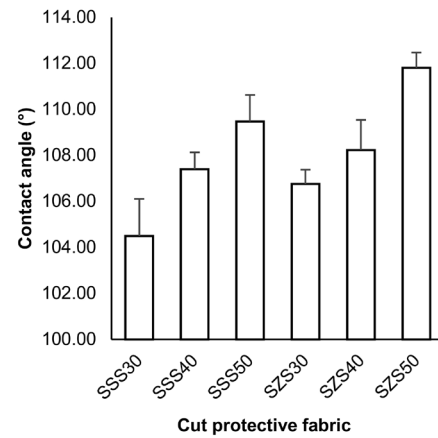


Figure 20: Influence of core material content (stainless-steel) and yarn structural parameters on wettability

Table 20: ANOVA test for the impact of core material (stainless-steel content) and yarn structural parameters on wettability

Source of variation	SS	df	MS	F	p-value	F _{critical}
Between groups	152.9957	5	30.59915	20.97844	4.75×10^{-8}	2.620654
Within groups	35.0064	24	1.4586			

Effect of glass content

Figure 21 indicates that the test results demonstrate a reduction in the contact angle as the amount of core material rises, indicating enhanced wettability. An increase in the core material leads to increased fabric thickness and reduced bulk density. The fabric specimens SSG10 and SZG10 showed a reduced contact angle. These fabric samples have a higher bulk density. Fabrics with higher bulk densities typically exhibit more density and smoother surfaces. When in contact with liquids, the smoother surface may have a lower contact angle, indicating enhanced wettability. Fluids exhibit greater surface tension on fabric, facilitating rapid absorption and potentially enhancing moisture retention. On the other hand, fabric manufactured from S-S twisted yarn has a

lower contact angle than fabric made from S-Z twisted yarn. Yarns with an S-S twist generally result in a denser and tightly woven fabric structure. The heightened density of this structure yields a more uniform cloth surface with less flaws. Applying liquids to smoother surfaces typically results in lower contact angles, indicating increased wettability. S-S twist yarns improve the wicking properties of fabrics, allowing liquids to spread more easily across the surface and be absorbed faster, perhaps leading to greater moisture retention. A one-way ANOVA test was also performed to determine how the core material (glass content) and yarn structure factors affected the ability to absorb water. Table 21 shows that the p-value is significant.

Table 21: ANOVA test for the impact of core material (glass content) and yarn structural parameters on wettability

Source of variation	SS	df	MS	F	p-value	F _{critical}
Between groups	294.331	5	58.8662	56.56631	1.7×10^{-12}	2.620654
Within groups	24.9758	24	1.040658333			

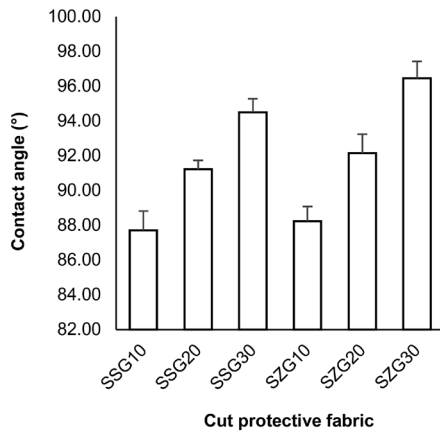


Figure 21: Influence of core material content (glass) and yarn structural parameters on wettability

3.9 Moisture wicking

Effective moisture wicking is crucial for improving the comfort of clothing by efficiently controlling moisture. The combined action of moisture wicking and evaporation results in a cooling sensation as moisture is extracted from the skin and heat is dissipated through evaporation. The cooling effect is especially advantageous during physical activity or in hot environments, thus aiding in the prevention of heat stress and maintaining a level of comfort.

Effect of stainless-steel content

Figure 22 presents the impact of core material content (stainless-steel) and yarn structural parameters on moisture wicking in the warp and weft direction. It can also be observed from Figure 22 that fabric sample SZS 30 performs better in terms of moisture

wicking height due to its bulk density, as seen in Table 5. Fabric specimens with a higher bulk density perform better in terms of moisture wicking. Fabrics with a higher bulk density often exhibit a more condensed and tightly packed structure, characterized by narrower gaps between individual fibres. The increased density of this structure facilitates capillary action, which refers to the fabric’s capacity to absorb moisture using small channels or capillaries present inside it. Moisture may be transported more effectively to the outside surface of the cloth for evaporation as it travels through these capillaries. It is also evident from Figures 22 a) and 22 b) that the S-Z twist direction of yarn has a greater influence on moisture wicking property than the S-S twist direction. Yarns that have an S-Z twist tend to create a fabric with a more porous and relaxed structure. This structure has the ability to generate larger capillaries and channels inside the fabric, which allows for the more effortless passage of moisture through the fabric. Fabrics with S-Z twist yarns often exhibit superior moisture wicking properties as a result of their heightened capacity to efficiently move moisture from the skin to the outside surface of the fabric. A one-way ANOVA test was also performed to examine the impact of the yarn structural parameters (warp and weft direction) and the core material (stainless-steel content) on moisture wicking. Fabric sample SZS 30 performs better in terms of moisture wicking height due to its bulk density, as seen in Table 5. Tables 22 and 23 show that the p-value is significant.

Table 22: ANOVA test for the impact of core material (stainless-steel content) and yarn structural parameters on moisture wicking (warp direction)

Source of variation	SS	df	MS	F	p-value	F _{critical}
Between groups	63	5	12.6	5.4	0.003315	2.772853
Within groups	42	18	2.333333			

Table 23: ANOVA test for the impact of core material (stainless-steel content) and yarn structural parameters on moisture wicking (weft direction)

Source of variation	SS	df	MS	F	p-value	F _{critical}
Between groups	58.25	5	11.65	4.003819	0.012844	2.772853
Within groups	52.375	18	2.909722			

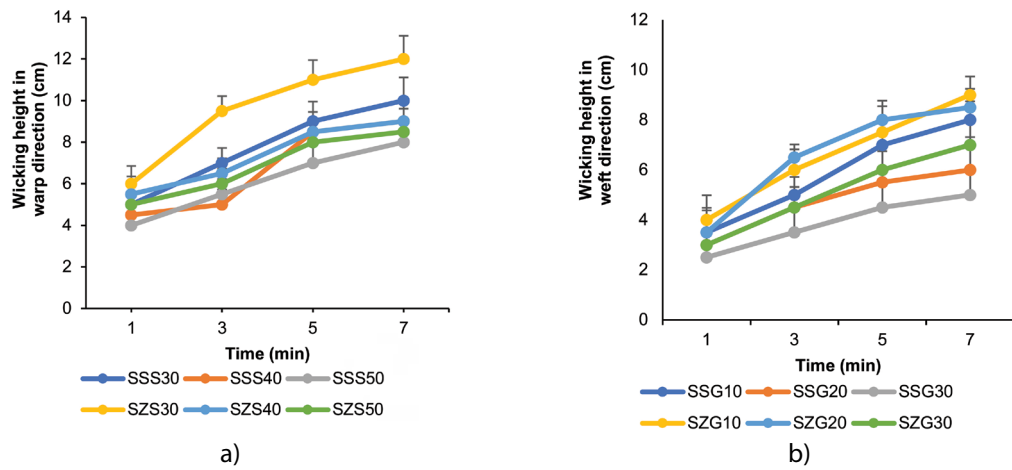


Figure 22: Influence of core material content (stainless-steel) and yarn structural parameters on moisture wicking: a) warp direction b) weft direction

Effect of glass content

Figure 23 illustrates the influence of the content of core material (specifically stainless-steel) and the structural characteristics of the yarn on the ability to absorb moisture in warp and weft directions. The figure shows that the fabric sample SZG 10 performs better in terms of moisture wicking height due to its bulk density, as seen in Table 6. Fabric specimens with a higher bulk density exhibit superior performance in terms of moisture wicking. Fabrics with a higher bulk density often have a more compact and tightly woven structure, which is characterised by fewer spaces between the individual threads. The higher density of this structure enhances capillary action, which is the ability of the fabric to absorb moisture through tiny pores or capillaries inside it. Moisture may be carried more efficiently to the outside surface of the fabric for evaporation as it moves through these capillaries. The impact of the S-Z twist

direction of yarn on the moisture wicking characteristic is more significant than that of the S-S twist direction, as seen in Figures 23 a) and b). Yarns with an S-Z twist tend to produce a fabric that is more permeable and has a looser structure. This structure possesses the capacity to produce larger capillaries and channels inside the fabric, facilitating the easier flow of moisture through the fabric. Fabrics with S-Z twist yarns frequently have enhanced moisture wicking characteristics due to their increased ability to effectively transport moisture from the skin to the external surface of the fabric. In order to examine the impact of the core material (glass content) and the structural characteristics of the yarn on moisture wicking in both the warp and weft directions, a one-way ANOVA test was conducted. Based on the data presented in Tables 24 and 25, the p-value demonstrates statistical significance.

Table 24: ANOVA test for the impact of core material (glass content) and yarn structural parameters on moisture wicking (warp direction)

Source of variation	SS	df	MS	F	p-value	F _{critical}
Between groups	25.5	5	5.1	3.221053	0.029905	2.772853
Within groups	28.5	18	1.583333			

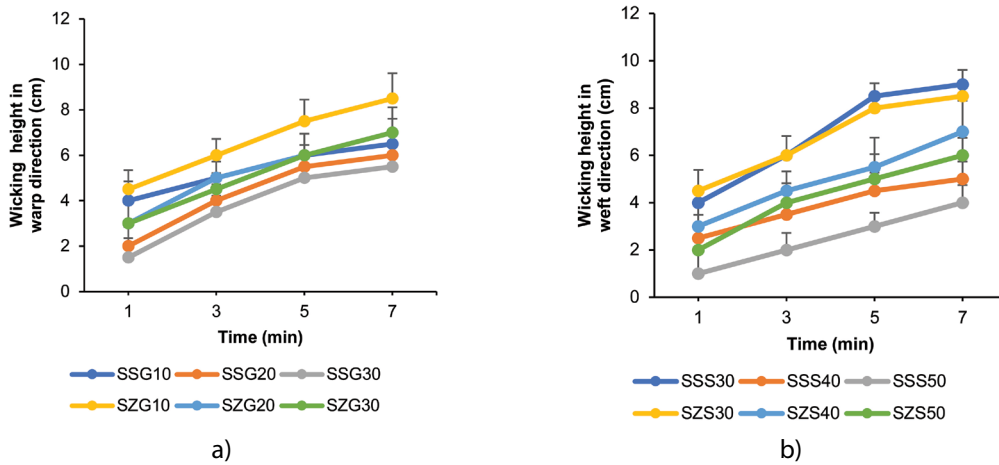


Figure 23: Influence of core material (glass content) and yarn structural parameters on moisture wicking in: a) warp direction b) weft direction

Table 25: ANOVA test for the impact of core material (glass content) and yarn structural parameters on moisture wicking (weft direction)

Source of variation	SS	df	MS	F	p-value	F _{critical}
Between groups	11.83333333	5	2.366667	2.84	0.046229	2.772853
Within groups	15	18	0.833333			

4 Conclusion

The objective of this study was to explore the thermo-physiological comfort characteristics of cut protective woven with filament twisted core sheath yarns, with the intention of using them to produce cut protective workwear fabrics. UHMWPE and PES filament fibres were used as the sheath and stainless-steel and glass filaments as the core to produce filament twisted core sheath yarns using a HKV141 hollow spindle wrapping machine. The fabricated filament twisted core sheath yarns were used to weave the cut protective fabrics, and the impact of the percentage of core material and yarn structural properties on the thermo-physiological comfort characteristics were analysed. Fabric sample SZS50 and SZG30 demonstrated higher values for air permeability, thermal conductivity and moisture permeability. On the other hand, fabric sample SZS30 and SZG10 performed better in terms of dry and evaporative heat resistance, wettability and

moisture wicking. Fabric with a higher thickness and lower bulk density performed better in terms of cut protection, with a moderate comfort level. On the other hand, the fabric produced from a coarser count with an S-Z twisted direction of yarns with less bulk density exhibited satisfactory results in thermophysiological comfort attributes, including air permeability, thermal conductivity, dry and evaporative heat resistance, moisture permeability, moisture wicking and wettability. Fabrics with a higher thickness and lower bulk density from the filament twisted core sheath yarns can be selected as cut protective workwear for better cut protection and enhanced thermo-physiological comfort. The fabrics mentioned above, which possess excellent cut protection and comfort features, are highly recommended for workwear, protective sleeves, military uniforms, cut-proof aprons and other similar applications.

Funding

This work was financially supported by the National Technical Textiles Mission, Ministry of Textiles, Government of India (Project Code: IITD/IRD/RP04561).

References

- HOLMER, I. Protective clothing in hot environments. *Industrial Health*, 2006, **44**(3), 404–413, doi: 10.2486/indhealth.44.404.
- Human thermal environments: the effects of hot, moderate, and cold environments on human health, comfort, and performance (3rd ed.)*. Edited by K. Parsons. Boca Raton : CRC Press, 2014, doi: 10.1201/b16750.
- LI, D.X. *Cut protective textiles*. Cambridge : Woodhead Publishing, 2020.
- DORMAN, L.E., HAVENITH, G. The effects of protective clothing on metabolic rate. In *Proceedings of 11th International Conference on Environmental Ergonomics*, 2005, 82–85 [online]. Loughborough University [accessed 11.9.2024]. Available on World Wide Web: <<https://hdl.handle.net/2134/2553>>.
- DORMAN, L.E., HAVENITH, G. The effects of protective clothing on energy consumption during different activities. *European Journal of Applied Physiology*, 2009, **105**(3), 463–470, doi: 10.1007/s00421-008-0924-2.
- HOLMER, I. Protective clothing and heat stress. *Ergonomics*, 1995, **38**(1), 166–182, doi: 10.1080/00140139508925093.
- RATHOUR, R., DAS, A., ALAGIRUSAMY, R. Studies on the influence of process parameters on the protection performance of the outer layer of fire-protective clothing. *Journal of Industrial Textiles*, 2022, **51**, 8107S–8126S, doi: 10.1177/15280837211054582.
- RATHOUR, R., DAS, A., ALAGIRUSAMY, R. Impact of repeated radiative heat exposure on protective performance of firefighter's protective clothing. *Journal of Industrial Textiles*, 2022, **52**, 1–30, doi: 10.1177/15280837221117610.
- PEASE, A.L. *Heat stress evaluation of protective clothing ensembles: Master Thesis*. Department of Environmental Occupational Health College of Public Health University of South Florida, 2010, <https://digitalcommons.usf.edu/etd/3485>.
- RAJPUT, B., MAHESH, N., RATHOUR, R., DAS, T., RAY, B., DAS, A., TALUKDAR, P. Performance analysis of multilayer flame-retardant fabric ensembles for different exposure conditions using numerical modeling. *The Journal of Industrial Textiles*, 2022, **115**(2), 218–227, doi: 10.1080/00405000.2022.2156717.
- FU, M., WENG, W., YUAN, H. Quantitative assessment of the relationship between radiant heat exposure and protective performance of multilayer thermal protective clothing during dry and wet conditions. *Journal of Hazardous Materials*, 2014, **276**, 383–392, doi: 10.1016/j.jhazmat.2014.05.056.
- O'BRIEN, C., BLANCHARD, L.A., CADARETTE, B.S., ENDRUSICK, T., XU, X., BERGLUND, L., SAWKA, M.N., HOYT, R.W. Methods of evaluating protective clothing relative to heat and cold stress: thermal manikin, biomedical modeling, and human testing. *Journal of Occupational and Environmental Hygiene*, 2011, **8**(10), 588–599, doi: 10.1080/15459624.2011.613291.
- KOFLER, P., HERTEN, A., HEINRICH, D., BOTTONI, G., HASLER, M., FAULHABER, M., BECHTOLD, T., NACHBAUER, W., BURTSCHER, M. Viscose as an alternative to aramid in workwear: influence on endurance performance, cooling, and comfort. *Textile Research Journal*, 2013, **83**(19), 2085–2092, doi: 10.1177/0040517513487784.
- YOO, S., BARKER, R.L. Comfort properties of heat-resistant protective workwear in varying conditions of physical activity and environment. Part I: thermophysical and sensorial properties of fabrics. *Textile Research Journal*, 2005, **75**(7), 523–530, doi: 10.1177/0040517505053949.

15. YOO, S., BARKER, R.L. Comfort properties of heat resistant protective workwear in varying conditions of physical activity and environment. Part II: perceived comfort response to garments and its relationship to fabric properties. *Textile Research Journal*, 2005, **75**(7), 531–539, doi: 10.1177/0040517505054190.
16. LEVINE, L., SAWKA, M.N., GONZALEZ, R.R. Evaluation of clothing systems to determine heat strain. *American Industrial Hygiene Association Journal*, 1998, **59**(8), 557–562, doi: 10.1080/15428119891010730.
17. SURI, M., RASTOGI, D., KHANNA, K., CHAKRABORTY, M. Development of protective clothing for pesticide industry. Part I: assessment of various finishes. *Indian Journal of Fibre & Textile Research*, 2002, **27**(1), 85–90.
18. MOHAMMADI, R.A., SHIRAZI, M., MOAREF, R., JAMALPOUR, S., TAMSILIAN, Y., KIASAT, A. Protective smart textiles for sportswear. In *Protective textiles from natural resources*. Edited by Md. Ibrahim H. MONDAL. Cambridge : Woodhead Publishing, 2022, 317–345, doi: 10.1016/B978-0-323-90477-3.00025-0.
19. MISHRA, K., DEDHIA, E. Balancing aesthetics, and functionality with comfort: compliance-friendly protective clothing. *International Journal of Home Science*, 2022, **8**(3), 7–15, doi: 10.22271/23957476.2022.v8.i3a.1342.
20. Wear comfort [Online]. Hohenstein [accessed 20 July 2024]. Available on World Wide Web: <<https://www.hohenstein.in/en-in/expertise/performance/comfort>>.
21. BARTKOWIAK, G. Liquid sorption by nonwovens containing superabsorbent fibers. *Fibres and Textiles in Eastern Europe*, 2006, **14**(1), 57–61.
22. GUIDOTTI, T.L. Human factors in firefighting: ergonomic-, cardiopulmonary-, and psychogenic stress related issues. *International Archives of Occupational and Environmental Health*, 1992, **64**, 1–12, doi: 10.1007/BF00625945.
23. NAYAK, R., PUNJ, S.K., CHATTERJEE, K.N., BEHRA, B.K. Comfort properties of suiting fabrics. *Indian Journal of Fibre & Textile Research*, 2009, **34**, 122–128.
24. SLATER, K. Comfort properties of textiles. *Textile Progress*, 1977, **9**(4), 1–70, doi: 10.1080/00405167.1977.10750095.
25. YAN, D., HAO, A. Functional protective clothing and new material application. *Cotton Textile Technology*, 2012, **40**(2), 65–68.
26. RATHOUR, R., DAS, A., ALAGIRUSAMY, R. Study on the influence of constructional parameters on performance of outer layer of thermal protective clothing. *The Journal of Textile Institute*, 2023, **114**(9), 1336–1346, doi: 10.1080/00405000.2022.2124650.
27. RATHOUR, R., DAS, A., ALAGIRUSAMY, R. Water vapor transmission and electromagnetic shielding characteristics of stainless steel/viscose blended yarn woven fabrics. *Journal of Industrial Textiles*, 2023, **53**(2), 1–20, doi: 10.1177/15280837221149217.
28. ZHOU, H., HUANG, X., FU, Y. A comparative study of China and Europe personal protective equipment standards. *China Personal Protective Equipment*, 2014, **2**, 26–41.
29. KIM, J. O., SPIVA, S.M. Dynamic moisture vapor transfer through textile Part II: Further techniques for microclimate moisture and temperature measurement. *Textile Research Journal*, 1994, **64**(2), 112–121, doi: 10.1177/004051759406400207.
30. DUTSCHK, V., SABBATOYSKIY, K.G., STOLZ, M., GRUNDKE, K., RUDOYR, V.M. Unusual wetting dynamics of aqueous surfactant solutions on polymer surfaces. *Journal of Colloid and Interface Science*, 2003, **267**(2), 456–462, doi: 10.1016/S0021-9797(03)00723-9.
31. SENGUPTA, A.K., SREENIVASA MURTHY, H.V. Wicking in ring spun vis- α -vis rotor spun yarns. *Indian Journal of Fibre & Textile Research*, 1985, **10**, 155–157.
32. DAS, A., ALAGIRUSAMY, R., KUMAR, K.P. Study of heat transfer through multilayer

- clothing assemblies: a theoretical prediction. *Autex Research Journal*, 2011, **11**(2), 54–60, doi: 10.1515/aut-2011-110205.
33. HOUSHYAR, S., PADHYE, R., NAYAK, R. Effect of moisture-wicking materials on the physical and thermophysiological comfort properties of firefighters' protective clothing. *Fibers and Polymers*, 2017, **18**(2), 383–389, doi: 10.1007/s12221-017-6746-2.
34. EN 388. Protective gloves against mechanical risks. Plzen : European Standard, 2016, 1-2.
35. The science of cut protection [online]. Dupont [accessed 20 July 2024]. Available on World Wide Web: <<https://www.rpta.org/safety/1Kevlar.pdf>>.
36. JHANJI, Y., GUPTA, D., KOTHARI, V.K. Thermal and mass transport properties of polyester-cotton plated fabrics in relation to back layer fibre profiles and face layer yarn types. *Journal of Industrial Textiles*, 2018, **109**(5), 669–676, doi: 10.1080/00405000.2017.1363948.
37. BIVAINYTĖ, A., MIKUČIONIENĖ, D., KERPUSKAS, P. Investigation on thermal properties of double-layered weft knitted fabrics. *Materials Science*, 2012, **18**(2), 167–171, doi: 10.5755/j01.ms.18.2.1921.
38. ONOFREI, E., ROCHA, A.M., CATARINO, A. The influence of knitted fabrics' structure on the thermal and moisture management properties. *Journal of Engineered Fibers and Fabrics*, 2011, **6**(4), 10–22, doi: 10.1177/155892501100600403.
39. SONG, G., PASKALUK, S., SATI, R., CROWN, E.M., DALE, J.D. Thermal protective performance of protective clothing used for low radiant heat protection. *Textile Research Journal*, 2011, **81**(3), 311–323, doi: 10.1177/0040517510380108.
40. *Textiles for protection*. Edited by R. A. Scott. Cambridge : Woodhead, 2005, 622–647.
41. BAGHERZADEH, R., GORJI, M., LATIFI, M., PAYYANDYP, P., KONG, L. Evolution of moisture management behavior of high-wicking 3D warp knitted spacer fabrics. *Fibers and Polymers*, 2012, **13**, 529–534, doi: 10.1007/s12221-012-0529-6.
42. HOUSHYAR, S., PADHYE, R., TROYNIKOV, O., NAYAK, R., RANJAN, S. Evaluation and improvement of thermo-physiological comfort properties of firefighters' protective clothing containing super absorbent materials. *The Journal of The Textile Institute*, 2015, **106**(12), 1394–1402, doi: 10.1080/00405000.2014.995930.
43. ISLAM, M.A., RATHOUR, R., AMIN, M.J.I., DAS, A., ALAGIRUSAMY, R. Protective and comfort performance of fire protective clothing. *Textile Leather Review*, 2024, **7**, 597–615, doi: 10.31881/TLR.2024.066.
44. DAS, B., DAS, A., KOTHARI, V.K., FANGUEIRO, R., de ARAÚJO, M. Moisture transmission through textiles. Part I: processes involved in moisture transmission and the factors at play. *Autex Research Journal*, 2007, **7**(2), 100–110, doi: 10.1515/aut-2007-070204.

Mehmet Karahan,^{1,2} Nevin Karahan¹

¹ Vocational School of Technical Sciences, Bursa Uludag University, 16059, Bursa, Türkiye

² Butekom Inc., Demirtas Dumlupinar OSB District, 2nd Cigdem Street No: 1/4, 16245, Osmangazi, Bursa, Türkiye

Stiffness Determination of Bi- and Triaxial Flat Braided Carbon/Vinyl Ester Composites Using Micromechanics Method

Določanje togosti kompozitov iz dvo- in triosnih ploskih pletiv iz ogljikovih vlaken in vinilestrske matrice z uporabo metode mikromehanike

Original scientific article/Izvirni znanstveni članek

Received/Prispelo 7–2024 • Accepted/Sprejeto 9–2024

Corresponding author/Korespondenčni avtor:

Prof. dr. Mehmet Karahan

E-mail: mkarahan@uludag.edu.tr

ORCID iD: 0000-0003-3915-5598

Abstract

This paper is concerned with geometric modelling and elastic properties of 2D biaxial and triaxial braided composites. A representative unit cell (RUC) of braid architectures is first identified along with its constituents. Geometric parameters of braided structures are compared with each other. A method of inclusions with the Mori-Tanaka homogenisation was used in the determination of elastic properties of the unit cell with the Tex-Comp software. As a result, a higher amount of crimp occurs in triaxial braided structures compared to biaxial structures generated using the same yarn and construction. Therefore, the elastic modulus of the triaxial structure diminishes compared to that of the biaxial structure. However, the axial yarn reinforcement in triaxial structures ensures four times higher axial strength in the axial direction related to the biaxial structures that it provides. The results were experimentally verified.

Keywords: carbon braided composites, modelling methodology, micromechanics

Izvleček

Avtor članka obravnava geometrijsko modeliranje in elastične lastnosti dvoosnih in triosnih pletenih kompozitov. Najprej je identificirana reprezentativna osnovna celica (RUC) pletenih struktur, vključno s sestavnimi deli. Primerjani so geometrijski parametri pletenih struktur. Pri določanju elastičnih lastnosti osnovne celice je bila s pomočjo programske opreme Tex-Comp uporabljena metoda vključkov z Mori-Tanaka homogenizacijo. Rezultati kažejo, da je pri triosnih pletenih strukturah več kodranja kot pri dvoosnih strukturah, izdelanih iz enakih prej in z enako vezavo. Zato se modul elastičnosti triosne strukture v primerjavi z dvoosno strukturo zmanjša. Kljub temu ojačitev v smeri osi preje pri triosnih strukturah zagotavlja štirikrat večjo trdnost v smeri kot pri dvoosnih strukturah. Rezultati so bili potrjeni s poskusi.

Ključne besede: pleteni kompoziti iz ogljikovih vlaken, metodologija modeliranja, mikromehanika



Content from this work may be used under the terms of the Creative Commons Attribution CC BY 4.0 licence (<https://creativecommons.org/licenses/by/4.0/>). Authors retain ownership of the copyright for their content, but allow anyone to download, reuse, reprint, modify, distribute and/or copy the content as long as the original authors and source are cited. No permission is required from the authors or the publisher. This journal does not charge APCs or submission charges.

1 Introduction

Braids are one of the most widely used reinforcements for textile composites. Braiding is the process of interlacing three or more threads in such a way that they cross one another in the diagonal formation. Flat, tubular or solid constructions may be formed in this way. Due to the fact that all fibres within a braided structure are continuous and mechanically locked, braid has a natural mechanism that evenly distributes load throughout the structure [1].

Biaxial braids are commonly defined as a $\pm 45^\circ$ orientation. The triaxial form involves adding a third set of yarns in the axial direction. This multidirectional braid achieves unidirectional and off-axis reinforcement within one layer. The introduction of the third set of axial yarns locks the diameter and stops the braid's natural tendency to expand and contract [1].

Two-dimensional braided structures are either biaxial or triaxial in configuration. The biaxial construction is most common and has two sets of yarns travelling in opposite directions, where yarns in one direction are passing under and over the other yarns. This is a popular structure as the construction is predictable, it has consistency in lay-up and the braid can match any shape. Biaxial braided sleeves can be draped over a mandrel with varying cross-sections without creating wrinkles [2, 3].

A triaxial braided fabric has basically three sets of yarns: braid (bias) and warp (axial). Braided yarns intertwine with each other around the axial yarns at an angle of about 45° , whereas axial yarns lie throughout in the structure. The intertwining is similar to that of a traditional braided fabric, which means $-$ braided yarns are above and below the $+$ braided yarns, and repeated throughout the fabric width and length [3, 4]. Axial yarns are often referred to as warp warp yarns. These warp yarns are not necessary for the braid formation; however, they provide the braid with its essential characteristics, e.g. tensile and compression strength in addition to an improved modulus in applications such as fibre-reinforced composites [5].

The microlevel scale of a textile composite is physically larger and geometrically more complex than a unidirectional composite. Even at the microscale, textile composites maintain a relatively complicated microstructure. Even under simple loading conditions, a textile microstress state will be shown to be quite complex, and elastic constants are non-uniform due to the waviness of a woven fibre tow. Laminate analysis, property homogenisation, and other common approaches will no longer apply. Thus, current designs of textile structures will not be optimised for maximum damage resistance and light-weight. Conventional micromechanics models for textile composites assume that the state of stress is uniform over a distance comparable to the dimensions of the representative unit cell (RUC). However, due to the complexity of the weave geometry, the size of RUC in textile composites can be large compared to structural dimensions. In such cases, severe non-uniformities in the stress state will exist and conventional models may fail [6].

Most of the micromechanics models are based on the well-known Classical Laminate Plate Theory (CLPT). Ishikawa and Chou [7–8] proposed and compared three stiffness and strength predictive models that formed the basis to many subsequent textile fabric composite models, i.e. the “mosaic”, “fibre undulation” and “bridging” models. The models use CLPT as the basis of the RUC analysis study. The properties of the unit cell are assumed to be representative of overall composites.

The internal geometry of textile reinforcement is an important factor of the reinforcement performance during composite manufacturing and in the service life of the composite material. For the former, impregnation of the reinforcement is governed by its porosity (size, distribution and connectivity of pores). For the latter, load transfer from the matrix to the reinforcement is governed by the fibre orientation, which plays a paramount role in the composite stiffness; stress–strain concentration loci, determining composite strength, is correlated with the resin rich zones and fibre/matrix interfaces, distributed

in the composite volume in accordance with the reinforcement geometry. When a 3D-shaped composite part is concerned, the reinforcement is locally deformed (compressed, stretched and sheared), and the geometrical model should account for this deformation.

A generalised description of the internal structure of a textile reinforcement has been developed in the university KU Leuven. It is the final result of a development that started in the middle of the 1990s with the work of Vandeurzen et al. [9, 10] on woven fabric composites and Gommers et al. [11] on knitted and woven fabric composites.

The major drawback of these early models was their dependency on empirically obtained descriptions of the textile internal geometry. This means that the textile first has to be produced and then measured, and that no predictions on the behaviour of yet non-existing textile composites can be made. In this way, the value of these predictive models is rather limited. A big development could be achieved when collaboration started with S. V. Lomov, who developed a model for the internal geometry of 2D- and 3D-weaves (the CETKA-model [12, 13]), based on a minimum number of topological data (weave style, inter-yarn distance) and yarn mechanical properties. The model is a mechanical model, as it applies a yarn deformation energy minimisation algorithm to predict the internal geometry of any 2D- and 3D-weave. Connecting this approach to the cell- or inclusion models of Gommers and Vandeurzen resulted in a more versatile way to calculate the homogenised properties of textile-based composites [14–18].

Since 1999, this approach has been systematically followed, extending the types of textiles to 2D- and

3D-woven [17–19], bi- and triaxial braided [20], weft-knitted [21] and non-crimp warp-knit stitched [22] fabrics and laminates [23]. The mechanical models not only generate the internal geometry of relaxed textiles, but also of textiles deformed in tension, compression and shear. The models are implemented in the software package Wise-Text.

A further step was the full integration of geometrical models with other predictive models relevant to composites processing and performance prediction. Permeability tensors can be predicted by modelling the resin flow through the reinforcement [24]; the homogenised mechanical properties, and the local stresses and strains can be generated by micromechanical calculations of properties of the composite [16, 17] and can then be further linked to a micro-macro analysis of the composite parts [25], finite element models [26–27] and virtual reality software [28]. The same model also has applications for both 2D- and 3D-woven composites [29–34]. All these models use a unified description of the geometry of the reinforcement unit cell.

The aim of the study was to analyse geometrically the triaxial and biaxial braided structures made of the same carbon tow and construction, and to model the unit cell of the structure. Furthermore, we focused on the generation of elastic properties of the unit cell impregnated with vinyl ester resin by using the micromechanics model.

2 Materials and methods

2.1 Biaxial and triaxial braided carbon/vinyl ester composites

The parameters of biaxial and triaxial dry preforms used in this study are shown in Tables 1 and 2.

Table 1: Parameters of biaxial and triaxial braided fabrics used in research [1]

Fabric type	Product code	Structure	Angle (°)	Yarn type (0/+45/–45)	Yield (m/kg)	Fabric areal density (g/m ²)
Biaxial	MR 4932	Regular braided	+45/–45	T700 12K/T700 12K	2.18	309
Triaxial	MR 4933	Regular braided	0/+45/–45	T700 24K/T700 12K/T700 12K	1.28	526

All preforms were taken from the A&P Technology.

The biaxial braid construction is a regular braided weave with two yarns crossing over and under

each other as $\pm 45^\circ$ orientation (Figure 1a). The triaxial braids involves adding a third set of yarns (T700 24K) in the axial direction (Figure 1b).

Table 2: Yarn properties of biaxial and triaxial braided fabrics [1]

Yarn type	Number of filaments	Linear density (tex)	Filament diameter (μm)	Tensile strength (GPa)	Tensile modulus (GPa)	Tensile strain (%)
T700 12K	12,000	800	6.92	4.9	230	2.1
T700 24K	24,000	1,650	7.05	4.9	230	2.1

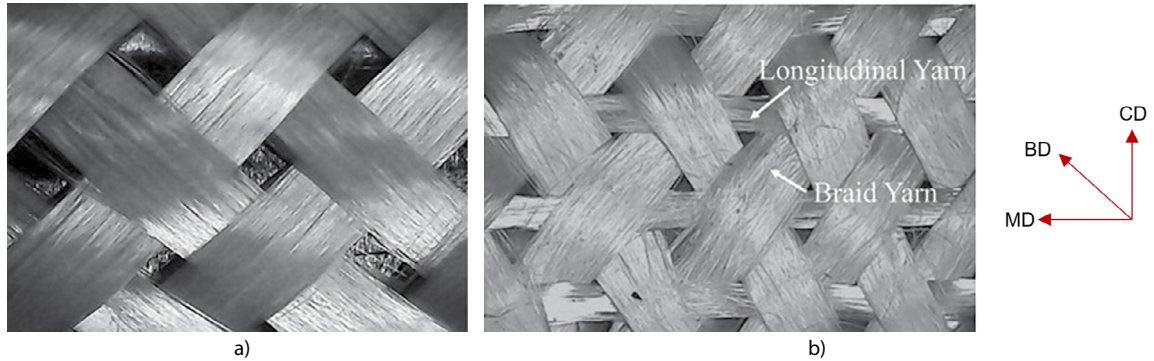


Figure 1: Braided fabrics: a) biaxial and b) triaxial (MD - machine direction, BD - bias direction, CD - cross direction)

Epoxy based Polives 702 Bisphenol-A type vinyl ester resin was used as the matrix material. Active methyl ethyl ketone peroxide in the ratio of 2% cobalt naphthalate in the ratio of 0.25% was used as a hardener. The properties of the used vinyl ester resin are given in Table 3. All composite plates were made of 4 fabric layers and were produced with the Vacuum Assisted Resin Infusion Method (VARIM) in size of 300 mm \times 300 mm.

Table 3: Mechanical properties of vinyl ester resin

Modulus of elasticity (GPa) Longitudinal = Transverse	Strain (%)	Poisson ratio (ν)
3	5	0.30

2.1 Methods

2.1.1 Geometric modelling and stiffness prediction

The geometrical modelling of biaxial and triaxial preforms was performed by employing the Wise-Tex software. Data given in Tables 1 and 2 were used in

the geometrical modelling. The method of inclusions with the Mori-Tanaka homogenisation was used in the determination of tensile modules [16, 17] with the Tex-Comp software. For that, the unit cell of a woven fabric modelled with the Wise-Tex program was used.

Method of inclusion

To apply the method of inclusions, implemented in the Tex-Comp software [16–19], the yarns in the unit cell were subdivided into a number of smaller segments, where each yarn segment was geometrically characterised by its total volume fraction, spatial orientation, cross-sectional aspect ratio and local curvature (all these parameters are readily provided by the geometrical model). Next, Eshelby's equivalent inclusion principle was adopted to transform each heterogeneous yarn segment into homogeneity with a fictitious transformation strain distribution. The solution makes use of a short fibre equivalent, which physically reflects the drop in the axial load

carrying capability of a curved yarn with respect to an initially straight yarn. Every yarn segment was hence linked to an equivalent short fibre, possessing an identical cross-sectional shape, volume fraction and orientation as the original segment it was derived from. The length of the equivalent fibre was on the other hand related to the curvature of the original yarn. For textiles with smoothly varying curvature radii, a proportional relationship between the short fibre length and the local yarn curvature radius is the most straightforward choice and sufficiently accurate for the present purpose.

The interaction problem between different reinforcing yarns was solved in the traditional way, i.e. by averaging out the image stress sampling over different phases. If the Mori-Tanaka scheme is used, the stiffness tensor C^C of the composite is obtained as:

$$C^C = [c_m C^m + (c_s C^s A^s)] [c_m I + (c_s + A^s)]^{-1} \quad (1),$$

where the subscripts m and s denote the matrix and yarn segment, respectively, c_i is the volume fraction of phase i ($= m, s$), and the angle brackets denote a configurational average.

2.1.2 Measurement of tensile modulus

The braided composite plates were cut perpendicular to three different directions, i.e. BD (braided direction), MD (machine direction) and CD (cross direction). Determining the tensile strength and modulus on composite samples in accordance with the ASTM 1D 638 standards was experimentally performed in an Instron testing machine with load cell of 100 kN capacity. For each direction, 5 samples were used. The test speed was 15 mm/min for all samples.

3 Results and discussion

3.1 Geometric modelling

The geometrical modelling of biaxial and triaxial carbon dry preforms generated by employing the Wise-Tex software using data from Tables 1, 2 and 4 is given in Figure 2. For the Wise-Tex modelling, the input data were measured from the samples. Each measurement was made at least 5 times and the average and standard deviation values were calculated. The appearance of yarn segments generating unit cell is demonstrated in Figure 3. The parameters which belong to unit cell modelling, generated by using the Wise-Tex software, are given in Tables 5 and 6 for biaxial and triaxial braided structures. In our study, we took into account all the conditions that the yarn is exposed to in the fabric structure. The data required to model the fabric geometry were obtained by measuring the composite material, meaning that the Wise-Tex smart application was not used. Consequently, lateral yarn pressures and bending rigidity values were not taken into account. The yarn widths, diameters and geometries were measured on composite samples. Thus, the existing data were obtained from the resin impregnated fabric structure. These data were used in the modelling. Accordingly, the width and diameter measurements of the cross-section of the yarn within the fabric structure were used, not the straight section. As a result, the model reflects the internal geometry of the braided structures virtually, which is relatively similar to the real fabric.

Table 4: Measured parameters to geometric modelling of biaxial and triaxial braided fabrics used in research

Fabric type	Braiding pattern	Braiding angle (°)	Braiding yarn width (mm)	Yarn spacing (mm)	Axial yarn width (mm)
Biaxial	2 × 2 diamond	91.3 ± 1.2	4.60 ± 0.62	5.27 ± 0.50	–
Triaxial	2 × 2 diamond	91.5 ± 0.9	4.13 ± 0.18	5.33 ± 0.17	4.33 ± 0.34

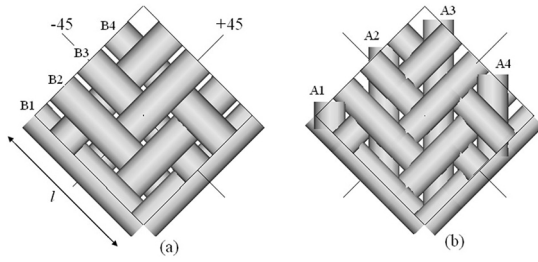


Figure 2: Geometric modelling of unit cell of: a) biaxial and b) triaxial braided fabrics (B1, B2, B3, and B4 are braided yarns, A1, A2, A3 and A4 are axial yarns, l is yarn length)

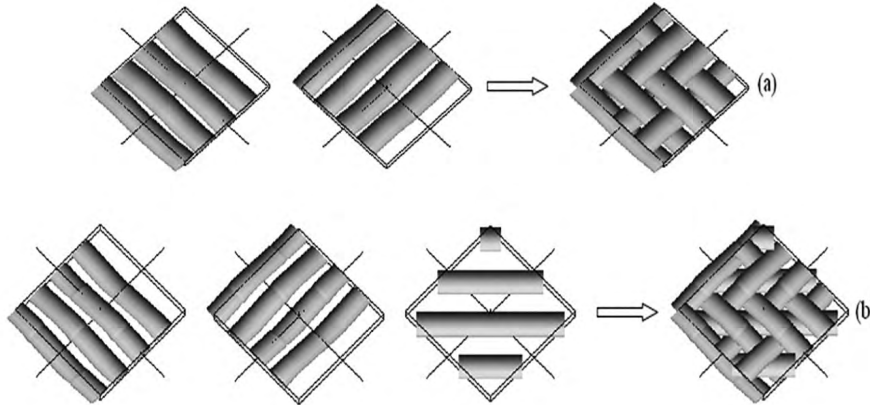


Figure 3: Appearance of yarn segments generating unit cell in: a) biaxial and b) triaxial braided structure

Table 5: Geometric modelling results of biaxial braided fabric

Unit cell size: 20.4 mm \times 20.4 mm \times 0.40 mm (length \times width \times thickness)

Areal density: 313.9 g/m²

Porosity (inter yarn): 29.1%

Fibre volume fraction (V_f): 44.6%

Yarn	Yarn thickness (mm)	Yarn width (mm)	Fibre volume fraction, V_f (%)	Yarn length (mm)	Crimp (%)
B1 (+45°)	0.20	4.60	63	20.41	0.1
B2 (+45°)	0.20	4.60	63	20.41	0.1
B3 (+45°)	0.20	4.60	63	20.41	0.1
B4 (+45°)	0.20	4.60	63	20.41	0.1
B1 (-45°)	0.20	4.60	63	20.41	0.1
B2 (-45°)	0.20	4.60	63	20.41	0.1
B3 (-45°)	0.20	4.60	63	20.41	0.1
B4 (-45°)	0.20	4.60	63	20.41	0.1

The data in Table 5 seem similar. There are 8 different yarns in the unit cell for biaxial braided structures. 4 of them are in the +45 degree direction while the other 4 are in the -45 degree direction. Since all yarns have the same density and yarn count in the structure, all data are the same. This is a result of the Wise-Tex geometric model. Here, if the yarn densities and/or yarn counts were different, these results would not be the same. All data in this table are the same; however, the results may change if the produc-

tion parameters change. Therefore, it is believed that retaining the data for the entire unit cell is useful.

In the research, it was established that the volume fractions of reinforcing yarns are the same in +45° and -45° directions in biaxial preforms. The total volume of reinforcing yarns in a unit cell was 70.9%. The volume of reinforcing yarns is 18.6% in +45° and -45° directions in triaxial preforms, while the amount is 12.8% of that of axial yarns; the total yarn fraction is 55.5% in the unit cell. It can be observed

that the porosity of the triaxial structure is by 42% higher than of the biaxial structure although both of them were manufactured using the same yarns and constructions. Nevertheless, it can be said that resin rich areas in the triaxial structure are larger com-

pared to the biaxial structures. One of the important parameters that affected the performance of the structure is yarn crimp. An increase in yarn crimp was observed in the triaxial structures. This increase negatively affects the stiffness of the structure.

Table 6: Geometric modelling results of triaxial braided fabric

Unit cell size: 21.3 mm × 21.3 mm × 0.656 mm (length × width × thickness)

Area density: 520.1 g/m²

Porosity (inter yarn): 50.1%

Fiber volume fraction (V_f): 37.7%

Yarn	Yarn thickness (mm)	Yarn width (mm)	Fibre volume fraction, V_f (%)	Yarn length (mm)	Crimp (%)
B1 (+45°)	0.20	4.13	70.1	21.39	0.3
B2 (+45°)	0.20	4.13	70.1	21.39	0.3
B3 (+45°)	0.20	4.13	70.1	21.39	0.3
B4 (+45°)	0.20	4.13	70.1	21.39	0.3
B1 (-45°)	0.20	4.13	70.1	21.39	0.3
B2 (-45°)	0.20	4.13	70.1	21.39	0.3
B3 (-45°)	0.20	4.13	70.1	21.39	0.3
B4 (-45°)	0.20	4.13	70.1	21.39	0.3
A1	0.33	4.33	84.8	3.77	0
A2	0.33	4.33	84.8	18.84	0
A3	0.33	4.33	84.8	26.38	0
A4	0.33	4.33	84.8	11.31	0

3.2 Stiffness prediction

The method of inclusions with the Mori-Tanaka (MT) homogenisation was used in the determination of elastic properties of the unit cell impregnated with vinyl ester resin (cf. Figure 2) with the Tex-Comp software. The results are given in Table 7 for each direction. V_f values are 44.6% and 37.7% for biaxial and triaxial braided structures, respectively.

E , G and ν indicate tensile modulus, shear modulus and Poisson ratio. Subscripts of YY , XX , XY and ZZ indicate the directions.

The results show that all values are the same for +45° and -45° directions in biaxial braided structures due to the construction of this directions being the same. The E_{xx} and E_{yy} values of BD are significantly higher than of MD. The E_{xx} and E_{yy} values belonging to the BD directions in the biaxial braided unit cell, these directions being fibre directions, are by 5 times higher than the values in the MD directions. When

the shear modules are compared, a worthy attractive difference is observed in the G_{xy} values. The values of G_{xy} in the MD direction are by almost 9 times higher than the values in the BD direction. The properties for the CD and MD directions are the same in the biaxial braided unit cell.

The E_{xx} and E_{yy} values in the BD direction are by 32% lower compared to the values in the MD direction in the triaxial braided unit cell. Since there is an axial fibre reinforcement in the MD direction, there is no significant difference in triaxial structures as there is in biaxial structures. The structure shows higher stiffness in the MD direction due to the axial yarn reinforcement in addition to that of the BD direction. A great increase did not occur in the G_{xy} values as it was the case in the biaxial structure. However, there is a 1.7 times rising available in G_{xy} in the MD direction when compared to that in the BD direction.

Table 7: Estimated homogenised elastic properties of unit cells

(E indicates tensile modulus, G shear modulus, and ν Poisson ratio, subscripts of YY, XX, XY and ZZ indicate the directions.)

Direction	Braiding type	E_{XX} (GPa)	E_{YY} (GPa)	E_{ZZ} (GPa)	G_{VZ} (GPa)	G_{XZ} (GPa)	G_{XY} (GPa)	ν_{VZ}	ν_{ZY}	ν_{ZX}	ν_{XZ}	ν_{XY}	ν_{YX}
BD (+45°)	Biaxial	55.4	55.4	6.07	2.16	2.16	2.92	0.037	0.34	0.34	0.037	0.033	0.033
	Triaxial	31.6	31.5	5.43	1.94	1.94	8.44	0.059	0.35	0.35	0.059	0.091	0.091
BD (-45°)	Biaxial	55.4	55.4	6.07	2.16	2.16	2.92	0.037	0.34	0.34	0.037	0.033	0.033
	Triaxial	31.5	31.6	5.43	1.94	1.94	8.45	0.059	0.35	0.35	0.059	0.091	0.091
MD	Biaxial	10.59	10.59	6.07	2.16	2.16	26.9	0.037	0.06	0.06	0.037	0.81	0.81
	Triaxial	46.2	15.1	5.43	1.91	1.97	14.5	0.11	0.29	0.10	0.012	0.23	0.70

It can be observed that the stiffness values in triaxial structures are low when the values of biaxial and triaxial braided structures are compared to each other. This situation can be explained with a higher fibre volume ratio of biaxial structures. In addition, the excess of yarn crimp in triaxial structures causes a decline in planar properties. However, when the properties in different directions are compared, it can be stated that triaxial structures are more favourable.

When evaluating the results, it can be seen that the values E_{XX} and E_{YY} in the biaxial structure are by 27.5% higher than those in the triaxial structure. This result can be explained with low yarn crimp values in the triaxial structure, which has a lower initial modulus value. Due to the significant fibre volume in the axial direction, the laid in axial yarns force added crimp in the bias yarns, causing the biases to lose in-plane properties. The axial fibres also tend to inhibit the distribution of loads within the laminate, yielding a lower tensile modulus. However, a significant increase was obtained in the

G_{XY} value in the axial yarn reinforcement. There was no significant decrease in the Poisson ratio observed when triaxial structures were compared to biaxial structures. In contrast, some increase was observed in the ν_{XY} values. These phenomena can be explained by increased space between the yarns.

3.3 Experimental results

Experimental values of modulus elasticity (E) are a result of tensile testing. The experimental results normalised for 40% fibre volume fraction are comparatively given to the values in Table 8 obtained according to the MT method. A typical load-displacement diagram obtained experimentally from bi- and triaxial carbon vinyl ester braided composite specimens is given in Figure 4. As seen from the diagram in Figure 4, high strength in biaxial structures can be obtained only in the BD direction; there is a decrease in the other directions. However, in the triaxial structures, a high level of strength can be reached in the MD direction due to the axial yarn reinforcement in addition to that of the BD direction.

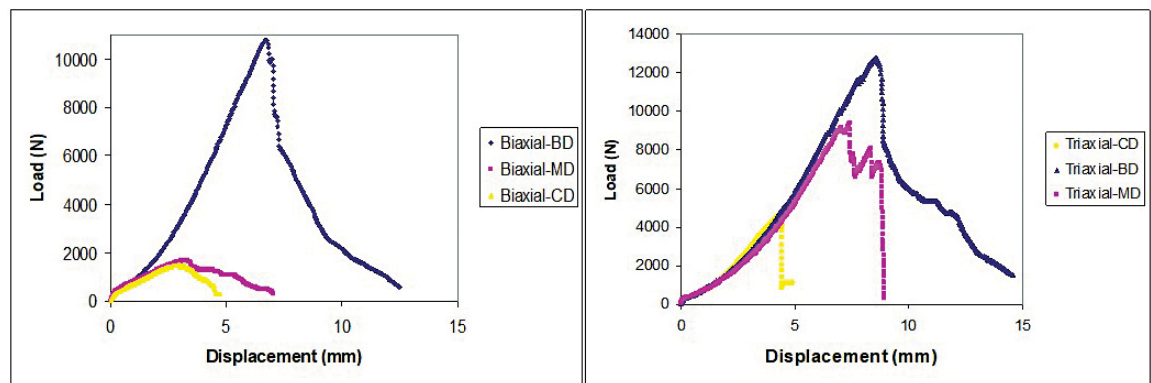


Figure 4: Load-displacement curves of biaxial and triaxial braided composites

When experimental data and numeric values are compared, it can be observed that the values are close. Nevertheless, a certain amount of deviation is observed in the BD direction in both biaxial and triaxial structures. This deviation can arise due to

the air within the gaps in composite specimens or the quality of samples. On the other hand, such a deviation may also be caused by a lack of information about real yarn crimp.

Table 8: Comparison of estimation values with experimental data

Direction	Braiding type	Tensile modulus, E (GPa) ^{a)}	Tensile modulus, E (GPa) ^{b)}	Difference (%)
BD	Biaxial	49.6 ± 2.3	55.4	10.5
	Triaxial	38.6 ± 2.3	31.5	18.4
CD	Biaxial	11.5 ± 0.7	10.59	7.9
	Triaxial	13.5 ± 0.7	15.1	10.6
MD	Biaxial	11.3 ± 0.8	10.59	6.7
	Triaxial	48.3 ± 2.8	46.2	4.5

^{a)} experimental for @ V_f 40%, ^{b)} MT estimation

4 Conclusion

In this study, structure parameters are predicted by geometrically modelling bi- and triaxial braided preforms. According to the model generated, the reinforcement in the axial direction causes an increase in crimp values of the yarns in triaxial structures. In addition, the reinforcement causes an increase in space between the yarns; resin rich areas hence increase as well.

Since lower porosity and a higher fibre volume ratio values can be reached in biaxial composite plates, the high stiffness values were achieved in this structure in the BD direction in relation to the triaxial structure. There is an impact of lower crimps in biaxial structures on these results. An increase in yarn crimp was a cause of a decline in planar properties. Tensile module triaxial composite structures were raised 4 times in relation to biaxial structures due to the axial yarn reinforcement. The results were also confirmed with experimental data. Yarn reinforcement in the axial direction caused a significant increase in the G_{xy} values. When triaxial structures were compared to biaxial structures, a significant decrease was not observed in the Poisson ratio, although significant increases in the ν_{xy} and ν_{yx} values were observed.

Acknowledgements

We thank to MTM KU Leuven and S.V. Lomov for supplying the Wise-Text and Tex-Comp software.

References

1. Making composites better with braid [online]. A&P Technology [accessed 23. 11. 2024]. Available on World Wide Web: <<https://braider.com/?s=Making+composites+better+with+braid+>>>.
2. POTLURİ, P., NAWAZ, S. Developments in braided fabrics. In *Specialist Yarn and Fabric Structures: Developments and Applications*. Edited by R.H. Gong. Oxford : Woodhead Publishing, 2011, 333–353, doi: [10.1533/9780857093936.333](https://doi.org/10.1533/9780857093936.333).
3. BİRKEFELD, K., PICKETT, A., MIDDENDORE, P. Virtual design and optimisation of braided structures considering production aspects of the preform. In *Comprehensive Composite Materials II*. Editors-in-Chief Peter W.R. Beaumont and Carl H. Zweben. Elsevier, 2018, 85–97, doi: [10.1016/B978-0-12-803581-8.10054-2](https://doi.org/10.1016/B978-0-12-803581-8.10054-2).
4. AROLD, B., GESSLER, A., METZNER, C., BİRKEFELD, K. Braiding processes for composites manufacture. In *Advances in Composites*

- Manufacturing and Process Design*. Edited by Philippe Boisse. Woodhead Publishing, 2015, 3–26, doi: [10.1016/B978-1-78242-307-2.00001-4](https://doi.org/10.1016/B978-1-78242-307-2.00001-4).
5. FANGUEIRO, R., SOUTINHO, F. Textile structures. In *Fibrous and Composite Materials for Civil Engineering Applications*. Edited by R. Figueiro. Woodhead Publishing, 2011, 62–91, doi: [10.1533/9780857095583.1.62](https://doi.org/10.1533/9780857095583.1.62).
 6. AYRANCI, C., CAREY, J. 2D Braided composites: a review for stiffness critical applications. *Composite Structures*, 2008, **85**(1), 43–58, doi: [10.1016/j.compstruct.2007.10.004](https://doi.org/10.1016/j.compstruct.2007.10.004).
 7. ISHIKAWA, T., CHOU, T.-W. Stiffness and strength behavior of woven fabric composites. *Journal of Material Science*, 1982, **71**(11), 3211–3220, doi: [10.1007/BF01203485](https://doi.org/10.1007/BF01203485).
 8. ISHIKAWA, T., CHOU, T.-W. In-plane thermal expansion and thermal bending coefficients of fabric composites. *Journal of Material Science*, 1983, **17**(2), 92–104, doi: [10.1177/0021998383017002](https://doi.org/10.1177/0021998383017002).
 9. VANDEURZEN, P. Structure-performance modelling of two-dimensional woven fabric composite: PhD Thesis. Leuven : Department of MTM, KU Leuven, 1999.
 10. VANDEURZEN, P., IVENS, J., VERPOEST, I. Micro-stress analysis of woven fabric composites by multilevel decomposition. *Journal of Composite Materials*, 1998, **32**(7), 623–651, doi: [10.1177/002199839803200702](https://doi.org/10.1177/002199839803200702).
 11. GOMMERS, B., VERPOEST, I., VAN HOUTTE, P. The Mori–Tanaka method applied to textile composite materials. *Acta Materialia*, 1998, **46**(6), 2223–2235, doi: [10.1016/S1359-6454\(97\)00296-6](https://doi.org/10.1016/S1359-6454(97)00296-6).
 12. LOMOV, S.V., TRUEVTZEV NN. A software package for the prediction of woven fabrics geometrical and mechanical properties. *Fibres & Textile in Eastern Europe*, 1995, **3**(2), 49–52.
 13. GUSAKOV, A.V., LOMOV, S.V. Parametric studies of the internal structure of 3D-woven fabrics. *Fibres & Textile in Eastern Europe*, 1998, **6**(2), 60–63.
 14. HUYSMANS, G., VERPOEST, I., VAN HOUTTE, P. A poly-inclusion approach for the elastic modelling of knitted fabric composites. *Acta Materialia*, 1998, **46**(9), 3003–3013, doi: [10.1016/S1359-6454\(98\)00021-4](https://doi.org/10.1016/S1359-6454(98)00021-4).
 15. HUYSMANS, G., VERPOEST, I., VAN HOUTTE, P. A damage model for knitted fabric composites. *Composites Part A: Applied Science and Manufacturing*, 2001, **32**(10), 1465–1475, doi: [10.1016/S1359-835X\(01\)00045-8](https://doi.org/10.1016/S1359-835X(01)00045-8).
 16. LOMOV, S.V., HUYSMANS, G., LUO, Y., PARNAS, R.S., PRODROMOU, A., VERPOEST, I., PHELAN, F.R. Textile composites models: modelling strategies. *Composites Part A: Applied Science and Manufacturing*, 2001, **32**(10), 1379–1394, doi: [10.1016/S1359-835X\(01\)00038-0](https://doi.org/10.1016/S1359-835X(01)00038-0).
 17. LOMOV, S.V., GUSAKOV, A.V., HUYSMANS, G., PRODROMOU, A., VERPOEST, I. Textile geometry preprocessor for meso-mechanical models of woven composites. *Composites Science and Technology*, 2000, **60**(11), 2083–2095, doi: [10.1016/S0266-3538\(00\)00121-4](https://doi.org/10.1016/S0266-3538(00)00121-4).
 18. LOMOV, S.V., HUYSMANS, G., VERPOEST, I. Hierarchy of textile structures and architecture of fabric geometric models. *Textile Research Journal*, 2001, **71**(6), 534–543, doi: [10.1177/004051750107100611](https://doi.org/10.1177/004051750107100611).
 19. LOMOV, S.V., TRUONG, VERPOEST, I., PEETERS, T., ROOSE, V., BOISSE, P., GASSER, A. Mathematical modelling of internal geometry and deformability of woven preforms. *International Journal of Form and Processing*, 2003, **6**(3–4), 413–442, doi: [10.3166/ijfp.6.413-442](https://doi.org/10.3166/ijfp.6.413-442).
 20. LOMOV, S.V., PARNAS, R.S., BANDYOPADHYAY GHOSH, S., VERPOEST, I., NAKAI, A. Experimental and theoretical characterization of the geometry of two-dimensional braided fabrics. *Textile Research Journal*, 2002, **72**(8), 706–712, doi: [10.1177/004051750207200810](https://doi.org/10.1177/004051750207200810).
 21. MOESEN, M., LOMOV, S.V., VERPOEST, I. Modelling of the geometry of weft-knit fabrics. In *Proceedings of the TechTextil 2003 Symposium: 10th International Symposium for Technical Textiles [CD edition]*, 2003.

22. LOMOV, S.V., BELOV, E.B., BISCHOFF, T., GHOSH, S.B., TRUONG CHI, T., VERPOEST, I. Carbon composites based on multiaxial multiply stitched preforms. Part 1: geometry of the preform. *Composites Part A: Applied Science and Manufacturing*, 2002, **33**(9), 1171–1183, doi: 10.1016/S1359-835X(02)00090-8.
23. LOMOV, S.V., VERPOEST, I., PEETERS, T., ROOSE, D., ZAKO, M. Nesting in textile laminates: geometrical modelling of the laminate. *Composite Science and Technology*, 2002, **63**(7), 993–1007, doi: 10.1016/S0266-3538(02)00318-4.
24. BELOV, E.B., LOMOV, S.V., VERPOEST, I., PEETERS, T., ROOSE, D., PARNAS, R.S. Modelling of permeability of textile reinforcements: lattice Boltzmann method. *Composite Science and Technology*, 2004, **64**(7–8), 1069–1080, doi: 10.1016/j.compscitech.2003.09.015.
25. VAN den BROUCKE, B., TUMER, F., LOMOV, S.V., VERPOEST, I., De LUCA, P., DUFORT, L. Micro–macro structural analysis of textile composite parts: case study. In *Proceedings of the 25th international SAMPE Europe conference, Paris, March 30th – April 1st 2004*, 194–199, <https://www.researchgate.net/publication/228406657>.
26. LOMOV, S.V., VERPOEST, I., KONDRATIEV, S.V., BOROVKOV, A.I. An integrated model strategy for processing and properties of textile composites: new results. In *Proceedings of the 22nd International SAMPE Europe Conference*, 2001, 379–389.
27. LOMOV, S.V., DING, X., HIROSAWA, S., KONDRATIEV, S.V., MOLIMARD, J., NAKAI, H., VAUTRIN, A., VERPOEST, I., ZAKO, M. FE simulations of textile composites on unit cell level: validation with full-field strain measurements: In *Proceedings of the 26th SAMPE-Europe conference, Paris; 5th – 7th April 2005 [CD edition]*, 2005.
28. LOMOV, S.V., MIKOLANDA, T. Textile virtual reality. In *Proceedings of TechTextil symposium, Frankfurt am Main, 2005 [CD edition]*, 2005.
29. BOGDANOVICH, A.E., KARAHAN, M., LOMOV, S.V., VERPOEST, I. Quasi-static tensile behavior and damage of carbon/epoxy composite reinforced with 3D non-crimp orthogonal woven fabric. *Mechanics of Materials*, 2013, **62**, 14–31, doi: 10.1016/j.mechmat.2013.03.005.
30. KARAHAN, M., LOMOV, S.V., BOGDANOVICH, A.E., MUNGALOV, C., VERPOEST, I. Internal geometry evaluation of non-crimp 3D orthogonal woven carbon fabric composite. *Composites Part A: Applied Science and Manufacturing*, 2010, **41**(9), 1301–1311, doi: 10.1016/j.compositesa.2010.05.014.
31. KARAHAN, M., KARAHAN, N. Influence of weaving structure and hybridization on the tensile properties of woven carbon-epoxy composites. *Journal of Reinforced Plastics and Composites*, 2014, **33**(2), 212–222, doi: 10.1177/0731684413504019.
32. KARAHAN, M. The effect of fibre volume fraction on damage initiation and propagation of woven carbon-epoxy multi-layer composites. *Textile Research Journal*, 2012, **82**(1), 45–61, doi: 10.1177/0040517511416282.
33. KARAHAN, M. Investigation of damage initiation and propagation in 2 × 2 twill woven carbon/epoxy multi-layer composites. *Textile Research Journal*, 2011, **81**(4), 412–428, doi: 10.1177/0040517510395996.
34. LOMOV, S.V., BOGDANOVICH, A.E., IVANOV, D.S., HAMADA, K., KURASHIKI, T., ZAKO, M., KARAHAN, M., VERPOEST, I. Finite element modelling of progressive damage in non-crimp 3D orthogonal weave and plain weave E-Glass composites. In *Second World Conference on 3D Fabrics and Their Applications, 2009, Greenville, South Carolina, USA*.

Vishal Trivedi, Pradeep Joshi

Amity School of Fashion Technology, Amity University, Sector 125, Noida, Uttar Pradesh, India

Exploring the Role of Situational Cues in Apparel Consumers' Impulsive Buying Behaviour

Raziskovanje vloge situacijskih dejavnikov pri impulzivnem nakupovalnem vedenju potrošnikov oblačil

Original scientific article/Izvorni znanstveni članek

Received/Prispelo 6–2024 • Accepted/Sprejeto 9–2024

Corresponding author/Korespondenčni avtor:

Dr. Vishal Trivedi, Assistant Professor (Garde-II)

E-mail: vishal.trivedi22@gmail.com

Mobile: +918006473336

ORCID iD: 00000-0001-6180-5572

Abstract

This study evaluates the role of situational cues (time availability, money availability, salesperson's behaviour, promotional offers and payment methods) on the impulse purchasing conduct of apparel buyers in brick-and-mortar stores. The study sheds light on the key determinants of impulse purchases in offline apparel shopping by delving into the dynamic interaction between situational cues (factors) and consumer impulse-buying decisions. A survey questionnaire was used, based on previous literature, to collect primary data from 325 respondents from Delhi (NCR), India in the sample. The data were examined using regression analysis, correlation analysis and factor analysis. According to the findings of the study, impulsive apparel shopping behaviour is significantly influenced by situational cues such as time availability, money availability, salesperson behaviour, promotional offers and payment methods. In addition, the findings indicate that salespeople's behaviour, promotional offers and payment methods are closely linked to apparel consumers' impulse buying behaviour. This study offers some recommendations for retailers to enhance their retail strategies to increase consumers' impulsive purchases of apparel.

Keywords: apparel consumer, impulse buying, promotional offers, payment methods, situational cues

Izvleček

Raziskava vrednoti vpliv situacijskih dejavnikov (razpoložljivost časa, razpoložljivost denarja, vedenje prodajalca, promocijske ponudbe in metode plačila) pri impulzivnem nakupovalnem vedenju kupcev oblačil v fizičnih trgovinah. Osvetljuje ključne dejavnike impulzivnih nakupov pri tradicionalnem nakupovanju oblačil, tako da se poglobi v dinamično interakcijo med situacijskimi dejavniki in odločitvami potrošnikov za impulzivni nakup. Za zbiranje podatkov je bil uporabljen anketni vprašalnik, oblikovan na podlagi obstoječe literature. Izpolnilo ga je 325 anketirancev iz New Delhija (NCR) v Indiji. Podatki so bili analizirani z uporabo regresijske analize, analize korelacije in faktorske analize. Pokazalo se je, da na impulzivno nakupovalno vedenje pomembno vplivajo situacijski dejavniki, kot so razpoložljivost časa in denarja, vedenje prodajalcev, promocijske ponudbe in načini plačila. Poleg tega so ugotovili, da so vedenje prodajalcev, promocijske ponudbe in načini plačila močno povezani z impulzivnim nakupovalnim vedenjem potrošnikov



Content from this work may be used under the terms of the Creative Commons Attribution CC BY 4.0 licence (<https://creativecommons.org/licenses/by/4.0/>). Authors retain ownership of the copyright for their content, but allow anyone to download, reuse, reprint, modify, distribute and/or copy the content as long as the original authors and source are cited. No permission is required from the authors or the publisher. This journal does not charge APCs or submission charges.

oblačil. Raziskava ponuja priporočila trgovcem za izboljšanje njihovih maloprodajnih strategij, da bi pri potrošnikih povečali število impulzivnih nakupov oblačil.

Ključne besede: potrošnik oblačil, impulzivni nakupi, promocijske ponudbe, načini plačila, situacijski dejavniki

1 Introduction

In today's dynamic retail landscape, impulsive buying behaviour among consumers has garnered significant attention from researchers and marketers alike. Impulsive buying, characterized by spontaneous and unplanned purchases, is particularly prevalent in the apparel industry, where consumers are often swayed by a variety of external factors. This phenomenon is not merely a product of individual predispositions but is also heavily influenced by situational cues present in the shopping environment. Understanding these situational cues is crucial for retailers aiming to enhance their marketing strategies and boost sales. Impulse buying, often characterized by unplanned and spontaneous purchases, is a pervasive phenomenon in consumer behaviour [1]. In the realm of marketing, impulsive purchasing behaviour is a mystery. Although this type of behaviour is socially unacceptable, it nonetheless accounts for a sizeable portion of the annual sales of items across a variety of product categories [1]. Making an unanticipated or spontaneous purchase without having made up your mind before entering a store is known as impulsive buying behaviour [2].

Hedonic purchases are driven by pleasure and excitement, often occurring without much thought, and lead to feelings of loss of control at the time of purchase and later regret [3, 4]. These purchases are defined as being motivated by emotions and social influences rather than practical benefits. Impulse buying is a self-regulation strategy used to alleviate negative emotions, especially when those emotions stem from not meeting personal ideals or having low self-esteem [5]. The rise of online shopping and new technologies, such as smartphones and digital platforms, has made it easier to access and purchase goods, increasing the frequency of impulsive buying

[6]. Research by Kacen and Baumeister [7, 8] suggests that people are more likely to give in to their impulses if they believe it will improve their mood. Understanding consumer behaviour, especially impulsive buying, is one of the most challenging aspects of marketing due to its complex nature. This study delves into the role of specific situational cues—time availability, money availability, salesperson's behaviour, promotional offers and payment methods—in shaping the impulsive buying behaviour of apparel consumers. These situational cues can significantly alter a consumer's decision-making process, tipping the scales towards an impulsive purchase. Time availability, or the perception of time constraints, often serves as a key factor that influences impulsive purchase behaviour. It is recognized that individuals with excess time during their shopping trips are more prone to making unplanned purchases [9]. The availability of money is another important situational aspect that impacts impulsive purchases. Consumers are naturally swayed by their perceived economic capacity and budgetary flexibility when contemplating spontaneous purchases. A surplus of available funds may embolden consumers to indulge their desires, while financial constraints may impose a greater degree of caution. The role of sales staff in the retail environment cannot be overstated. The efforts, attitude and persuasiveness of salespersons often play a decisive role in shaping the shopping experience and, consequently, impulsive buying tendencies [10]. The interactions between consumers and sales staff can either foster an environment conducive to impulsive purchases or deter potential buyers. Discounts and promotional offers are powerful triggers for impulsive buying behaviour. The allure of a limited-time discount, a special offer or a 'buy one, get one free' deal can sway consumers to deviate from their original shopping

plans and make unplanned apparel purchases [11]. Such incentives tap into consumers' desire for value and savings, prompting immediate action. Payment methods, both traditional and digital, constitute yet another dimension of situational factors. The ease, convenience and security associated with various payment options influence the likelihood of consumers making impulsive purchases [12]. Rapid advancements in digital payment technology have further complicated the landscape, offering consumers novel avenues for instant gratification.

Impulse buying behaviour is a critical area of study in consumer behaviour research, as it represents spontaneous, unplanned purchases that can significantly impact retail sales. Understanding the importance of impulse buying behaviour is crucial for retailers and marketers [13]. Impulse purchases can contribute substantially to a retailer's overall sales, often accounting for a significant portion of revenue. Encouraging impulse buys can enhance the shopping experience, making it more engaging and enjoyable for customers. Insights into impulse buying behaviour can help form the development of targeted marketing strategies, promotions and in-store displays [14].

This study aims to explore situational cues to provide a comprehensive understanding of their impact on the impulsive buying behaviour of apparel consumers. The research seeks to assess how situational cues influence impulsive purchasing behaviour among apparel consumers. Specifically, the purpose is to determine the effect of situational circumstances on customers' impulsive apparel purchases. The objectives of this research are as follows:

- a. To evaluate the influence of time availability on apparel consumer's impulse purchasing behaviour.
- b. To identify the influence of money availability on apparel consumer's impulse purchasing behaviour.
- c. To identify the influence of salesperson's behaviour on apparel consumer's impulse

purchasing behaviour.

- d. To assess the influence of promotional offers on apparel consumer's impulse purchasing behaviour.
- e. To assess the influence of various payment methods on apparel consumer's impulse purchasing behaviour.

1.1 Apparel consumer impulse purchasing behaviour

Impulse buying is a common occurrence in the apparel retail industry, marked by spontaneous and immediate purchase decisions [13–15]. Unlike planned purchases, which involve careful consideration and planning, impulse buys happen with little to no prior thought [16, 17]. This behaviour is influenced by various external factors present at the point of sale, often referred to as situational cues, which play a significant role in driving impulse purchases in the retail sector [18–21]. These include time availability, money availability, salesperson's behaviour, promotional offers and payment methods. Limited time to make a purchasing decision can create a sense of urgency, leading to quick and unplanned purchases [22, 23]. Flash sales and limited-time offers capitalize on this behaviour by pressuring consumers to buy before the opportunity expires [24]. The amount of disposable income or available credit can impact a consumer's likelihood of making an impulse purchase. When consumers feel financially secure, they are more likely to indulge in spontaneous buying [25]. Promotions that make products seem more affordable, such as discounts or instalment plans, can also trigger impulsive decisions [26, 27]. The interaction with sales personnel can significantly affect impulse buying. A persuasive, friendly and knowledgeable salesperson can create a positive shopping experience, encouraging consumers to make impulsive purchases [28]. Personalized recommendations and the effective communication of product benefits are key strategies used by sales staff to drive impulse buys. Discounts, special deals and loyalty programs create a sense of urgency and

perceived value, prompting consumers to buy on impulse [29, 30]. Limited-time promotions and ‘buy one, get one free’ offers are common tactics used to stimulate impulsive buying behaviour [31]. The ease and convenience of modern payment methods, such as contactless payments, mobile wallets and buy-now-pay-later options, reduce friction in the purchasing process. When payment is quick and effortless, consumers are less likely to hesitate and more likely to make spontaneous purchases [32].

1.2 Situational cues and impulse buying behaviour

Situational cues, such as the availability of time/money, promotional offers, salesperson’s behaviour and payment methods [32–35], are linked to the impulse purchases of consumers. Time constraints can contribute to impulsive behaviour in consumer decision-making [32]. When individuals are under time pressure, they are more likely to make quick and spontaneous purchasing decisions without thoroughly evaluating alternatives. Limited time availability may lead consumers to rely on heuristics or emotional responses, potentially increasing the likelihood of impulse buying [6]. All of a person’s available funds on a given day are considered to be their money availability [19]. Cash accessibility is a significant factor in the course of incautious purchasing [19]. If a consumer has more money, they could change their planned shopping schedule. Buying power is thus raised [32]. There is a positive and significant connection between consumers’ impulse purchasing behaviour and limited-time promotions, as demonstrated by studies linking discount offerings to impulsive buying [36]. Many studies have demonstrated the positive connection between discounts, promotions and impulse buying [14, 16]. Salespersons play a pivotal role in fostering impulse buying through actions such as sharing product information, expressing admiration and addressing consumer queries [37, 38]. Professional assistance from employees alleviates consumer frustration during shopping [39]. The importance of employee friendliness in the retail context suggests that amiable

staff contribute to consumer satisfaction by aiding decision-making and providing product-related information [40]. Cashless payment methods may weaken consumers’ impulse control, as cashless payments are considered less painful than cash payments [41]. Yan’s [42] study found that QR codes and mobile payment methods have a positive impact on impulse buying behaviour. Existing studies have shown that non-cash payment options, such as the use of credit cards, enabled consumers to make both planned and spontaneous purchases [43, 44]. The connection between impulsive behaviour and actual purchasing behaviour weakens if a consumer perceives impulsive buying as inappropriate for certain reasons. In such cases, even a highly impulsive customer is less likely to act on their desire to purchase. [45, 46].

Drawing from critiques in prior literature, this study suggests that situational cues impact the impulsive purchasing behaviour of apparel consumers. The study’s suggested framework and developed hypotheses are shown in the figure below.

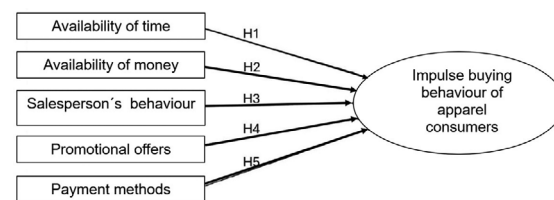


Figure 1: Proposed research framework

- H1: The availability of time positively influences the impulsive buying behaviour (IBB) of apparel consumers.
- H2: The availability of money positively influences the impulsive buying behaviour (IBB) of apparel consumers.
- H3: A salesperson’s behaviour positively influences the impulsive buying behaviour (IBB) of apparel consumers.
- H4: Promotional offers positively influence the impulsive buying behaviour (IBB) of apparel consumers.
- H5: Payment methods positively influence the impulsive buying behaviour (IBB) of apparel consumers.

2 Methodology

A research design serves as a fundamental approach, guiding the stages of data collection and analysis. It provides the framework outlining the nature of the data to be gathered, the sources thereof and the collection process. This study adopted a descriptive strategy, as it primarily focuses on examining the phenomenon of impulse purchase behaviour. A cross-sectional research design was chosen for this study, which was conducted in a specific period with a predetermined segment of the population. In this study, the non-probability sampling technique was used because not every respondent had an equal chance of being selected. Specifically, the convenience method of non-probability sampling was employed, as samples were chosen based on convenience. The study's outcomes, which rely on information gathered from the specified sample population to address the research questions, are primarily based on primary data.

A structured questionnaire was used for this study. The data were gathered with an individualized webpage-based online survey and social groups. The study's sample size was 325 respondents, while the questionnaire was sent to 370 respondents and received 350 responses. After cleaning the data, 325 respondents were left for further analysis. The five-point Likert scale was used for the development of the questionnaire, where 1 indicates strongly disagree and 5 indicates strongly agree, 1 indicates least important and 5 indicates most important options discussing a degree of agreement and disagreement and importance over different situational factors on apparel impulse buying. The questionnaires took into account the objective of the study to achieve perfection. The measurement items related to variables were taken from previous studies and modified for this study (refer to Appendix 1). The survey questionnaire has six main key variables (IBB, AT, AM, SB, PO, and PM). In the questionnaire, IBB has five items, and the rest of the other variables (AT, AM, SB, PO, and PM) have four items each. The scale of

impulse buying behaviour was taken from the study of Trivedi et al. [31]. Availability of time (AT) was measured using a scale developed and modified from the studies of Turley [32], and Atulkar [33]. The availability of money (AM) was measured using a scale developed and modified from the studies of Gehrt [34] and Mohan et al. [35]. Similarly, the scale of salesperson behaviour (SB) was measured using a scale developed by Zhuang et al. [36]. Further, for promotional offers (PO) and payment methods (PM), scales were used from the studies of Akram [42] and Badgaiyan [43]. The survey data was analysed using descriptive statistics. Statistical software, such as SPSS and Microsoft Excel, was employed to visually present the information and illustrate the relationships between dependent and independent variables.

2.2 Data analysis

SPSS software, version 29, was used to analyse the data. Described below is the analysis plan. SPSS software was used to first generate descriptive statistics and the frequency of demographics. Second, the loading scores of each item were ascertained using factors analysis (PCA), while the reliability of the data was evaluated using Cronbach's alpha. Third, the relationship between situational circumstances and apparel buyers' impulsive purchasing behaviour was examined using the Pearson correlation test. Regression analysis was used to assess the hypotheses and determine the relationship between both dependent and independent variables.

The demographic profile of the respondents and descriptive statistics are summarized in Tables 1 and 2. Table 3 presents principal component analysis (PCA) with a Cronbach's alpha value (reliability test). Each item's factor loading was greater than 0.6, indicating that it belonged to a single group. According to the findings, all variables had Cronbach's values above the 0.7 threshold (minimum) [47], indicating that the data were statistically appropriate and trustworthy for further investigation.

Table 1: Demographic profile of respondents

Demographic		Frequency	Percentage (%)
Gender	Male	156	47.96
	Female	168	51.72
	Others	1	0.31
Age	18-25	170	52.35
	25-35	87	26.64
	35-45	40	12.22
	45 and above	28	8.77
Occupation	Student	113	34.79
	Employed	137	42
	Self-employed	66	20.37
	Homemaker	9	2.82

Table 2: Descriptive statistics for variables

Variables	N	Mean	Std. deviation
Impulse buying behaviour	325	2.93	0.86
Availability of time	325	4.04	0.93
Availability of money	325	3.85	0.84
Salesperson's behaviour	325	3.47	0.80
Promotional offers	325	3.61	0.80
Payment methods	325	4.06	0.72

Table 3: Results of PCA with reliability test

Factors	Item	Loading value	Eigen value	Variance (%)	Alpha value
Impulse buying behaviour (IBB)	IBB1	0.698	3.250	54.609	0.787
	IBB2	0.701			
	IBB3	0.688			
	IBB4	0.722			
	IBB5	0.679			
Availability of time (AT)	AT1	0.799	0.964	61.043	0.792
	AT2	0.765			
	AT3	0.677			
	AT4	0.771			
Availability of money (AM)	AM1	0.781	0.416	63.127	0.731
	AM2	0.790			
	AM3	0.699			
	AM4	0.682			
Salesperson's behaviour (SB)	SB1	0.801	0.482	82.471	0.878
	SB2	0.789			
	SB3	0.747			
	SB4	0.775			

Promotional offers (PO)	PO1	0.782	0.636	70.313	0.825
	PO2	0.764			
	PO3	0.698			
	PO4	0.721			
Payment methods (PM)	PM1	0.711	0.253	72.119	0.810
	PM2	0.701			
	PM3	0.693			
	PM4	0.646			

Table 4: Correlation test analysis

Variables	Coefficient (<i>r</i>)	Significance (<i>p</i>)
Availability of time (AT)	0.221	0.001
Availability of money (AM)	0.263	0.003
Salesperson's behaviour (SB)	0.649	0.000
Promotional offers (PO)	0.406	0.005
Payment methods (PM)	0.442	0.0002

Table 5: Regression analysis

Hypothesis	B (unstandardized coefficients)	<i>p</i> -value	Beta (standardized coefficients)	t-statistics	Remarks
H1: The availability of time significantly influences the impulsive buying behaviour of apparel consumers (AT)	0.219	0.001	0.221	4.032	Accepted
H2: The availability of money significantly influences the impulsive buying behaviour of apparel consumers (AM)	0.344	0.000	0.263	4.844	Accepted
H3: A salesperson's behaviour significantly influences the impulsive buying behaviour of apparel consumers (SB)	0.648	0.002	0.649	15.205	Accepted
H4: Promotional offers significantly influence the impulsive buying behaviour of apparel consumers (PO)	0.445	0.003	0.406	7.916	Accepted
H5: Payment methods significantly influence the impulsive buying behaviour of apparel consumers (PM)	0.626	0.001	0.442	8.782	Accepted

3 Results and discussion

The percentage of respondents by age group is 52.35% (18–25 age), 26.64% (25–35 age), 12.22%

(35–45 age) and 8.77% (45 age and above). The majority of respondents (42%) are employed, followed by students (34.79%), self-employed (20.37%) and homemakers (2.82%).

The relationship between the independent variable – time availability, money availability, salesperson behaviour, promotional offers and payment methods and the dependent variable, impulse buying behaviour – was evaluated using Pearson correlation tests. In addition, to test the hypotheses, a multiple regression analysis was carried out with impulse buying behaviour as the dependent variable and the availability of time, money, salesperson behaviour, promotional offers and payment methods as the independent variables to see if any relationships could be used to determine the relative importance of these influences on apparel consumers' impulse buying behaviour. The following proposed hypothesis is explained:

H1: Availability of time positively influences the IBB of apparel consumers.

The results of the correlation test (see Table 4) indicate a strong link between impulsive purchasing and time availability, with an r -value of 0.221 and a p -value less than 0.05. A regression study also showed that time availability has a significant impact on consumers' impulsive apparel purchases. Table 5 indicates that because the p -value is less than the alpha threshold, the hypothesis is supported.

H2: The availability of money positively influences the IBB of apparel consumers.

Table 4 indicates that there is a substantial link (p -value less than 0.05 and r -value of 0.263) between the availability of money and impulsive purchases. Additionally, the results of the regression analysis showed that consumers' impulse purchase behaviour for clothes is significantly influenced by their financial situation. The p -value is less than the alpha threshold, supporting the hypothesis (see Table 5).

H3: A salesperson's behaviour positively influences the IBB of apparel consumers.

Table 4 indicates that the correlation test, with a p -value less than 0.05 and an r -value of 0.649, demonstrates a strong relationship between impulse buying and a salesperson's behaviour. Additionally,

the results of the regression analysis showed that consumers' impulsive apparel purchases are significantly influenced by the behaviour of salespeople. The p -value is below the alpha threshold, which supports the hypothesis (see Table 5).

H4: Promotional offers positively influence the IBB of apparel consumers.

There is a significant correlation between impulse buying and promotional offers, according to the correlation test (see Table 4), with a p -value of less than 0.05 and an r -value of 0.406. Additionally, the results of the regression analysis showed that promotional offers had a significant impact on consumers' impulsive apparel purchases. Table 5 shows that because the p -value is less than the alpha threshold, the hypothesis is supported.

H5: Payment methods positively influence the IBB of apparel consumers.

The results of the correlation test (see Table 4) indicate a strong link ($p < 0.05$) between payment methods and impulsive purchases, with an r -value of 0.442. Additionally, the results of the regression analysis showed that payment methods had a significant impact on consumers' impulsive apparel purchases. The fact that the p -value is less than the alpha threshold supports the hypothesis (see Table 5).

As a result, the final multiple regression equation (1) was developed using unstandardized coefficients (B):

$$IBB = 3.401 + 0.219 \times AT + 0.344 \times AM + 0.648 \times SB + 0.445 \times PO + 0.625 \times PM \quad (1),$$

where IBB is for impulse buying behaviour, AT is for availability of time, AM is for availability of money, SB is for salesperson behaviour, PO is for promotional offers, and PM is for payment methods.

Additionally, the beta value (β) of the regression analysis can be used to identify dependent factors that have a greater impact on consumers' impulsive apparel purchases [48]. According to the beta coefficient (β) results, salesperson's behaviour, followed

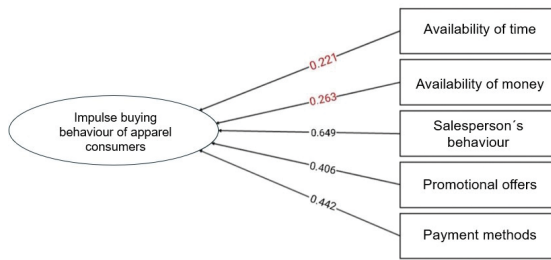


Figure 2: Research framework between situational cues and impulse buying behaviour of apparel consumers

by payment methods and promotional offers ($\beta = 0.649$, 0.442 , and 0.406), had a greater influence on IBB for apparel consumers, respectively, while the availability of time ($\beta = 0.221$) and availability of money ($\beta = 0.263$) had a lesser influence than other situational factors (salesperson behaviour, payment methods and promotional offers). The structural model in Figure 2 presents the effects of situational factors related to the IBB of apparel consumers.

4 Conclusions and implications

This study assessed a primary model to determine the connection between situational variables and apparel consumer's impulse purchasing behaviour. The model aids retailers and researchers in examining the underlying connections between situational factors and the impulse purchasing behaviour of apparel shoppers. The findings of the study indicate that situational factors such as the availability of money, availability of time, salesperson's behaviour, promotional offers and payment methods all have a significant impact on the IBB of apparel consumers. Moreover, the findings indicate that a salesperson's behaviour, promotional offers and payment methods are highly correlated with apparel consumer's impulse buying behaviour. This suggests that these elements work as drivers that stimulate arousal and eventually persuade a buyer to make impulsive purchases, especially when it comes to clothing.

Apparel retailers should focus on salesperson's behaviour, promotional offers and payment meth-

ods since these factors contribute significantly to impulse purchases and might increase sales and generate revenue. This study offers sufficient evidence that salesperson's behaviour, promotional offers and payment methods lead to impulse purchasing decisions. Furthermore, the research suggests that an increase in personal income or the availability of extra money made consumers buy more impulsive, while the limited availability of money reduces the chances of impulse purchasing.

This study also suggested that if consumers have more time to shop, they tend to do more impulse buying rather than consumers having limited time to shop. According to the study, retailers should pay more attention to salespersons' behaviour and conduct, as an effective salesperson can encourage customers to buy more. Additionally, retailers should focus on offering more promotional discounts and deals to motivate consumers to shop more. Moreover, the findings of the study also suggest that easy payment options, such as UPI, credit/debit cards phone banking, etc., also contribute to the impulsive buying behaviour of apparel consumers. These findings can help retailers to attract more consumers and influence the purchasing decisions of apparel customers.

Managerial implication

Apparel retailers can enhance the shopping experience by minimizing waiting times and optimizing the store layout, making it efficient and enjoyable. For time-constrained shoppers, clear signage and easy access to popular items can boost impulse purchases. Retailers should adopt flexible pricing strategies, offering products at various price points to accommodate different budgets. Investing in comprehensive training for sales staff is crucial, as well-trained, friendly and knowledgeable salespeople can drive impulse buying by providing personalized recommendations and fostering a positive shopping environment. Additionally, retailers should create attractive promotional offers, such as limited-time discounts, buy-one-get-one-free deals and exclu-

sive member discounts. Offering diverse payment options, including contactless payments, mobile wallets and credit/debit cards, and streamlining the checkout process can further reduce friction and enhance the likelihood of impulsive purchases.

Limitations and future recommendation

This study is hampered by some limitations. The first is the study's sample size, i.e. 325 respondents, which is a small sample size when compared to the magnitude of India's population and geographical location. Another limitation of this study is that the research was performed only on the offline shopping of apparel consumers, while online impulse buying is not considered in this study. The results may vary depending on the online shopping environment of apparel consumers.

Research in the future should employ a mixed-method approach, using both qualitative and quantitative techniques. Investigating impulse purchasing through TV, online shopping, mobile commerce and other non-store formats would be interesting. Since apparel was the primary focus of this study, additional products, such as footwear, cosmetics and other categories, can be used in future research.

Acknowledgments

We are thankful that AUUP, Uttar Pradesh, allowed us to contribute to the writing of this research paper.

References

- ROOK, D.W., FISHER, R.J. Normative influences on impulse buying behaviour. *Journal of Consumer Research*, 1995, **22**(33), 305–313, doi: [10.1086/209452](https://doi.org/10.1086/209452).
- GEORGE, B.P., YAOYUNYONG, G. Impulse buying and cognitive dissonance: a study conducted among the spring break student shoppers. *Young Consumers*, 2010, **11**(4), 291–306, doi: [10.1108/17473611011093925](https://doi.org/10.1108/17473611011093925).
- ARNOLD, M.J., REYNOLDS, K.E. Hedonic shopping motivations. *Journal of Retailing*, 2003, **79**(2), 77–95, doi: [10.1016/S0022-4359\(03\)00007-1](https://doi.org/10.1016/S0022-4359(03)00007-1).
- PENTECOST, R., ANDREWS, L. Fashion retailing and bottom line: the effects of generational cohorts, gender, fashion fanship, attendance and impulse buying on fashion exploration. *Journal of Retailing and Consumer Services*, 2010, **17**(1), 43–52, doi: [10.1016/j.jretcnser.2009.09.003](https://doi.org/10.1016/j.jretcnser.2009.09.003).
- BAUMGARTNER, H. Toward a personology of the consumer. *Journal of Consumer Research*, 2002, **29**(2), 286–292, doi: [10.1086/341578](https://doi.org/10.1086/341578).
- VERPLANKEN, B., HERABADI, AG. Individual differences in impulse buying tendency: feeling and no thinking. *European Journal of Personality*, 2001, **15**(1), 71–83, doi: [10.1002/per.423](https://doi.org/10.1002/per.423).
- KACEN, J.J., LEE, A.J. The influence of culture on consumer impulsive buying behaviour. *Journal of Consumer Psychology*, 2002, **12**(2), 163–176, doi: [10.1207/S15327663JCP1202_08](https://doi.org/10.1207/S15327663JCP1202_08).
- BAUMEISTER, R.F. Yielding to temptation: self-control failure, impulsive purchasing and consumer behaviour. *Journal of Consumer Research*, 2002, **28**(4), 670–676, doi: [10.1086/338209](https://doi.org/10.1086/338209).
- VERHAGEN, T., VAN DOLEN, W. The influence of online store beliefs on consumer online impulse buying: a model and empirical application. *Information & Management*, 2011, **48**(8), 320–327, doi: [10.1016/j.im.2011.08.001](https://doi.org/10.1016/j.im.2011.08.001).
- BATEMAN, C., VALENTINE, S. The impact of salesperson customer orientation on the evaluation of a salesperson's ethical treatment, trust in the salesperson, and intentions to purchase. *Journal of Personal Selling & Sales Management*, 2015, **35**(2), 125–142, doi: [10.1080/08853134.2015.1010538](https://doi.org/10.1080/08853134.2015.1010538).
- DHOLAKIA, U.M. Temptation, and resistance: An integrated model of consumption impulse formation and enactment. *Psychology & Marketing*, 2000, **17**(11), 955–982, doi: [10.1002/1520-6793\(200011\)17:11<955::AID-MAR3>3.0.CO;2-J](https://doi.org/10.1002/1520-6793(200011)17:11<955::AID-MAR3>3.0.CO;2-J).

12. SRINIVASAN, R., ANDERSON, R., PON-NAVOLU, K. Customer loyalty in e-commerce: an exploration of its antecedents and consequences. *Journal of Retailing*, 2002, **78**(1), 41–50, doi: [10.1016/S0022-4359\(01\)00065-3](https://doi.org/10.1016/S0022-4359(01)00065-3).
13. CLOVER, V.T. Relative importance of impulse-buying in retail stores. *Journal of Marketing*, 1950, **15**(1), 66–70, doi: [10.1177/002224295001500110](https://doi.org/10.1177/002224295001500110).
14. STERN, H. The significance of impulse buying today. *Journal of Marketing*, 1962, **26**(2), 59–62, doi: [10.2307/1248439](https://doi.org/10.2307/1248439).
15. ROOK, D.W. The buying impulse. *Journal of Consumer Research*, 1987, **14**(2), 189–199, doi: [10.1086/209105](https://doi.org/10.1086/209105).
16. ABRATT, R., GOODEY, S.D. Unplanned buying and in-store stimuli in supermarkets. *Managerial and Decision Economics*, 1990, **11**(2), 111–121, doi: [10.1002/mde.4090110204](https://doi.org/10.1002/mde.4090110204).
17. JUNG CHANG, H., YAN, R.N., ECKMAN, M. Moderating effects of situational characteristics on impulse buying. *International Journal of Retail & Distribution Management*, 2014, **42**(4), 298–314, doi: [10.1108/IJRDM-04-2013-0074](https://doi.org/10.1108/IJRDM-04-2013-0074).
18. ROOK, D.W., GARDNER, M.P. In the mood: impulse buying's affective antecedents. *Research in Consumer Behavior*, 1993, **6**(7), 1–28.
19. BEATTY, S.E., FERRELL, M.E. Impulse buying: modeling its precursors. *Journal of Retailing*, 1998, **74**(2), 169–191, doi: [10.1016/S0022-4359\(99\)80092-X](https://doi.org/10.1016/S0022-4359(99)80092-X).
20. BAYLEY, G., NANCARROW, C. Impulse purchasing: a qualitative exploration of the phenomenon. *Qualitative Market Research*, 1998, **1**(2), 99–114, doi: [10.1108/13522759810214271](https://doi.org/10.1108/13522759810214271).
21. BLOCK, L.G., MORWITZ, V.G. Shopping lists as an external memory aid for grocery shopping: influences on list writing and list fulfillment. *Journal of Consumer Psychology*, 1999, **8**(4), 343–375, doi: [10.1207/s15327663jcp0804_01](https://doi.org/10.1207/s15327663jcp0804_01).
22. ENGEL, J.F., BLACKWELL, R.D. *Consumer Behaviour*. 4th ed. Hinsdale : Dryden Press, 1982.
23. NANDA, A.P., BANERJI, D., SINGH, N. Situational factors of compulsive buying and the well-being outcomes: what we know and what we need to know. *Journal of Macromarketing*. 2023, **43**(3), 384–402, doi: [10.1177/02761467231180091](https://doi.org/10.1177/02761467231180091).
24. TAN, L., LI, H., CHANG, Y.W., CHEN, J., LIOU, J.W. How to motivate consumers' impulse buying and repeat buying? The role of marketing stimuli, situational factors, and personality. *Current Psychology*, 2023, **42**(36), 32524–32539, doi: [10.1007/s12144-022-04230-4](https://doi.org/10.1007/s12144-022-04230-4).
25. HUO, C., WANG, X., SADIQ, M.W., PANG, M. Exploring factors affecting consumer's impulse buying behavior in live-streaming shopping: an interactive research based upon SOR model. *SAGE Open*, 2023, **13**(2), 1–15, doi: [10.1177/21582440231172678](https://doi.org/10.1177/21582440231172678).
26. ROBERT, D., JOHN, R. Store atmosphere: an environmental psychology approach. *Journal of Retailing*, 1982, **58**(1), 34–57.
27. YUNIARTI, Y., SYAFRI, R.A. The effect of price promotion time limit on consumer impulse buying through situational factors as intervening variables. In *4th Green Development International Conference (GDIC 2022)*. Atlantis Press, 2023, 1097–1107, doi: [10.2991/978-2-38476-110-4_106](https://doi.org/10.2991/978-2-38476-110-4_106).
28. SAHARI, N., OTHMAN, A.A., ALI, N.M., DJAJANTI, A., KAMAROLZAMAN, N. Unravelling the impact of visual merchandising on consumer impulse buying behaviour in hypermarket. *Environment-Behaviour Proceedings Journal*, 2024, **9**(28), 39–45, doi: [10.21834/e-bpj.v9i28.5874](https://doi.org/10.21834/e-bpj.v9i28.5874).
29. VERHAGEN, T., SWEN, E., FELDBERG, F., MERIKIVI, J. Benefitting from virtual customer environments: an empirical study of customer engagement. *Computers in Human Behavior*, 2015, **48**, 340–357, doi: [10.1016/j.chb.2015.01.061](https://doi.org/10.1016/j.chb.2015.01.061).
30. BABIN, B.J., DARDEN, W.R., GRIFFIN, M. Work and/or fun: measuring hedonic and utilitarian shopping value. *Journal of Consumer Research*, 1994, **20**(4), 644–656, doi: [10.1086/209376](https://doi.org/10.1086/209376).

31. TRIVEDI, V., JOSHI, P., CHATTERJEE, K.N., SINGH, G.P. Impact of store ambience on impulse purchasing of apparel consumers. *Tekstilec*. 2022, **65**(2), 147–156, doi: [10.14502/tekstilec.65.2022015](https://doi.org/10.14502/tekstilec.65.2022015).
32. TURLEY, L.W., MILLIMAN, R.E. Atmospheric effects on shopping behavior: a review of the experimental evidence. *Journal of Business Research*, 2000, **49**(2), 193–211, doi: [10.1016/S0148-2963\(99\)00010-7](https://doi.org/10.1016/S0148-2963(99)00010-7).
33. ATULKAR, S., KESARI, B. Role of consumer traits and situational factors on impulse buying: does gender matter? *International Journal of Retail & Distribution Management*, 2018, **46**(4), 386–405, doi: [10.1108/IJRDM-12-2016-0239](https://doi.org/10.1108/IJRDM-12-2016-0239).
34. GEHRT, K.C., YAN, R.N. Situational, consumer, and retailer factors affecting Internet, catalog, and store shopping. *International Journal of Retail & Distribution Management*, 2004, **32**(1), 5–18, doi: [10.1108/09590550410515515](https://doi.org/10.1108/09590550410515515).
35. MOHAN, G., SIVAKUMARAN, B., SHARMA, P. Impact of store environment on impulse buying behavior. *European Journal of Marketing*, 2013, **47**(10), 1711–1732, doi: [10.1108/EJM-03-2011-0110](https://doi.org/10.1108/EJM-03-2011-0110).
36. ZHUANG, G., TSANG, A.S., ZHOU, N., LI, F., NICHOLLS, J.A. Impacts of situational factors on buying decisions in shopping malls: an empirical study with multinational data. *European Journal of Marketing*, 2006, **40**(1/2), 17–43, doi: [10.1108/03090560610637293](https://doi.org/10.1108/03090560610637293).
37. YU, C., BASTIN, M. Hedonic shopping value and impulse buying behaviour in transitional economies: a symbiosis in the Mainland China marketplace. *Journal of Brand Management*, 2010, **18**(2), 105–114, doi: [10.1057/bm.2010.32](https://doi.org/10.1057/bm.2010.32).
38. PARBOTEEAH, D.V. A model of online impulse buying: an empirical study (Doctoral dissertation). Washington State University, 2005, <https://hdl.handle.net/2376/387>.
39. BAKER, J., PARASURAMAN, A., GREWAL, D., VOSS, G.B. The influence of multiple store environment cues on perceived merchandise value and patronage intentions. *Journal of Marketing*, 2002, **66**(2), 120–141, doi: [10.1509/jmkg.66.2.120.18470](https://doi.org/10.1509/jmkg.66.2.120.18470).
40. PRADHAN, D., ISRAEL, D., JENA, A.K. Materialism and compulsive buying behaviour: the role of consumer credit card use and impulse buying. *Asia Pacific Journal of Marketing and Logistics*, 2018, **30**(5), 1239–1258, doi: [10.1108/APJML-08-2017-0164](https://doi.org/10.1108/APJML-08-2017-0164).
41. YAN, LY., TAN, G.W., LOH, X.M., HEW, J.J., OOI, K.B. QR code and mobile payment: the disruptive forces in retail. *Journal of Retailing and Consumer Services*, 2021, **58**, 1–9, doi: [10.1016%2Fj.jretconser.2020.102300](https://doi.org/10.1016%2Fj.jretconser.2020.102300).
42. AKRAM, U., PENG, H., KHAN, M., YASIR, T., KHALID, M., WASIM, A. How website quality affects online impulse buying: moderating effects of sales promotion and credit card use. *Asia Pacific Journal of Marketing and Logistics*, 2017, **30**(1), 235–256, doi: [10.1108/APJML-04-2017-0073](https://doi.org/10.1108/APJML-04-2017-0073).
43. BADGAIYAN, A.J., VERMA, A., DIXIT, S. Impulsive buying tendency: measuring important relationships with a new perspective and an indigenous scale. *IIMB Management Review*, 2016, **28**(4), 186–199, doi: [10.1016/j.iimb.2016.08.009](https://doi.org/10.1016/j.iimb.2016.08.009).
44. REDINE, A., DESHPANDE, S., JEBARAJA-KIRTHY, C., SURACHARTKUMTONKUN, J. Impulse buying: a systematic literature review and future research directions. *International Journal of Consumer Studies*, 2023, **47**(1), 3–41, doi: [10.1111/ijcs.12862](https://doi.org/10.1111/ijcs.12862).
45. RODRIGUES, R.I., LOPES, P., VARELA, M. Factors affecting impulse buying behavior of consumers. *Frontiers in Psychology*, 2021 **12**, 1–3, doi: [10.3389/fpsyg.2021.697080](https://doi.org/10.3389/fpsyg.2021.697080).
46. MANDOLFO, M., LAMBERTI L. Past, present, and future of impulse buying research methods: a systematic literature review. *Frontiers in Psychology*, 2021, **12**, 1–11, doi: [10.3389/fpsyg.2021.687404](https://doi.org/10.3389/fpsyg.2021.687404).
47. NUNNALLY, J.C. *Psychometric Theory 3E*. Tata McGraw-Hill Education. 1994.
48. SCHROEDER, L.D., SJOQUIST, D.L., STEPHAN, P.E. *Understanding Regression Analysis*. Newbury Park : Sage Publication, 1986.

Appendix 1

Table 6: Measurement items and content

Variable	Measurement	Content	References
Impulse Buying Behaviour (IBB)	IBB1	When I see a new trend in apparel, I buy it instantly.	[31]
	IBB2	When I go apparel shopping, I buy apparel that I had not intended to buy.	
	IBB3	I cannot suppress the desire of wanting to buy a new style of apparel spontaneously.	
	IBB4	I frequently purchase apparel items without any prior thought.	
	IBB5	Based on your past experiences of apparel shopping, do you agree that you buy apparel products on impulse?	
Availability of Time (AT)	AT1	If I have enough time to spend, I make more purchases.	[32, 33]
	AT2	Does more time for shopping result in unplanned purchase?	
	AT3	When I have time constraints, I buy only items that I actually need.	
	AT4	When I have little time, I buy those items that are on my shopping list.	
Availability of Money (AM)	AM1	Does money availability impact your purchasing behaviour?	[33–35]
	AM2	Do you agree that you buy apparel products that are low price, even if you do not plan to make a purchase?	
	AM3	When I feel financially comfortable, I tend to make more impulse purchases.	
	AM4	I often control my feelings to buy something impulsively because of my limited budget.	
Salesperson's Behaviour (SB)	SB1	Are the efforts of sales staff important in impulse purchases?	[36]
	SB2	Does sales staff directly influence your impulse purchase?	
	SB3	Does the sales staff's ability to create a sense of urgency or excitement about a product or offer lead to your impulse purchases?	
	SB4	How likely are you to make an impulsive purchase primarily because of a persuasive salesperson?	
Promotional Offers (PO)	PO1	When I see a special promotional sign in a store, I go to look at the products.	[43, 44]
	PO2	I am more likely to make unplanned purchases if the apparel product has a sale sign.	
	PO3	If you see discount price, you tend to buy impulsively.	
	PO4	Any offer, such as BUY one GET one and so on, organized by stores affects your buying behaviour	
Payment Methods (PM)	PM1	Do you think payments using cards, UPI, Paytm, etc. are more convenient than cash payments?	[42, 43]
	PM2	Do you think the ability to make payments using debit or credit cards increases impulse purchase?	
	PM3	Do you believe that the ease of using a different payment method, such as credit cards, UPI, Paytm, etc., encourages you to make more impulse purchases?	
	PM4	Do you agree that offers (cash back, discount, etc) for using digital payments methods, such as credit cards, UPI, Paytm, etc., increase impulse purchases?	

Ambreen, Kashif Javed, Asfandyar Khan, Faiza Anwar, Imran Ahmad Khan, Mumtaz Hassan Malik
Department of Textile and Apparel Science, University of Management and Technology, Lahore-54470, Pakistan

Analysis of Identifying and Correcting the Digital Printing Defects in Pakistan's Textile Industry

Analiza prepoznavanja in odpravljanja napak pri digitalnem tisku v pakistanski tekstilni industriji

Original scientific article/Izvorni znanstveni članek

Received/Prispelo 6-2024 • Accepted/Sprejeto 11-2024

Corresponding author/Korespondenčni avtor:

Imran Ahmad Khan

Tel: +92-3139374141

E-mail: enggimran110@gmail.com

ORCID iD: 0000-0002-7127-5509

Abstract

This paper provides an in-depth examination of the issues hindering the adoption of digital textile printing in Pakistan. It presents background on commonly used printing techniques, and analyses industry data to identify major printing defects using quality tools such as Pareto charts and correlation analysis. The root causes of the main defects were determined through cause-effect diagrams and the 5 Whys approach. Preventive solutions are proposed in connection with fabric preparation, process controls, equipment maintenance, training, and sustainable practices. Instead of recommending broad strategies, the study focused on actionable solutions for addressing specific challenges in digital printing, including practical measures for improving operational efficiency in recycling. The analysis provides a comprehensive roadmap for Pakistan's textile industry to overcome current limitations and successfully transition to digital systems for improved productivity, innovation, profitability and global competitiveness.

Keywords: digital printing, textile industry, Pakistan, printing defects, challenges and solutions, sustainability

Izveček

V članku je podana poglobljena analiza problemov, ki ovirajo usvojitve digitalnega tekstilnega tiska v Pakistanu. Predstavljene so pogosto uporabljene tehnike tiskanja ter podani rezultati analize podatkov iz industrijske prakse, ki so osredinjeni na ugotavljanje glavnih napak pri tisku. Analiza je bila izvedena s pomočjo orodij za oceno kakovosti, tj. Paretovimi grafikoni in korelacijsko analizo. Temeljni razlogi glavnih napak so bili določeni iz diagramov vzrokov in posledic in s pomočjo rezultatov analize "strategije petih zakajev". Predlagane so preventivne rešitve, ki vključujejo pravo tkanin, nadzor procesov, vzdrževanje opreme, usposabljanje in trajnostne prakse. Namesto priporočanja široko zasnovane strategije študija predlaga uporabne rešitve za posebne izzive v digitalnem tiskanju, vključno s praktičnimi ukrepi za izboljšanje operativne učinkovitosti recikliranja. Analiza ponuja celovit načrt za pakistansko tekstilno industrijo, da premaga trenutne omejitve in uspešno preide na digitalne sisteme za izboljšano produktivnost, inovativnost, dobičkonosnost in globalno konkurenčnost.

Ključne besede: digitalni tisk, tekstilna industrija, napake pri tiskanju, izzivi in rešitve, trajnost



Content from this work may be used under the terms of the Creative Commons Attribution CC BY 4.0 licence (<https://creativecommons.org/licenses/by/4.0/>). Authors retain ownership of the copyright for their content, but allow anyone to download, reuse, reprint, modify, distribute and/or copy the content as long as the original authors and source are cited. No permission is required from the authors or the publisher. This journal does not charge APCs or submission charges.

1 Introduction

Digital printing and imaging technologies are revolutionizing textile design and production worldwide [1]. Unlike conventional methods that require screens or engraved rollers, digital printing uses digital data and software to guide printer heads, depositing ink directly onto fabric based on the desired pattern [2]. This approach enables on-demand printing, rapid design adjustments, high colour vibrancy, reduced material waste and customized small-batch production [3]. Among digital printing techniques, ink-jet printing is a practice that facilitates printing on various textile substrates, such as cotton, bamboo and silk, without direct contact between the substrate and ink. It has gained attention due to its simplicity, speed, and reduced material usage [4–6]. Common defects in digital printing include fabric distortion, registration errors, ink smudging, nozzle blockages and colour matching problems [5]. Addressing these defects and process limitations is essential for the widespread adoption of digital printing in Pakistan's textile sector.

Pakistan's textile and apparel sector is a key industry, accounting for about 60% of the country's exports. However, the adoption of digital processes has lagged behind major competitors such as China, India and Bangladesh due to limited technical expertise. Digital printing and imaging offer significant advantages, including the ability to create customized, photorealistic prints in small batches with reduced material waste. This technology eliminates the need for the physical screens and rollers used in conventional printing [6]. Digital printing allows for last-minute design changes, on-demand printing and reduced setup costs, making it ideal for small-batch production. It also enables faster time-to-market, the ability to quickly switch between designs and photorealistic quality with unlimited colour options [7]. Despite these advantages, Pakistan's textile sector faces the challenge of limited infrastructure and technical expertise in digital

printing, which hinders the industry's ability to fully capitalize on this technology and remain competitive in the global market.

This paper presents an in-depth examination of impediments to the introduction of digital printing in Pakistan's textile sector. It analyses empirical industry data to quantify major printing defects and utilizes quality tools such as Pareto charts, correlation analysis, and cause-effect diagrams to investigate the root causes. Targeted solutions are proposed, encompassing fabric pretreatment, process controls, equipment maintenance and training. The analysis also provides strategies to tackle broader challenges regarding rising costs, technology investments, business acquisition, cash flows and environmental sustainability. The examination culminates in recommendations to promote digital printing's growth through synergistic initiatives between industry stakeholders, research institutions and policy bodies. By applying the proposed solutions, Pakistan's textile sector can overcome current limitations in quality, productivity and capabilities. The transition to digital technologies and systems will bolster the industry's competitiveness and exports through enhanced flexibility, efficiency and sustainability.

2 Materials and methods

The materials used in this study were mainly industrial grades such as sodium alginate, urea, sodium bicarbonate and a non-ionic detergent. The study was conducted at Maa Textiles, which operates an MS JP5 Evo inkjet printer from Kyocera's KJ4 series for digital textile printing. The printer uses water-based reactive dye inks (Xennia Amethyst Evo RC, acquired from Sun chemicals), specifically formulated for cellulosic fabrics. The primary substrate used in this study was 100% cotton fabric with a weight of 150 g/m².

2.1 Pre-treatment of fabric

Prior to printing, fabric undergoes a specialized pre-treatment process crucial for digital printing success. The fabric was pretreated to optimize ink reception and colour development during digital printing. A pretreatment solution was prepared containing sodium alginate (50 g/L) as a thickener to control ink spread, urea (100 g/L) to enhance dye solubility and distribution, sodium bicarbonate (20 g/L) as an alkali to facilitate dye-fibre bonding and a non-ionic detergent (5 g/L) to improve wetting and ink penetration. The fabric was padded with this solution to achieve an 80% wet pick-up and subsequently dried at 100°C for 2 minutes. This pretreatment ensured the fabric's suitability for the subsequent printing and steaming processes.

2.2 Data collection

The research encompassed the direct empirical observation of the “Maa Textiles” industry in Pakistan to determine the types and prevalence of printing defects encountered in real production settings. Maa Textiles operates an MS JP5 Evo inkjet printer from Kyocera's KJ4 series for digital textile printing operations. Quantitative data was gathered regarding the various defect categories observed during digital printing runs over a one-month period. On average, around 10 production runs were conducted daily, with each run comprising 50–100 meters of printed fabric. Approximately 5–7 defects occurred during each run. The frequency of the total defects that occurred during the printing process is presented in Table 1. The data was analysed using *Pareto analysis* to prioritize the defects based on occurrence and *correlation analysis* to identify relationships between the defects.

Table 1: Types of defects and the effects thereof

Defect Type	Production Effect	No of failures/month
Plate tear (A)	CTP (aluminium) plates were cracked due to marks on paper.	90
Zero setting (B)	Make-in key was not properly set.	0
Solid problem (C)	Printed areas appear darker due to excessive ink deposition, resulting in reduced print quality.	60
Wiper issue (D)	A wiper issue occurred with the same frequency. It indicates problems related to the wiper component in the printing process.	4
Doubling (E)	Design overlap occurred due to doubling, reducing clarity and precision.	120
Leakage (F)	Due to environmental changes and various problems such as seal kit, air leakage elbow, etc.	2
Impression setting (G)	Registration problems and plate tear problems.	4
Nozzle missing (H)	This issue occurred most frequently, making it the highest priority for resolution. The absence of a nozzle can lead to significant problems in the process or system.	450

3 Results and discussion

Pareto analysis, also referred to as the 80/20 rule, arranges issues based on severity, frequency or economic impact [8]. It draws attention to the vital few defects causing the majority of problems. Addressing these few high-impact vital factors yields disproportionately large gains. Figure 1 displays the Pareto chart

for observed defects. The top four issues based on frequency are as follows: nozzle missing (450 instances). This is the most common defect, arising almost 1.5 times per production run. Missing nozzles significantly hamper the print quality; colour matching errors (300 instances). Wrong or inaccurate colour reproduction occurred in 1 out of 3 runs; doubling defects (120 instances). This involves repeated or

overlapping prints arising due to improper ink drying before overlaying subsequent layers; and plate tears (90 instances). This includes the damage and tearing of printing plates made from fragile photopolymer materials. The remaining defect types occurred sporadically, with leakage and blockages being rare. Prioritizing improvements for the top four vital issues can yield substantial gains.

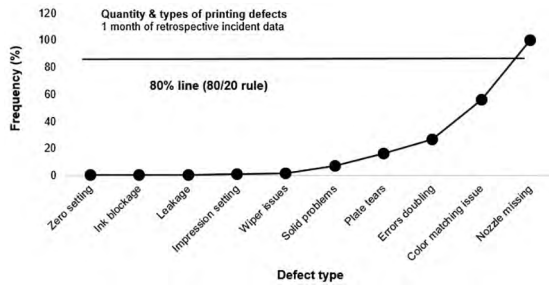


Figure 1: Printing defects applying the 80/20 rule

3.1 Correlation analysis

Correlation analysis quantifies the strength of the relationship between two variables, with the correlation coefficient (r) ranging from -1 to 1. Values nearing -1 or 1 indicate strong negative and positive correlations respectively, while 0 denotes no correlation [9]. Table 2 provides the calculated r values (calculated using equation 1) between the observed defect types. The strongest positive correlation of 0.6 exists between plate tears and impression-setting adjustments. Enhancing impression settings may also reduce plate tears. The strongest negative correlation (-0.4) occurs between wiper issues and impression setting. As wiper problems decrease, impression-setting defects may rise. Analysing correlations enables focused solutions targeting interconnected defects. For example, the positive correlation between plate tears and impression setting indicates that enhancing impression systems can also mitigate the occurrence of plate tears.

$$r = \frac{\sum(x_i - \bar{x})(y_i - \bar{y})}{\sqrt{\sum(x_i - \bar{x})^2 \sum(y_i - \bar{y})^2}} \quad (1)$$

Table 2: Pearson correlation coefficient for each pair of defect types

Defect 1	Defect 2	Correlation coefficient (r)
Plate tear	Zero setting	0.05
Plate tear	Solid problem	0.2
Plate tear	Wiper issue	-0.1
Plate tear	Doubling	0.4
Plate tear	Leakage	0.1
Plate tear	Impression setting	0.6
Zero setting	Solid problem	0.3
Zero setting	Wiper issue	0.2
Zero setting	Doubling	0.1
Zero setting	Leakage	0.4
Zero setting	Impression setting	0.2
Solid problem	Wiper issue	-0.2
Solid problem	Doubling	0.3
Solid problem	Leakage	0.1
Solid problem	Impression setting	0.5
Wiper issue	Doubling	-0.1
Wiper issue	Leakage	-0.3
Wiper issue	Impression setting	-0.4
Doubling	Leakage	0.2
Doubling	Impression setting	0.3
Leakage	Impression setting	0.1

The heatmap illustrates the relative strength of the correlations, with darker colours indicating stronger correlations (both positive and negative) as shown in Figure 2. Light blue shades indicate a weak positive correlation. Dark red shades indicate a strong negative correlation. For example, the darkest red square shows a -0.4 correlation between wiper issue and impression setting. Light red shades indicate a weak negative correlation. White indicates no correlation (a correlation coefficient of 0). This correlation analysis provides insights into relationships between the different defects. A company could use these results to prioritize the resolution of addressing defects that are strongly correlated, as fixing one issue may also reduce the occurrence of related defects.

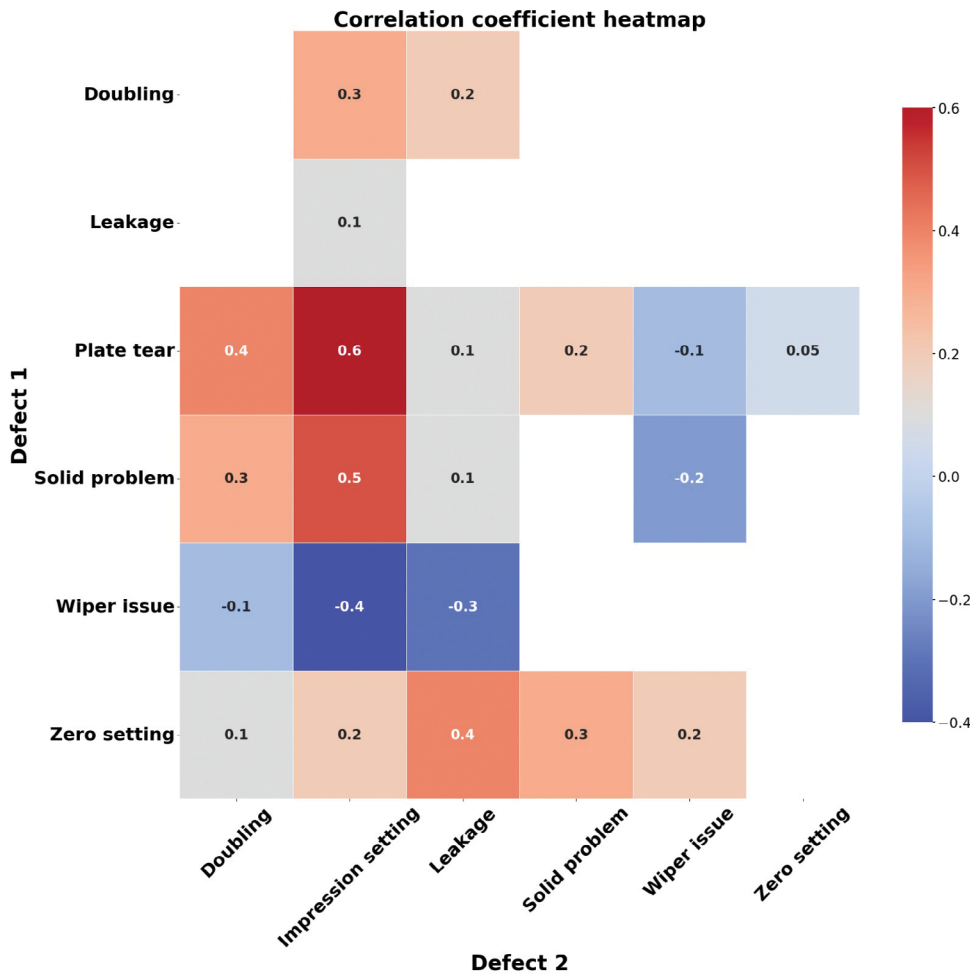


Figure 2: Heatmap analysis of the relative strength of the correlations

3.2 Cause and effect analysis

Structural tools such as cause-effect diagrams, 5 Whys analysis and failure mode analysis help determine the latent factors responsible for producing visible printing defects. The fishbone diagram links defects through progressive causal relationships to reveal their main sources as depicted in Figure 3 for the most important issues identified. A fishbone diagram (3a) illustrates the potential causes of the “tear plate” problem. These causes are categorized into gear condition (issues related to the physical state of the gear, such as misalignment, missing teeth or inaccurate physical dimensions), plate mounting, physical gear accuracy, magnet function, cylinder position, ink/grease accuracy, cylinder/plate condition and impression cylinder concentricity. By identifying these

causes, it is possible to investigate and address the root cause of the problem. Figure 3b presents a fishbone diagram for the potential causes of “zero setting” issues in the printing process. These causes are categorized into material, human (i.e. human factors that may influence zero setting, including improper ink setting techniques, unclean ink ducts and variations in ink setting.), method and measurement. Figure 3c presents a fishbone diagram for the leakage issue, and depicts various sources of ink or chemical leakage in the printing system, including equipment wear and environmental factors. Once we have isolated these contributing elements, we can pinpoint the root of the issue and implement appropriate remedies.

3.3 Proposed solutions

3.3.1 Nozzle clogging

Nozzle clogging was the most frequent defect, occurring 450 times due to dried ink or dust blocking nozzle openings, resulting in missed spots and lines on printed fabric. Ink pigments and additives also accumulate over time, causing defects only after a coverage threshold is reached [10]. Solutions include preventative maintenance with pressurized, filtered ink delivery, covering idle printheads and routine cleaning methods, such as back-flushing, vacuum extraction and ultrasonic cleaning. Purging and priming can flush out obstructions, while automated vision systems enable the proactive detection of nozzle issues. A combination of preventative maintenance, regular cleaning and advanced monitoring addresses nozzle clogging effectively [11].

3.3.2 Colour matching errors

Inaccurate colour reproduction, the second most frequent defect occurring 300 times, resulted from deviations between desired and digital artwork colours due to several factors. Software issues, such as glitches in raster image processors and incorrect colour management settings, contributed to the problem. Hardware limitations, inadequate fabric pretreatment and variable room conditions also affected colour accuracy. Ceramic ink requires proper viscosity and surface tension, along with dispersion stability of the inorganic pigments [10]. The purpose of this study is the formulation of an environment-friendly ceramic ink with a water-based system; using nano-sized CoAl_2O_4 pigment as a raw material, ink should have dispersion stability to prevent nozzle clogging during ink-jet printing process. In addition, the surface tension of the ceramic ink was optimized with the polysiloxane surfactant according to the surface tension requirement (20 - 45 mN/m). Solutions include adhering to manufacturer colour profiling guidelines, optimizing software settings, matching fabric pretreatment to ink chemistry, maintaining a stable room temperature and humidity, and using a spectrophotometer for colour testing.

Effective colour management, software adjustments, hardware upgrades, controlled conditions and proactive testing can resolve these issues.

3.3.3 Ghosting and doubling defects

Ghosting and doubling defects, which occurred 120 times, arise when subsequent ink layers are applied before the initial layer dries, causing the ink to spread. Contributing factors include high production speeds, excessive ink limits, high print densities, improper printhead height, and variable humidity and temperature. Solutions include reducing machine speed, lowering ink densities, adjusting printhead height, adding drying systems and controlling ambient conditions [12]. These adjustments can prevent defects by ensuring proper drying between layers.

3.3.4 Plate tears and damage

Photopolymer printing plates, which showed tearing in 90 runs, are prone to damage from pressure and mechanical stress. Factors include defective plates with micro-fissures, improper press roller settings, mishandling leading to bends and nicks, and debris causing abrasion [13]. Solutions involve using smooth rollers and cushioned mounting blankets, following correct mounting procedures, regularly cleaning presses to remove debris, avoiding contact with hard surfaces and inspecting equipment to screen out defective plates. Proper material selection, careful handling, press maintenance and inspection can mitigate tearing issues [14].

3.3.5 Fabric pretreatment

Based on the root cause analysis, the following solutions are proposed to address the major printing defects and limitations. Proper fabric selection and pretreatment are crucial for eliminating impurities and enhancing ink absorption capacity. Pretreatment processes adjust surface properties to align with ink chemistry and facilitate dye fixation. For successful digital printing, fabric pretreatment is crucial to ensure optimal ink absorption and colour

development. The pretreatment process for digital printing typically involves the following steps:

- i. the application of a thickening agent (e.g., sodium alginate) to control ink spread and prevent bleeding;
- ii. the addition of hygroscopic substances such as urea to keep the fabric moist during steaming, promoting dye migration and fixation;
- iii. the incorporation of alkali (e.g., sodium bicarbonate) to facilitate the reaction between dye and fibre;

- iv. the use of sequestering agents to prevent interference from water hardness ions; and
- v. the application of a wetting agent to ensure even distribution of the pretreatment chemicals and subsequent ink penetration.

This specialized pretreatment is distinct from conventional textile preparation processes and is tailored to the specific requirements of digital reactive dye printing on cellulosic fabrics.

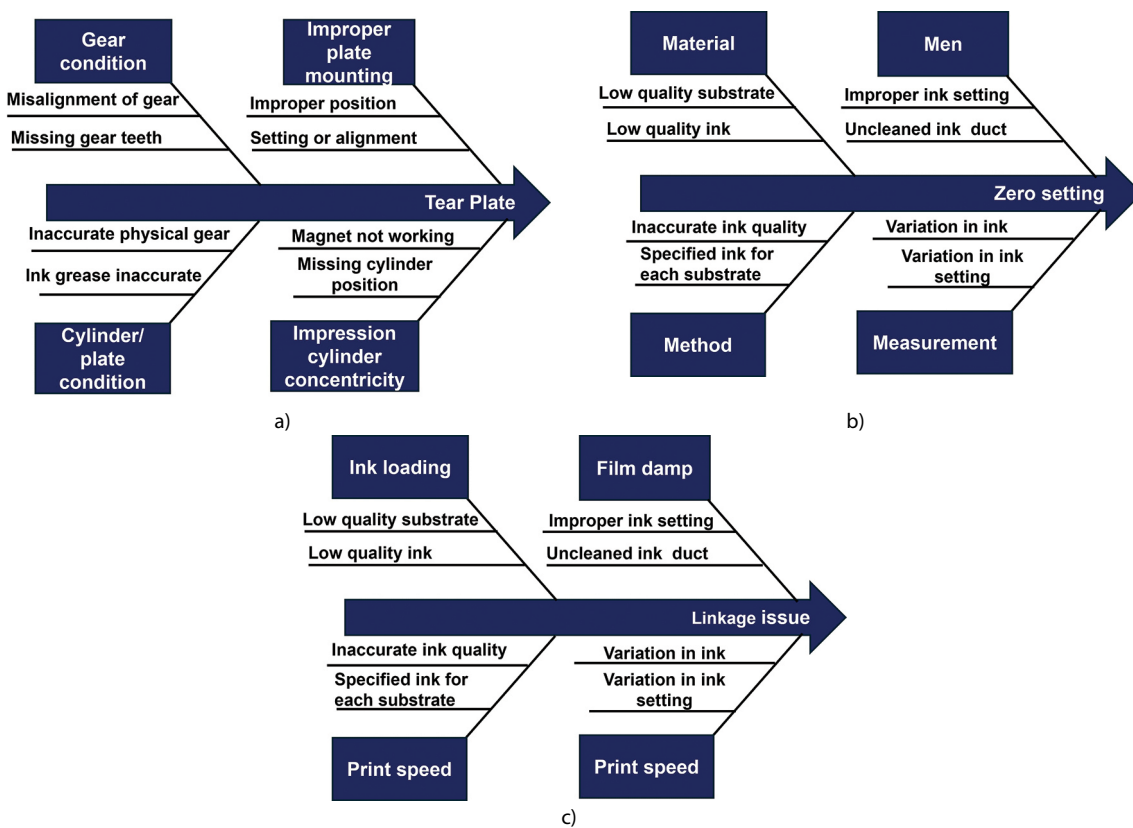


Figure 3: Fishbone diagrams for a) tear plate, b) zero setting and c) leakage issue

3.3.6 Controlled material handling

Fabric requires careful handling during printing to avoid stretching and distortion leading to misregistration errors. Integrating motorized roll tension controls provides the required tautness. Guidelines include avoiding sharp redirection over rollers and hardware edges, incorporating electronic yarn break

detectors to stop machines, maintaining tension within manufacturer's recommended range, employing edge guide sensors to prevent lateral drift and using pneumatic tension control for precise force regulation [15].

3.3.7 High-performance Inks

Specialty inks designed for specific fabric types enable optimal ink-fibre bonding while resisting cracking, bleeding and fading. Variables include pigment versus dye, where pigments have higher lightfastness but less saturation, while dyes offer vivid hues but moderate wash fastness [16]. Nanoscale pigment dispersion provides stable colloidal inks. Rheological additives provide favourable viscosity, density and surface tension. Binders enhance pigment adhesion to the fabric surface. Surfactants lower surface tension enabling smoother ink flow [17].

3.3.8 Printer maintenance

Regular maintenance procedures are imperative for preserving printhead health, nozzle integrity and colour consistency. Best practices involve automated cleaning cycles to prevent dried ink accumulation, printhead priming and purging to unclog nozzles, monitoring nozzle status through drop detection systems, spectrophotometry and densitometry to calibrate colour, and the timely replacement of worn printer components such as belts and rollers [18].

3.3.9 Operator training

Focused training programmes continually raise worker expertise in areas such as fabric inspection procedures to identify defects prior to printing, colour management principles for reliable colour matching, standard operating procedures for machine operation and maintenance, instructional videos and demonstrations for hand-eye coordination, and certifications through testing on process parameters and variables [19].

3.3.10 Tighter process controls

Enhancing process controls and monitoring enables quicker defect detection and minimizes material losses. Strategies comprise real-time machine vision systems to detect defects and abnormal process conditions. Integrating statistical process control charts can be used to reduce variability. Barcode tracking for materials can be used to pinpoint error sources.

Automated alerts using sensors can be used to notify inconsistencies. Data analytics can be used to identify high-waste processes needing improvement [20].

4 Conclusion

This research provides a detailed analysis of defects impeding the introduction of digital textile printing in Pakistan, paired with targeted solutions and future recommendations. Industry data was rigorously examined to identify and prioritize the most prevalent printing issues using Pareto, descriptive and correlational techniques. The root causes for key defects were determined using structured tools such as cause-effect diagrams and 5 Whys analysis. Solutions were proposed encompassing fabric pre-treatment, controlled handling, high-performance inks, vigilant printer maintenance, operator training, process controls and sustainable recycling. Rather than proposing broad strategies, the study concentrated on actionable solutions to address specific challenges in digital printing, including practical measures for enhancing operational efficiency and advancing recycling practices. Finally, recommendations were presented on collaborative initiatives, training programmes, research and development, access to finance, new markets and environmental sustainability to propel digital printing forward. By applying these proposed solutions, Pakistan's textile sector can overcome current limitations in quality, productivity and capabilities. The transition to digital technologies will enhance flexibility, efficiency, sustainability and global competitiveness. The analytical techniques, findings and recommendations provide a comprehensive roadmap to accelerate digital printing's future expansion.

Challenges and future progress

This study focused on one printer to facilitate an in-depth analysis of the occurrence of defects and the underlying causes thereof. However, the importance of expanding this research has been noted, and

future studies will include additional printers. These investigations can consider various factors, such as substrate types, external conditions and printer age, to validate and extend the findings. Several broader challenges impede the extensive introduction of digital printing in Pakistan's textile sector. Escalating raw material, energy, labour and financing costs strain traditionally low-profit margins in printing businesses. Management tactics to lower expenses include the bulk purchasing of fabrics and chemicals, negotiating discounts with suppliers, utilizing government incentives and loans for equipment, enhancing production efficiency and diversifying product offerings to maximize asset utilization. Generating adequate print orders to warrant investments in digital printers poses difficulties. Strategies to attract new clients include offering specialized niche printing services, actively communicating expanded capabilities to customers, obtaining client referrals and testimonials, participating in textile trade fairs and exhibitions, and developing an online presence and social media marketing campaigns. New printing technologies provide advantages but require carefully planned implementation. Principles for technology integration encompass realistically assessing return on investment and payback periods, prioritizing upgrades that deliver maximum productivity gains, initially adopting smaller-scale innovations to minimize risk and extensively training workers on the functioning of new equipment. Managing cash flows is also imperative for printing businesses with thin margins. Tactics to improve liquidity include requesting advance payments from clients, providing discounts for early invoice settlement, rigorously following up on late payments, accurately forecasting cash inflows and outflows, and maintaining liquid reserves and access to working capital.

To spur digital printing's continued expansion, collaborative initiatives between textile firms, original equipment manufacturers (OEMs), chemical providers and academic institutes can facilitate co-developing solutions through knowledge transfer.

Comprehensive workforce training programmes on digital printing best practices are vital for enhancing product quality and equipment capabilities. Ongoing research and development projects with industry and academia can refine printing techniques, specialty inks, pre-treatments and process automation. Providing flexible credit lines and subsidized loans would enable firms to invest in advanced digital equipment. Exploring new geographical regions and product segments opens additional market opportunities for digitally printed textiles. Adopting green initiatives in the areas of energy, water, effluents, and waste reduction contributes to environmental sustainability. By proactively addressing challenges and implementing these recommendations, Pakistan's textile industry can fully capitalize on digital printing's benefits. The solutions and future progress strategies will assist the sector in overcoming limitations, thereby boosting productivity and flexibility, achieving global competitiveness and establishing leadership in digital textile manufacturing.

Conflicts of interest

The authors hereby declare that there were no potential conflicts of interest concerning the research, authorship and/or publication of this article.

Funding

The authors received no financial support for the research, authorship and/or publication of this article.

References

1. KUMELACHEW, D.M., WAGAYE, B.T., ADAMU, B.F. Digital textile printing innovations and the future. In *Digital Textile Printing*. Edited by H. Wang and H. Memon. Woodhead Publishing, 2023, 241–259, doi: 10.1016/B978-0-443-15414-0.00009-1.
2. UGUR KOSEOGLU, A. Innovations and analysis of textile digital printing technology. *International Journal of Science, Technology and Society*, 2019, 7(2), 38–43, doi: 10.11648/j.ijsts.20190702.12.
3. NTIM, C.K., OCRAN, S.P., ACQUAYE, R. Digital textile printing: a new alternative to short-run textile printing in Ghana. *International Journal of Technology and Management Research*, 2(1), 60–65, doi:10.47127/ijtmr.v2i1.51.
4. ARSHAD, M.Z. Internal capabilities and SMEs performance: a case of textile industry in Pakistan. *Management Science Letters.*, 2019, 9(4), doi: 10.5267/j.msl.2019.1.001.
5. IQBAL, T., HUQ, F., BHUTTA, M.K.S. Agile manufacturing relationship building with TQM, JIT, and firm performance: an exploratory study in apparel export industry of Pakistan. *International Journal of Production Economics*, 2018, 203, 24–37, doi: 10.1016/j.ijpe.2018.05.033.
6. GOOBY, B. The development of methodologies for color printing in digital inkjet textile printing and the application of color knowledge in the Ways of Making project. *Journal of Textile Design Research and Practice*, 2020, 8(3), 358–383, doi: 10.1080/20511787.2020.1827802.
7. JUNG, J.J., KIM, S., PARK, C.K. Optimization of digital textile printing process using Taguchi method. *Journal of Engineered Fibers and Fabrics*, 2016, 11(2), 1–9, doi:10.1177/155892501601100207.
8. RASHID, M.R., GHOSH, S.K., ALAM, M.F.B., RAHMAN, M.F. A fuzzy multi-criteria model with Pareto analysis for prioritizing sustainable supply chain barriers in the textile industry: evidence from an emerging economy. *Sustainable Operations and Computers*, 2024, 5, 29–40, doi: 10.1016/j.susoc.2023.11.002.
9. YILMAZ, T. The relationship between capital structure and return on capital: a canonic correlation analysis on textile industry. *PressAcademia*, 2022, 15, 84–88, doi: 10.17261/pressacademia.2022.1582.
10. KWON, J.W., SIM, H.S., LEE, J.H., HWANG, K.T., HAN, K.S., KIM, J.H., KIM, U.S. Optimization of aqueous nano ceramic ink and printing characterization for digital ink-jet printing. *Journal of the Korean Ceramic Society*, 2017, 54(6), 478–483, doi: 10.4191/kcers.2017.54.6.01.
11. ISLAM, M.R., AFROJ, S., YIN, J., NOVOSELOV, K.S., CHEN, J., KARIM, N. Advances in printed electronic textiles. *Advanced Science*, 2024, 11(6), 1–50, doi: 10.1002/advs.202304140.
12. SMITH C. Inkjet technology within the label converting market. In *Handbook of Industrial Inkjet Printing: a Full System Approach*. Edited by Werner Zapka. John Wiley & Sons, 2017, 681–722, doi: 10.1002/9783527687169.
13. MEERADEVI, T., SASIKALA, S. Automatic fabric defect detection in textile images using a labview based multiclass classification approach. *Multimedia Tools and Applications*, 2024, 83, 65753–65772, doi: 10.1007/s11042-023-18087-7.
14. *The Printing Ink Manual*. Edited by R.H. Leach. Springer Science & Business Media, 1993, 804–864.
15. TADESSE, M.G., NAGY, L., NIERSTRASZ, V., LOGHIN, C., CHEN, Y., WANG, L. Low-stress mechanical property study of various functional fabrics for tactile property evaluation. *Materials*, 2018, 11(12), 1–13, doi: 10.3390/ma11122466.
16. LI, L., CHU, R., YANG, Q., LI, M., XING, T., CHEN, G. Performance of washing-free printing of disperse dye inks: influence of water-borne polymers. *Polymers*, 2022, 14(20), 1–13, doi: 10.3390/polym14204277.
17. ELSHEMY, N.S., HAGGAGE, K., EL-SAYED, H. A critique on synthesis and application of binders in textiles pigment printing. *Egyptian*

- Journal of Chemistry*, 2022, **65**(9), 539–549, doi: 10.21608/EJCHEM.2022.116492.5264.
18. CORRALL, J. Konica Minolta's inkjet print-head technology. In *Handbook of Industrial Inkjet Printing: a Full System Approach*. Edited by Werner Zapka. Wiley, 2017, doi: 10.1002/9783527687169.ch14.
 19. WARDANI, I.K., IFTADI, I., ASTUTI, R.D. Design of tools to reduce the risk level of work postures at warping station. *Jurnal Sistem Dan Manajemen Industri*, 2020, **4**(1), 30–40, doi: 10.30656/jsmi.v4i1.1997.
 20. SHANG, S.M. Process control in printing of textiles. In *Process Control in Textile Manufacturing*. Edited by Abhijit Majumdar, Apurba Das, R. Alagirusamy and V.K. Kothari. Woodhead Publishing, 2012, 339–362, doi: 10.1533/9780857095633.3.339.

Mehmet Karahan,^{1,2} Muhammad Ali Nasir,³ Rizwan Ahmed Malik⁴

¹ Vocational School of Technical Sciences, Bursa Uludag University, 16059, Bursa, Türkiye

² Butekom Inc., Demirtas Dumlupinar OSB District, 2nd Cigdem Street No:1/4, 16245, Osmangazi, Bursa, Türkiye

³ Department, of Mechanical Engineering, University of Engineering, and Technology, Taxila, 47080, Pakistan

⁴ Department of Mechanical Engineering, College of Engineering, Prince Sattam bin Abdulaziz University, Al-Kharj 11942, Saudi Arabia

Effect of Fibre Type and Fabric Structure on Composite Materials Under Ballistic Shock Impact

Vpliv vrste vlaken in strukture ploskovne tekstilije kompozitnih materialov pri balističnem udaru

Original scientific article/Izvirni znanstveni članek

Received/Prispelo 7–2024 • Accepted/Sprejeto 11–2024

Corresponding author/Korespondenčni avtor:

Prof. Dr. Mehmet Karahan

E-mail: mkarahan@uludag.edu.tr

ORCID iD: 0000-0003-3915-5598

Abstract

This study analysed the effect of fibre type and fabric structure on the behaviour of aramid and ultra-high molecular weight polyethylene (UHMW PE) composite plates under ballistic shock loading. A specific test system that simulates a ballistic shock wave was prepared in this context. Aramid composite plates are reinforced with three types of fabric structure, while UHMW PE composite plates are reinforced with a single fabric structure. The plates were cured in an autoclave. The ballistic explosion behaviour of composite plates was evaluated in terms of trauma depth, trauma diameter and absorbed energy at the ballistic limit. The results of the ballistic tests showed that GS3000-reinforced composites demonstrated the highest energy absorption. In contrast, UHMW PE composite plates exhibited higher ballistic energy absorption on a unit-weight basis than other plates. UHMW PE fabric-reinforced composites showed approximately 30% higher energy absorption per unit area density than other composites. Biaxial aramid fabric composite plates exhibited 10% higher energy absorption per unit area density than woven aramid fabric composite plates. Additionally, UD-aramid GS3000 reinforced composite demonstrated the lowest trauma depth of all tested composites, showing 90% less trauma depth than UHMW PE fabric-reinforced composites.

Keywords: composites, ballistic, shock loading, aramid, UHMW PE

Izveček

V raziskavi je analiziran vpliv vrste vlaken in strukture ploskovnih tekstilij iz aramidnih vlaken in vlaken iz polietilena ultra visoke molekulske mase (UHMW PE) na obnašanje kompozitnih plošč pri balistični udarni obremenitvi. V ta namen je bil pripravljen poseben testni sistem, ki simulira balistično udarno valovanje. Kompozitne plošče so bile ojačene z aramidnimi ploskovnimi tekstilijami treh različnih struktur in eno polietilensko (UHMW PE) ploskovno tekstilijo ter utrjene v avtoklavu. Balistično obnašanje kompozitnih plošč je bilo ocenjeno glede na globino poškodbe, premer



Content from this work may be used under the terms of the Creative Commons Attribution CC BY 4.0 licence (<https://creativecommons.org/licenses/by/4.0/>). Authors retain ownership of the copyright for their content, but allow anyone to download, reuse, reprint, modify, distribute and/or copy the content as long as the original authors and source are cited. No permission is required from the authors or the publisher. This journal does not charge APCs or submission charges.

poškodbe in absorbirano energijo pri balistični meji. Rezultati balističnih testov so pokazali najvišjo absorpcijo energije pri kompozitu, ojačenem z enoosno orientirano tekstilijo Aramid UD GS3000. V nasprotju s tem pa so kompozitne plošče, ojačene z enoosno orientirano tekstilijo UHMW PE UD Dyneema H62, dosegle za približno 30 odstotkov višjo absorpcijo balistične energije na enoto ploščinske mase kot druge plošče. Kompozitne plošče, ojačene z aramidnimi dvoosno usmerjenimi tekstilijami brez tkanja, so dosegle za 10 odstotkov višjo absorpcijo energije na enoto ploščinske mase kot kompozitne plošče, ojačene z aramidno tkanino. Poleg tega je kompozit, ojačen z UD aramidno ploskovno tekstilijo GS3000, dosegel najmanjšo globino poškodbe v primerjavi z drugimi kompoziti, pri čemer je bila globina poškodbe za 90 odstotkov manjša kot pri kompozitih, ojačenih s tkanino iz UHMW PE.

Ključne besede: kompoziti, balistika, udarna obremenitev, aramid, UHMW PE

1 Introduction

The need to provide personal protection against explosives and ballistic threats using lightweight materials is rising [1–3]. High-performance fibres and associated fabrics, such as aramid and ultrahigh molecular weight polyethylene (UHMW PE), are widely used in personnel armour systems against exploding ammunition fragments, such as protective helmets and armour panels [1, 4, 5]. Manufacturers often use these fibres as reinforcement in the form of continuous filaments or woven fabric embedded in a resin [5–7].

Behaviour under ballistic shock waves refers to the response of composite materials when subjected to high-velocity impacts or explosions. The effect of manufacturing parameters on various composite plates under ballistic impact was studied, and provided insights into how different parameters influence the blast behaviour of composites. Understanding behaviour under ballistic shock waves is crucial for designing materials that can withstand such extreme conditions. Comparative analysis of fibres as composite reinforcement provides valuable information on how to enhance the ballistic blast resistance of composites. Understanding how composite materials respond to ballistic shock waves is essential for defence, aerospace and other high-impact scenario applications.

The behaviour of composite materials under high-velocity impact loading is complex and needs to be better understood. The structure of reinforcing

fabric makes this situation even more complicated.

Optimizing the layers of composites for ballistic application maximizes energy absorption performance. The two main types of reinforcement materials in ballistic applications are para-aramid and UHMW PE [8, 9]. Para-aramid fibres, such as Kevlar, offer remarkable tensile strength and resistance to impact. Certain UHMW PE fabrics, such as unidirectional (UD) Dyneema, provide exceptional strength and rigidity in the direction of the fibres. Additionally, they have exceptional strength relative to their weight and exhibit remarkable impact absorption capabilities, making them ideal for lightweight ballistic armour applications [9]. Some researchers are studying the effect of UD reinforcement on the mechanical and impact properties of composites. These include Barhoumi et al., who investigated the mechanical properties of fibres and fabrics used in ballistic protection [10]. M. Bajya et al. investigated the effectiveness of soft armour panels for ballistic protection. They tested these panels at a speed of 430 m/s and against 9 mm bullets. UHMW PE UD reinforced panels have been replaced with woven fabric reinforced panels [11]. While 2D-woven composite materials have outstanding strength-to-weight ratios and can be easily shaped into complex forms, they have limitations, including poor impact properties. Some researchers, including Guowei Zhou et al., who studied the effect of 2D woven composites on mechanical and impact properties, stated that knitting models significantly affect parameters such as stress-strain curves and Poisson's ratio. Lower crimp ratios were associated

with linear stress-strain curves and higher strength and elasticity, while higher crimp ratios exhibited nonlinear behaviour. They concluded that the crimp ratio directly affects flexibility [12]. Lopresto et al. investigated the mechanical properties of 2D-woven plain and twill-woven fabrics. According to this study, plain weaving is better than twill weaving for tensile and bending strength because it has a more compact structure. However, twill weaving is better than plain weaving for energy absorption performance, such as fracture toughness and shear strength, because of its reduced waviness/lower crimp [13].

The ballistic performance of high-performance fibres and composites has been investigated in various studies found in literature. Gao et al. investigated the anti-explosive characteristics of aramid-steel composite target plates, highlighting the superior anti-explosion effect of aramid laminates on the back explosion surface compared to single-layer steel plates. The study confirmed that pasting aramid laminates on the back surface of steel plates significantly enhances their anti-explosion performance, reducing the centre deflection and diameter of explosion pits. Various structural configurations of aramid-steel composite target plates were analysed, and showed that aramid laminates on the back surface effectively improve explosion resistance and reduce centre displacement deflection, aligning well with numerical simulation results [14]. Butola et al. focused on preparing multi-layered flexible composites using high-performance fabrics such as Kevlar and UHMW PE for ballistic applications through a compression moulding technique, and showed better performance in tensile and impact testing than stitched samples. Kevlar fabric composites demonstrated higher impact energy absorption. In contrast, all UHMW PE and hybrid composites exhibited superior peak force and energy till failure, which was attributed to better bonding in all UHMW PE composites by LDPE. Poor bonding in all Kevlar samples led to yarn pull-out, reducing peak total energy absorption and peak force, highlighting the importance of proper bonding for ballistic performance [15]. Karahan et al., showed

that, unidirectional fabric-reinforced composites demonstrated higher ballistic limit velocity and energy absorption per unit areal density than other plates. Composite laminates with biaxial aramid fabric exhibited higher ballistic limit and energy absorption per unit areal density than those with woven aramid fabric. Additionally, UD-aramid GS3000 reinforced composite displayed better ballistic limit and energy absorption than others composites, while UD-UHMW PE-H62 reinforced composites showed good ballistic performance per unit areal density. Fabric orientation had an immaterial effect on the ballistic performance of composites, regardless of the reinforcement type [7].

There are many studies on how fibres dissipate the energy on fabric or plate surfaces. Jashi et al. [16] performed a critical analysis of internal factors, such as fibre properties, resin characteristics, interphase properties and composite architecture, and external factors, such as projectile type, environmental conditions and impact velocity as they influence the impact response of UHMW PE fabric and composites. Okhawilai et al. [17] investigated the energy absorption capabilities of aramid fibre-reinforced poly(benzoxazine-co-urethane) composites at different urethane mass concentrations under ballistic impact. Wong et al. [18] reported that they increased the friction between threads through the modification of LDPE and graphene in aramid fabrics and thus increased ballistic resistance approximately twofold. They investigated the energy absorption capacity of ballistic fabrics using the finite element method. Wang et al. [19] investigated the ballistic resistance of soft panels made of UHMW PE fabrics. In this study, the energy absorption properties of fabrics used in different ply numbers and the damage propagation characteristics depending on the deformations on the fabric surface after impact were investigated. Wang et al. [20] simulated the energy absorption and dissipation properties of UHMW PE fabrics under impact using FE modelling.

In woven fabrics, crimp is formed in warp and weft yarns due to interlacing. The load affecting the

yarn during ballistic impact applies some tension to the yarn through its axes. Due to the crimp, tension affects the fabric plane as well as the vertical direction to the fabric plane. Load in the vertical direction to the fabric plane affects the back of the panel. This causes the yarns to displace towards the back of the fabric panel more, and forms a deeper trauma or less energy absorption [21]. To minimize this disadvantage, unidirectional (UD) fabric structures are produced by placing warp and weft yarns at right angles (at 0° and 90°) on top of each other and then sticking them by using polyethylene film. Forming UD fabric structures is also possible by placing yarns at angles different than 90°. No interlacing and crimp exist in such structures, as the yarns are stuck with each other with the help of temperature and pressure using a thermoplastic resin. Thus, the majority of impact stress is propagated on the fabric plane, and less is transmitted to the back of the fabric layers. This forms a smaller trauma or higher energy absorption.

Our previous studies investigated the energy absorption properties of [1, 6, 22] and the ballistic protection properties [7] of various aramid and UHMW PE fabric composites. These studies discussed the ballistic properties of thermoplastic composites made from different aramid and UHMW PE fabrics used to produce ballistic protective composites. The aim of this study was to determine the behaviour of aramid and UHMW PE composites

under explosion load with a simulated test method. In this study, three aramid fabric structures (woven, biaxial and unidirectional), used as reinforcement in our previous studies and composites manufactured using aramid and UHMW PE, were investigated using a blast test system that simulates behaviour under a ballistic shock wave. Thanks to this system, the behaviour of composites against ballistic shock waves could be analysed. This study also investigated optimum combinations of different fabric structures, fibre types and hybrid composite architectures for developing high-performance composites. This will make achieving higher levels of protection in defence, security and civilian applications easier.

2 Materials and methods

2.1 Materials

Five different ballistic fabrics, whose properties are given in Table 1 and the structures shown in Figure 1, were used as reinforcement, while Nolax A21.2007 low density polyethylene (LDPE) adhesive film (density 0.94 g/cm³, melting temperature 80–90 °C and melt flow rate of 6–9 g/10 min) was used as a matrix system. The properties of the fibres that were used in the preparation of reinforcement structures are presented in Table 2.

Table 1: Properties of reinforcements used in this study

Reinforcement type	Code	Producer	Weave type	Linear density (tex)		Warp/Fill (or 0°/90° yarns)		Yarn density (warp/fill) (cm ⁻¹)	Areal density (g/m ²)	Crimp (warp/fill) (%)	Thickness (mm)
				Warp	Fill	Warp	Fill				
Aramid woven fabric – CT 736	R ₁	Teijin	2×2 basket weave	336	336	Twaron 2000	Twaron 2000	127/127	410	0.8/0.8	0.60
Aramid Bi-axial non-crimp fabric-XA450	R ₂	Saertex	Bi-axial non-crimp	336	-	Twaron 2000	Twaron 2000	127/127	465	Non-crimp	0.40
Aramid UD GS3000	R ₃	FMS	UD	126	-	Kevlar 49/ Kevlar 49	-	^{a)}	510	Non-crimp	0.50
UHMW PE UD Dyneema H62	R ₄	FMS	UD	176	-	Dyneema SK62	-	^{a)}	262	Non-crimp	0.25
Aramid woven fabric- Artec	R ₅	Pro-System	1×1 plain weave	58	58	Artec	Artec	116/116	135	0.2/0.2	0.23

^{a)} Fabric structure is not woven; it is unidirectional in which yarns are placed only in one direction. Yarn density can be measured in this structure.

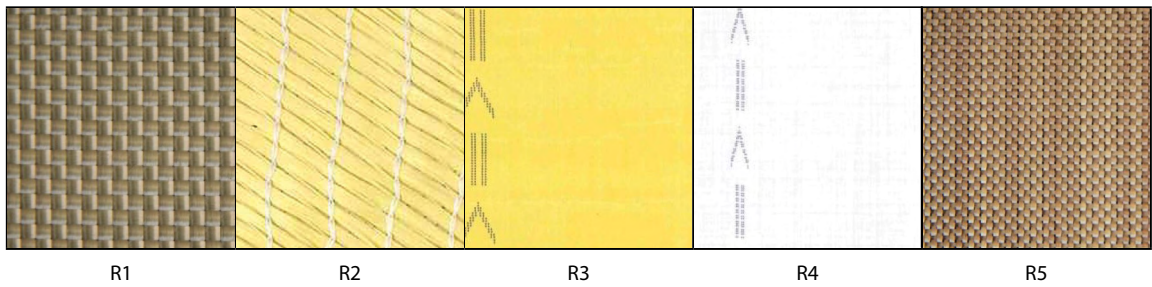


Figure 1: Ballistic fabrics used as reinforcements

Table 2: Parameters of the aramid and UHMW PE fibres used in this study

Fibres	Young modulus (GPa)	Strength (cN/tex)	Ultimate elongation (%)	Density (g/cm ³)
Twaron 2000 (aramid)	85	235	3.5	1.44
Kevlar 49 (aramid)	112	208	2.4	1.44
Dyneema SK62 (UHMW PE)	113	338	3.6	0.97
Artec Russian aramid	103	181	2.8	1.44

2.2 Composite manufacturing

The ballistic fabrics were cut to a size of 400 mm × 400 mm, and composite laminates were prepared, with same number of fabric layers and different panel thickness, different fabric layers and same panel thickness, different orientation of fabric layers and same panel thickness, and different number of fabric layers and different panel thickness, using the autoclave process. The temperature of the process was maintained at 110 °C, while the pressure of the vacuum was maintained at 14.8 bar. Figure 2 shows the different stages of the manufacturing process. Table 3 shows the details of composite produced

from different reinforcements. The fibre volume fraction (V_f) of all composite panels was calculated using the following equation [23]:

$$V_f = \frac{n \times m}{\rho \times h} \times 100 \quad (1)$$

where n represents the number of fabric plies, m represents the fabric areal density, ρ represents the fibre density and h represents the panel thickness. V_f values of hybrid samples were calculated for each reinforcement separately.



Figure 2: Different stages of the composite manufacturing process

Table 3: Properties of the composite plates used in this study

Sample code	Reinforcement type	Reinforcement layer number	Stacking direction	Resin	Plate thicknesses (mm)	Fibre volume fraction (%)	Areal density (g/m ²)
C1	R1	25	0°/90°	LDPE	10 ± 0.23	54.6	10.150
C2	R2	24	45°/-45°	LDPE	10 ± 0.39	54.0	9.660
C3	R3	21	0°/90°	LDPE	10 ± 0.45	65.0	10.710
C4	R4	31	0°/90°	LDPE	10 ± 0.25	66.4	8.153
C5	R1+R2	25	0°/90°/45°/-45°	LDPE	10 ± 0.40	54.3	9.875
C6	R1+R5	44	0°/90°	LDPE	10 ± 0.50	59.6	10.050
C7	R3+R4	26	0°/90°	LDPE	10 ± 0.27	67.5	9.020

2.3 Blast simulation projectile (BSP) tests

BSP tests were used to determine the energy absorption capacities of different materials during the blast and their damage behaviour against the blast. BSP tests were performed at an energy level close to the energy to which the reinforcement materials are used as boot sole reinforcement materials that can be blasted in explosion tests. The average weight of the ammunition used in these tests was 41.6 g. Its dimensions were cylindrical, with a diameter of 18.34 mm and a length of 33.3 mm. The content of the ammunition consisted of 95% iron powder and 5% paraffin. This ammunition was fired from a particular barrel to hit the target at a speed of approximately 700 m/s (Figure 3).

The bullet used was made of compressed iron powder. This bullet breaks up when it hits the target. It thus does not have a penetrating feature, but applies a kinetic energy directly proportional to its mass

and speed to the target. It therefore causes damage other than penetrating the target. The purpose of performing this test was to learn about the damage behaviour and energy absorption capacity that will occur under ballistic shock applied to composites in the explosion test. Explosion tests are difficult, expensive and risky. With this method, a comparison could be made between different samples, thus determining both their energy absorption capacity and damage behaviour. The results provided a comparison opportunity between different materials used in ballistic protection.

In these tests, materials of constant and equal thickness were subjected to BSP tests, and their deformation states were determined. The effect of fibre type and hybridization was investigated in the tested samples. BSP tests were carried out at Nurok Technology Ballistic Test Laboratory.



Figure 3: Ammunition – compressed iron powder (a) and barrel used in BSP tests (b)

2.4 Determination of trauma depth and diameter

If bullets cannot pass through the plates after the shot, a specific diameter and depth gap is formed in the backing material. This gap is called trauma depth. The depth of this gap shows the impact of the blast on the back of the panel. If ballistic plates emit more energy, the cavity depth decreases, while the cavity diameter increases. Otherwise, the cavity diameter will be small and its depth will be large. After the shooting, each cavity's depth and diameter were measured with a 1% precision micrometre. A cavity mould was then prepared to obtain the cavity or trauma geometry.

2.5 Determination of energy absorption of samples

Formation of trauma geometry using moulds

The energy absorption capabilities of the ballistic panels were determined depending on trauma depth and diameter in the tests. The volume of trauma geometry was taken as a basis to find the energy absorption capacity of panels. Trauma geometry may show small differences from shooting to shooting. In this work, as the number of measurements was too high, trauma geometry was obtained depending on depth and diameter based on some assumptions.

An exact mould of trauma geometry was obtained for each test result using mould clay. Millimetrical divisions were formed on the mould clay by showing the diameter axis using 'x' and depth using 'z'. With the help of these millimetrical divisions, depth values were obtained for each value of diameter. The curves were then fitted to these 'x' and 'z' values using Maple 10 software [24]. Among polynomial, rational polynomial and spline curve fitting techniques, the spline curve fitting technique was found to be the most suitable for the purpose of this research [25]. Figure 4 shows three-dimensional trauma shape obtained by turning the spline curve around the 'y' axis.

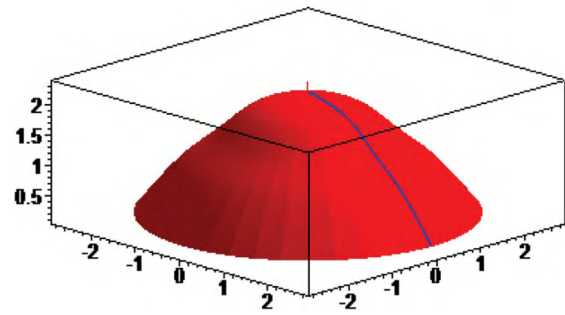


Figure 4: View of three-dimensional model of trauma obtained using the spline curve fitting method [5, 23]

Curves forming each trauma geometry were obtained using the spline curve fitting technique and Maple 10 software. Data obtained from fitted curves were transferred to Inventor 10 CAD software, which is a solid modelling software, while the volumes of trauma were calculated for each sample.

2.6 Calibration of backing material and determination of energy absorbed and transmitted to the back side

A calibration test was conducted to determine the trauma on the backing material created by the bullet. After the tests, energy required per unit volume of trauma on the backing material was calculated. In the tests, a cylindrical iron bar weighing 1 kg and measuring 45 mm in diameter with a semi-spherical tip was dropped on the backing material from heights of 0.5 m, 1.5 m and 2 m, respectively, from a hollow tube. Trauma depth and diameter were measured for each case. The shape of trauma was taken as the semi-spherical shape of the tip of the iron bar. Trauma volumes were calculated using Inventor CAD software, with the depth and diameter values obtained in this way. Unit trauma energies were calculated for heights of 0.5 m, 1.5 m and 2 m, and a linear relationship was found between unit volume trauma energy and dropping height. The results of the tests were found to be within the interval of the results recommended by the NIJ 0101.03 standard for a height of 2 m. Tests were repeated five times for each height. The potential energy of the weight

dropped was calculated using the equation below and the results are given in Table 4.

$$EP_{cal} = mgh \tag{2}$$

where EP_{cal} represents the potential energy of the iron weight dropped (J), m represents the weight of the iron bar with a semi-spherical tip (kg), g represents the gravitational acceleration (m/s^2) and h represents the dropping height (m).

Table 4: Dropping test results (average values)

Height (m)	Trauma depth (mm)	V_{cal}^a (mm ³)	EP_{cal}^b (J)	E_{unit}^c (J/mm ³)	$E_{av_{unit}}$ (J/mm ³)
2	22.5	23.860	19.62	8.22×10^{-4}	8.72×10^{-4}
1.5	17.6	16.020	14.72	9.18×10^{-4}	8.72×10^{-4}
0.5	12.8	11.360	8.00	8.8×10^{-4}	8.72×10^{-4}

a) volume of the trauma formed by weight dropped on the backing material

b) potential energy of the iron weight dropped

c) energy per unit volume

d) average energy per unit volume

According to the data presented in Table 4, it is evident that trauma depth changes linearly with a change in dropping height. According to the NIJ standard, a dropping test using a 2 m dropping height is sufficient for calibration. However, dropping tests with different heights were also conducted in this work to ensure the alignment of the test results with the results recommended by the NIJ standard. Using the test results, the calibration of the backing material was carried out and energy per unit volume (E_{unit}) was calculated. Average unit volume energy was found to be 8.72×10^{-4} J/mm³. The unit volume of energy was calculated using the following equation:

$$E_{unit} = \frac{EP_{cal}}{V_{cal}} \tag{3}$$

where E_{unit} represents the energy absorbed by unit volume of trauma (J/mm³), EP_{cal} represents potential energy, and V_{cal} represents the volume of the trauma formed by the weight dropped on the backing material (mm³).

Energy absorbed and transmitted by the fabric was determined by establishing a relation between the trauma volume after shooting tests (V_{test}) and trauma volume (V_{cal}) created by a known potential energy (EP_{cal}) on the backing material.

In the calculation of V_{test} , the following relationship was obtained using a polynomial curve, as shown in Figure 3. The volume of the body formed

by turning the curve 360° around the y axis is found using the following equation:

$$V_{test} = 2\pi \int_0^x xf(x)dx \tag{4}$$

where V_{test} represents the volume of the trauma formed on the backing material due to shooting tests (mm³), $f(x)$ represents the equation of the polynomial curve fitted using the spline curve fitting method and x represents the radius of the trauma formed on the backing material (mm).

Trauma energy (E_{test}) is found to be dependent on the trauma volume for each test as follows:

$$E_{test} = E_{av_{unit}} \times V_{test} \tag{5}$$

The kinetic energy of the bullet just before it touches the fabric is as follows:

$$EK_p = \frac{m \times v^2}{2} \tag{6}$$

where EK_p represents the kinetic energy of the bullet just before it touches the fabric (J), m represents the mass of the bullet (kg) and v represents the speed of the bullet (m/s).

When panel layers prevent the bullet from passing to the other side, the majority of the energy is absorbed by fabric layers and spread on the fabric surface, while a smaller amount passes to the back side. The energy absorbed by the fabric (EA_{fabric}) is

calculated using the following equation:

$$EA_{fabric} = EK_p - E_{test} \quad (7)$$

The energy creating the trauma is calculated by multiplying the unit volume energy obtained during calibration tests ($8.72 \times 10^{-4} \text{ J/mm}^3$) by the trauma volume for each shooting. Energy absorbed by the fabric can also be calculated by subtracting this energy from the kinetic energy of the bullet.

3 Results and discussion

Table 5 and Figure 5 show the BSP test results of different composite samples. For each test, bullet velocity was measured using a chronograph. Bullet velocities were recorded as $700 \text{ m/s} \pm 5 \text{ m/s}$ on average. The resulting impact energy is thus much higher than the energy level obtained in other ballistic shooting tests. In addition, the ammunition consists of compressed iron powder, and because it disperses into powder when it hits the target, a shock wave is applied instead of penetrating the target. After each shooting test, the depth and diameter of the trauma on the back surface of the samples were measured. The measured trauma depth and the diameter's statistical significance were determined using one-way variance analysis with a 95% confidence interval. It was determined that fabric types affect trauma depth and diameter. Table 5 shows the change in average trauma depth and diameter obtained from Student–Newman–Keuls (SNK) tests according to

the number of fabric layers and the type used in the panels. According to the results, the highest trauma depth was recorded for C4 at 81 mm. This is due to the relatively low bending strength of the UHMW PE fabric, the high trauma depth and the inward collapse of the composite plate after the shots.

C3 gave the best result. The fact that the trauma depth is lowest at 38 mm and interlayer delamination is limited proves that this material performs best against blast. The trauma depth is approximately 90% lower than that recorded for C4.

In the C7 hybrid composite, the displacement value decreased by 33% from 72 mm to 54 mm compared to C4. However, it was found to be relatively weak in terms of interlayer delamination. It was observed that the layers were almost completely separated from each other, and it was predicted that the load-carrying capacity would be limited in the face of explosion loading.

The behaviours of specimens C1, with a trauma depth of 57 mm, and C2, with a trauma depth of 53 mm, are quite similar to each other. It was observed that both trauma values and damage characteristics were quite close. The trauma depth of C5, formed by hybridizing these two materials, decreased by 18%, but the trauma diameter increased slightly. This shows that the energy spreads over a wider area. The C6 hybrid gave very successful results with trauma depth and trauma diameter values. There was a 10% decrease in trauma depth compared to C1. Contributing significantly to this was the thinner thread structure of Artec aramid fabric.

Table 5: BSP test results

Sample code	Trauma depth (mm)	Trauma diameter (mm)	Trauma volume after shooting tests, V_{test} (mm ³)	Trauma energy, E_{test} (J)	Energy absorbed by the fabric, $E_{a, fabric}$ (J)	Absorbed energy/ areal density, E_a/AD (Jm ² /kg)
C1	57	60	53721.2	46.8	10145.2	999.5
C2	53	56	43513.2	37.9	10154.1	1051.1
C3	38	41	16723.2	14.6	10177.4	950.3
C4	72	81	123671.9	107.8	10084.2	1236.9
C5	48	62	48305.1	42.1	10149.9	1027.8
C6	52	43	25171.5	21.9	10170.1	1011.9
C7	54	57	45931.7	40.1	10151.9	1125.5

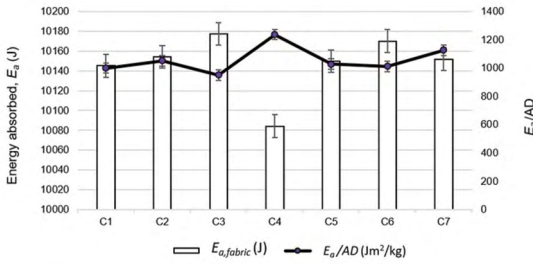


Figure 5: Ballistic behaviour of composites reinforced with different numbers of fabric plies and the same thickness

The C3 composite plate reinforced with UD aramid-GS3000 absorbs more energy than the aramid-CT736 reinforced plate, as shown in Table 5 and Figure 5. The values of the other plates are obvious. It is more convenient to compare the E_a/AD of composites to see how different types of materials affect ballistic performance. It is assumed that the higher areal density of the fabric, the composite panel it reinforces and the UD architecture of the fabric may contribute to this result. The E_a and E_a/AD hierarchy of composites is as follows:

$$E_a \quad C_3 > C_6 > C_2 > C_7 > C_5 > C_1 > C_4 \quad (8)$$

$$E_a/AD \quad C_4 > C_7 > C_2 > C_5 > C_6 > C_1 > C_3 \quad (9)$$

It is important to note that the hierarchies given in equations (8–9) are different. The E_a/AD of both UHMW PE fabric-reinforced composites is higher than that of aramid fabrics-reinforced plates, as shown in Figure 5. C4 composite plates reinforced with UD-UHMW PE-Dyneema H62 show the best results: E_a/AD values are 24% higher than aramid CT736 reinforced plates and 30% higher than UD-aramid-GS3000 reinforced plates. It is known that materials with high modulus and low density quickly disperse the strain wave away from the impact point, thus dispersing the energy over a larger area and preventing immense strain from occurring at the impact point. The materials' high specific strength, as well as their high modulus and low density, also contribute to better energy absorption and ballistic performance. UD-UHMW PE-Dyneema

H62 has high specific toughness, high modulus and low density compared to the aramids used in this study (Table 2). Additionally, it is known that UD fabric plates absorb more energy than woven fabric plates in terms of unit area density. These parameters contribute to the better E_a/AD values of UHMW PE-reinforced composite plates. Analysis of variance also revealed that the number of fabric layers had a statistically significant effect on E_a/AD with a 95% confidence interval ($\alpha \leq 0.05$).

The leading cause of shear deformation in woven aramid CT736 reinforced plates is the crimp between warp and weft threads (Figure 6a). The tension arising from the ballistic impact of the woven aramid-reinforced C1 and C5 samples caused tension along the fabric plane (57 mm displacement diameter) as well as in the vertical direction of the fabric plane (60 mm displacement diameter) due to the crimp in the threads. This situation caused the threads to slide towards the back of the fabric, resulting in a higher trauma depth. However, as seen in Figure 6b, the stress of aramid (GS3000) fabric-reinforced plates with UD structure is spread in the fabric plane due to ballistic impact. In this case, most of the shock wave spread in the fabric plane and the energy transmitted to the back of the fabric decreased. Thus, the collapse displacement of the C3 sample had the lowest trauma depth at 38 mm.

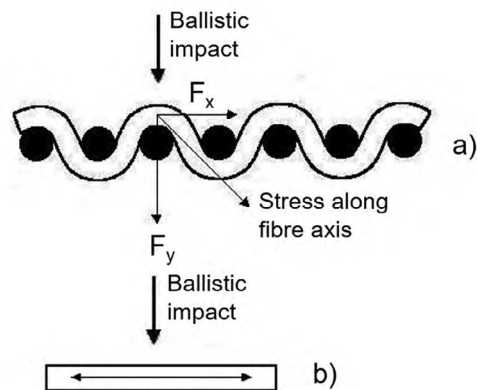


Figure 6: Stress formation behaviour of (a) woven and (b) unidirectional non-woven fabric structures after a ballistic shock [5]

The performance of the reinforcement material is susceptible to changes in fabric properties. This can be attributed to the difference in areal density, tensile modulus and reinforcement material design. The fabric used to reinforce composite panel C3 has a higher areal density, larger tensile modulus and a unidirectional structure. In contrast, the R1 reinforcement used in the C1 composite panel was woven with basket weave with a 0.8% crimp. The undesirable effect of this bend was excessive bending of the panel during loading. This caused the panel to have the lowest peak voltage value at different speeds. The thicker yarn linear density (336 tex) in reinforcement R1 also contributed to the lower value of the peak tension. A thin thread offers more surface area and can carry more load than a thick thread. C3 confirmed this effect, reinforced with fabric R3 (no crimp and fine yarn linear density), with the highest E_a value.

According to the results, the energy absorption of C6 hybrid composite plates reinforced with aramid CT736 and Artec Russian aramid was the highest after C3. C6 showed better energy absorption than other hybrid composite plates C5 and C7. These hybrid plates (C5 and C7) gave similar results. The better energy absorption of the C6 hybrid composite plates can be attributed to woven reinforcement. It is a hybrid composite produced by reinforcing two woven fabrics: Twaron CT 736 and Russian aramid. Woven fabric was produced by intertwining two sets of threads and has greater integrity. Twaron CT 736 has a basket weave, while Russian aramid has a plain weave. The interlocking of warp and weft caused the load to be transferred to more than one thread. When subjected to a load, these threads contribute as a whole and absorbed more energy before breaking. Thus, the energy absorption of woven hybrid composite plates C6 is higher than that of other woven composite plates.

Another factor affecting energy absorption is material density. Dyneema H62 (UHMW PE) had the lowest density. The C4 sample produced entirely based on this reinforcement thus showed the lowest

energy absorption. Hybrid plates were produced using high-density aramid-reinforced Dyneema H62, and the energy absorption of the C7 sample was 100 J higher than that of C4.

Damage analysis

Damage occurred after shooting tests is shown as an example in Figure 7. Damage models due to ballistic impact from the front, bottom and sides of composites reinforced with aramid woven fabric – CT 736, aramid woven fabric – Artec, Aramid UD GS3000 and UHMW PE UD Dyneema H62 samples are presented in Table 6 and Figure 8. Different failure modes were observed, such as shear clogging, fibre breakage, fibre stretching, bulging, delamination and fibrillation. During the study, it was noted that ballistic impact parameters such as bullet mass and bullet diameter were kept the same. In the C4 and C7 samples reinforced with UHMW PE UD Dyneema H62, it was observed that the extent of the damage around the impact point on the front of the plates was more significant and complete delamination occurred. For all impact composite plates, the damage density in the inner region was found to be more significant than in the outer region. The damage was more localized on the front of the aramid CT 736 and biaxial aramid XA450 reinforced plates. The relationship between energy absorption capacity and damage mechanisms is as follows: Only fibre breakage occurred in the C3 sample reinforced with Aramid UD GS3000, which has the highest E_a value. Fibre breakage is an indication that it is absorbing more energy. The broken fibres in the composite after the ballistic impact show that the fibres went through this energy absorption process before breaking, making maximum use of their high tensile strength and elongation performance. While fibre breakage contributes significantly to energy absorption, it is known that other mechanisms, such as delamination, shear clogging and friction, also affect the overall ballistic performance of the composite material [26]. In the biaxial aramid composite (C2), the fibre stretching mechanism was essential in absorbing

the bullet's kinetic energy, which plays a crucial role. The high tensile strength and elongation abilities of aramid fibres, together with their biaxial orientation, enable effective energy distribution through fibre tension and deformation processes at the molecular level. However, fibre breakage, fibre stretching, swelling, peeling and complete delamination occurred in the C4 and C7 hybrid samples reinforced with UHMW

PE UD Dyneema H62, which had the lowest E_a value. Fibre regions separated from the composite provide energy absorption through fibre pulling and friction mechanisms. The mechanisms of delamination, swelling and peeling suggest that matrix cracking, interlaminar shear and fibre-matrix separation play a role in dissipating the projectile's energy through fracture and friction processes.

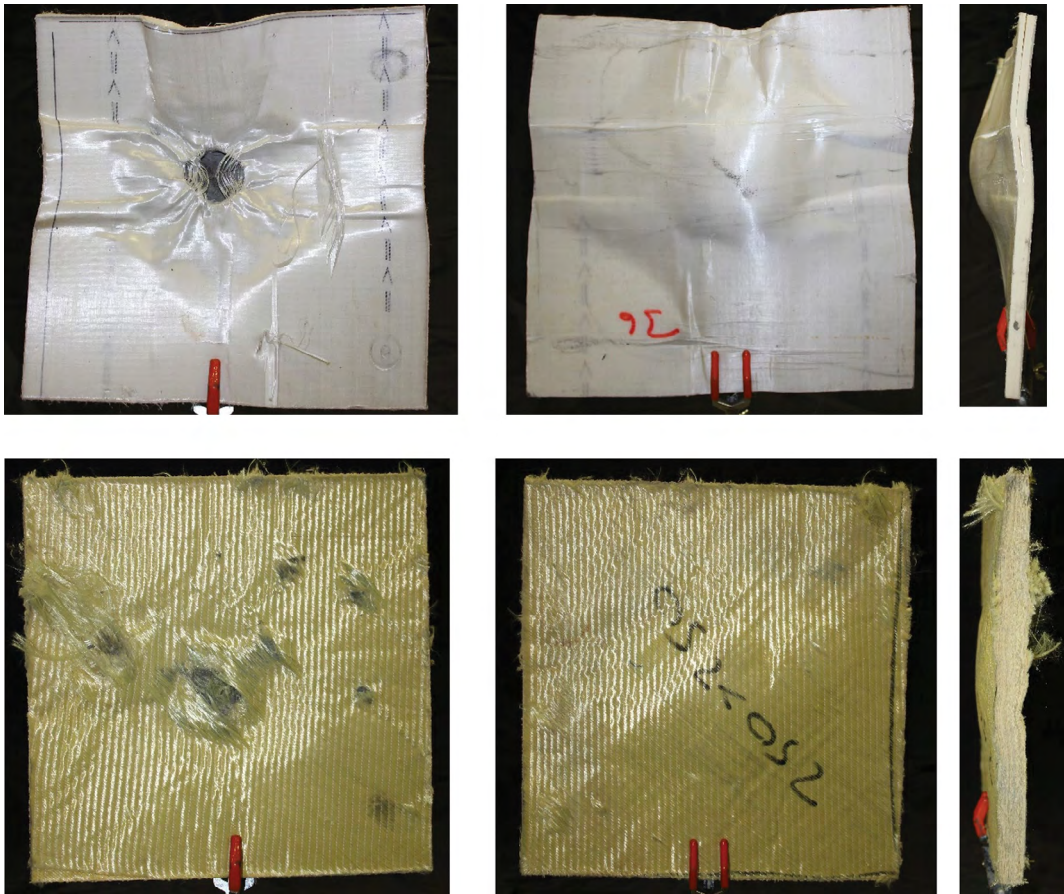


Figure 7: Examples showing the front (left), back (middle) and sectional (right) views of the damage incurred in UHMW PE (above) and aramid (below) samples after the shooting tests

Table 6: Summary of damages in samples after BSP tests

Sample code	Shear plugging	Fibre breakage	Fibre tension	Fibre stretching	Bulging	Delamination	Fibrillation	Stip
C1	+				+			
C2			+				+	
C3		+						
C4		+	+		+	+		+
C5	+		+				+	
C6				+	+			
C7			+		+	+		+

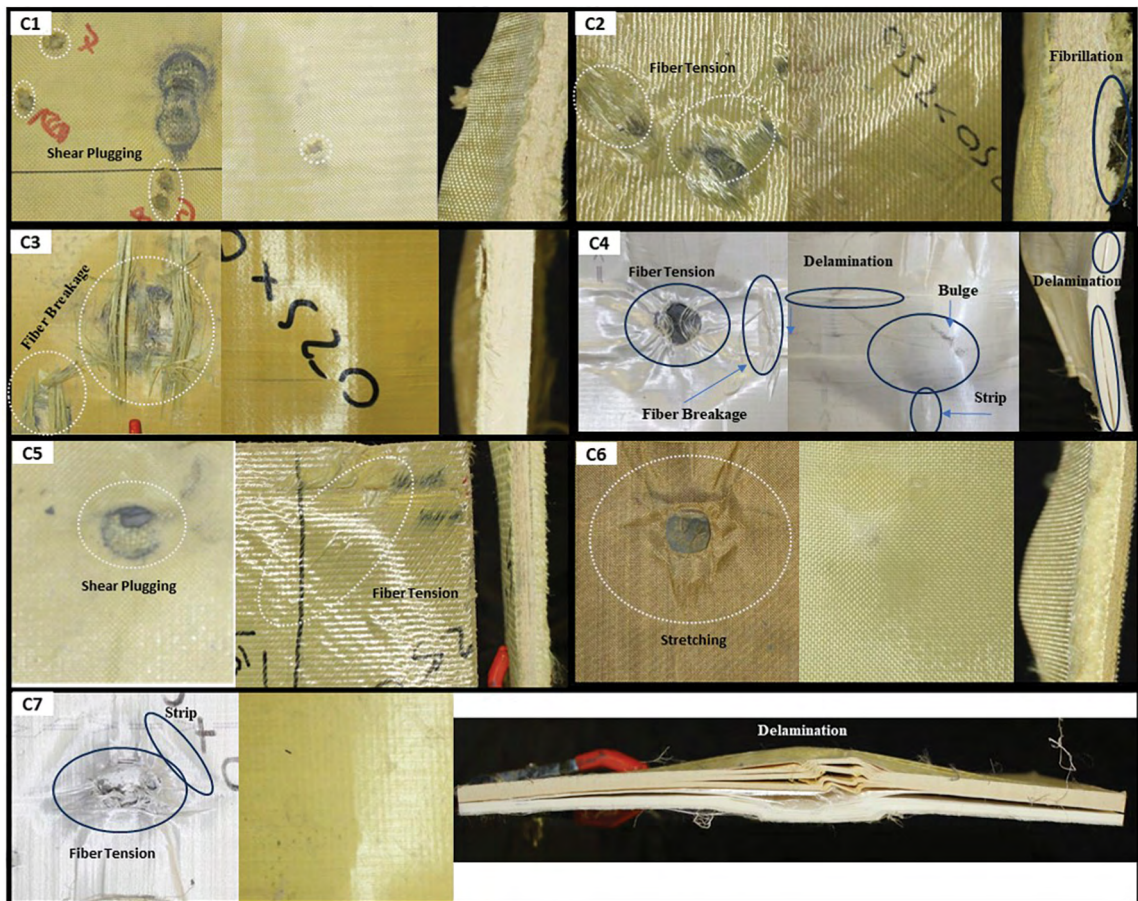


Figure 8: Damage patterns of composite reinforced with C1, C2, C3, C4, C5, C6, and C7 samples

Similar deformations and fibre direction-dependent energy dissipation were also observed in tests performed on composite samples in our previous study [6]. In these tests, it was observed that the energy dissipation directions increased depending on the fibre direction in the sample. All these results are compatible with available literature [27].

Figure 9 shows that as the fibre direction increases, the energy dissipation on the composite surface increases. There is a correlation between the energy distribution or damage occurring on the composite plate and the fibre directions. As the fibre direction increases in the composite structure, the energy distribution direction or the direction of the fibre damage increases. Generally, fibre breaking and fibre tension damage occur around the impact point, while fibre tension, shear and delamination damages occur in the areas around the impact point.

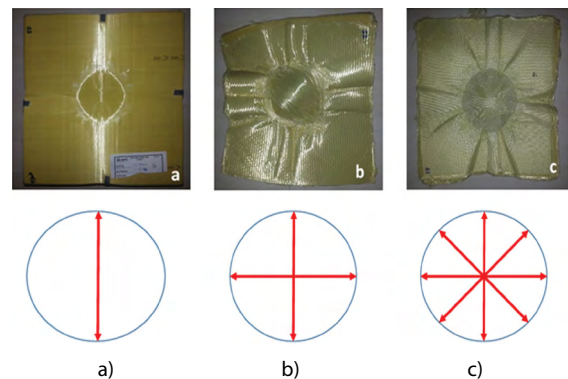


Figure 9: Schematic representation of the deformation and energy dissipation directions occurring after low-speed impact in aramid plates with: a) unidirectional, b) bidirectional and c) multi-directional fibre direction [6]

The increase in area around the impact point indicates that more energy is absorbed, but it also indicates that the composite structure no longer

has a load-carrying capacity, probably due to delamination damage. While the increase in the fibre direction increases the direction in which the energy is distributed, since the fibre volume fraction ratio in each direction decreases, the energy absorption performance of the structure also decreases. For this reason, UD structures absorb more energy.

Figure 10 schematically shows energy distribution under different loading conditions. The damage types in low-velocity impact, ballistic projectile and shock loading tests are presented as a comparison. Here, two-zone damage occurs with a low-velocity impact. In ballistics tests, there is three-zone damage occurs. The first region shown in red here is the area directly hit by the impact. Fibre breakage and fibre tensile damage generally occur in this area. The second area is the blue coloured area and is the area where the shock wave generated by the impact spreads. In this area, delamination and shear damage generally occurred in the samples shown in Figures 10b and 10c. The area shown in green is the third area where the shock wave spreads, while fibre tensile and delamination damage mainly occurred in this region.

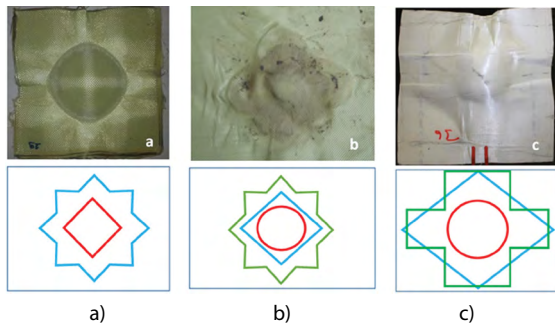


Figure 10: Deformation and illustration of different composite plates under: a) low-speed, b) ballistic and c) shock loading impact [4, 6]

4 Conclusion

This study experimentally investigated the effects of composite plates produced using different fibre types and fabric structures on trauma depth, diameter

and energy absorption. The results obtained are as follows:

- Considering plates of the same thickness, the UD-aramid GS3000 reinforced composite had the lowest trauma depth compared to other composites. The trauma depth of this composite was approximately 90% lower than that of the UD-UHMW PE-H62 reinforced composite. It was also observed that the trauma depth of the hybrid composite produced by the reinforcement of these two fabrics was 33% lower than the trauma depth of the UD-UHMW PE-H62 reinforced composite alone.
- The trauma depth of the composite created by hybridizing Twaron CT 736-Baixaal aramid fabrics decreased by 18% compared to non-hybrid composites. However, a slight increase in trauma diameter was observed. This shows that the energy is spread over a wider area.
- The UD-aramid GS3000 reinforced composite recorded the highest energy absorption. However, the UD-UHMW PE-H62 reinforced composite showed the best energy absorption per unit area density. This value is 24% higher than CT736 reinforced wafers and 30% higher than UD-aramid GS3000 reinforced wafers.
- Biaxial aramid fabric composite plates exhibited approximately 10% higher energy absorption per unit area density than woven aramid fabric composite plates.
- Woven and biaxial fabric reinforced plates showed local damage with very little delamination. In contrast, UD-UHMW PE-H62 reinforced plates had large damage areas, primarily including delamination and bulging. This damage includes mechanisms such as fibre withdrawal, inter-fibre delamination, fibrillation and fibre breakage.

References

1. KARAHAN, M., KARAHAN, E.A. Development of an innovative sandwich composite material for protection of lower limb against landmine explosion: mechanical leg test results. *Textile Research Journal*, 2016, **87**(1), 15–30, doi: 10.1177/0040517515624880.
2. KAMBEROĞLU, M., KARAHAN, M., ALPDOĞAN, C., KARAHAN, N. Evaluation of foot protection effectiveness against AP mine blasts: effect of deflector geometry. *Journal of Testing and Evaluation*, 2024, **45**(2), 356–368, doi: 10.1520/JTE20150171.
3. KARAHAN, M., KARAHAN, E.A., KARAHAN, N. Blast performance of demining footwear: numerical and experimental trials on frangible leg model and injury modeling. *Journal of Testing and Evaluation*, 2018, **46**(2), 666–679, doi: 10.1520/JTE20160340.
4. KARAHAN, M., KUŞ, A., EREN, R. An Investigation into ballistic performance and energy absorption capabilities of woven aramid fabrics. *International Journal of Impact Engineering*, 2008, **35**(6), 499–510, doi: 10.1016/J.IJIMPENG.2007.04.003.
5. KARAHAN, M. Comparison of ballistic performance and energy absorption capabilities of woven and unidirectional aramid fabrics. *Textile Research Journal*, 2008, **78**(8), 718–730, doi: 10.1177/0040517508090487.
6. KARAHAN, M., YILDIRIM, K. Low velocity impact behaviour of aramid and UHMW PE composites. *Fibres & Textiles in Eastern Europe*, 2015, **23**(3), 97–105, doi: 10.5604/12303666.1152522.
7. KARAHAN, M., JABBAR, A., KARAHAN, N. Ballistic impact behavior of the aramid and ultra-high molecular weight polyethylene composites. *Journal of Reinforced Plastics and Composites*, 2015, **34**(1), 37–48, doi: 10.1177/0731684414562223.
8. ZHOU, W., WENTE, T., LIU, D., MAO, X., ZENG, D., TORAB, H., DAHL, J., XIAO, X. A comparative study of a quasi 3D woven composite with UD and 2D woven laminates. *Composites Part A: Applied Science and Manufacturing*, 2020, **139**, 1–11, doi: 10.1016/J.COMPOSITESA.2020.106139.
9. TAM, T., BHATNAGAR, A. High-performance ballistic fibers and tapes. In *Lightweight Ballistic Composites: Military and Law-Enforcement Applications*. Edited by Ashok Bhatnagar. Woodhead Publishing, 2016, 1–39, doi: 10.1016/B978-0-08-100406-7.00001-5.
10. BARHOUMI, H., BHOURI, N., FEKI, I., BAF-FOUN, A., HAMDALOU, M., BEN ABDESSALEM, S. Review of ballistic protection materials: properties and performances. *Journal of Reinforced Plastics and Composites*, 2022, **42**(13-14), 685–699, doi: 10.1177/07316844221137920.
11. BAJYA, M., MAJUMDAR, A., BUTOLA, B.S., ARORA, S., BHATTACHARJEE, D. Ballistic performance and failure modes of woven and unidirectional fabric based soft armour panels. *Composite Structures*, 2021, **255**, 1–11, doi: 10.1016/J.COMPSTRUCT.2020.112941.
12. ZHOU, G., SUN, Q., MENG, Z., LI, D., PENG, Y., ZENG, D., SU, X. Experimental investigation on the effects of fabric architectures on mechanical and damage behaviors of carbon/epoxy woven composites. *Composite Structures*, 2021, **257**, 1–13, doi: 10.1016/J.COMPSTRUCT.2020.113366.
13. LOPRESTO, V., LEONE, C., DE IORIO, I. Mechanical characterisation of basalt fibre reinforced plastic. *Composites Part B: Engineering*, 2011, **42**(4), 717–723, doi: 10.1016/J.COMPOSITESB.2011.01.030.
14. GAO, Z., CHEN, Y., WANG, Z., LI, S., WEI, W., CHEN, J. Shattering effect study of aramid–steel composite target plates under localized blast loading. *Sustainability*, 2023, **15**(5), 1–26, doi: 10.3390/SU15054160.

15. BUTOLA, B.S., MAJUMDAR, A., JAIN, A., KAUR, G. Multilayered flexible uni-polymer and hybrid composites for ballistic applications. *Fibers and Polymers*, 2017, **18**, 786–794, doi: 10.1007/S12221-017-6959-4.
16. JOSHI, A., MISHRA, A., SAXENA, V.K. Impact response and energy absorption mechanisms of UHMW PE fabric and composites in ballistic applications: a comprehensive review. *Composites Part A: Applied Science and Manufacturing*, 2024, **185**, 1–27, doi: 10.1016/J.COMPOSITE-SA.2024.108314.
17. OKHAWILAI, M., PARNKLANG, T., MORA, P., HIZIROGLU, S., RIMDUSIT, S. The energy absorption enhancement in aramid fiber-reinforced poly (benzoxazine-co-urethane) composite armors under ballistic impacts. *Journal of Reinforced Plastics and Composites*, 2019, **38**(3), 133–146., doi: 10.1177/0731684418808894.
18. WANG, H., HAZELL, P.J., SHANKAR, K., MOROZOV, E. V., ESCOBEDO, J.P., WANG, C. Effects of fabric folding and thickness on the impact behaviour of multi-ply UHMW PE woven fabrics. *Journal of Materials Science*, 2017, **52**, 13977–13991, doi: 10.1007/S10853-017-1482-Y.
19. WANG, Z., ZHANG, H., DONG, Y., ZHOU, H., HUANG, G. Ballistic performance and protection mechanism of aramid fabric modified with polyethylene and graphene. *International Journal of Mechanical Sciences*, 2023, **237**, 1–14, doi: 10.1016/J.IJMECSCI.2022.107772.
20. WANG, H., WEERASINGHE, D., MOHOTTI, D., HAZELL, P.J., SHIM, V.P.W., SHANKAR, K., MOROZOV, E. V. On the impact response of UHMW PE woven fabrics: experiments and simulations. *International Journal of Mechanical Sciences*, 2021, **204**, 1–15, doi: 10.1016/J.IJMECSCI.2021.106574.
21. FREESTON, W.D., CLAUS, W.D. Strain-wave reflections during ballistic impact of fabric panels. *Textile Research Journal*, **43**(6), 348–351, doi: 10.1177/004051757304300606.
22. SHAKER, K., JABBAR, A., KARAHAN, M., KARAHAN, N., NAWAB, Y. Study of dynamic compressive behaviour of aramid and ultrahigh molecular weight polyethylene composites using Split Hopkinson Pressure Bar. *Journal of Composite Materials*, 2017, **51**(1), 81–94, doi: 10.1177/0021998316635241.
23. KARAHAN, M., KARAHAN, N. Influence of weaving structure and hybridization on the tensile properties of woven carbon-epoxy composites. *Journal of Reinforced Plastics and Composites*, 2014, **33**(2), 212–222, doi: 10.1177/0731684413504019.
24. RICHARDS, D. *Advanced Mathematical Methods with Maple*. Cambridge : Cambridge University Press, 2009.
25. WEISS, V., ANDOR, L., RENNER, G., VÁRÁDY, T. Advanced surface fitting techniques. *Computer Aided Geometric Design*, 2002, **19**(1), 19–42, doi: 10.1016/S0167-8396(01)00086-3.
26. GAMA, B.A., GILLESPIE, J.W. Punch shear based penetration model of ballistic impact of thick-section composites. *Composite Structures*, 2008, **86**(4), 356–369, doi: 10.1016/J.COMPSTRUCT.2007.11.001.
27. ZHOU, H., MIN, S., CHEN, X. A numerical study on the influence of quasi-isotropic structures on the ballistic performance of para-aramid woven composites. *Composite Structures*, 2021, **275**, 1–12, doi: 10.1016/J.COMPSTRUCT.2021.114489.

Viktorija Diak,¹ Andrii Diak²

¹ Institute of Art Research, Vilnius Academy of Arts, Maironio str. 6, LT-01124 Vilnius, Lithuania

² NTUU KPI, Kyiv, Ukraine

Features and Limitations of Fused Deposition Modelling (FDM) in Obtaining Textile-like Structures

Značilnosti in omejitve tehnologije modeliranja s spajanjem slojev (FDM) pri pridobivanju tekstilu podobnih struktur

Scientific review/Pregledni znanstveni članek

Received/Prispelo 9–2024 • Accepted/Sprejeto 12–2024

Corresponding author/Korespondenčna avtorica:

Viktorija Diak

E-mail: vk.diak@gmail.com

ORCID iD: 0009-0002-8665-0348

Abstract

In contemporary production processes and customisation, 3D printing has emerged as a prominent method for prototyping. It offers flexibility to create objects of diverse shapes, structures, sizes and materials. However, integrating this technology into the textile industry to achieve textile-like structures poses challenges. The fused deposition modelling (FDM) method is currently the closest approach to prototyping such structures due to its ability to extrude monofilaments resembling traditional threads. Regrettably, attempts to produce structures with properties akin to textiles, including flexibility, durability, breathability, lightness and fineness, have been unsuccessful due to various limitations inherent in the technical setups of 3D printers. This study analyses the key features of FDM printing that determine the feasibility of achieving authentic textile-like printed structures while clarifying the underlying logic behind their future purpose. Our aim was to assist future researchers in achieving the production of thin 3D-printed fibres (diameter ~0.1 mm) regardless of structure type.

Keywords: 3D printing, f-fibre, 3D-printed textile, quasi-fabric, textile structure

Izvleček

3D tiskanje se v sodobnih proizvodnih procesih in prilagoditvah pojavlja kot pomembna metoda za izdelavo prototipov. Kljub temu, da mogoča fleksibilnost pri ustvarjanju predmetov različnih oblik, struktur, velikosti in materialov, predstavlja vključevanje 3D tiskanja v tekstilno industrijo za doseganje struktur, podobnih tekstilu, poseben izziv. Tehnologija modeliranja s spajanjem slojev (FDM; angl. fused deposition modelling) je trenutno najboljši način za izdelavo prototipov takšnih struktur, saj lahko iztisne monofilamente, ki so podobni tradicionalni niti. Žal so bili poskusi izdelave struktur z lastnostmi, podobnimi tekstilu, vključno s prožnostjo, trajnostjo, zračnostjo, lahkotnostjo in finostjo, neuspešni zaradi različnih omejitev, povezanih s tehničnimi nastavitvami 3D tiskalnikov. Raziskava analizira ključne značilnosti tiskanja s tehnologijo FDM, ki določajo izvedljivost doseganja pristnih tiskanih struktur, podobnih tekstilu, hkrati pa pojasnjuje možnosti uporabe v prihodnosti. Namen raziskave je bil olajšati delo bodočim raziskovalcem pri izdelavi tankih 3D tiskanih vlaken (premer ~0,1 mm), ne glede na vrsto strukture.

Ključne besede: 3D tisk, f-vlakno, 3D tiskani tekstil, kvazi-tkanina, tekstilna struktura



Content from this work may be used under the terms of the Creative Commons Attribution CC BY 4.0 licence (<https://creativecommons.org/licenses/by/4.0/>). Authors retain ownership of the copyright for their content, but allow anyone to download, reuse, reprint, modify, distribute and/or copy the content as long as the original authors and source are cited. No permission is required from the authors or the publisher. This journal does not charge APCs or submission charges.

1 Unveiling logic behind obtaining 3D-printed quasi-fabric

Weaving has stood unchanged as the fundamental technique for textile production over millennia as its simplicity and efficiency have rendered it unparalleled thus far. Incremental improvements have solely focused on enhancing machines performing routine operations. With the advent of plastics and synthetic fibres derived from them, an opportunity arose to enhance existing fabric types significantly while maintaining traditional thread weaving methods. Technological advancements subsequently led to composite materials combining different substances (e.g. cotton and elastane), followed by membranes comprising layered combinations of thin synthetic selective films intertwined with nonwoven fabrics [1]. The manufacturing process for such structures transcended conventional weaving techniques while modern developments in smart textiles incorporating synthetic coatings, Shape Memory Materials (SMMs), conductive threads, sensors, micro power sources etc. [2] necessitated even more sophisticated technological advancements. For instance, the mere “attachment” of electronics to textiles proved impractical for creating active smart textiles. Consequently, achieving their seamless and organic integration with traditional ones requires novel unified technologies capable of merging textile production with microelectronics [3]. The solution may lie in the application of additive technologies that can amalgamate diverse approaches and production methods [4][5][6]. The rationale behind creating 3D-printed quasi-fabrics lies in providing transitional forms for the textile industry to utilise as a multi-component composite foundation. Further advancement in 3D-printed electronics will enable the seamless integration of any smart structures into existing textiles [8]. However, while there is an active trend in developing 3D printing for smart structures and microelectronics, a similar trend has not emerged in achieving 3D-printed textiles [7][8]. Our objective

is to comprehend why manufacturing quasi-textile remains an unresolved challenge. We think that one of the primary reasons for these setbacks lies in the lack of understanding regarding the technological causes and limitations inherent in Fused Deposition Modelling (FDM) method that impede positive outcomes. In other words, gaining deeper insights into the problem can significantly expedite its resolution by future researchers.

2 Methods

The research methodology hinges on a critical review of FDM 3D printing practices. By drawing upon personal practical experience alongside logical reasoning, we conducted an extensive analysis of internal technical factors that actively influence the current possibilities and constraints associated with the FDM technology's ability to fabricate thin textile-like structures comparable to traditional textiles.

2.1 3D printing methods for textile-like structures and their limitations

Despite its capacity to produce various structures and combine different materials, 3D printing has been unable to replicate the intricate textile fabrics achieved through weaving/knitting techniques. The primary reason for this shortcoming lies in the complex and specific process of obtaining and weaving fibres. Textile yarn entails intricate preprocess steps [9] that are absent in 3D printing. To create a textile analogue, we must concurrently generate a composite fibre and perform the weaving within a single 3D printing process, which poses an exceedingly challenging task even for highly advanced machines. Moreover, achieving a basic (woven, knitted) structure using 3D printing methods presents considerable difficulties [10, 11] in terms of quality. The predicament arises from the fact that additive technologies focus on bonding layers together, whereas weaving endeavours to keep these layers separate and free from fusion. There are attempts to

obtain structures with weaving/knitting techniques, e.g. employing the PolyJet method [13], where printed structures resembling threads possess a diameter measuring 1.3 mm, the selective laser sintering (SLS) method [12], with tube sizes in structures measuring 0.6 mm, and the FDM method [10, 11], with extrusion “fibre” (f-fibre) diameter measuring 1–2 mm. Unfortunately, these 3D-printed structures only mimic traditional woven textiles superficially without capturing their essence in other aspects, such as fineness, flexibility, lightness, durability and stretchability. Efforts have also been made to print basic structures, typically consisting of single-layered or multi-layered meshes without interlacing technology; however, these structures tend to be rigid and have height greater than 1 mm [14, 10].

In conventional manufacturing processes, a multifilament yarn is typically composed of a bundle of exceedingly fine uniform fibres, referred to as monofilaments, which possess diameters ranging from approximately 0.01 mm to 0.05 mm (10–50 μm) [38]. These fibres are twisted together to create a thread, generally exhibiting a standard diameter between 0.05 mm and 0.5 mm. The characteristics inherent in these threads significantly influence the desired properties of fabrics; however, contemporary advancements in 3D printing textile-like materials markedly fall short of achieving these specifications. It is posited that the capability to produce structures comprising homogeneous monofilaments (as f-fibres) with diameters of at least approximately 0.1 mm (100 μm) [7] could facilitate the development of 3D-printed structures that emulate the properties of traditional textiles. This assertion is supported by methodologies such as DefeXtiles [15], which demonstrated flexibility – without incorporating rubber-like materials – despite overall thickness of approximately 0.45 mm due to the utilisation of short f-fibres (less than 2 mm) with diameters varying from 0.09 mm to 0.75 mm, anchored between “drops” of extrudate. On the other hand, there is a challenge. These short f-fibres namely tend to thin out during the printing process (potentially resulting

to breakage), thereby hindering the production of long, fine (< 0.75 mm) and uniformly continuous f-fibres with this technique. A prospective alternative may lie in another 3D printing approach used for fabricating hair-like structures [39], which involves drawing extremely fine f-fibres from the extrudate with diameters less than 0.1 mm and variable lengths. Nonetheless, this method also presents several limitations concerning the requisite presence of extruded “anchor drops”, uncontrolled variability in the f-fibre diameter, difficulties associated with maintaining uniformity in the f-fibre deposition and random breakages. Additionally, the method may face challenges related to bonding or intertwining layers to achieve a final quasi-textile product.

In contrast, standard FDM printing can also yield f-fibres with diameters below 0.15 mm, while effectively controlling their homogeneity and permitting potentially infinite lengths (restricted solely by printbed dimensions). Nevertheless, attaining such outcomes necessitates addressing numerous issues that arise during the prototyping phase for textile-like structures characterised by minimal extrusion f-fibre values.

2.2 FDM method

It is known [16] that the filament diameter for FDM is 1.75 mm (or 2.85 mm), while the standard nozzle diameter (D) is 0.4 mm. Typically, the calculation for print layer height (Lh) follows the recommended formula $D(\text{nozzle})/2$; however, acceptable print boundaries encompass a wider range and may practically fall within 0.1–0.3 mm (for $D_n = 0.4$ mm). In theory, using one of the simplest materials for printing, e.g. polylactic acid (PLA), it is feasible to achieve a uniform f-fibre with dimensions of (Width) \times (Height) = 0.4 \times 0.2 mm. Nevertheless, in practice, accomplishing this (for basic layer) becomes challenging for various reasons, particularly when striving for a homogeneous structure without breaks in f-fibre continuity [14]. The task becomes even more complex when attempting to reduce the required cross-section thickness or utilising more

intricate printing materials. One significant aspect of 3D printing is the repeatability of the printing structure, which also introduces a wide range of errors that can affect the quality of the final printed structure. Various factors, e.g. the influence of the initial model, constituent elements and their sizes, number of print layers, print speed, temperature and other parameters, can also significantly alter the printing conditions and subsequently impact the end result.

In the forthcoming sections, an in-depth analysis will be conducted on distinctive technological attributes associated with the FDM method. This examination will include a thorough review of important components and features of a common FDM 3D printer that impact the ability to produce fine textile-like structures.

3 Analysis of limits

3.1 Base layer printing

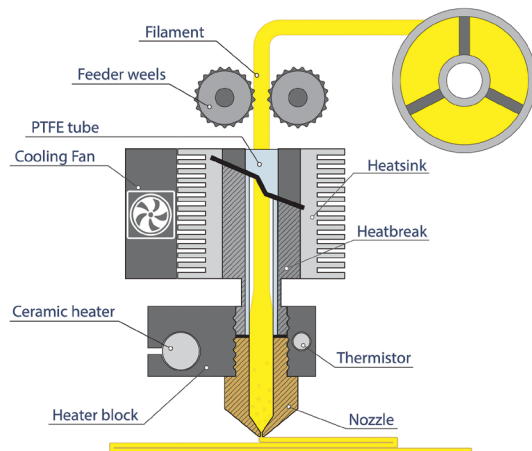


Figure 1: FDM 3D printer components description

Traditional fabrics consist of relatively thin fibres ($D \sim 0.1\text{--}0.4$ mm). Therefore, imitating these fabrics using additive technologies involves printing only a few layers (usually 1–5 layers, depending on the structure) with $Lh \sim 0.05\text{--}0.2$ mm.

Consequently, obtaining a high-quality base print layer becomes crucial for successfully

3D-printed textile-like structures (referring specifically to the first layer of the target structure while excluding any support structures) (Figure 2A). However, an inherent challenge in 3D printing lies in thermoplastic adhesion to the printbed surface during the initial layer deposition. When aiming for thinner f-fibre dimensions, achieving a high-quality base layer becomes even more demanding. Specific solutions such as vertical printing [11, 15] or using a raft [16] can be considered to address this issue. In standard horizontal printing, adjusting the distance (gap) between the nozzle and printbed (Figure 2B, b2) becomes a priority, as failure to adhere to this requirement cannot be resolved through alternative methods. Attention should also be given to the flatness of the printbed itself (Figure 2B, b1). When deviations exceed ± 50 μm , precise printing of thin structures with linewidths < 0.3 mm and heights $\sim 0.1\text{--}0.2$ mm becomes unpredictable or even impossible without employing a raft. Failure to meet these criteria can manifest through secondary signs during direct printing (without a raft) (Figure 2C).

Another factor influencing f-fibre adhesion is the choice of the printbed surface material. Different thermoplastics exhibit varying adhesive properties with different materials. Adhesive capability is also influenced by both melt and printbed surface temperature. By altering the material or temperature of the bed coating, it is possible to enhance or diminish adhesion and subsequently improve the print quality. Various materials/coatings are available for this purpose, including borosilicate glass, silicone, polyetherimide (PEI) films, polyethylene terephthalate (PET) films, polyimide (PI) and other tapes. In-depth research studies can provide a more comprehensive understanding of how these materials affect adhesion and aid in selecting an appropriate option [17, 18].

A partial detachment of printed structures from the printbed due to uneven crystallisation and resulting warping (Figure 2C, c5) is a common issue occurring during 3D printing processes [16, 19]. The issue can be addressed by establishing printing conditions that allow for slow and uniform cooling

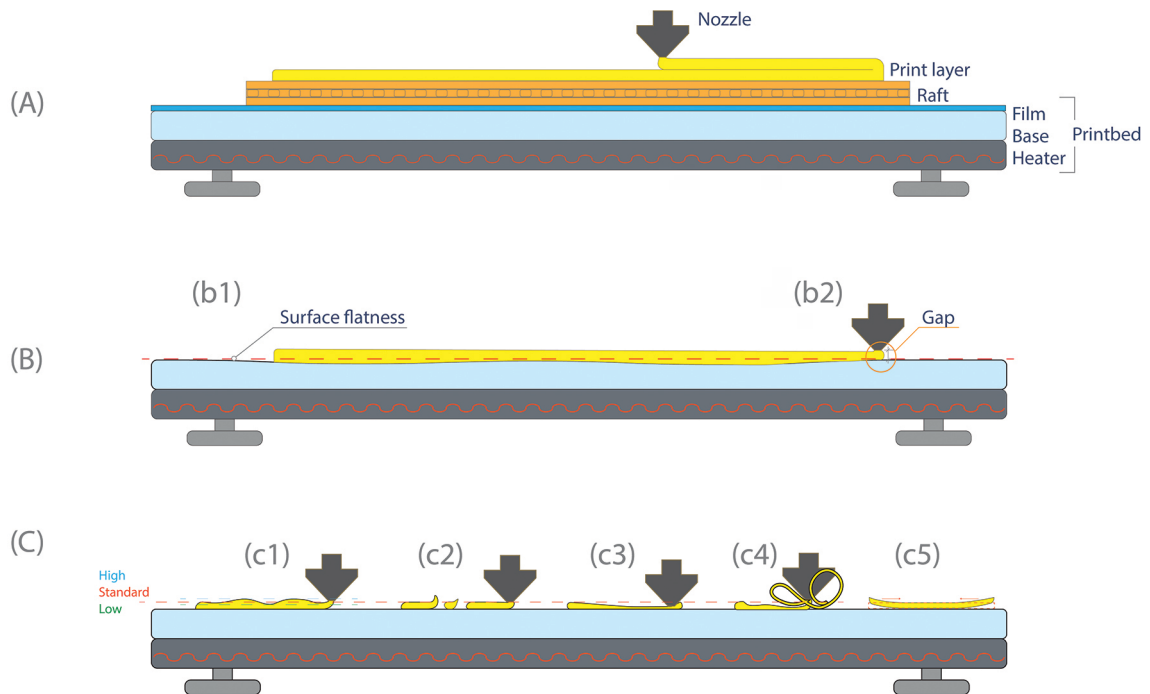


Figure 2: Printbed and nozzle impact on print results: (A) description, (B) printed flatness, (C) nozzle position and print issues: (c1) inconsistency in f-fibre width/height within significant limits; (c2) breaks in f-fibre; (c3) imprinting of f-fibre into printbed causing its height to approach zero while significantly increasing its width, making it impossible to remove print from bed; (c4) “spaghetti” effect where partial or complete “extrusion in mid-air” occurs, hindering further printing and leading to material accumulation on nozzle; (c5) warping effect

of the material during printing. Alternatively, the use of glue can be considered as a solution.

When aiming for thinner f-fibres ($D < 0.2$ mm), reducing the contact area between the f-fibre and the printbed surface during printing decreases adhesion, leading to detachment or breakage of f-fibre during extrusion. Hence, the precise adjustment of the gap between the nozzle and the printing surface becomes essential (Figure 2C), especially when aiming for reduced f-fibre thickness (this also rely heavily on the kinematic precision of the printer itself). Failure to achieve this calibration may render the printing of such minute components technically unviable. In instances where challenges arise in adjusting the gap, employing specialised adhesive [20] is a common solution that proves effective for the structure height of more than 1 mm. However, it can complicate removing prints from the bed when dealing with smaller elements, as it presents a

labour-intensive task that poses a risk of accidental damage, particularly when working with an overall structure height of less than 0.4 mm.

In general, poor adhesion may occur due to a simple reason – a dirty or greasy surface. Therefore, thorough cleaning of the surface before and after printing is recommended, especially when changing materials. On the other hand, some thermoplastics leave behind a micro-film during printing that significantly improves adhesion for subsequent prints by acting as a micro-initial layer.

Slicer settings also play a significant role in achieving high-quality base layer prints. Parameters such as print speed, extrusion rate, retraction and its speed have an active influence on achieving extrusion thermodynamic stability and require personal testing considering different input parameters specific to the printhead characteristics as well as material type and preparation.

3.2 Nozzle and extrusion coefficient ratio

As previously mentioned, the attainment of textile-like structures relies on the ability to produce f-fibres with $D < 0.2$ mm. The influence of the nozzle plays a significant role in this process, as its flow capacity and print quality are dependent on factors such as its diameter (specifically the smallest hole of the nozzle), material feed rate, nozzle's material composition and filament material (Figure 1) [22, 23]. There are specific limits for melt volume associated with each material case, beyond which extruding f-fibre without the mechanical "grip and stretching" (Figure 3) becomes unfeasible.

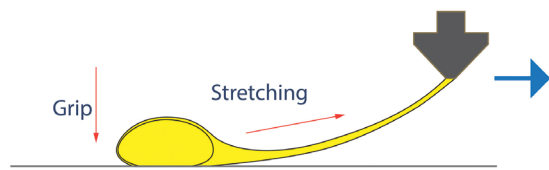


Figure 3: "Grip and stretching" extrusion process

Attempts to increase temperature in order to reduce viscosity and induce oozing only provide marginal assistance since without a sufficient mechanical grip onto the printing surface, the molten

material tends to clog or adhere to the nozzle itself right after extruding. Moreover, there is a correlation between the material feed rate and nozzle diameter; exceeding certain limits leads to unpredictable extrusion outcomes, resulting in either highly uneven extrusion (wherein droplets of molten plastic are partially expelled) (Figure 2C, c4) or clogging (Figure 7B) that necessitates the mechanical cleaning of the nozzle. Moreover, if the nozzle diameter decreases, then achieving f-fibre thinning becomes increasingly challenging without compromising the print speed or precise control over the melt temperature and pressure in the hotend. To comprehensively understand these phenomena, it is recommended to conduct research specific to each material.

There is an alternative method for reducing f-fibre cross-section without altering the nozzle diameter by implementing underextrusion (Figure 4A) that involves decreasing the extrusion flow while maintaining constant printing speed, resulting in a "drops and hairline" thinning effect on the melted filament. Depending on the degree of underextrusion applied (ranging from 10–20% to 50–70%) and on the material, variations in droplet size and hairline thinning occur.

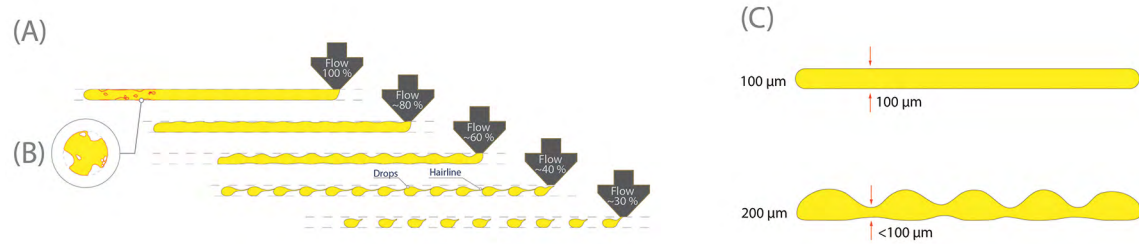


Figure 4: Extrusion flow rate: (A) flow rate and underextrusion; (B) hygroscopicity effects on filament extrusion; (C) f-fibre extrusion issues (homogeneity)

This effect has enabled the DefeXtiles method [15] to develop the technique for creating a tulle-like quasi-textile, wherein periodic anchor drops (~0.5 mm long) are formed based on the degree of underextrusion and filament feed rate. These drops fuse together through thin hairlines ($D \sim 45$ µm average), resulting in a fabric-like structure. This technology visually demonstrates the principle of semi-automatic "stretch-

ing" of the hairline by the drop itself, which would be challenging to achieve without this programmable extrusion process. Nevertheless, it should be noted that this method has strict limitations regarding hairline length (< 2 mm according to conducted tests) due to the impossibility of creating drops larger than the nozzle diameter using underextrusion. Moreover, reducing the nozzle diameter results in even shorter hairlines.

Additionally, it is not feasible to eliminate anchor drops as they form the foundation of this technology. Unfortunately, DefeXtiles represents a highly specialised production method that cannot produce homogeneous f-fibres $D < 0.1$ mm or diverse fabric-like structures without incorporating anchor drops ($D \sim 0.5$ mm).

The existing approach of 3D printing hairs [39] also addresses the challenge of reducing extrusion to levels below 0.1 mm; nonetheless, it also necessitates the incorporation of “anchor” points between which the “hair” is elongated. Despite the potential to produce long and thin f-fibres, the primary obstacle lies in the lack of control over such extrusion, thereby hindering the attainment of uniformity or

the fabrication of arbitrary shapes within the print design. Additionally, there are concerns regarding the formation of a quasi-fabric made from these “hairs”, as they need to be intertwined with each other (due to the nature of this printing method that does not allow for direct bonding between them). Addressing these complications presents a notably intricate challenge compared to direct printing techniques and falls outside the scope of this investigation.

When considering how nozzles affect extrusion quality and their ability to produce fine f-fibres, it is crucial to consider their internal parameters [21] such as material composition, inner surface quality, shape and physical dimensions (Figure 5).

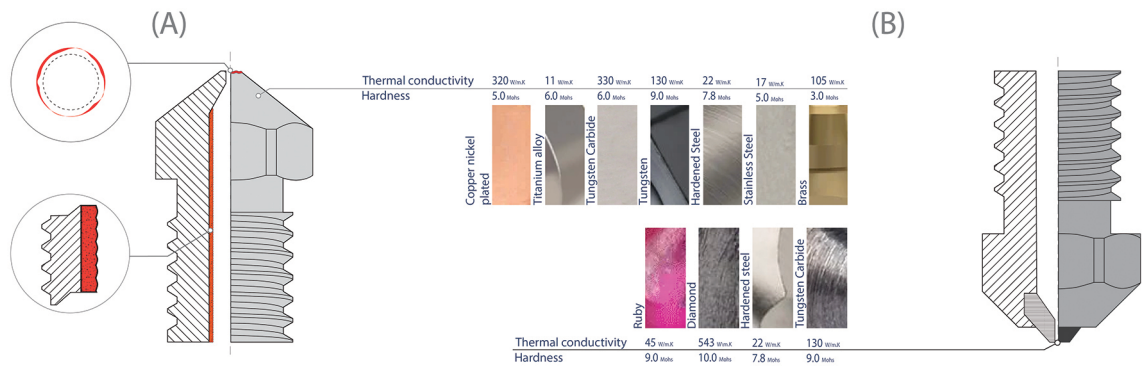


Figure 5: Nozzle: (A) inner defects and (B) thermal conductivity/hardness

Each of these factors significantly impacts print quality, speed, temperature control and even the ability to extrude certain materials. For example, nozzles crafted from materials with higher thermal conductivity allow for lower printing temperatures, while smoother walls melt flowability. It is worth noting that different thermoplastic composites require nozzles with increased hardness (Figure 5B) in their construction material to prevent rapid wear [25] and uphold the quality of f-fibre prints.

The market offers various types and models of nozzles with distinct characteristics and lifecycles [24]. However, conducting comprehensive tests is necessary to understand their influence on achieving textile-like f-fibres based on the material used, the nozzle material itself and its diameter dependencies.

3.3 Materials

A wide range of thermoplastic materials is available [27], each possessing unique characteristics; hence, establishing appropriate settings is crucial for successful printing. For instance, adjusting print temperature alone will not suffice when transitioning from printing with the polylactic acid (PLA) material to polyamide (PA) material while maintaining the same level of quality. Each material necessitates specific printing settings that can vary significantly. Furthermore, even variations in manufacturing processes [26] for the same filament material can impact its properties, requiring further adjustments.

It should be noted that the quality and structure of filaments differ considerably among different materials when maximum f-fibre print quality is achieved.

For example, PLA can be printed as a high-quality homogeneous f-fibre (if properly prepared), whereas thermoplastic polyurethane (TPU) cannot achieve the same result [37], despite being stronger and more durable as initial material (as filament) (Figure 6). Additionally, the type of the material itself affects the minimum nozzle diameter limits, particularly in composite materials where additional inclusions may exceed the nozzle diameter and cause clogging. While PLA is widely utilised for its ease of 3D printing, its characteristics may render it problematic for applications in the textile industry [9].



Figure 6: Printed samples – PLA and TPU f-fibre (macro photo): (A) TPU material with high porosity issues; (B) PLA (transparent) material

A simple example highlighting peculiarities in printing materials can be observed with TPU [28, 37], which demonstrates significant property variations based on its hardness coefficient. Usual challenges arise regarding the extrusion of flexible materials through the hotend (Figure 7B, b1), thereby establishing a minimum requirement for utilising direct drive 3D printers, maintaining low print speeds (< 15 mm/s), and implementing substantial reductions in acceleration and jerk rates. Decreasing Shore hardness coefficients result in feeding issues and frequently lead to clogging. The softening of TPU causes it to adhere inside the hotend tube (Shore hardness < 80 A), hindering filament extrusion and causing irregular extrusion patterns (Figure 2C, c1). Consequently, a smooth hotend (Figure 1) (referring to the inner feeding tube) with low adhesion properties and capable of withstanding elevated temperatures (up to 260 °C) becomes imperative. The application of the polytetrafluoroethylene (PTFE) material/coating serves as a must-have solution, while mirror-polished internal channels within the hotend feeding tube are also utilised, although it may be less suitable for TPU, but more appropriate for high-temperature plastics.

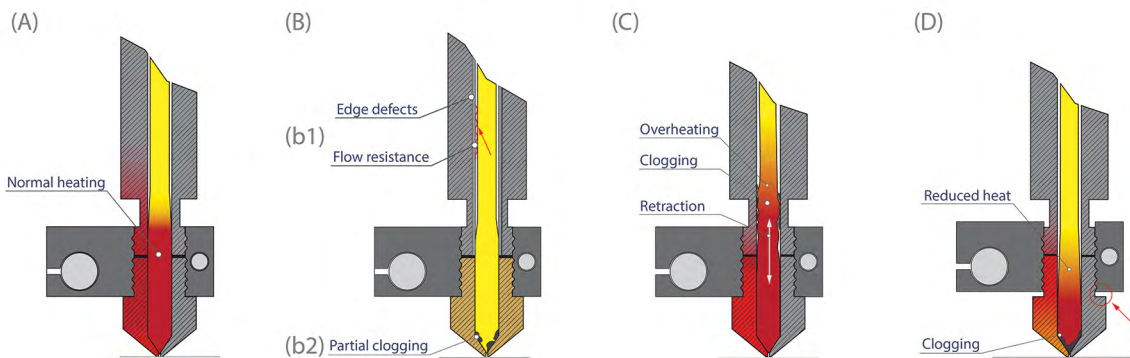


Figure 7: Printhead issues during printing process: (A) normal extrusion, (B) heatbreak wall surface defects, (C) heatbreak overheating, (D) wrong nozzle installation/contact

A precise calibration of temperature, speed and extrusion coefficient becomes paramount in achieving consistent extrusion without interruptions. While TPU offers a wide working temperature range

that allows for printing without material degradation or crystallisation, successful printing is confined to a narrow window of only ± 5 °C. Particularly when working with rubber-like materials with low

Shore hardness, adjusting the extrusion coefficient assumes significant importance. This serves as a clear illustration of the intricate dependence inherent in regular TPU printing, not to mention the challenges associated with achieving thin f-fibres that necessitate even more meticulous adjustments.

A practical demonstration of these challenges can be observed in the case of the DefeXtiles method [15], which exhibits reservations about conducting tests involving rubber-like materials. Our analysis indicates that this reluctance stems from the challenges encountered when decreasing the extrusion coefficient of TPU (assuming usage of the most basic and rigid type 95 A in case of DefeXtiles), since it often leads to issues such as uneven “drop-hairline” extrusion, resulting in structural inconsistencies, breakages, clogging, and finally to a non-working method (Figure 2C). Moreover, deliberately introducing breaks in the f-fibre structure (when we have to use retraction) poses a significant challenge with TPU (the lower the Shore value and the higher the printing temperature, the more pronounced these challenges become). However, a refinement (f-fibre thinning) of such flexible materials primarily hinges upon the nozzle diameter. By ensuring a precise regulation of temperature, print speed and extrusion coefficient, problems are generally mitigated even at minimal nozzle diameters (e.g. 0.2 mm).

In other cases where PLA or PET is used, underextrusion may be justifiable in the pursuit of smaller filament diameters; although it should be noted that this often leads to considerable irregularities in resulting f-fibres and consequently compromises their mechanical properties akin to the “drop-hairline” effect. This bears significance as these areas are prone to breakage under load.

Regrettably, there is currently an absence of comprehensive tests that offer clarity regarding the limits of underextrusion for each type of a material available on the market. Without such data at our disposal, it remains impossible to evaluate their potential for achieving thin and homogeneous f-fibres measuring < 0.1 mm.

One notable advantage of FDM printing lies in its ability to utilise composites [29], which can be classified into two main types. The first type (Figure 8A) comprises, during filament manufacturing process, a base material augmented with supplementary inclusions such as carbon, aramid, or glass short fibres (typically less than 2 mm in length) or powders consisting of small particles usually measuring less than 20 μm derived from various materials like wood, metal or glass. The second type (Figure 8B) involves the amalgamation of two or more materials, e.g. polycarbonate and acrylonitrile butadiene styrene (PC/ABS) blend or polylactic acid and polyhydroxyalkanoates (PLA/PHA) blend. However, the first type is not without drawbacks; these additives can have detrimental effects on the nozzle and may cause clogging due to particle or fibre sizes that impede nozzle openings as they fail to melt (Figure 5A). Consequently, this limits the potential for reducing the nozzle diameter. Furthermore, the quality of powder grinding or the length and orientation of short fibres directly influence f-fibre quality and subsequently impact its strength based on inclusion type and orientation.

Another approach to creating composites (the third type) presents one of the key advantages of FDM 3D printing in addressing future challenges pertaining to smart textiles. This method is known as direct printing with multimaterials and enables a simultaneous integration of different materials during printing, resulting in what is referred to as a composite structure (Figure 8C). This capability proves immensely valuable when aiming to obtain textile-like materials since it allows for potential modifications or enhancements in structural functions and characteristics. It also facilitates the creation of diverse constraints and offers opportunities for working with smart structures and conductors [6]. Developing this area necessitates extensive research as it presents boundless possibilities.

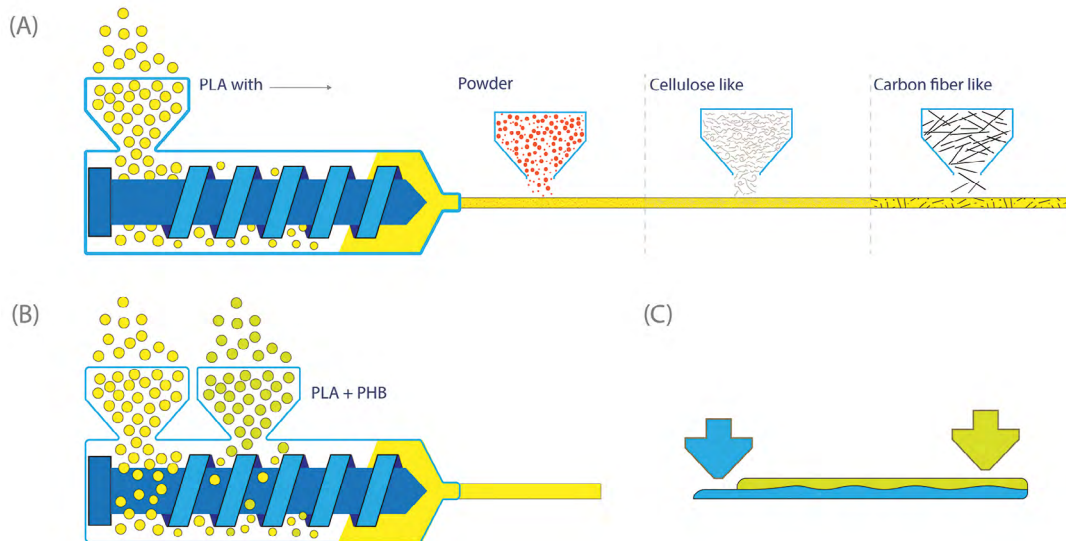


Figure 8: Filament manufacturing processes: (A) first type: raw material pellets + fibre/powder inclusions; (B) second type: mix of two raw materials; and (C) third type: creation of composite during printing process

Having a closer look at some general characteristics that demand consideration when working with any material, we must take into account material hygroscopicity – referring to its capacity to rapidly absorb moisture from the surrounding environment [30, 31] – as it significantly impacts printing outcomes, particularly when dealing with thin f-fibres exposed to high temperatures. The rapid evaporation of moisture within the melt during printing leads to micro-breaks (Figure 4B) that detrimentally affect extrusion uniformity and structural integrity. The severity of this damage is directly proportional to the moisture content of the initial material. Therefore, minimising moisture becomes a top priority when aiming to achieve high-quality f-fibres devoid of breaks or damage. Different materials exhibit varying levels

of hygroscopicity and absorption rates. Consequently, this issue warrants meticulous attention and extensive research to address concerns regarding appropriate drying and storage practices for materials.

It is also important to acknowledge that not all types of thermoplastics are suitable for producing fabric-like structures. Despite the wide array of plastics available, including emerging biobased and biodegradable varieties, the textile industry predominantly relies on a limited selection [32] due to practical limitations, safety considerations, maintenance requirements and disposal challenges. These principles likely extend to 3D printing materials as well, underscoring the significance of studying their physico-chemical properties in facilitating the material selection for future applications.

3.4 Structures

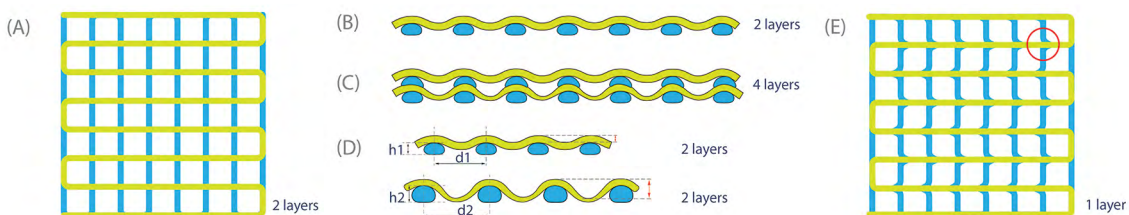


Figure 9: (A) 3D-printed mesh (grid) structure top view; (B) 2-layers mesh side view; (C) 4-layers mesh side view; (D) f-fibre sagging side view; and (E) 1-layer print top view

While traditional fabrics consist of interwoven independent threads, additive printing endeavours to create a fusion between layers or fibres (Figure 2A, 9A). Therefore, achieving an equivalent nonwoven fabric structure (comprising thermally bonded micro-sized fibres randomly intertwined) using the FDM methodology appears theoretically possible due to inherent filament bonding in 3D printing. For instance, adaptations of electrospinning [33, 34] or methods similar to paint spraying utilising molten plastic exposed to hot air flow can generate multiple chaotic threads that adhere to any surface and form a nonwoven structure [35]. Unfortunately, a precise control over such nano-threads remains elusive at present, impeding our ability to create fabric-like materials through this approach. On the other hand, standard FDM 3D printing enables the production of mesh (grid) structures (Figures 9A, 6, 10) that lie somewhere between nonwoven and woven structures – referred to as 3D-printed mesh structures – which can be expanded upon extensively. This aspect highlights one of the advantages of 3D printing, as it allows for the combination of volumetric (semi)rigid elements with flexible thin fabric-like structures (Figure 10).

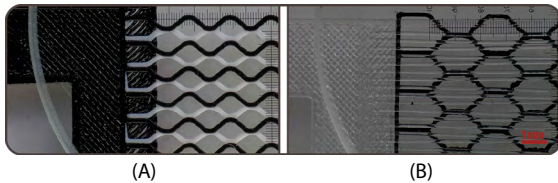


Figure 10: Printed samples (macro photo) – connection of rigid structure and *f*-fibres within one process: (A) PLA black and white material and (B) PA6 transparent and PLA black material

Any material or a combination thereof can be employed, along with any desired number of layers or coatings. Such structures possess the potential to realise a wide range of smart functionalities given that their production foundation (through 3D printing methods) facilitates the integration of different materials and printing technologies, such as the

addition of the direct ink writing (DIW) method.

One notable advantage of 3D printing lies in its capacity to generate multiple layers. As previously mentioned, the print quality of subsequent layers surpasses that of the initial layer; however, they also have certain limitations. When discussing a grid structure in printing, the second and following layers (in contrast to the base layer) are essentially printed in mid-air and only make contact with the *f*-fibres of the lower layer at specific points (Figure 9B). If the grid fill density is low and *f*-fibres are thin, they become more susceptible to breakage during movement between these connection points. This issue becomes less significant when $Lh < 100 \mu\text{m}$ or when the grid fill density is increased. Naturally, as Lh increases, this problem worsens, resulting in sagging, and breaks in the printed structure (Figure 9D). For conventional 3D printing tasks, this issue can be addressed through specific slicer bridging settings [37]. However, when working with thin textile-like structures such as ours, different settings are required that heavily depend on factors such as material type and melting temperature.

Structures exist where both horizontal and vertical (similar to weft and warp threads of traditional textile) *f*-fibres are printed within a single layer (Figure 9E). This inevitably leads to disruptions at intersections where *f*-fibres with different orientations meet, necessitating duplicate layers to conceal errors. Previous attempts to mimic textile-like materials often adopt this printing principle [14]; however, unless absolutely necessary, we do not recommend it due to its detrimental effect on filament integrity and overall structural strength. Attempting to rectify this by adding more layers compromises textile-like properties and results in a plastic-rigid structure with compromised strength.

The height of each individual layer as well as the overall structure plays a vital role; thus, striving for minimal values is paramount for achieving flexibility in printed structures. Our research indicates that when the structure resembles that shown in Figure 9A, specific layer height (Lh) checks apply to

maintain textile-like properties (the total height of the 3D-printed structure must remain below 0.5 mm and the fibre width is less than 200 μm). If $Lh < 150 \mu\text{m}$, a maximum of three printing layers is possible. For cases where $Lh < 100 \mu\text{m}$, up to five layers are possible; and if $Lh < 50 \mu\text{m}$, seven printing layers are possible.

Another challenge that must be addressed is the uniformity and homogeneity of f-fibres without breaks. When attempting to reduce f-fibre cross-sections, it is crucial to consider maintaining continuous accuracy during the melt extrusion process, which requires a more precise feeding mechanism (Figure 1). This issue can manifest as an error resulting from reducing the extrusion coefficient (slicer settings), leading to the formation of sagging (Figure 9D) or “drop-hairline” f-fibres (Figure 4A). In other words, filament delivery necessitates a different level of precision (smooth pressure via feeding mechanism) that has the potential to significantly enhance f-fibre quality when compensating for underextrusion. With low-quality 3D printer kinematic precision, we can encounter a situation where f-fibre thickness of, e.g., 200 μm (extruded using underextrusion methods) exhibits even poorer strength limits compared to a homogeneous f-fibre with a thickness of 100 μm (Figure 4C).

Regarding traditional weaving techniques, while it may be theoretically feasible to create structures that mimic them, this does not negate the fundamental principle of achieving f-fibres $D < 100 \mu\text{m}$ for them. Without a requirement like this, such prototype structures would merely resemble a fabric in appearance but lack its inherent flexibility, delicacy and functionality. This can be observed through various examples [10–13]. Furthermore, we believe that implementing such structures (given the current stage of advancement in 3D printing within the textile sector) becomes significantly more complex compared to grid-based structures and necessitates the adoption of innovative methodologies.

4 Conclusion

Despite additive technologies still being in their nascent stages of development with respect to textile manufacturing, it is evident that they already demand a high level of expertise from specialists. Even printing a simple structure requires knowledge about various software packages, technical aspects of 3D printers, material properties etc. When striving to achieve 3D-printed textiles comparable to traditional ones, it is safe to say that there are currently no straightforward solutions available. This conclusion is supported by existing accomplishments and our analysis of the limitations and peculiarities inherent in the FDM technology. Nonetheless, the rationale behind pursuing such structures lies in the technological advantages offered by additive technologies for the realisation of future smart structures. We firmly believe that our research can contribute to taking the next step towards materialising these structures, provided that our observations are taken into account and existing limitations in achieving minimal filament thicknesses are overcome. Our comprehensive analysis also reveals that we are still at an early stage of comprehending and applying the FDM technology. Therefore, further extensive testing is imperative to achieve practical quality (and diversity) of 3D-printed fabric-like structures.

Funding details: This work was supported by the Research Council of Lithuania (LMTLT) under Grant No: S-PD-22-44

Conflicts of interest: No potential conflict of interest was reported by the author(s).

Data availability statement: The data that support the findings of this study are available on request from the corresponding author.

References

- ZHANG, Y., LIN, J.H., CHENG, D.H., LI, X., WANG, H.Y., LU, Y.H., LOU, C.W. A study on Tencel/LMPET-TPU/triclosan laminated membranes: excellent water resistance and antimicrobial ability. *Membranes*, 2023, **13**(8), 1–13, doi: 10.3390/membranes13080703.
- RUCKDASHEL, R.R., VENKATARAMAN, D., PARK, J.H. Smart textiles: a toolkit to fashion the future. *Journal of Applied Physics*, 2021, **129**(13), 1–18, doi: 10.1063/5.0024006.
- JÚNIOR, H.L.O., NEVES, R.M., MONTICELI, F.M., DALL AGNOL, L. Smart fabric textiles: recent advances and challenges. *Textiles*, 2022, **2**(4), 582–605, doi: 10.3390/textiles2040034.
- WU, S., ZENG, T., LIU, Z., MA, G., XIONG, Z., ZUO, L., ZHOU, Z. 3D printing technology for smart clothing: a topic review. *Materials*, 2022, **15**(20), 1–15, doi: 10.3390/ma15207391.
- XU, Y., WU, X., GUO, X., KONG, B., ZHANG, M., QIAN, X., MI, S., SUN, W. The boom in 3D-printed sensor technology. *Sensors*, 2017, **17**(5), 1–37, doi: 10.3390/s17051166.
- PARK, S., SHOU, W., MAKATURA, L., MATUSIK, W., FU, K.K. 3D printing of polymer composites: materials, processes, and applications. *Matter*, 2022, **5**(1), 43–76, doi: 10.1016/j.matt.2021.10.018.
- CHATTERJEE, K., GHOSH, T.K. 3D printing of textiles: potential roadmap to printing with fibres. *Advanced Materials*, 2020, **32**(4), 1–24, doi: 10.1002/adma.201902086.
- MANAIA, J.P., CEREJO, F., DUARTE, J. Revolutionising textile manufacturing: a comprehensive review on 3D and 4D printing technologies. *Fashion and Textiles*, 2023, **10**(1), 1–28, doi: 10.1186/s40691-023-00339-7.
- RANA, S., PICHANDI, S., PARVEEN, S., FANGUEIRO, R. Biosynthetic fibres: production, processing, properties and their sustainability parameters. In *Roadmap to sustainable textiles and clothing: eco-friendly raw materials, technologies, and processing methods*. Edited by Subramanian Senthilkannan Muthu. Springer, 2014, 109–138, doi: 10.1007/978-981-287-065-0_4.
- MELNIKOVA, R., EHRMANN, A., FINSTERBUSCH, K. 3D printing of textile-based structures by Fused Deposition Modelling (FDM) with different polymer materials. *IOP conference series: materials science and engineering*, 2014, **62**(1), 1–7, doi: 10.1088/1757-899X/62/1/012018.
- JAYSWAL, A., ADANUR, S. Effect of heat treatment on crystallinity and mechanical properties of flexible structures 3D printed with fused deposition modelling. *Journal of Industrial Textiles*, 2022, **51**(2_suppl), 2616S–2641S, doi: 10.1177/15280837211064937.
- BEECROFT, M. Digital interlooping: 3D printing of weft-knitted textile-based tubular structures using selective laser sintering of nylon powder. *International Journal of Fashion Design, Technology and Education*, 2019, **12**(2), 218–224, doi: 10.1080/17543266.2019.1573269.
- WIRTH, M., SHEA, K., CHEN, T. 3D-printing textiles: multi-stage mechanical characterization of additively manufactured biaxial weaves. *Materials & Design*, 2023, **225**, 1–14, doi: 10.1016/j.matdes.2022.111449.
- ARIKAN, C. O., DOĞAN, S., MUCK, D. Geometric structures in textile design made with 3D printing. *Tekstilec*, 2022, **65**(4), 307–321, doi: 10.14502/tekstilec.65.2022092.
- FORMAN, J., DOGAN, M. D., FORSYTHE, H., ISHII, H. DefeXtiles: 3D printing quasi-woven fabric via under-extrusion. In *Proceedings of the 33rd Annual ACM Symposium on User Interface Software and Technology*, 2020, 1222–1233, doi: 10.1145/3379337.3415876.
- BAECHLE-CLAYTON, M., LOOS, E., TAHERI, M., TAHERI, H. Failures and flaws in fused deposition modelling (FDM) additively manufactured polymers and composites. *Journal of Composites Science*, 2022, **6**(7), 1–17, doi: 10.3390/jcs6070202.

17. KAŠČAK, J., KOČIŠKO, M., VODILKA, A., TÖRÖK, J., CORANIČ, T. Adhesion testing device for 3D printed objects on diverse printing bed materials: design and evaluation. *Applied Sciences*, 2024, **14**(2), 1–14, doi: 10.3390/app14020945.
18. PŁACZEK, D. Adhesion between the bed and component manufactured in FDM technology using selected types of intermediary materials. In *9th International Conference on Manufacturing Science and Education – MSE 2019 “Trends in New Industrial Revolution”*. Edited by I. Bondrea, N.F. Cofaru and M. Intă. *MATEC Web of Conferences*, 2019, **290**, 1–9, doi: 10.1051/mateconf/201929001012.
19. NAZAN, M.A., RAMLI, F.R., ALKAHARI, M.R., ABDULLAH, M.A., SUDIN, M.N. An exploration of polymer adhesion on 3D printer bed. *IOP Conference Series: Materials Science and Engineering*, 2017, **210**(1), 1–10, doi: 10.1088/1757-899X/210/1/012062.
20. CAVALCANTI, D.K.K., MEDINA, M., DE QUEIROZ, H.F. M., NETO, J. S. S., CHAVES, F.J.P., BANEJA, M.D. Recent advances in adhesive bonding of 3D-printed parts and methods to increase their mechanical performance. *Annals of “Dunarea de Jos” University of Galati. Fascicle XII, Welding Equipment and Technology*, 2023, **34**, 17–24, doi: 10.35219/awet.2023.02.
21. SCHULLER, T., JALAAL, M., FANZIO, P., GALINDO-ROSALES, F.J. Optimal shape design of printing nozzles for extrusion-based additive manufacturing. *Additive Manufacturing*, 2024, **84**, 1–18, doi: 10.1016/j.addma.2024.104130.
22. CZYŻEWSKI, P., MARCINIAK, D., NOWINKA, B., BOROWIAK, M., BIELIŃSKI, M. Influence of extruder’s nozzle diameter on the improvement of functional properties of 3D-printed PLA products. *Polymers*, 2022, **14**(2), 1–17, doi: 10.3390/polym14020356.
23. BUTT, J., BHASKAR, R., MOHAGHEGH, V. Investigating the influence of material extrusion rates and line widths on FFF-printed graphene-enhanced PLA. *Journal of Manufacturing and Materials Processing*, 2022, **6**(3), 1–19, doi: 10.3390/jmmp6030057.
24. MELO, J.T., SANTANA, L., IDOGAVA, H.T., PAIS, A.I.L., ALVES, J.L. Effects of nozzle material and its lifespan on the quality of PLA parts manufactured by FFF 3D Printing. *Engineering Manufacturing Letters*, 2022, **1**(1), 20–27, doi: 10.24840/2795-5168_001-001_0005.
25. BIANCHI, I., MANCIA, T., MIGNANELLI, C., SIMONCINI, M. Effect of nozzle wear on mechanical properties of 3D printed carbon fibre-reinforced polymer parts by material extrusion. *The International Journal of Advanced Manufacturing Technology*, 2024, **130**(9), 4699–4712, doi: 10.1007/s00170-024-13035-7.
26. ANDRONOV, V., BERÁNEK, L., KRŮTA, V., HLAVŮŇKOVÁ, L., JENÍKOVÁ, Z. Overview and comparison of PLA filaments commercially available in Europe for FFF technology. *Polymers*, 2023, **15**(14), 1–21, doi: 10.3390/polym15143065.
27. DEY, A., ROAN EAGLE, I.N., YODO, N. A review on filament materials for fused filament fabrication. *Journal of Manufacturing and Materials Processing*, 2021, **5**(3), 1–40, doi: 10.3390/jmmp5030069.
28. KORGER, M., GLOGOWSKY, A., SANDULOFF, S., STEINEM, C., HUYSMAN, S., HORN, B., ERNST, M., RABE, M. Testing thermoplastic elastomers selected as flexible three-dimensional printing materials for functional garment and technical textile applications. *Journal of Engineered Fibres and Fabrics*, 2020, **15**, 1–10, doi: 10.1177/1558925020924599.
29. WICKRAMASINGHE, S., DO, T., TRAN, P. FDM-based 3D printing of polymer and associated composite: a review on mechanical properties, defects and treatments. *Polymers*, 2020, **12**(7), 1–42, doi: 10.3390/polym12071529.
30. HAMROL, A., GÓRALSKI, B., WICHNIAREK, R. The influence of moisture absorption and desorption by the ABS filament on the properties

- of additively manufactured parts using the fused deposition modelling method. *Materials*, 2024, **17**(9), 1–16, doi: 10.3390/ma17091988.
31. ANISKEVICH, A., BULDERBERGA, O., STANKEVICS, L. Moisture sorption and degradation of polymer filaments used in 3D printing. *Polymers*, 2023, **15**(12), 1–23, doi: 10.3390/polym15122600.
 32. TIAN, W., HUANG, K., ZHU, C., SUN, Z., SHAO, L., HU, M., FENG, X. Recent progress in biobased synthetic textile fibres. *Frontiers in Materials*, 2022, **9**, 1–12, doi: 10.3389/fmats.2022.1098590.
 33. YANG, D.L., FARAZ, F., WANG, J.X., RADACSI, N. Combination of 3D printing and electrospinning techniques for biofabrication. *Advanced Materials Technologies*, 2022, **7**(7), 1–27, doi: 10.1002/admt.202101309.
 34. EJIHOUO, O. A perspective on the synergistic use of 3D printing and electrospinning to improve nanomaterials for biomedical applications. *Nano Trends*, 2023, **4**, 1–13, doi: 10.1016/j.nwnano.2023.100025.
 35. KARA, Y., KOVÁCS, N. K., NAGY-GYÖRGY, P., BOROS, R., MOLNÁR, K. A novel method and printhead for 3D printing combined nano-/microfibre solid structures. *Additive Manufacturing*, 2023, **61**, 1–13, doi: 10.1016/j.addma.2022.103315.
 36. KUIPER, P., WIJNIA, S. Improved bridging in FFF [online]. Technical Disclosure Commons [accessed 6. 7. 2024]. Available on World Wide Web: <https://www.tdcommons.org/cgi/viewcontent.cgi?article=6454&context=dpubs_series>.
 37. RODRÍGUEZ, L., NAYA, G., BIENVENIDO, R. Study for the selection of 3D printing parameters for the design of TPU products. *IOP Conference Series: Materials Science and Engineering*, 2021, **1193**(1), 1–9, doi: 10.1088/1757-899X/1193/1/012035.
 38. SABIR, T. Fibres used for high-performance apparel. In *High-performance apparel: materials, development, and applications*. Edited by John McLoughlin and Tasneem Sabir. Woodhead Publishing, 2017, 7–32, doi: 10.1016/B978-0-08-100904-8.00002-X.
 39. LAPUT, G., CHEN, X.A., HARRISON, C. 3D printed hair: fused deposition modelling of soft strands, fibres, and bristles. In *Proceedings of the 28th annual ACM Symposium on User Interface Software & Technology*, 2015, 593–597, doi: 10.1145/2807442.2807484.

SHORT INSTRUCTIONS FOR AUTHORS OF SCIENTIFIC ARTICLES

Scientific articles categories:

- **Original scientific article** is the first publication of original research results in such a form that the research can be repeated and conclusions verified. Scientific information must be demonstrated in such a way that the results are obtained with the same accuracy or within the limits of experimental errors as stated by the author, and that the accuracy of analyses the results are based on can be verified. An original scientific article is designed according to the IMRAD scheme (Introduction, Methods, Results and Discussion) for experimental research or in a descriptive way for descriptive scientific fields, where observations are given in a simple chronological order.
- **Review article** presents an overview of most recent works in a specific field with the purpose of summarizing, analysing, evaluating or synthesizing information that has already been published. This type of article brings new syntheses, new ideas and theories, and even new scientific examples. No scheme is prescribed for review article.
- **Short scientific article** is original scientific article where some elements of the IMRAD scheme have been omitted. It is a short report about finished original scientific work or work which is still in progress. Letters to the editor of scientific journals and short scientific notes are included in this category as well.

Language: The manuscript of submitted articles should be written in UK English or in Slovene with bilingual Figures and Tables. The authors responsibility to ensure the quality of the language.

Manuscript length: The manuscript should not exceed 30,000 characters without spacing.

Article submission: The texts should be submitted only in their electronic form in the *.doc (or *.docx) and *.pdf formats, where for each author must be given:

- first name and family name
- title
- full institution address
- ORCID ID
- e-mail.

The name of the document should contain the date (year-month-day) and the surname of the corresponding author, e.g. 20140125Novak.docx. The manuscripts proposed for a review need to have their figures and tables included in the text.

Detailed information on the preparation and submission of the manuscript is available on the website:

<https://journals.uni-lj.si/tekstilec/about/submissions>.

Reviewer suggestions

Authors can suggest potential reviewers. Please provide their titles, ORCID IDs, institutions, and e-mail addresses. The proposed referees should not be current collaborators of the co-authors nor should they have published with any of the co-authors of the manuscript within the last three years. The proposed reviewers should be from institutions other than the authors.

Authors may also provide the names of potential reviewers they wish to exclude from reviewing their manuscript during the initial submission process.

Peer-review process

All submitted articles are professionally, terminologically and editorially reviewed in accordance with the general professional and journalistic standards of the journal Tekstilec. All articles are double-blind reviewed by two or more reviewers independent of editorial board.

The review process takes a minimum of two weeks and a maximum of one month. The reviewers' comments are sent to authors for them to complete and correct their manuscripts. If there is no consensus among the reviewers, the editorial board decides on the further procedure. We accept the articles for publication based on a positive decision.

Copyright corrections

The editors are going to send computer printouts for proofreading and correcting. It is the author's responsibility to proofread the article and send corrections as soon as possible. However, no greater changes or amendments to the text are allowed at this point.

Colour print of hard copies

Colour print is performed only when this is necessary from the viewpoint of information comprehension, and upon agreement with the author and the editorial board.

Copyright Notice

Authors who publish with this journal agree to the following terms:

- Authors are confirming that they are the authors of the submitting article, which will be published (print and online) in journal Tekstilec by University of Ljubljana Press / Faculty of Natural Sciences and Engineering, University of Ljubljana, Aškerčeva 12, SI-1000 Ljubljana, Slovenia).
- Author's name will be evident in the article in journal. All decisions regarding layout and distribution of the work are in hands of the publisher.
- Authors guarantee that the work is their own original creation and does not infringe any statutory or common-law copyright or any proprietary right of any third party. In case of claims by third parties, authors commit their self to defend the interests of the publisher, and shall cover any potential costs.
- Authors retain copyright and grant the journal right of first publication with the work simultaneously licensed under a Creative Commons Attribution CC BY 4.0 that allows others to share the work with an acknowledgement of the work's authorship and initial publication in this journal.
- Authors are able to enter into separate, additional contractual arrangements for the non-exclusive distribution of the journal's published version of the work (e.g. post it to an institutional repository or publish it in a book), with an acknowledgement of its initial publication in this journal.
- Authors are permitted and encouraged to post their work online (e.g., in institutional repositories or on their website) prior to and during the submission process, as it can lead to productive exchanges, as well as earlier and greater citation of published work.

Privacy Statement

The personal data entered in this journal site, like names and addresses, will be used exclusively for the stated purposes of this journal and will not be made available for any other purpose or to any other party.

